Further Immunohistochemical (IHC) Characterisation of Devil Facial Tumour Disease 1 (DFT1) in the Tasmanian Devil (Sarcophilus harrisii)

By

Dane A. Hayes

BBiomedSc, CT(ASC)

School of Health Sciences

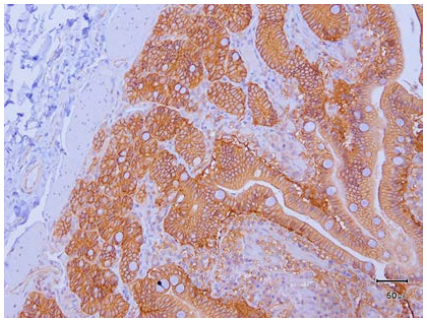

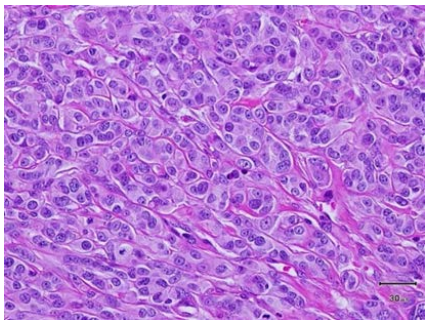

Submitted in fulfilment of the requirements for the Doctor of Philosophy

University of Tasmania 10th of December 2018

Declaration of Originality

'This thesis contains no material which has been accepted for a degree or diploma by the University or any other institution, except by way of background information and duly acknowledged in the thesis, and to the best of my knowledge and belief no material previously published or written by another person except where due acknowledgement is made in the text of the thesis, nor does the thesis contain any material that infringes copyright.'

Candidate: Dane Hayes Date: 10th December 2018

Authority of access

'This thesis is not to be made available for loan or copying for two years following the date this statement was signed due to pending publication of Chapter 1 of this thesis. Following that time, the thesis may be made available for loan and limited copying and communication in accordance with the Copyright Act 1968.'

Candidate: Dane Hayes Date: 10th December 2018

Published work contained in this thesis

'The publishers of the papers contained in chapters 1-3 of this thesis hold copyright for the content and access to the material should be sought from the respective journals. The remaining content of the thesis may be made available for loan and limited copying and communication in accordance with the Copyright Act 1968.'

Candidate: Dane Hayes Date: 10th December 2018

Animal ethics statement

'All Tasmanian devil serum and paraffin embedded tissues were accessed from the Animal Health Laboratory archive, samples were collected by DPIPWE veterinary staff for the Save the Tasmanian Devil Program (STDP) http://www.tassiedevil.com.au/tasdevil.nsf *encompassing health checks, field trapping trips, or autopsy due to animal welfare reasons therefore, samples and did not require ethics approval.'*

Candidate: Dane Hayes Date: 10th December 2018

Statement of Co-Authorship

The following people and institutions contributed to the publication of work undertaken as part of this thesis:

Candidate, Dane A. Hayes**,** School of Health Sciences, University of Tasmania.
Author 2, Sukhwinder S. Sohal, (supervisor), School of Health Sciences, University of Tasmania.
Author 3, Elizabeth. T. Snow, (supervisor), School of Health Sciences, University of Tasmania.
Author 4, Mathew Eapen, School of Health Sciences, University of Tasmania.
Author 5, Elizabeth Murchison, Department of Veterinary Medicine, University of Cambridge.
Author 6, Graeme Knowles, Department of Primary Industries, Parks, water and Environment.

Author details and their roles:
Devil Facial Tumour 1 (DFT1) Immunophenotype Reveals a Progenitor-Like Cell with Schwann cell, Melanocyte and Self-renewal Characteristics.

Located in chapter 1

Dane Hayes was the primary author and responsible for the conception and design of the research project, contributed approximately 80% to the planning, execution and preparation. Performed immunohistochemistry, photography, compiled and interpreted results and drafted the paper.
Sukhwinder Sohal, supervisor, contributed to the concept and design of the research project, critically reviewed, read and approved the paper.
Elizabeth Snow, supervisor, contributed to the concept and design of the research project, critically reviewed, read and approved the paper.
Mathew Eapen applied statistical analysis and presented data figures, read and approved the paper.
Elizabeth Murchison provided gene data from previously published work for expressional comparison, read, critically assessed and approved the paper.
Graeme Knowles, assessed the histomorphology of the DFT1 strains, read and approved the paper.

Candidate, Dane A. Hayes**,** School of Health Sciences, University of Tasmania.
Author 2, Sukhwinder S. Sohal, School of Health Sciences, University of Tasmania.
Author 3, Elizabeth. T. Snow, School of Health Sciences, University of Tasmania.
Author 4, Dale Kunde, School of Health Sciences, University of Tasmania.
Author 5, Robyn L. Taylor, School of Zoology, University of Tasmania.
Author 6, Stephen B. Pyecroft, School of Animal & Veterinary Sciences, University of Adelaide.

Author details and their roles:

ERBB3: A Potential Serum Biomarker for Early Detection and Therapeutic Target for Devil Facial Tumour Disease (DFTD)

Located in chapter 2

Dane Hayes was the primary author and responsible for the conception and design of the research project, contributed approximately 85% to the planning, execution and preparation. Performed immunohistochemistry, photography, compiled and interpreted results and drafted the paper.
Sukhwinder Sohal, supervisor, contributed to the concept and design of the research project, critically reviewed, read and approved the paper.
Elizabeth Snow, supervisor, contributed to the concept and design of the research project, critically reviewed, read and approved the paper.
Dale Kunde performed the ELISA assay, interpreted the assay data, read and approved the paper.
Robyn Taylor retrieved serum, performed the ELISA assay, read and approved the paper
Stephen Pyecroft, supervisor, read and approved the paper.

Signed:
Dr Sukhwinder Sohal
Supervisor
School of Health Sciences
University of Tasmania
Date: 26/11/18

Signed:
Prof Nuala Byrne
Head of School
School of Health Sciences
University of Tasmania
5/12/18

Acknowledgements

I would like to express my sincere gratitude to my supervisor's Dr Sukhwinder Sohal and especially Associate Professor Elizabeth Snow (Ret.) for their academic guidance during my research. I am incredibly grateful to the following colleagues:

- My graduate research coordinators Professor Dominic Geraghty and Dr Karin Ahuja for their continued support.
- My co-authors Dr Dale Kunde, Robyn Taylor, Dr Stephen Pyecroft, Dr Mathew Eapen, Dr Graeme Knowles and Dr Elizabeth Murchison for their invaluable assistance and contribution to my research and manuscripts.
- This research was not possible without funding from the Eric Guiler Save The Tasmanian Devil Program research grant (STDP) and University of Tasmania, in kind and financial support from the Tasmanian government Department of Primary Industries, Parks, Water and Environment (DPIPWE) and the University of Adelaide.
- STDP manager David Pemberton for his critical manuscript reviews and the STDP/DPIPWE staff especially Sarah Peck, Collette Harmsen and David Schaap for their field expertise, Greg Woods and Alex Kreiss for their insights into DFTD.
- Ruth Pye and Max Stammnitz for inviting me to collaborate on their Tasmanian devil facial tumour 2 (DFT2) research projects.
- Veterinary pathologist's Dr Richmond Loh, Dr Jim Taylor, Dr Philip Ladds (Dec.), Dr Roy Mason, Dr Tony Ross and Dr Andrew Davis for their insights into Tasmanian devil pathology and provision of histological tissues.
- DPIPWE staff Jeremy Carson, Richard Morrison, Teresa Wilson, and Catherine Marshall. Margaret Quill and Tony Venettacci for journal article procurement and Anne-Maree Pearce and Kate Swift for Tasmanian devil cytogenetics.
- Alistair Townsend, Tony Van Galen, Dhirendra Prasad, Mike Burley, Jann Brauer, Karen Wolfswinkel and Dr Terry Brain for histological and immunohistochemical support and advice.
- Committees of the Molecular an Experimental Pathology Society of Australasia, National Histology Conference and Histology Group of Victoria for their continued support of veterinary pathology and research.

To my family,

It is with heartfelt appreciation and deepest gratitude that I thank Melissa and Lydia for their encouragement and support during my research. I thank Sam, Audrey, Rocky and Molly for their companionship during the wee small hours.

Published articles and conference presentations

Co-author published papers pre-candidature:

1. Loh R, Bergfeld J, Hayes D, O'Hara A, et al. **The pathology of devil facial tumor disease (DFTD) in Tasmanian devils (Sarcophilus harrisii)**. Vet Pathol. 2006;43(6):890-5. doi: 10.1354/vp.43-6-890. (appendix 1)
2. Loh R, Hayes D, Mahjoor A, O'Hara A, et al. **The immunohistochemical characterization of devil facial tumor disease (DFTD) in the Tasmanian Devil (Sarcophilus harrisii)**. Vet Pathol. 2006;43(6):896-903. doi: 10.1354/vp.43-6-896. (appendix 2)
3. Pyecroft SB, Pearse AM, Loh R, Swift K, Belov K, Fox N, et al. **Towards a case definition for devil facial tumour disease: What is it?** EcoHealth. 2007;4(3):346-51. doi: 10.1007/s10393-007-0126-0. (appendix 3)

1st Author manuscript published during candidature:

4. Hayes DA, Kunde DA, Taylor RL, Pyecroft SB, Sohal SS, Snow ET. **ERBB3: A potential serum biomarker for early detection and therapeutic target for devil facial tumour 1 (DFT1)**. PLoS One. 2017;12(6). doi: 10.1371/journal.pone.0177919. (appendix 4)

1st Author manuscript completed during candidature, submission imminent.

5. Dane A. Hayes, Mathew Eapen, Elizabeth P Murchison, Graeme Knowles, Elizabeth T. Snow, Sukhwinder Singh Sohal. **Devil Facial Tumour 1 (DFT1) Immunophenotype Reveals a Progenitor-Like Cell with Schwann cell, Melanocyte and Self-renewal Characteristics.**

Co-author papers on DFT2 during candidature:

6. Pye RJ, Pemberton D, Tovar C, Tubio JMC, Dun KA, Fox S, et al. **A second transmissible cancer in Tasmanian devils**. Proc Natl Acad Sci U S A. 2016;113(2):374-9. doi: 10.1073/pnas.1519691113. (appendix 5)

7. Stammnitz MR, Coorens THH, Gori KC, Hayes D, Fu BY, Wang JH, et al. **The Origins and Vulnerabilities of Two Transmissible Cancers in Tasmanian Devils**. Cancer Cell. 2018;33(4):607-+. doi: 10.1016/j.ccell.2018.03.013. (appendix 6)

Conference presentations:

1. Molecular an Experimental Pathology Society of Australasia (Oral presentation: Further Immunohistochemistry of DFTD, Sydney, 2013, Received travel grant prize.)
2. Histology group of Victoria (Oral presentation: Further Immunohistochemistry of DFTD, Hobart 2014)
3. National Histology Conference (Oral presentation: Further Immunohistochemistry of DFTD, Brisbane 2015)
4. National Histology Conference (Poster presentation of ERBB3 paper - Received 1st Prize [international judges], Hobart 2017, appendix 7)
5. Molecular an Experimental Pathology Society of Australasia (Oral presentation: Further Immunohistochemistry of DFTD, Sydney, 2017, Received travel grant prize.)

Table of Abbreviations:

Note: Primary antibody and therapeutic abbreviations are located in **Table 2** and **Table 7** respectively.

ABC	Avidin-Biotin Complex
AML	Angiomyolipoma
AR	Amphiregulin
B2M	β_2 microglobulin
BAC	Bacterial artificial chromosome
BCs	Boundary cap cells
bFGF	Basic fibroblast growth factor
BSC	Bungner Schwann cell
BTC	Beta- cellulin
C	Chondrocytes
CCST	Clear cell sugar carcinoma
CD	Cluster of Differentiation

CE	Stochastic/clonal evolution
CHD	Clinically healthy Tasmanian devils
CHDD	Localised skin non-DFT1 dermatopathy
CHJD	Clinically healthy juvenile Tasmanian devils
CL	Cutaneous Lymphoma
CME	Clathrin mediated endocytosis
CNC	Cranial neural crest
CNS	Central nervous system
CNVs	Copy number variants
CREB1	cAMP responsive element binding protein 1
CSC	Cancer stem cell
CSIRO	Commonwealth Scientific and Industrial Research Organisation
CTC	Circulating tumour cell
CTLA-4	Cytotoxic T Lymphocyte Antigen 4
DAB	3,3'- Diaminobenzidine
DCT	Tyrosinase related protein 2/dopachrome tautomerase
DFT1	Devil Facial Tumour Disease 1
DFT2	Devil Facial Tumour Disease 2
DFTD	Devil Facial Tumour Disease
DM	Double minute chromosomes
DMB	MHC class II DM beta
DNMT	DNA methyltranferases
DPIPWE	Department of Primary Industries, Parkes, Water and Environment
DPSC	Dental pulp stem cells
DREZ	Dorsal root entry zones
DRG	Dorsal root ganglia

ECD	Extracellular domain
EDN3	Endothelin 3
EDNRB	Endothelin receptor type B
EGF	Epidermal growth factor
EGFR	Epidermal growth factor receptor/Erb-B2 Receptor Tyrosine Kinase 1/HER1
EIER	Enzyme induced epitope retrieval
ELISA	Enzyme linked immunosorbent assay
EMPNST	Epithelioid malignant peripheral nerve sheath tumour
EMT	Epithelium-to-mesenchymal transition
ENS	Enteric nervous system
EPG	Epigen
EPI-NCSC	Epidermal neural crest stem cells
EPR	Epiregulin
ERAD	Endoplasmic reticulum – associated degradation pathway
ERBB	Avian erythroblastosis oncogene, v-erbB/ Erb-B2 receptor tyrosine kinase
ERBB2	Erb-B2 Receptor Tyrosine Kinase 2/HER2
ERBB3	Erb-B2 Receptor Tyrosine Kinase 3/HER3
ERBB4	Erb-B2 Receptor Tyrosine Kinase 4/HER4
F	Myofibroblast
FOXD3	Forkhead box D3
FPSC	Fungiform papilla of the tongue
FZD	Frizzled receptor
G	Glial
GDNF	Glial derived neurotrophic factor
GN	Ganglioneuroma

GRN	Gene regulatory network
HAP	Hair follicle-associated stem cells
HB-EGF	Heparin binding EGF-like growth factor
HCC	Hepatocellular carcinoma
HER	Human epidermal growth factor receptor
HIER	Heat induced epitope retrieval
HIF2A	Hypoxia inducible factor 2α pathway
IFN- γ	Interferon -γ
IGF1	Insulin like growth factor 1
IGFBP1	Insulin like growth factor binding protein 1
IHC	Immunohistochemistry
IL4	Interleukin 4 (IL4)
ISC	Immature Schwann cells
JNK	c-Jun N-terminal kinase
KITLG	KIT ligand, steel factor, SCF/stem cell factor
LAM	Lymphangioleiomyomatosis
lncRNAs	Long ncRNAs
LRC	Leukocyte Receptor Complex
LRP5/6	Low density lipoprotein related protein 5/6
M	Melanocyte
M1	DFTD karyotype marker 1
M2	DFTD karyotype marker 2
M3	DFTD karyotype marker 3
M4	DFTD karyotype marker 4
M5	DFTD karyotype marker 5
MAPK	Mitogen activated protein kinase pathway

MBD	Methyl-CpG binding domain protein
MBD2	Methyl-CpG binding domain protein 2
MBD4	Methyl-CpG binding domain protein 4
MCAM	CD146, is also known as melanoma cell adhesion molecule
MDA-BF-1	Bone metastasis factor
MEP	Motor exit points
MET	MET proto-oncogene, receptor tyrosine kinase/ hepatocyte growth factor receptor/HGFR
MHC	Major Histocompatibility Complex
miRNAs	MicroRNAs
MPDZ	Multiple PDZ crumbs cell complex polarity complex component
MPNST	Malignant peripheral nerve sheath tumour
MSC	Myelinating Schwann cells
N	Neural
NC	Neural crest
NCC	Neural crest cells
ncRNAs	Non-coding RNAs
NCSC	Neural crest stem cell
ND	Clinically healthy adults with no visible disease/DFTD1
NEDD4	Neural cell precursor expressed, developmentally down-regulated 4, E3 ubiquitin protein ligase
Nf1	Neurofibromatosis 1
NF2	Neurofibromatosis 2, Neurofribromin 2
NKC	Natural killer Complex
NMJ	Neuromuscular junction
NMSC	Non-myelinating Schwann cell
NOD/SCID	Non-obese diabetic/severe combined immunodeficiency

NRDP1	Neuregulin Receptor Degradation Protein -1
NRG	Neuregulin
NRG1/2	Neuregulin 1/2
NSCLC	Non-small cell lung cancer
O	Osteocytes
OEC	Olfactory ensheathing cells
OMLP	Oral mucosa lamina propria
OMSC	Oral mucosa stem cells
PCP	Planar cell polarity pathway
PDL1	Programmed cell death 1 ligand 1
PEComa	Perivascular epithelioid cell tumour
PI3K	Phoshatidylinositide 3-Kinase pathway
PKC	Protein kinase C
PMEL	Premelanosome protein/Pmel17/HMB45/gp100
PNCSC	Palatal neural crest stem cells
PNS	Peripheral nervous system
PTCH1	Patched receptor
RAD	Restriction site associated DNA sequencing
RNF41	Ring Finger 41, E3 Ubiquitin Protein Ligase
rRNA	Ribosomal RNA
RSPO3	R-spondin 3
RTK	Receptor tyrosine kinase
SC	Schwann cell
SCPs	Schwann cell precursors
sERBB3	Secreted ERBB3
siRNAs	Short interfering RNAs

SKPs	Skin derived stem cells
SMO	Smoothened receptor
sncRNAs	Small ncRNAs
SNP	Single nucleotide polymorphism
SRY	Gene found on Y chromosome
STAT3	Signal transducer and activator of transcription 3
STC	Satellite cells
STDP	Save the Tasmanian Devil Program
SUFU	Suppressor of fused receptor
TAA's	Tumour associated antigens
TAP1/2	Transporter 1/2 ATP binding cassette SUB-family B member
TAZ	WW domain containing transcription regulator 1/WWTR1
TCF/LEF	Transcription factor/lymphoid enhancer binding factor
TG	Terminal Glia or Teloglia
TGFα	Transforming growth factor-alpha
Th1	T-helper 1 cells
TIC	Tumour initiating cell
TOR	Mammalian target of rapamycin
TPA	12-O-tetradecanoylphorbol-18-acetate
tRNA	Transfer RNA
TYRP1	Tyrosinase related protein 1
USP8	Ubiquitin Specific Peptidase -8
WNT	Wingless-type MMTV integration site family
WNT/STOP	WNT dependent stabilisation of proteins
x-DFT1	Xenograft DFT1
YAP1	YES associated protein 1

Table of Contents

List of Figures

List of Tables

1.0 Contextual Statement

As a veterinary histologist at Tasmania's Animal Health Laboratory, Department of Primary Industries, Parks, Water and Environment (DPIPWE), I am positioned to respond to any emerging biosecurity risk. It was incomprehensible in 2002 to foresee how sectioning and staining the first of an extraordinary number of Tasmanian devil tumours would influence my professional life as a medical scientist. Tasmanian devil numbers plummeted and the likelihood of losing Tasmania's iconic marsupial to 'Devil Facial Tumour Disease' (DFTD) became clearly evident. Research into the aetiology of the transmissible cancer became paramount. I was a co-author on two initial papers by Richmond Loh et al. (1, 2) describing the immunohistochemistry and pathology of DFTD followed by a broader paper by Stephen Pyecroft et al. (3) integrating the histopathology, cytogenetics and epidemiology of this unusual transmissible tumour. Our immunohistochemical research continued to investigate tissue specific markers that define DFTD and its transmissible nature. I dovetailed my research at the Animal Health Laboratory through graduate research at the University of Tasmania where I secured two research grants offered by 'Save the Tasmanian Devil Program' (STDP), funding crucial to advancing our research findings. During my candidature, I have tested and validated over 150 commercially available anti-human antibodies on Tasmanian devil (marsupial) tissues, unfortunately sequence homology was not always one hundred percent with approximately half failing to recognise marsupial protein sequences.

DFTD is a clonally evolved tumour of Schwann cell origin (4) affecting Tasmanian devils (*Sarcophilus harrisii*) and is transferred by biting. This thesis presents my research as two major chapters. Firstly, a very comprehensive immunohistochemical approach investigating neural crest derived Schwann cell and melanocyte associated markers. These findings are novel and will contribute significantly to the understanding of the pathobiology of this unusual tumour. I have prepared the following manuscript pending submission, presented in chapter 1.

Devil Facial Tumour 1 (DFT1) Immunophenotype Reveals a Progenitor-Like Cell with Schwann cell, Melanocyte and Self-Renewal Characteristics.

In addition to gene and protein expression by DFTD, I wanted my immunohistochemical research findings to be applied in a practical way. I identified ERBB3 as a biomarker that can be utilised in both the early detection of DFTD and the identification of potential therapeutic regimes that could be applied therapeutically to wild Tasmanian devils to eradicate this disfiguring and terminal disease. This article was published in 2017 (chapter 2) ahead of the main body of my research (chapter 1) to expedite modes of DFT1 treatment, prevention and eradication which is a high priority of the STDP.

ERBB3: A potential serum biomarker for early detection and therapeutic target for devil facial tumour 1 (DFT1).

In summary, my research has comprehensively redefined the immunophenotype of DFTD, expressing novel proteins not available in the current literature. I show divergent origins of DFTD, a progenitor like cell with Schwann cell and melanocyte lineages, self-renewal characteristics that contributes to MHC down regulation and therefore enhanced transmissibility. I describe for the first time the histomorphology of the 5 strains of DFTD and extensively immunohistochemically stain these strains to determine any variation present. My findings are drafted for imminent manuscript submission. From my research, I published the first description of the expression of ERBB3 by DFTD and its possible early detection and possible therapeutic approach. I also first reported the expression of ERBB3 in cutaneous lymphoma in Tasmanian devils. It is reassuring

that two subsequent publications, like ourselves, found ERBB3 to be important in DFTD tumourigenesis (5, 6).

As unbelievable as it seems researching a transmissible tumour in Tasmanian devils, it would be inconceivable to think I would be involved in a second transmissible tumour however, this is exactly what has happened. At DPIPWE I was involved in the Histology and immunohistochemistry of this newly described Tasmanian devil tumour. During my candidature I collaborated with fellow Tasmanian devil researchers Ruth Pye et al. (7) and Max Stammnitz et al. (8) through STDP by providing histological and immunohistochemical components of the research defining this second devil facial tumour. Our research findings have therefore renamed the original DFTD as DFT1, with the newly described tumour named DFT2, its intention to avoid confusion in the literature. My contribution to DFT2 is outlined in chapter 3 of my thesis. My future directions are to publish unfinished immunohistochemical work completed during my candidature and continue researching DFT1 and DFT2 by collaboration with Tasmanian devil researchers as well as continue histological and immunohistochemical support at the Animal Health Laboratory, DPIPWE.

Dane Hayes

PhD candidate,
University of Tasmania,
School of Health Sciences,
Launceston.

Medical Scientist, Cytotechnologist CT (ASC),
Animal Health Laboratory
Department of primary Industries, Parks, Water and Environment (DPIPWE)
Launceston.

2.0 Introduction: Tasmanian Devil Facial Tumour Disease (DFTD/DFT1) and the discovery of a second Transmissible Devil Facial Tumour (DFT2)

2.1 The Emergence of Devil Facial Tumour Disease (DFTD)

The Tasmanian devil (*Sarcophilus harrisii*) belongs to the Dasyuridae family, it is a carnivorous marsupial that is extinct on mainland Australia, now found only on the island of Tasmania. Superficial dermal cutaneous lesions of wild Tasmanian devils can be found commonly in the form of skin sores (9) and neoplasia (10). Multiple spontaneous neoplasms in captive Tasmanian devils have been recorded, including squamous cell carcinoma of the lip and gingiva, dermal lymphosarcoma (11), trichoepithelioma, papilloma and keratoacanthoma (12) and a single devil with multiple unrelated tumours involving internal organs in combination with skin (13), suggestive of potential metastasis. Similar observations were made while reviewing Dasyurid archival material at the Australian Registry of Wildlife Health (14) and recently, two captive female devils with pruritus and dermatitis were diagnosed with cutaneous T-cell lymphoma (15). None of the recorded neoplastic superficial lesions found in captive or wild Tasmanian devils appeared to mimic the newly described firm, flattened centrally ulcerated soft tissue lesions of DFTD affected Tasmanian devils (1).

The first evidence of DFTD in wild populations occurred in 1996 when several Tasmanian devils with facial lesions were photographed by Christo Baars in the north east of the state; however, a tissue diagnosis was not obtained until 2001 (16). Review of Tasmanian devil archival slides submitted to the Animal Health Laboratory, DPIPWE, revealed a single case in 1997 that was consistent with DFTD (1, 17) indicating that this tumour had been present in Tasmania for at least 5 years prior to tissue diagnosis. An emerging disease was finally recognised in 2003 (17) because of the prevalence of DFTD during the previous two to three years. The disease had spread from

the north east of the state both south and westward with high mortality rates of up to 90% in some areas leaving very few animals over twelve months old. Thus, a transmissible viral aetiology was suspected such as those induced by cancer-causing retroviruses similar to feline leukaemia virus or Koala retrovirus. Speculation was that a viral agent directly transferred from animal to animal by biting while engaged in fighting results in the tumours, which arise at the site of inoculation, typically affecting the mouth and facial areas. However, extensive testing by the Australian Animal Health Laboratory, CSIRO by cell culture and electron microscopy (unpublished data, DH, Alex Hyatt, AAHL, CSIRO) has not isolated a viral agent (3).

Histologically, the 'facial tumours' consist of round cells with a high nuclear to cytoplasmic ratio but are not limited to the face as the neoplastic lesions metastasise to local draining lymph nodes and bone marrow. The breakthrough report came from Pearse et al. proposing that DFTD is transmitted by allograft, an infectious cell line, transferring cells of friable tumours from devil to devil through biting (18). The karyotype of a normal devil consists of fourteen chromosomes including XX or XY chromosomes however; the Karyotype of DFTD contains only thirteen chromosomes and is grossly abnormal. Both chromosomes two, one chromosome six, both sex chromosomes are missing, deletion of the long arm of chromosome one and four unidentified marker chromosomes are also present. Characterisation was further determined by G-banding by Pearse et al. (18) and has subsequently been reassessed in 2012 by Deakin et al. (19) using chromosome painting highlighting minor chromosome misidentification (see Genomic Investigation of the Tasmanian devil and DFTD below for details).

The interesting fact was that all eleven tumours studied (early, late and metastasis) had exactly the same complex abnormal karyotype, all with no apparent intermediate stages between normal and tumour chromosomes present, suggesting that a single breakpoint was unlikely. Further support for the allograft theory was the absence of both sex chromosomes regardless of

the sex of the affected devils and the discovery of a pericentric inverted chromosome 5 in one devil that was not reflected in its tumour karyotype, being present only in cultures of its normal tissues, a result that was unexpected.

2.3 Initial Pathology and Immunohistochemistry of DFTD

A comprehensive study of the pathology of DFTD by Loh et al. in 2006 (1) revealed tumours tended to be located on the face, lips and oral mucosa. Most tumours were well circumscribed, firm soft tissue masses, flattened and centrally ulcerated and exudative. The cut surface was pale, and visible fibrous septae gave the tumour a multinodular appearance, sometimes the tumours were necrotic centrally. Almost equal numbers of male and female devils with DFTD were examined suggesting neither sex was favoured for transmission and devils with DFTD were greater than two years of age suggesting younger devils perhaps avoid confrontation.

Histopathology revealed all tumours examined were microscopically similar originating in the dermis or submucosa of the oral tissues. The cells were pleomorphic round cells with single nucleus without nucleoli, high nuclear to cytoplasmic ratio, little eosinophilic cytoplasm with often indistinct cell borders forming bundles, cords, packets, palisades, nests or sheets depending on the tumour, forming vascularised nodular aggregates that were minimally infiltrative. Metastasis was apparent in sixty-five percent of cases with regional lymph nodes involved as well as distant organs including lungs, heart, kidney, spleen, mammary, adrenal, pituitary, rib and ovary. Electron microscopy revealed few specialised organelles but occasional ribosome-lamellar complexes, secretory granules, myelin bodies and desmosome like structures were recorded. Together, the comparable histopathology and electron microscopy observations suggest that DFTD is derived from a single cell type.

In addition to the pathology of DFTD above, Loh et al. 2006 also comprehensively described the immunohistochemical features of DFTD by the application of antibodies commonly used to differentiate tumours of unknown origin. These antibodies would detect any differentiating features associated with DFTD in order to classify this very unusual transmissible tumour (2). No immunoreactivity for CD16, CD57 and CD3 was evident indicating that the tumour does not originate from the myeloid/lymphoid lineages and therefore initial histological classification of DFTD being a possible lymphosarcoma would appear unlikely. It was noticed that very few lymphocytes infiltrate the tumour perhaps suggesting support for the allograft theory. No reactivity for Von Willebrand Factor excludes the possibility of an endothelial cell derived tumour. No reactivity to pan-Cytokeratin AE1/AE3 and epithelial membrane antigen (EMA) also excludes epithelial carcinomas. No reactivity to smooth muscle antigen (SMA) and desmin excludes a muscle origin. No reactivity to glial fibrillary acidic protein (GFAP) would exclude glial origins. The immuno-positive staining for S100 protein, vimentin (VIM), Melan-A (MLANA), neuron specific enolase (ENO2), chromogranin A (CHGA) and synaptophysin (SYN) would suggest neural crest derived tumour including sarcoma, melanoma and undifferentiated neuroendocrine tumour. Because DFTD is non-pigmented, an amelanotic melanoma was excluded on the basis that no pre-melanosomes or melanosomes were identified during electron microscopical examination and histochemical staining such as Masson Fontana were also negative. In conclusion, the immunohistochemical expression of neuroendocrine markers CHGA, SYN, ENO2, mesenchymal marker VIM and neural crest marker S100 indicated that DFTD is of neuroectodermal origin.

The next exciting research chapter published by Murchison et al. in 2010 (4) used large scale genetic analysis including microsatellite genotyping, mitochondrial genome analysis and deep sequencing of the DFTD and microRNAs that revealed the clonal transmissible DFTD was of Schwann cell origin. The genetic analysis revealed that nine of twenty genes validated were actually involved in the myelination pathway and the cells responsible for myelination are central

nervous system oligodendrocytes and peripheral nervous system Schwann cells. Myelin surrounds nerve axons providing the necessary insulation for nerve impulse conduction. Key genes identified by transcriptome analysis identified as structural components of myelin included myelin protein zero (MPZ), peripheral myelin protein 22 (PMP22), myelin basic protein (MBP) and specifically the peripheral nervous system myelin protein periaxin (PRX). Protein expression was also documented for PMP22, MPZ, MBP and PRX with immunohistochemical expression confirmed for PMP22, MBP and PRX. PRX was expressed in all DFTD samples and therefore it was proposed that PRX be used as a marker for DFTD. Additionally several genes involved in transcription of myelination were also identified such as SRY-box 2 (SOX2), SRY-box 10 (SOX10), c-JUN (JUN) and POU Class 3 Homebox 1 (POU3F1) and neural crest markers nerve growth factor (NGFR) and intermediate filament nestin (NES). This research reinforces previous research that DFTD is of neural crest origin but provides the genetic and expressional evidence that the Schwann cell is likely to be the origin of DFTDs. The significance of neuroendocrine markers expression is yet to be elucidated and I will discuss this further in chapter one of this thesis.

A paper by Tovar et al. in 2012 stemming from Murchison et al. 2010 further examines Schwann cell and neural crest markers and demonstrates once again the positive immunohistochemical staining of PRX, PMP22, MBP, NGFR, NES and S100. This study showed reduced EN02 and no CHGA staining which is in contrast to the original studies by Loh et al. (2); however, the antibodies used in this research were different. For example, the ENO2 used by Tovar et al (20) was a different mouse clone and CHGA was a mouse monoclonal, whereas Loh et al. (2) employed a rabbit polyclonal. I have also noticed that monoclonal CHGA and SYN do not stain DFTD however; the converse applies when using polyclonal antibodies thus indicating that different antigens are targeted, specific sequences in the case of the monoclonal and a variety of antigens for the polyclonal (DH, unpublished observation). It was noted on immunohistochemistry that MBP had cross reactivity with epithelium and connective tissue, which may indicate that the monoclonal

antibody used may be less specific as only two out of twenty samples showed immuno-reactivity. I further examine MBP in detail in chapter one of my thesis to further determine this myelin structural protein. This research demonstrates overwhelming evidence that PRX is an excellent diagnostic marker for DFTD and this has proven to be the case over the ensuing years as I employ PRX as a diagnostic marker in the routine laboratory (DH, personal observation).

2.4 Investigation of the Immune system of the Tasmanian devil

The Tasmanian devils immune system has come under considerable investigation in attempt to ascertain possible deficiencies that would allow transmission of an allograft. Very few CD3 positive T-cell lymphocytes are seen infiltrating the tumour (2) thus, immune surveillance failure must be considered contributory to tumour dispersal. Early examination of Tasmanian devil immune system by Woods et al. (21) and Kreiss et al. (22, 23) demonstrated similar characteristic as placental mammals with an expected range of white blood cells including neutrophils, lymphocytes, monocytes, basophils and eosinophils present in peripheral blood smears. Thymic tissues was found in juveniles and subadults, splenic architecture displayed typical red and white pulp with B-cells located in the white pulp and T-cells located near arterioles. Lymph nodes also displayed a typical arrangement of B-cell follicles located in the cortex and T-cell areas in the paracortex. B-cell areas appeared activated and there were numerous plasma cells noted in the spleen and lymph nodes of devils with DFTD. When the immune system was challenged with T-cell mitogens such as phytohemagglutanin and concanavalin-A and T- and B-cell mitogen pokeweed mitogen, all induced lymphocyte proliferation but there is a diversity of responses among the devils tested. The subcutaneous injection of horse red blood cells into male and female Tasmanian devils produced a strong antibody response demonstrating an appropriate humoral response. The observed phagocytosis of bacteria by neutrophils showed the innate immune system is functional.

These experiments demonstrate that the Tasmanian devil is certainly capable of stimulating lymphocyte proliferation and therefore infer that the Tasmanian devil's immune system is completely competent. Interestingly, when mixed lymphocyte reactions were performed measuring the allogenic T-cell response, no proliferation of lymphocytes occurred raising the possibility that lack of diversity at the major histocompatibility complex (MHC) may contribute to the allograft not being recognised as 'non-self' by the host's immune system.

Kreiss et al. (24) immunohistochemically examined Tasmanian devil lymph nodes employing CD3 (T-cell), CD79b (B-cell) and HLA-DR (MHC-II antigen presenting cells – dendritic, macrophage, lymphocytes -B-cell, activated T-cell) to reveal the outer cortex rich in lymphoid follicles containing CD79b (mantle zone) and HLA-DR (germinal centre) positive cells whereas, CD3 positive cells were located within the inner cortex. The architecture and specific cell identity reported here further support that the Tasmanian devil immune system has the necessary components of an adaptive immune system and adequate response. Kreiss et al. (25) demonstrated that despite little or no MHC-I and -II mismatches, all five allograft skin grafts were rejected, most within as little as fourteen days. A mixed lymphocyte reaction was performed again employing devils from the skin graft experiment. These devils were from different geographical locations with some proliferation occurring, noticeably between eastern and western Tasmanian devils, indicating some allelic differences between them. Evaluation of cytotoxicity responses was performed by Brown et al. (26) finding that Tasmanian devils elicited either very little cytotoxic response or none at all to the injection of irradiated DFTD cells with montanide adjuvant whereas injected human K562 cells (erythroleukaemia) did develop a cytotoxic response. Antibody dependent cell-mediated cytotoxicity occurred within four hours, less time than is needed than cytotoxic T-cell response of at least 18 hours, upon exclusion of monocytes, neutrophils and T-cells would indicate the presence of Natural Killer cells are the likely effector cells responding to the xenogenic tumour

cells. Natural killer receptors (natural killer complex - NKC and leukocyte receptor complex - LRC) have been identified in the genome of the Tasmanian devil (27), with six assumed NKC genes located on chromosome five and forty-three open reading frame LRCs located on chromosome three.

Howson et al. (28) further classifies subpopulations of T-cell (CD4 and CD8) and B-cells (IgG and IgM) by the production of specific Tasmanian devil monoclonal antibodies against CD4, CD8, IgG and IgM. Dendritic cells are also identified by antibodies MHC-II, CD1a and CD83, in addition to classic antibodies CD3, CD79b and MHC-II. Immunohistochemical expression of these markers showed no B-cell markers within DFTD; however, CD3, CD4 and CD8 were present in all tumour samples with CD8 easily identified in the stroma, although CD4 was not always present. Intratumourally all eight samples stained for CD3 and CD8 but only three stained for CD4. Within and surrounding DFTD, MHC-II stained antigen presenting cells (presumed macrophages) and dendritic cells staining with CD1a were observed surrounding the tumour but not within the tumour. However, no CD83 positivity for activated dendritic cells was seen. The surprising finding was that the majority of T-cells within the tumour were CD8 and not CD4 as expected.

Why is it that Tasmanian devils less than one year of age do not succumb to DFTD? An explanation was offered by Cheng et al. (29) who found that as devils develop and reach puberty (sub adults) there is a noticeable alteration in immune system. Abundance of lymphocytes decreased at puberty for both male and female devils thus an increased neutrophil-lymphocyte ratio occurs negatively affecting the balance between innate and adaptive immunity. Additionally a lower interferon (IFN)-γ-interleukin 4 (IL4) ratio occurs where the IFN-γ/T-helper 1 (Th1) cells, such as cytotoxic and NK T-cells are inhibited by IL4 forcing differentiation of T-cells toward Th2 cells, or a humoral response. A murine xenograft model for DFT1 reported by Kreiss (30) showed conclusively that tumours grown in laboratory mice mimicked transmissible DFT1. Inoculation of

DFT1 Cell cultures into 17 non-obese diabetic/severe combined immunodeficiency (NOD/SCID) mice resulted in all mice developing tumours (x-DFT1). In addition, 7 NOD/SCID mice were inoculated with viable cultures from x-DFT1, a second passage, with all mice once again producing tumours. This suggests self-renewal characteristics and I discuss this in depth in chapter 1 of my thesis. All x-DFT1 tumours appeared histologically identical to the original DFT1 and the x-DFT1 karyotype was essentially similar to the pseudodiploid clone although an increase in the near triploid clone was observed. Neither immune competent BALB/c mice nor non-viable freeze/thaw tumour cells produced tumours and the tumours were all PRX positive.

2.5 Experimental immunisation procedures and immunotherapy

Kreiss et al. (31) showed evidence of humoral and cytotoxic immune responses when Tasmanian devils were immunised by killed DFTD cells. Two devils were immunised with DFTD strain two inactivated by freeze/thaw containing montanide adjuvant, two devils were immunised with DFTD strain three inactivated by sonication containing montanide and CpG 1668 adjuvant and four devils were immunised with DFTD strain 3 cells inactivated by irradiation containing montanide and CpG 1668 or CpG 1585 adjuvant. One devil that received freeze/thaw cells did produce antibodies, both devils that received sonicated cells produced antibodies and cytotoxic responses and all four devils receiving irradiated cells developed cytotoxic responses with three of those devils producing antibodies. Previous irradiated DFTD cells that were used to immunise devils did not produce antibodies or cytotoxic responses (26) may be explained perhaps by genetic diversity among Tasmanian devils however, this research uses CpG adjuvant which acts via Toll like receptor nine (TLR9) activating innate immune cells circumventing immune ignorance. Two of the above eight Tasmanian devils were challenged with live DFTD strain 3 cells; those that received

freeze/thaw containing montanide adjuvant, one devil produced tumour, but the second devil only produced tumour (strain 3) when challenged a second time. Interestingly, this particular devil also had an antibody response and thus may provide evidence that immunisation did provide some protection. Because these devils developed tumours, it was deemed unethical to challenge the other six devils. Evidence of immune recognition occurring in wild Tasmanian devils had been disappointing until a large survey conducted by Pye et al. (32) showed a limited, but positive response. This research encompassed fifty-two wild Tasmanian devils; serum was collected over a 7-year period with forty-five of those devils comprising multiple collections. The sera was tested for IgG antibodies to DFTD MHC-I negative cells, and DFTD MHC-I positive cells interferon γ (IFN-γ) exposed which can also be stained for β_2 microglobulin (B2M), a component of the MHC I molecule. Of the 52 wild Tasmanian devils, forty six did not produce detectable IgG antibodies to DFTD regardless of MHC-I status, however the remaining six devils had detectable levels of IgG against MHC I DFTD positive cells, but not MHC-I DFTD negative cells. These six devils were DFTD free when initially sampled but developed DFTD during the study therefore, anti-DFTD antibodies were detected as clinical signs progressed. Remarkably four of the six devils actually exhibited tumour regression. Previously it has been shown experimentally that captive Tasmanian devils immunised with killed DFTD cells can elicit an immune response (31) but this study demonstrates that naturally occurring immunity also occurs in a small number of individuals. The potential for wild Tasmanian devils to be immunised against DFTD was approached comprehensively by Tovar et al. (33) who experimented with four different immunisation and booster protocols that included heat treated, freeze/thawed, sonicated and irradiated DFTD cells. Protocols that involved treatment of these DFTD cells with a number of molecules including IFN-γ, Trichostatin A, TD2-Ga (histone deacetylase inhibitor) or TD3-Ty (upregulates MHC-I). Vaccines also utilised a number of adjuvants including ISCOMATRIX™, PolyIC and CpG. Devils immunised with sonicated and IFN-γ treated DFTD cells together with multiple adjuvants ISCOMATRIX™, PolyIC and CpG appeared to

produce IgG antibodies to both DFTD MHC-I positive and DFTD MHC-I negative cells. One devil failed to produce DFTD and two other devils exhibited delayed onset of DFTD, suggesting some immune protection against DFTD occurs. Pye et al. (34) are currently monitoring two different vaccination strategy trials involving the wild release of vaccinated Tasmanian devils at two sites: a northern location at Narawntapu National Park and the northeastern location of Stoney Head. Narawntapu National Park released devils vaccine consisted of sonicated and irradiated DFTD MHC-I positive cells with adjuvants ISCOMATRIX™, PolyIC and CpG as outlined above (33). Stony Head released devils vaccine consisted of sonicated and irradiated DFTD MHC-I positive cells with adjuvants ISCOMATRIX™, PolyICLC (Histonol®) and imiquimod. This protocol change was implemented following experimentation (35) finding these adjuvants induced a more rapid antibody response that was sustained longer and was also able to shorten this vaccine protocol which is quite practical when confronted with wild animal recapture. At the conclusion of both trials, seventeen of nineteen Narawntapu and all thirty-three Stoney Head devils had seroconverted following immunisation of DFTD. Five months after the primary course the Stoney Head devils had higher overall antibody levels than the Narawntapu devils despite receiving only two immunisations compared to up to four immunisations received by the Narawntapu devils. This trial is ongoing and we eagerly await the degree of success that immunisation against DFTD offers.

2.6 Major Histocompatibility Complex in the Tasmanian devil

The first characterisation of Tasmanian devil MHC genes was reported by Siddle et al. (36), describing six unique class II β-chain sequences from at least three loci (marsupial class II DA family), thirteen unique class I sequences from at least seven loci. MHC consists of multiple genes

encoding for molecules that recognise foreign antigens and evoke adaptive immunity through interaction with T-cells, providing resistance and recognising self from non-self. MHC contains class I molecules consisting of two chains; α- and β_2 microglobulin and Class II molecules also consist of two chains, α- and β-. Siddle et al. (37) found that DFTD cells expressed both MHC class I and class II genes, but because the class I sequences show little variation it was suggested that transmission of DFTD without recognition by the immune system may be a result of low MHC diversity. Additionally, MHC class II, usually expressed by haematopoietic cells such as macrophages and monocytes, was also expressed by DFTD. Comprehensive screening of MHC class I α1 by Siddle et al. (38) revealed twenty five different MHC types (types A-V and type 1) with some differences noted between the eastern and western populations of Tasmanian devils where ten of the twenty five types were found only in western devils. Class I sequences can be divided into group I and group II where eighty percent of the range of devils contained both, as did DFTD cells leaving twenty percent of individuals that had a restricted MHC range. The difference in individual sequence variants (0-6 group I, 0-4 group II) was found to be allelic copy number variation, thus the MHC diversity is low in Tasmanian devils. Subsequent testing using MHC linked microsatellite markers found that there was no variation in copy number of alleles (39, 40). It was also suggested that a genetic sweep might have occurred affecting class I genes resulting in similarity in allelic content and gene copy number of eastern devils. Importantly, most Tasmanian devils studied had MHC types similar to those of DFTD although some do not. It is these restricted MHC types that could potentially offer immune response to DFTD. A comprehensive study of MHC class II genes by Cheng et al. (41) also revealed that genetic diversity is low. Marsupials typically have two classical MHC class II gene families designated as DA; a single α chain gene – *Saha-DAA* and three DA β chain genes *Saha-DAB1, 2 and 3*) and DB which so far has only revealed a pseudogene *DBB*. In the Tasmanian devil population studied (60), the DA-α chain is invariable and the β chain genes show restricted polymorphism. It would appear that Tasmanian devil has only a

functional MHC class II DA family whereas the DB genes are likely to be lost in its genome. This study illustrates low diversity of MHC class II, likely attributed to genetic drift on the island as well as founder effects after population bottlenecks. The above studies by Siddle et al. and Cheng et al. together show reduced MHC I and II diversity in Tasmanian devils. Using bacterial artificial chromosome (BAC) libraries Cheng at al. (42) describes further MHC class I and class II regions of the Tasmania devil based on BAC contigs. A total of five class I genes were identified and named *Saha-UA, UB, UC, UD* and *UK* and a total of four class II genes all belonging to the DA gene family; *Saha DAA*, *Saha-DAB1, DAB2* and *DAB3*. A deletion was found in *Saha-UA* and was found to be present in fifty four percent of tested northwest devils but none in the south, and variation with east and central Tasmanian populations. Recent investigations by Siddle et al. (43) has shown that surface MHC class I are not expressed on the surface of DFTD cells due to down regulation of genes such as B2M, TAP1, TAP2 (Transporter 1 or 2, ATP binding cassette SUB-family B member) and MHC class II DM beta, (DMB) associated with this pathway. Production of two devil specific antibodies; a monoclonal antibody against class I heavy chain employed in western blot analysis and polyclonal antibody against B2M employed Immunohistochemically, enables cellular expression of MHC class I. Very little class I was detected on western blots and no B2M was detected on DFTD cell culture cells. If DFTD cells were treated with Trichostatin A or recombinant devil IFN-γ down regulated B2M, TAP1, TAP2 were also shown to be restored suggesting that these genes are structurally sound and gene suppression is related to acetylation state of histones. As this down regulation is reversible, this has practical applications in vaccine development.

2.7 Genomic Investigation of the Tasmanian devil and DFTD

Whole genome analysis by Miller et al. (44) was performed on two four-year-old Tasmanian devils (one female, one male) and their DFTDs from northern and southern Tasmanian geographic locations. The genome was found to be 3.3 gigabase pairs. Their analysis revealed that their tumours were not from the host however, it was estimated that the tumours may contain thirty percent of nuclear DNA and fifteen percent of mitochondrial DNA could be from the host devil. Because DFTD is transmissible then the diploid genome of both the original and present host and tumour as well somatic mutations of the tumour have to be taken into account when analysing DFTD. Murchison et al. (45) assembled the genome of a female Tasmanian devil using Phusion2 pipeline, estimated at 2.89 and 3.17 gigabase pairs using both sequencing and flow cytometry. Chromosome homology of the Tasmanian devil was compared to that of the opossum and genes were identified using Ensembl genome annotation pipeline. As previously reported neither sex chromosomes are identifiable in the DFTD karyotype, therefore the gender of the founder devil is unknown. Murchison et al. searched for the Y chromosome (*SRY* gene) which was amplified in a male devil but not in the female as expected; however, this is not amplified in DFTD. The X chromosome was searched for using reverse chromosome painting experiments and copy number analysis and it was determined that there were approximately two copies present, likely to be homologous pairs rather than recent duplicates. This suggests that the original DFTD founder devil was a female. It was also found that geographically distant DFTD subclones are acquiring new variations in karyotype, DNA sequences and genomic copy number indicating ongoing somatic change but despite this, DFTD is a relatively stable lineage and the transmissible cancer is most likely not due to genomic instability. Demonstration of evolutionary changes in DFTD by Pearse et al. (46) documents at least four novel chromosomal variants (strains), from two hundred and sixty nine diseased devils at different sites around Tasmania, from 2004-2011. Strain one is the simplest

karyotype, the original karyotype reported by Pearse et al. (18) in 2004 from Bronte Park. Strain two was first observed in 2005 and within its karyotype is a fifth marker which appears to be a duplication of the p-arm of marker one. Strain three was detected in 2005 and found exclusively on Forestier Peninsula in southeast Tasmania. A variant of strain three was recorded containing an interstitial inversion in the q-arm of the non-deleted chromosome three. Strain four was recorded in 2006 but only found in five devils from Freycinet Peninsula and is similar to strain two but has additional chromosome rearrangements including; interstitial deletion of the p-arm of chromosome five, translocation involving chromosome six and of marker two and variable number of double minute chromosomes (DM).

Karyotype examination of DFTD samples from between 1996 (disease emergence) prior to testing in 2004 were not available. No intermediate karyotype between the normal devil and strain one has been detected. It is possible that strain two was the original transmissible tumour type whereby strain one is derived from strain two with the loss of marker five or, strain two could have derived from strain one by a single chromosomal rearrangement by duplication of the short arm of marker one. Examination of karyotypes revealed both diploid and tetraploid cells of strain one since 2004 but in 2006, animals with only tetraploid strains one and two have been identified. Low frequency strain four may represent a more aggressive strain because it is fast growing in vitro and the presence of DM indicated instability, thus host death would occur more rapidly reducing transmission rates. Pearse et al. (46) noticed that more complex chromosomal rearrangements do occur in advanced primary tumours and metastasis alongside the four strains described. These rearrangements have not been seen in any two devils from the same population and therefore it is unlikely that these evolved tumours are transmissible.

Deakin et al. (19) combined chromosome painting and gene mapping (BAC clones) to determine the complex chromosomal rearrangements of 105 genes, including three strains of DFTD. This

analysis identified chromosome mismatches when comparing the previously reported karyotype by Pearce et al. (18). The Deakin et al. karyotype shows both chromosome one are absent and both chromosome two are present, both chromosome six and one chromosome five are present (Originally, the Pearse et al. karyotype had both chromosome twos missing, both chromosome ones present and chromosome fives were present with one chromosome six absent). Additionally, Deakin et al. found that the p-arm of one homologue of chromosome two contained translocated regions from chromosome one and the X chromosome and one of homologue of chromosome six had a translocated region from the X chromosome. Comparison of Tasmanian devil, opossum and wallaby show there is considerable rearrangement within some gene blocks by multiple inversions with the most conserved among marsupials being the long arm of chromosome three. This makes construction of a virtual map difficult and more genes would be required but sufficient to predict the gene content of each chromosome. The DFTD karyotype is remarkably stable in-vivo with only minor cytogenetic strain differences, stability after multiple passages with no progressive chromosomal rearrangements detected in-vitro is also apparent. Tumour evolution, as represented by strains one to three in this study, can be identified by G-banding but chromosome painting allows much more precise characterisation. Chromosome painting of DFTD strain one revealed that the marker chromosome M1 was predominantly made up of chromosome one and a small portion of the X chromosome. M2 was predominantly chromosome five and a small proportion of chromosome one and X chromosome. M3 was predominantly chromosome one and a small proportion of X chromosome and finally M4 consisted entirely of chromosome five. Gene mapping revealed only subtle differences between strains such as the presence of M5 containing one gene from chromosome one and one from the X chromosome present in strains two and three. The list of all the genes that were identified in relation to the strains is beyond the scope of this review but is available in detail (19). It is noteworthy that my research in chapter two of my thesis does assess over 40 genes and their expression in each of the strains of DFTD, contributing

additional information on gene expression in DFTD strains. In conclusion, this research maps chromosome restructuring and gene rearrangements comprising DFTD and suggest that the founder devil was female. It is also suggested by Deakin et al. (19) that the original tumourigenesis was triggered by chromothripsis, a shattering of the chromosomes, and in the case of DFTD restructuring has elicited a stable, transmissible, clonal tumour.

Taylor et al. (5) employed the BAC library and fluorescent in situ hybridisation (FISH) to map candidate genes commonly associated with peripheral nerve sheath tumours and cancers in general. Current data was overlayed with previous mapping to provide a visual comprehensive gene mapping of chromosome one showing the relocation of genes to markers M1, M2 and M3. Two genes associated with Schwann cell tumours are epithelial growth factor receptor (EGFR, or ERBB1) and insulin like growth factor binding protein 1 (IGFBP1), which are located on devil chromosome 1 but located on DFTD markers M1q and M3q are involved in driving of tumourigenesis. Genes of interest associated with malignancy that were not located on chromosome one was *ERBB3* (also from the epithelial growth factor family/HER3) and *TP53*, a tumour suppressor. ERBB3, normally located on chromosome five, is located differently in DFTD appearing on 4p with a copy gain located on marker chromosome M4q. My research had previously identified ERBB3 at an expression level as well as detecting it in the serum of devils, thus promoted ERBB3 as both an early biomarker of DFTD as well as a possible therapeutic target (47). This is covered in detail in chapter two of my thesis. TP53 is located on devil chromosome four and for the most part remained unchanged in DFTD but one sample did show an increased copy number with translocation to DFTD markers M1p and M5p. This gene is important in regulating cell cycle and preventing genomic mutations. TP53 along with IGF2R (insulin like growth factor receptor two) and nerve growth factor (NGF) both located on chromosome four were also

highlighted as potential gene candidates and these genes are discussed in more detail in chapter one of my thesis.

It is well established that DFTD is a clonal tumour being transmitted from one host to the next, exposing the tumour to different genetic backgrounds and tumour microenvironments therefore, the role of epigenetics was explored by Ujvari et al. (48). Epigenetic processes are heritable changes not caused by DNA sequence changes but involve DNA methylation, the addition of a methyl group to cytosine at the five-carbon position, essential to gene expression. This research investigated the DNA methyltranferases (DNMT) responsible for methylation and Methyl-CpG binding domain (MBD) proteins responsible for demethylation to ascertain DNA methylation regulation. DFTD had a higher number of methylation sites (amplified fragment length polymorphism sites) when compared to non-peripheral nervous tissue (liver, heart, kidney, brain) but a similar number of methylation sites when compared to peripheral nervous tissue (sciatic nerve). The mean number of hemimethylated sites were significantly higher in DFTD samples when compared to sciatic nerve and other tissues. These results suggest that DFTD has active demethylation occurring, possibly through increased *MBD2* and *MBD4* genes, thus despite being genetically stable DFTD is evolving through epigenetic modifications, although no significant differences were seen between DFTD strains. Ingles et al. (49) employed immunoflourescent staining using 5-methylcytosine antibody to assess methylation status of chromosomes. All DFTD chromosomes, including rearranged marker chromosomes displayed strong telomeric methylation but little interstitial. What was interesting was that the rearranged chromosomes had restored telomeric methylation despite their initial loss. Ingles et al. documented in detail the immunofluorescent characteristics of the DFTD chromosomes, for example, the short arm of M1 was hypermethylated, M4 was the most hypermethylated being on both telomeric ends and M5, present on all strains except strain 1, was intensely hypermethylated particularly the short arm. In

conclusion, no changes in DNA methylation was observed in DFTD over time with the fluorescent method used, contrary to Ujvari (48) but this could be attributed to hemimethylated sites rather than fully methylated or the semiquantitative immunofluorescent method used by Ingles et al.

In addition to epigenetic responses of DFTD, Ujvari (50) also provides evidence that an anthropogenic selection has occurred at Forestier Peninsula, a selective sweep in fact. It has been suggested that the active removal of diseased individuals at this site increases DFTD response and evolution with increased tetraploid tumours, thus selection of a slower growing tumour.

Ujvari et al. (51) found that DFTD has short telomeres and the copy number has increased over time in the tumour but no difference has been noted between geographical locations or strains. Telomerase is greatly upregulated in DFTD and this prevents cells entering replicative senescence with telomere elongation kept in check by the shelterin complex, perhaps offering genetic stability and increased proliferation. The characteristic short telomeres of DFTD were also reported by Bender et al. (52), who also found telomere dimorphism was not present in DFTD tumour cells.

Genetic assessment of 433 tissue samples from devils within the northwest and western Tasmanian region was performed between 2000-2006, while taking founder devils into the captive breeding program, over an area of approximately 250,000 km^2 area. Storfer et al. (53) used microsatellite analysis finding that genetic structure was present and populations appeared to consist of two or three clusters within the study area south, northeast and northwest. Another study using ten microsatellite loci to investigate genetic diversity in areas affected by DFTD compared to those areas not affected during 1999 and 2006-2007 was analysed by Bruniche-Olsen et al. (54). Results indicated that since the onset of DFTD no decline in diversity was evident, perhaps due to the short duration of population decline or because of low variability in the microsatellite loci there is insufficient statistical power to detect short-term loss of genetic

diversity. There was stable genetic structuring in geographic locations and DFTD mediated changes in gene flow following DFTD spread.

Ensuring that the Tasmanian devil insurance populations are genetically as diverse as possible is difficult when employing microsatellite markers because distinguishing closely related individuals is difficult. Wright et al. (55) has used single nucleotide polymorphisms (SNPs) which has benefits over other genotyping methods because it is better able to assess familial relationships among devils, particularly offspring. This enables an accurate pedigree, breeding recommendations, continued monitoring of genetic diversity of Tasmanian devils, the reduction of inbreeding and increased success when insurance population devils are reintroduced back into the wild. Morris et al. (56) employed SNPs to examine 167 genes immune related genes including interferon, chemokine, cytokine and natural killer T-cell receptor families. Their findings were that genetic diversity at functional loci is seriously low however, some diversity remains such as MHC, which is crucial to disease resistance. Hendricks et al. (57) employed restriction site associated DNA sequencing (RAD) to identify and genotype SNPs from thirty-eight geographic locations around Tasmania. They found limited genetic diversity, largely agreeing with previous data above, grouping north-western populations and central plateau and east coast populations as the two major clusters. It was noted that there were also sites intermediate to the two clusters above, those being central-west and Macquarie Harbour (Macquarie Heads) also previously identified by Brunichen et al. (58) as well as broad scale geographic structure within the two major regions. This methodology makes available data for future management of insurance populations whereby individuals from the intermediate zones, central-west and Central Plateau can be considered alongside the western and northern central coast individuals currently selected in the insurance population.

2.8 Tasmanian devil populations: Impact and insurance population strategies

In 2006, a decade after the first description of tumours characteristic of DFTD, Hawkins et al. (16) reported that approximately fifty one percent of Tasmania had been infiltrated with histologically confirmed DFTD from forty one geographic sites. The numbers of devils affected at each site varied with up to eighty three percent of trapped adults affected and in addition, spotlight sightings also declined simultaneously by eighty percent, indicating population decline. It was reported by Lachish et al. (59) that an increase in DFTD affected subadults (1-2 year's old) was occurring which will have an adverse effect on the number of devils reaching adulthood (>2 year's old). The mark-recapture trapping program found wild populations of the Tasmanian devil have been significantly reduced in Tasmania where the possibility of extinction either locally within 10-15 years or completely within 25-35 years (60) was predicted at the time.

The disease has impacted on the life history of the Tasmanian devil. Normally, the marsupial will begin seasonal breeding at age two having annual litters until age five and death at age six. Jones et al. (61) found in disease ravished populations, females were only able to survive one breeding season and may not survive to rear the litter and that precocial breeding in one-year olds was on the increase. This documents that wild populations of Tasmanian devils were adapting to the disease impacts by early reproduction however, what genetic effects or resistance it has on the population remains to be seen. In 2009 McCallum et al. (62) found that disease levels were persistently high at fifty percent in two to three year old devils despite population density declined up to ninety percent in these areas. This data is inconsistent with density dependent transmission of DFTD, rather transmission is independent of density but dependent on frequency reaffirming that extinction of this iconic marsupial is a real possibility. One particular site monitored by Hamede et al. (63) at West Pencil Pine found that when compared to other devil populations (Freycinet, Fentonbury, and Forestier) the West Pencil Pines population continued to have a range

of ages (> 3 year olds) and a contrasting less than twenty percent of one to two year old breeding females. Hamede et al. (63) reported that DFTD was tetraploid in this area and that these tumours may be less proliferative or perhaps this population engage in aggressive biting behaviour less often. Further to this Hamede et al. (64) found that at West Pencil Pine devils with fewer bites were more likely to develop DFTD suggesting dominant devils may be inoculated by biting affected subordinate devils with DFTD. Further to this, Wells et al. (65) found that those devils with the greatest reproductive value, often the socially dominant devils, are most affected by DFTD when compared to non-infected individuals. This finding would suggest that infection of DFTD selectively removes the fittest devils from the population and this would have long term implications to both genetic diversity and social structure of surviving Tasmanian devils. As reported above, West Pencil Pine had reduced prevalence of DFTD during the first five years of the disease outbreak with a tetraploid strain predominating. Hamede et al. (66) reported increased disease prevalence rates at his site when the tetraploid lineage was replaced with a diploid lineage where causative mechanisms include spread from adjacent populations, virulence of tumour ploidy, transmission rates and genetic differences. As of 2017 Lazenby et al. (67) reported that the disease now covers eighty percent of Tasmania, a thirty percent increase since reported in 2006 by Hawkins et al. (16), with a similar degree of decline in spotlight sightings (eighty three percent) and population densities (seventy seven percent) in affected locations. Fentonbury was the only location where a slight population increase was recorded and investigations here are ongoing. Recently Grueber et al. (68) reported in a landscape level analysis of field data publications, that indeed devils were significantly younger in DFTD affected sites. The females in these sites were also more likely to demonstrate evidence of breeding than those devils in sites unaffected by DFTD, where this could not be attributed to body condition or age difference. In a spatially explicit metapopulation model study, Siska et al. (69) predicted that the long term persistence of both DFTD and its host, the Tasmanian devil, but the population size would be approximately nine percent of the original

healthy population size that was previously enjoyed in Tasmania prior to the emergence of DFTD. This study highlights that this considerable reduction in population density has already altered the usual age structure of wild Tasmanian devils. Compounded by loss of genetic diversity in an environment where loss of habitat and road kill are continuing pressures, further endeavours in conservation of this iconic species are required. The timeframe of the pre-clinical stage of DFTD remains largely undetermined with observations ranging from 2-13 months (16, 32, 62, 64, 70) but as little as 1 month has been recorded (DH, manuscript in preparation, laboratory records DPIPWE). In a quest to discover a pre-clinical marker for DFTD, Hayes et al. (47) identified ERBB3 as the first potential serum biomarker for DFTD. My research found that serum ERBB3 was elevated in devils with advanced DFTD when compared to healthy non-infected devils and therefore the possibility to use ERBB3 as a screening method is proposed. ERBB3 is now recognised as a therapeutic target and therefore the potential exists to consider modes of administration in addition to existing whole cell vaccination such as ERBB3 monoclonal antibody, peptide or xenogeneic vaccines including checkpoint inhibitors. A combinatorial immunotherapeutic approach will enhance cytotoxic destruction, provide long-term immunity from DFT1 and therefore eradicate this transmissible tumour from the wild. Additionally, elevated serum ERBB3 levels was also detected in Tasmanian devils with cutaneous lymphoma (15), a T-cell lymphoma affecting older devils whose appearance is not confused with DFTD. In depth analysis of ERBB3 as an early serum biomarker, immunohistochemical expression and therapeutic applications are discussed in chapter two of my thesis.

In an attempt to suppress the spread of DFTD, selective culling of DFTD affected devils was performed at Forestier Peninsula during extensive trapping (four hundred and forty eight devils) and recording expeditions 2004-2008. A control population at Freycinet Peninsula (six hundred and thirty three devils), was exposed to the same rigorous trapping regime as Forestier Peninsula but devils with DFTD were not removed from the population. Lachish et al. (71) compared the two

populations finding that selective culling was ineffective and did not slow the rate of disease progression or reduced the population-level impacts, put simply, the trial really only culled those individuals that would die of the disease naturally in the wild. Population modelling by Beeton et al. (72) also came to the same conclusion as Lachish et al. (71) that managing DFTD through selective culling did not appear to be a practicable approach to managing DFTD in the wild. Two studies used chemotherapeutic approaches to establish possible treatment modalities employed vincristine (73) and doxorubicin and carboplatin (74) trials none of which DFTD responded to, therefore chemotherapy would not be an effective form of treatment for wild Tasmanian devils.

Given the precipitous population decline in wild Tasmanian devils and dire forecast of 2007, strategies to retain wild populations of devils began in earnest. Jones et al. (75) in 2007 suggested the establishment of an 'ark' or 'insurance' population, consisting of both captive and wild-living populations isolated from DFTD as a priority for the conservation management of the Tasmanian devil. Possible methods of maintaining a disease free insurance population include zoos, wildlife parks, fostering orphaned young from diseased mothers, fenced in enclosures and free ranging island populations. Modelling wildlife disease has its challenges when compared to human or livestock disease situations, no one strategy appears superior to the other, modelling may therefore need a number of different approaches (76). The main focus of the initiation of insurance populations in 2006 was simply to save the Tasmanian devil from extinction with local and national wildlife parks, free-range enclosures and Maria Island. Hogg et al. (77) reports that the success of this breeding program has realised its goal by reaching a carrying capacity of 600 devils retaining ninety nine percent of founding gene diversity. Hogg et al. also highlights that there was no influence on pairing success in regards to zoo or wild-born origins but wild-born females produced more joeys per female and downward trend in the number of joeys from captive females between respective generations in captivity. This has modified intake of founder

devils for insurance populations because of the better understanding of genetic providence and birth origin, for example accepting orphaned female devils (77). A recent report by Rogers et al. (78) followed up on twenty eight captive raised devils (nineteen from intensive captive management and nine from free range enclosures [twenty two hectares]) found ninety six percent of the devils had survived the first year following release onto Maria Island. The research also found that irrespective of captive management, the devils gained weight and intensive captive management does not diminish their instinctive behaviour of scavenging and hunting, showing captive bred devils, regardless of management, can be released successfully onto offshore islands as a viable conservation strategy. A second study of fourteen of the translocated devils to Maria Island by Thalman et al. (79) concurred with the above report by Rogers et al. (78). They were able to show that the devils frequented agricultural and urban habitats avoiding wet eucalypt forests. One devil died not from malnutrition but misadventure such as fighting or collapse of a wombat burrow where the body was recovered. Pedigree modelling on the Maria Island population by McLennan et al. (80) predicted genetic diversity of ninety-five percent for another two years and would drop to seventy seven percent after forty years. If however ten new founder female devils were introduced every three years this would preserve the ninety-five percent gene diversity until 2056. Forestier Peninsula has been subject to removal of DFTD since 2012 and declared disease free towards the end of 2015 whereupon a devil proof fence was erected across the 800m isthmus connecting the peninsula to mainland Tasmania. Here thirty five captive bred adult devils free of DFTD were reintroduced to Forestier Peninsula in November 2015 and ten captive bred juveniles were reintroduced in February of 2016 forming part of the Tasmanian devil insurance population (81). While captive breeding is crucial to survival of the Tasmanian devil, Grueber et al. (82) noted that nineteen of the fifty devils included in their study of reintroduced captive bred devils into Forestier Peninsula and Narawntapu National Park, were victims of vehicular road kill suggesting captive bred devils may be naïve to such post-release risks.

Together, there is a strong collaborative approach to saving the Tasmanian devil by integrating multidisciplinary laboratory based research within a conservation management framework devised by the Save the Tasmanian Devil Program (STDP) (83). This cooperative approach has witnessed great advancement in understanding the nature and origins of DFTD by identifying both genetic and expressional proteins, molecular markers for genetic diversity in founder populations and vaccine development in wild Tasmanian devils. Paramount to STDP is conservation management and the complete success of insurance populations of intensive, free-range enclosure or Island relocation, all of which are triumphantly at capacity, providing individuals suitable for relocation to decimated devil populations within Tasmania.

2.9 DFT2: A second transmissible Tasmanian devil facial tumour

The comprehensive sixteen-year overview above focuses solely on research and conservation management directed at DFTD. Unfortunately, for the Tasmanian devil a second transmissible tumour has been identified in this species, now termed Devil Facial Tumour 2 (DFT2), seemingly restricted to the Channel Peninsula south of Hobart. A comprehensive overview of DFT2 and my collaboration is provided in chapter three of my thesis but briefly outlined below for completion of devil Facial Tumour literature review.

Pye et al. (7) identified five cases from twelve in the Channel Peninsula as non-classical DFTD, despite the external appearance of facial tumours indistinguishable to DFTD. It was noted that the histomorphology was not consistent with typical pleomorphic small round cells forming distinct bundles, cords or packets of DFTD (1) in contrast, these cases had pleomorphic sheets containing amorphic, stellate and fusiform cell types with the distinct bundles, cords or packets characteristic of DFTD noticeably absent. Periaxin Immunohistochemical staining was performed which is

expressed by DFTD but was negative on two unusual facial tumours. As previously discussed, the distinctive DFTD karyotype has both chromosome two homologs absent, one of the chromosome 5 homolog absent, both X sex chromosomes absent and the presence of four abnormal marker chromosomes. In contrast to DFTDs karyotype, the unusual tumours karyotype has additional material on chromosomes one, two and four, a deletion involving chromosome 5 and monosomy for chromosome six. Both X and Y sex chromosomes were present. Of greatest significance was that all five tumours had the identical complex karyotype and therefore conceivable that they were derived from a single clone and for this reason we named the tumour DFT2, a second transmissible devil facial tumour. Previous investigations using fluorescent insitu hybridization had identified two X chromosome copies in DFT1 ((19, 45) and further examination by Pye et al. (7) of 10 X chromosome variants all mapping to the X chromosome only, confirms that DFT1 carries two homologous X chromosomes and the tumour probably arose from a female devil originally. Because the DFT2 karyotype is completely different to DFT1 and carries a Y chromosome indicating the origin of DFT2 was from a male devil, and DFT2 is negative for Periaxin, together the evidence supports that a single clonal origin of DFT1 and DFT2 is discordant. This discovery of DFT2 certainly provides some insight into the vulnerabilities of the Tasmanian devil given this is the second transmissible tumour in the species within twenty-two years, with DFT2 appearing as recently as 2014. We further investigated and reported by Stammitz et al. (8) the functional and genetic characteristics of DFT1 and DFT2 in an attempt to elucidate any commonalities between the two transmissible tumours. Our panel of IHC showed similar characteristics with both DFT1 and DFT2, both being positive for S100, ENO2 and VIM and negative for SMA and CK. As previously reported, DFT1 is strongly positive for PRX (20) which is routinely used for a diagnostic marker; however, in contrast to DFT1, DFT2 is negative for PRX, providing an expressional distinction. Genotyping DFT1 and DFT2 at 320 nuclear polymorphic loci, and compared to previous data (84) found that DFT1 arose geographically in the North East of Tasmania Mt William area however,

DFT2 arose in the south east Channel Peninsula area. Essentially, DFT1 and DFT2 appear to have emerged independently at separate locations. Interestingly, because DFT2 contains a Y chromosome it was noticed that of the now eleven DFT2 tumours identified (85) nine of these tumour were grafted into male hosts, one a female host and the other female host the Y chromosome was not detected. It remains to be seen if female devil hosts provide some type of immunological resistance to DFT2. In wrapping up our research we screened a number of drugs for potential therapeutic agents. It was found that both DFT1 and DFT2 were sensitive to receptor tyrosine kinases (RTK), particular DFT1s sensitivity to ERBB2 mediated Afatinib which is reassuring as our ERBB3 studies suggested a number of regimes that included the dimer ERBB2/ERBB3. DFT2 had sensitivity to Axitinib, which is active against PDGFR and KIT, both of which are discussed in depth in chapter 1 of my thesis. In a recent publication Caldwell et al. (86) found that DFT2 expresses B2M as well as classical and non-classical MHC class I heavy chains, which is contrary to DFT1 which has lost expression of MHC class I molecules. Results showed that expression of MHC class I alleles varied on DFT2 tumours with the highest expression of classic MHC-I allele also found present within host devils. This research by Caldwell et al. (86) suggests that loss of MHC is not necessary for tumour transmission because of varied expression however, subclones may be selected upon transmission if they have downregulated MHC as the tumour encounters different devils immune systems. It is predicted that DFT2 is likely to be losing MHC antigens already and this could lead to widespread transmission throughout the remaining fragile wild populations of Tasmanian devils, on the back of the decimation caused by DFT1. Evidence would suggest that the Tasmanian devil may well be prone to transmissible cancers, increasing the urgency of biomarkers for earlier identification and therapeutic intervention.

3.0 Methodology

3.1 Standard Histology and Immunohistochemistry chapters 1-3.

Devil Facial Tumour 1 (DFT1) Immunophenotype Reveals a Progenitor-Like Cell with Schwann cell, Melanocyte and Self-renewal Characteristics (Chapter 1).

ERBB3: A potential serum biomarker for early detection and therapeutic target for devil facial tumour 1 (DFT1) (Chapter 2).

DFT1 and DFT2 histology and immunohistochemistry (Chapter 3)
A second transmissible cancer in Tasmanian devils
The Origins and Vulnerabilities of Two Transmissible Cancers in Tasmanian Devils

3.2 Standard Histology

Tasmanian Devil tissues were fixed in 10% Neutral Buffered Formaldehyde (Confix, ACFC, Australian Biostain, Traralgon, Victoria, Australia) for 24 hours and selected tissues were cassetted and processed overnight using a standard 15 hour overnight procedure in the TP1050 tissue processor (Leica Microsystems, Wetzlar, Germany). Tissues were orientated on the EG1160 (Leica), embedded in paraffin wax (Surgipath Paraplast, 39601006, Leica), sectioned at 3 microns using Leica RM2245 microtome, adhered to microscope slides (Menzel Glaser, Braunschweig, Germany) and dried for 20 minutes at 60^{O}C. Sections were deparaffinised, rehydrated and stained using Jung autostainer XL (Leica) for Haematoxylin (Harris' Haematoxylin, AHHNA, Australian Biostain) and Eosin, dehydrated cleared and mounted in CV Mount (Leica, 046430011).

3.3 Standard Immunohistochemistry

Archival Tasmanian devil tissues and tumours were sectioned at 3 microns, floated onto Superfrost plus slides (Menzel Glaser) and subjected to standard deparaffinisation and rehydration techniques using an automated stainer (Leica). Antigen retrieval in tissue sections was conducted in citrate buffer at pH 6.0 (Reveal Decloaker, Biocare Medical, California, USA) at 120^{0}C for 8

minutes using a Pascal pressure chamber (Dako, Glostrup, Denmark) then cooled to 20^{o}C. Endogenous peroxidase activity was quenched using 3% hydrogen peroxide (Ajax Finechem, Sydney, Australia, 260) in methanol (Ajax, 723) for 30 minutes. Detection of primary antibodies was achieved using Mach1 Universal HRP-Polymer detection kit (Biocare Medical, California, USA, M1U539GL10). Protein block (Background Sniper BS966L10) was applied for 20 minutes prior to application of primary antibodies. Primary antibodies were applied to both devil tumour and normal devil control tissues at room temperature for 30 minutes. Negative control was omission of primary antibody with buffer substitution. Universal HRP-polymer was applied for 30 minutes (MRH538L10) followed by 1 drop of Betazoid DAB Chromogen 3,3'- Diaminobenzidine (BDB900G) in 1ml of substrate buffer (DB900) applied for 4 minutes. Tris buffered saline (Biocare Medical, TWB945) was used to rinse between all steps. Slides were rinsed, stained with Carazzi's Haematoxylin for 5 minutes, washed for 3 minutes in tap water, dehydrated, cleared and mounted in CV mount. Sections were viewed under light microscopy using Olympus BX41 (Olympus corporation, Tokyo, Japan) and selected areas were photographed using an Olympus digital camera (DP20).

3.4 Immunohistochemical detection systems

There are many choices of immunohistochemical kits available on the market today. One of the most common older technologies utilized is the **A**vidin-**B**iotin **C**omplex or the "ABC" methodology (figure 1). This relies on two major components; avidin, a large glycoprotein extracted from egg white that has four high affinity binding sites to Biotin which is the second major component, a low molecular weight vitamin. Biotin conjugated enzyme (peroxidase) and Avidin are allowed to react together to form a complex, this is then added to the tissue section which has a secondary biotinylated antibody attached. The biotinylated antibody binds to the ABC complex forming a

larger complex to which the chromogen (DAB) is added in order to reacted with the enzyme resulting in a brown colour change (87).

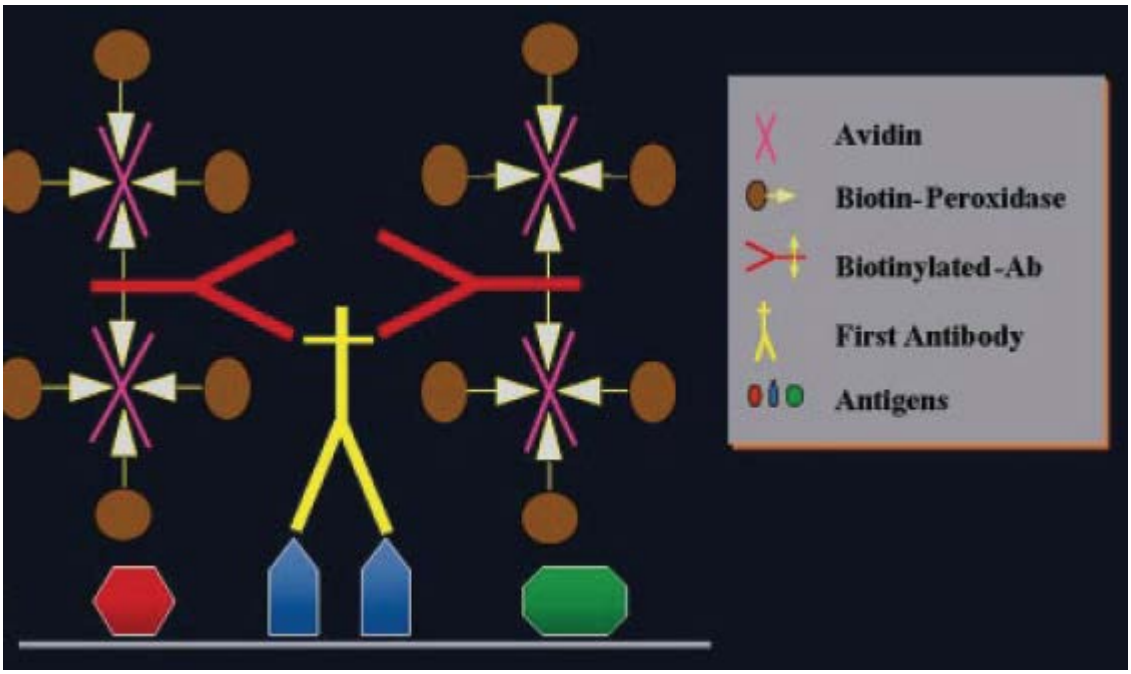

Figure 1: Diagrammatic representation of the ABC method of detection.

Diagram reference: Ramos-Vara et al.(87)

I previously used the ABC method but more recently substituted this method with the LSAB method. The LSAB method is similar but substitutes Avidin with Streptavidin (from the bacterium *Streptomyces avidinii*). This reduces the higher non-specific background staining caused by Avidin cross-reacting with lectins. An additional problem with both methods is that endogenous biotin (such as in liver or kidney tissue) can also contribute to background staining, making interpretation problematic. One such method that avoids both Avidin and Biotin non-specific staining is to use systems that employ polymer-based technology such as the Biocare micropolymer technology (Figure 2), which I utilised for my thesis. This method is able to increase the number of enzyme linked polymers adhered to antibody, is more compact than the 'ABC' complex, thus offering less steric hindrance and resulting in an intense signal with less non-specific background staining (87).

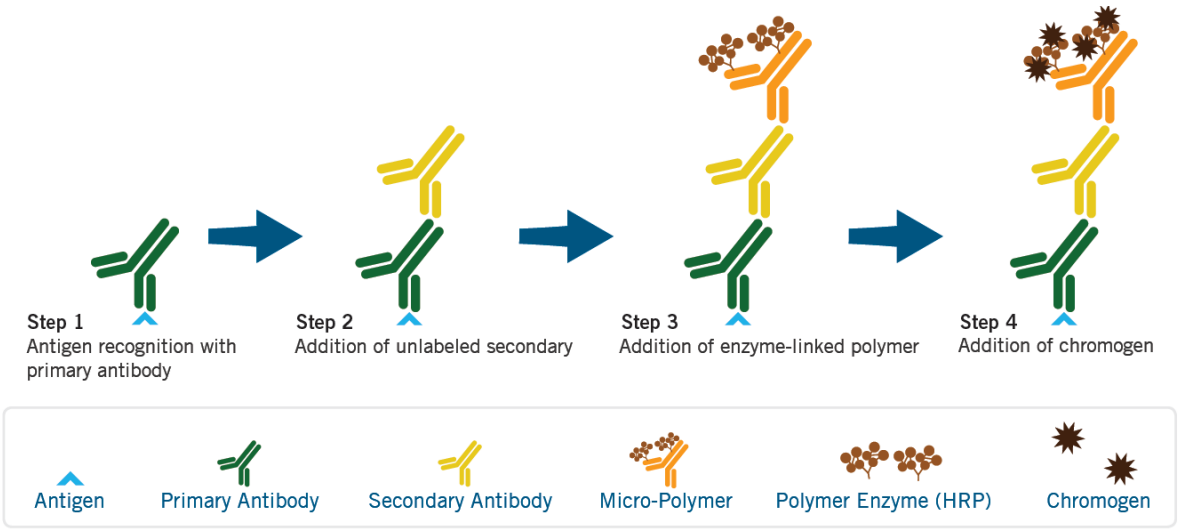

Figure 2: Avidin Biotin free enzyme linked micropolymer technology.

Diagram reference: Biocare https://biocare.net/wp-content/uploads/MACH103.pdf

3.5 Antigen (Epitope) retrieval

Formaldehyde is the preferred choice of histologists for fixing tissues as this small aldehyde infiltrates tissue and provides crosslinks between some amino acids and peptides. At a molecular level (figure 3) the formaldehyde reacts with hydrogen on the amino groups forming hydroxymethyl compound, crosslinks form and further reaction with hydrogen forms a methylene bridge. These crosslinks cause a conformational change (mainly tertiary and quaternary) in the peptides three-dimensional structure obscuring or masking potential antigens/epitopes for immunohistochemistry.

1. Formation of addition products

$$\underset{\text{Reactive hydrogen on tissue}}{\text{Protein-H}} + \underset{\text{Formaldehyde}}{CH_2O} \rightarrow \underset{\text{Reactive hydroxymethyl compound addition product}}{\text{Protein-}CH_2OH}$$

2. Formation of methylene bridges

$$\underset{\text{Reactive hydroxymethyl compound addition product}}{\text{Protein-}CH_2OH} + \underset{\text{Second reactive hydrogen on the protein}}{\text{Protein-H}}$$

$$\rightarrow \underset{\text{Methylene bridge cross-link}}{\text{Protein-}CH_2\text{-Protein}} + H_2O$$

Figure 3:Cross-linking induced by formaldehyde fixation at a molecular level.

Diagram reference: Ramos-Vara et al. 2005 (87).

In most cases, for the application of immunohistochemistry to formalin fixed paraffin embedded (FFPE) tissue sections, crosslinking caused by formaldehyde fixation must be reversed to “reveal” the antigens/epitopes (figure 4) for successful antibody adherence. This can be achieved by using either heat induced epitope retrieval (HIER) or enzyme induced epitope retrieval (EIER). HEIR involves the use of heat in various buffers and pH such as citrate pH 6.0 or EDTA pH 9.0 and is successfully achieved using a pressure cooker-like device (Figure 5), typically with programmable temperature and time for precise control over retrieval conditions. My experimentation found that epitope retrieval was best achieved using citrate pH 6.0, 8 minutes at 120 ^{o}C with relatively little background staining whereas higher pH buffers introduced some background or non-specific staining at this temperature. While pressure cookers are still currently in use in small laboratories or the research setting, they have largely been replaced by lower temperature longer time antigen/epitope retrieval technologies (e.g. routine human diagnostic high throughput laboratories) where the high pH buffers are used commonly.

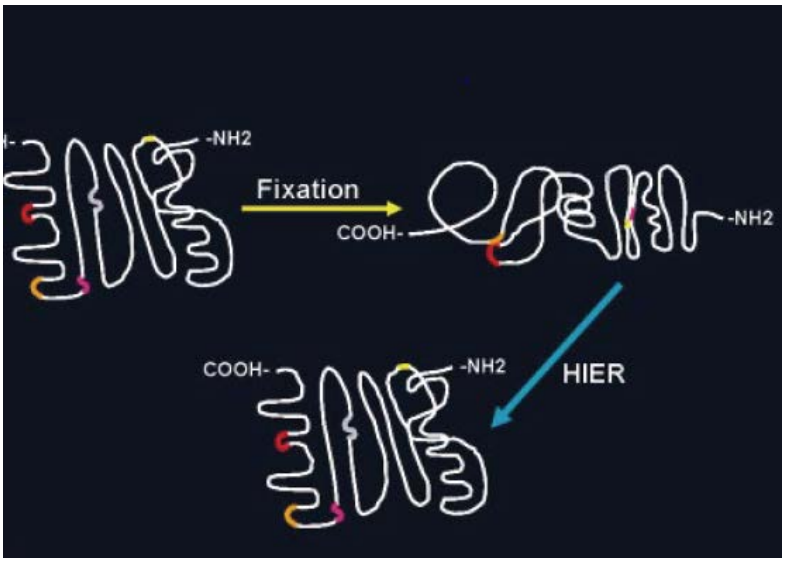

Figure 4: Antigen retrieval reverses the conformational changes revealing antigen/epitopes.

Diagram reference: Romos-Vara et al 2005.(87)

Figure 5: Antigen retrieval Pascal pressure cooker.

(Dako/Agilent https://www.agilent.com/)

3.6 Monoclonal and polyclonal antibodies

The targeting of marsupial cellular tissue antigens/epitopes by immunohistochemistry is a difficult task because virtually all commercial antibodies, whether monoclonal or polyclonal, are antibodies

produced using human immunogens. The host species for the polyclonal antibodies used in my research were rabbits, immunised with purified antigen, producing antibodies against this specific antigen. However, rabbit polyclonal antibodies have both advantages and disadvantages in their application. The advantage of a polyclonal antibody, providing the antisera is affinity purified, is it will contain a mixture of different antibodies directed at different epitopes present on a given protein immunogen. Essentially this does provide multiple epitope recognition, which can be particularly advantageous for non-human species. This feature is useful when identifying marsupial epitopes, where the marsupial-human amino acid sequence homology of the many antibodies present may range from fifty to one hundred percent. The disadvantage with the polyclonal antibody is that some of the antibodies may cross react with other cellular epitopes on non-target proteins. Thus, while polyclonal antibodies have higher affinity and wide reactivity they have lower specificity when compared to monoclonal antibodies (87). Monoclonal antibodies in contrast to polyclonal antibodies are most commonly produced in mouse, although rabbit monoclonal antibodies are becoming increasingly popular in the market place. Following immunisation of the mouse with purified antigen, antibody producing B-cells are harvested from the spleen and fused with mouse myeloma cells conferring immortality on the hybrid. Because B-cells will produce a variety of antibodies, the hybridomas can be screened for specificity and selected on this basis. Generally, monoclonal antibodies are more specific with less non-specific staining than polyclonal antibodies although the possibility of cross-reaction with non-target epitopes can occur if the initial antigen used comprised a small amino acid sequence (87). The choice of using monoclonal or polyclonal antibodies for a given marsupial epitope depends primarily on whether the amino acid sequence of the antigen is known. The Tasmanian devil genome has been sequenced and is available at Ensembl gene browser (https://www.ensembl.org/) therefore, I was able to use the orthologue protein alignment tool for human and Tasmanian devil amino acid sequences for the given gene of interest and compare the homology of the two

sequences. Exact comparison is only possible when manufacturers provide the actual position of the amino acids or the actual amino acid sequence from which I could deduce the actual position within the gene. For example, if we compare human and Tasmanian devil orthologue sequences

Species	Gene ID	Peptide ID
Human (*Homo sapiens*)	ENSG00000064300	ENSP00000172229
Tasmanian devil (*Sarcophilus harrisii*)	ENSSHAG00000006168	ENSSHAP00000007097

```
CLUSTAL W (1.81) multiple sequence alignment


ENSP00000172229/1-427    MGAGATGRAMDGP----RLLLLLLLGVSLGGAKEACPTGLYTHSGECCKACNLGEGVAQP
ENSSHAP00000007097/1-431 RGSGGSGRAMEGPCRLLLLLLLLLLGVSMGEVTEDCATNLYTESGECCRACNLGEGVAQP
                          *:*.:****:**     **********:* ..* *.*.***.*****:**********


ENSP00000172229/1-427    CGANQTVCEPCLDSVTFSDVVSATEPCKPCTECVGLQSMSAPCVEADDAVCRCAYGYYQD
ENSSHAP00000007097/1-431 CGVNQTVCEPCLDSVTFSDTISATEACKPCTECVGLQSMSAPCVEADDAVCRCAYGYYQD
                         **.****************.:****.**********************************


ENSP00000172229/1-427    ETTGRCEACRVCEAGSGLVFSCQDKQNTVCEECPDGTYSDEANHVDPCLPCTVCEDTERQ
ENSSHAP00000007097/1-431 EESGLCKPCSVCEPGSGLVFSCQDKQNTVCEVCPEGTYSDEANHVDPCLPCTACEETERE
                         * :* *:.* ***.**************** **:*****************.**:***:


ENSP00000172229/1-427    LRECTRWADAECEEIPGRWITRSTPPEGSDSTAPSTQEPEAPPEQDLIASTVAGVVTTVM
ENSSHAP00000007097/1-431 TRECTRWSDRECEEIPARWTTRTTPLLGSDSPPPITQDLPEPPEPEAEASTVADVVTTVM
                          ******:* ******.** **:**  ****..* **:   *** :  *****.******


ENSP00000172229/1-427    GSSQPVVTRGTTDNLIPVYCSILAAVVVGLVAYIAFKRWNSCKQNKQGANSRPVNQTPPP
ENSSHAP00000007097/1-431 GSSQPVVTRGTTDNLIPVYCSILAAVVVGLLAYIVFKRWNSCKQNKQGANNRPVNQTPSP
                         ******************************:***.***************.*******.*


ENSP00000172229/1-427    EGEKLHSDSGISVDSQSLHDQQPHTQTASGQALKGDGGLYSSLPPAKREEVEKLLNGSAG
ENSSHAP00000007097/1-431 EGEKLHSDSGISVDSQSLHDQQPQTQTAQVQALKGDGGLYSSLPAAKREEVEKLLNSSSG
                         ************************:****. **************.***********.*:*


ENSP00000172229/1-427    DTWRHLAGELGYQPEHIDSFTHEACPVRALLASWATQDSATLDALLAALRRIQRADLVES
ENSSHAP00000007097/1-431 DTWRHLAGELGYLPEHIDSLNREDCPVRALLDSWAAQDSATLDALYAALRRIQRGDIVEN
                         ************ ******:.:* ******* ***:********* ********.*:**.


ENSP00000172229/1-427    LCSESTATSPV
ENSSHAP00000007097/1-431 LYSESTATSPV
                         * *********
```

Figure 6: Orthologue protein alignment of nerve growth factor receptor (NGFR).

Figure reference: Ensembl gene browser (https://www.ensembl.org/)

of nerve growth factor receptor (NGFR) (figure 6) we can determine mismatch amino acid regions of the manufactures antigen to deduce the anti-human antibody with the most sequence homology to the Tasmanian devil sequence. In practice, if manufacturer-A's antigen sequence is aa's 1-38 and manufacturer-B's antigen sequence is aa's 88-120 we can see that both of the these illustrate amino acid mismatches with homology only at approximately fifty percent. However, if

manufacturer-C's antigen sequence is aa's 121-142 it has one hundred percent homology and therefore this antibody would be worthy of immunohistochemical evaluation. Some genes are conserved across species for example, proliferating cell nuclear antigen (PCNA) has one hundred percent homology (figure 7) and therefore any number of antibodies would be suitable.

Species	Gene ID	Peptide ID
Human (*Homo sapiens*)	ENSG00000132646	ENSP00000368458
Tasmanian devil (*Sarcophilus harrisii*)	ENSSHAG00000011654	ENSSHAP00000013638

```
CLUSTAL W (1.81) multiple sequence alignment


ENSP00000368458/1-261     MFEARLVQGSILKKVLEALKDLINEACWDISSSGVNLQSMDSSHVSLVQLTLRSEGFDTY
ENSSHAP00000013638/1-261  MFEARLVQGSILKKVLEALKDFINEACWDISSGGVNLQSMDSSHISLVQLTLRSEGFDTY
                          ********************:**********.**********:***************


ENSP00000368458/1-261     RCDRNLAMGVNLTSMSKILKCAGNEDIITLRAEDNADTLALVFEAPNQEKVSDYEMKLMD
ENSSHAP00000013638/1-261  RCDRNLAMGVNLTSMSKILKCASNEDIITLRAEDNADTLALIFEAPNQEKVSDYEMKLMD
                          **********************.*****************:*****************


ENSP00000368458/1-261     LDVEQLGIPEQEYSCVVKMPSGEFARICRDLSHIGDAVVISCAKDGVKFSASGELGNGNI
ENSSHAP00000013638/1-261  LDVEQLGIPEQEYSCVVKMPSGEFARICRDLSHIGDAVVISCAKDGVKFSASGELGSGNV
                          ************************************************************.**:


ENSP00000368458/1-261     KLSQTSNVDKEEEAVTIEMNEPVQLTFALRYLNFFTKATPLSSTVTLSMSADVPLVVEYK
ENSSHAP00000013638/1-261  KLSQTSNVDKEEEAVTIEMNEPVQLTFALRYLNFFTKATPLSPTVTLSMSADVPLVVEYK
                          ****************************************.****************


ENSP00000368458/1-261     IADMGHLKYYLAPKIEDEEGS
ENSSHAP00000013638/1-261  IADMGHLKYYLAPKIEDEGGS
                          ***************** **
```

***Figure 7*: Orthologue protein alignment for proliferating cell nuclear factor (PCNA).**

Figure reference: Ensembl gene browser (https://www.ensembl.org/)

When only polyclonal antibodies are available or perhaps only monoclonal with unknown immunogens then it is a matter of trial and error in these cases.

Chapter 1

4.0 Devil Facial Tumour 1 (DFT1) Immunophenotype Reveals a Progenitor-Like Cell with Schwann cell, Melanocyte and Self-renewal Characteristics

Dane A. Hayes [1, 2, 3 *], Mathew Suji Eapen [3], Elizabeth P Murchison [4], Graeme Knowles [1], Elizabeth T. Snow [3], Sukhwinder Singh Sohal [3].

[1]Department of Primary Industries, Parks Water and Environment, Animal Health Laboratory, Launceston, Tasmania, Australia.

[2]Save the Tasmanian Devil Program, University of Tasmania, Hobart, Tasmania, Australia.

[3]School of Health Sciences, Faculty of Health, University of Tasmania, Launceston, Tasmania, Australia.

[4]Transmissible Cancer Group, Department of Veterinary Medicine, University of Cambridge, Cambridge, CB3 0ES, United Kingdom

***Corresponding author:**

E-mail: dane.hayes@dpipwe.tas.gov.au (DH)

Funding: This research was funded by the Dr Eric Guiler Tasmanian Devil Research Grant through the University of Tasmania and the Save the Tasmanian Devil Appeal (STDP) to DH and SS http://www.tassiedevil.com.au/tasdevil.nsf. The Department of Primary Industries water and Environment (DPIPWE) and the University of Adelaide provided financial and in-kind support.

Competing interests: The authors declared that there were no competing interests.

4.1 Abstract

Devil Facial Tumour 1 (DFT1) is a clonally evolved tumour of Schwann cell origin affecting Tasmanian devils (*Sarcophilus harrisii*). Transferred by biting, it is now one of two transmissible neoplasms in this species. The orofacial regions of the Tasmanian devil are a rich source of peripheral nerves often injured during mastication or aggression between individuals, initiating a cascade of molecular signals transdifferentiating Schwann cells into Bungner Schwann cells, augmenting axonal repair within the wound microenvironment. We hypothesised that DFT1 may have originated from malignant transformation of the Bungner Schwann cell where, theoretically, the wound microenvironment, or niche, would provide the necessary trophic factors crucial to DFT1 transmission, survival and proliferation. Our extensive research explores immunohistochemical expression of common progenitor and developmental cell markers of the Schwann and Melanocyte lineages including self-renewal. Our results reveal DFT1 is a progenitor-like cell with Schwann cell, melanocyte and self-renewing characteristics.

4.2 Introduction

4.2.1 Vertebrate Neural crest

The neural crest (NC), is unique to the vertebrate embryo and advocated as the fourth germ layer (88) due to the diversity of cell types derived from the NC. Induction of the NC occurs at the neural plate border between the neural plate and the non-neural ectoderm where NC cells (NCCs) are specified and reside within the elevating neural folds and dorsal neural tube after its closure. Delamination, a process whereby partial or complete epithelium-to-mesenchymal transition (EMT) separates the NC from the surrounding neuroepithelial cells, now transitory and multipotent, migrates extensively throughout the developing embryo. Induction and migration phases are

highly dynamic and governed by the NC gene regulatory network (GRN) permitting NCCs interpretation of signals from the microenvironment, including other NCCs, navigation of embryonic pathways and their terminal differentiation depends on the axial level of the NCCs origin. The cranial NC (CNC) is the origin of ectomesenchymal cells of craniofacial skeleton, including bone, cartilage, connective tissue and most of the dental tissues. The trunk NC (TNC) is responsible for secretory cells of the adrenal (chromaffin) and thyroid (parafollicular) glands, form dorsal root ganglia (DRG) and autonomic nerves. The vagal NC contributes the enteric nervous system (ENS), cardiac mesenchyme and smooth muscle vasculature. NCCs from all axial levels differentiate into melanocytes and contribute to the peripheral nervous system (PNS) delivering sensory, sympathetic and parasympathetic neurons and glia to the developing embryo (above paragraph reviewed in (89-92)).

4.2.2 Marsupial neural crest

Studies on chick, mouse, rat and others provides extensive knowledge of vertebrate embryonic development. Although closely aligned, differences in NC development between species exist (89). Marsupial (metatherian) young are born extremely immature or altricial when compared to eutherian (placental) newborns, following a short intrauterine gestation and even shorter period of organogenesis yielding minimal respiratory, urogenital, skin, digestive and cardiovascular function for extrauterine survival (93-95). The degree of development in marsupials is narrow but the Dasyurids, the group to which Tasmanian devils belong to, are at the extreme end and therefore classed as ultra-altricial with the newborn weighing 5-20mg. Despite its embryonic state, the marsupial neonate must have considerable functional independence enabling movement. The marsupial neonate exhibits advanced features essential for survival; including movement from the birth canal to the teat area or pouch, recognition of the nipple, attachment and suckling (reviewed in (95-97)). Studies on the grey short tailed opossum, *Monodelphis domestica*, show early

differentiation and migration of the neural crest is responsible for advanced development of craniofacial region giving rise to most of the bone, cartilage and connective tissues and patterning for musculature (96, 97) necessary for orofacial development. Relative advancement of the forelimb of the marsupial, including the Tasmanian devil (98, 99), and the neuromuscular junction of the western grey kangaroo, *Macropus fuliginosus* (100) are considered crucial to neonate movement, specifically, Tasmanian devil metacarpals are developed but phalanges have not yet differentiated (96). Relative to its body size, precocious development of the trigeminal sensory pathway in the eastern quoll, *Dasyurus viverrinus*, is evident, possibly augmenting somatosensory signals from the face (101). The olfactory system is thought to guide the neonate to the mothers pouch and while the tammar wallaby, *Macropus eugenii*, shows early nerve fibres it was deemed insufficient for reception (102) however, it was concluded that the olfactory systems was developed at birth because the neonate is directionally influenced by the mothers pouch odours (103). Innervation of the mystacial vibrissae follicles in the brush tail possum, *Trichosurus vulpecula,* reveal Merkel cell-neurite complexes as well as specialised Schwann cell (SC) processes at terminal nerves called Palisade, Bulbous and Compound endings (104). Merkel cells present in the northern native cat, *Dasyurus hallucatus*, and other marsupials are highly sensitive touch receptors, present around the oral region and fusion area on the lips would aid the neonate to sense attachment to the teat (105, 106). Melanocytes are seen in the dermis and epidermis of the brush tail possum as early as two days (107) and 10 days in the northern native cat (108). These comparative marsupial studies illustrate the relative shift in timing of development compared to eutherian vertebrates. Advancement of the neonate, particularly early neural crest differentiation, migration for craniofacial formation, forelimb development, neuronal and sensory networks interconnecting basic organ function is crucial to the marsupial neonatal survival.

4.2.3 Schwann cell linage

The NC derived glial components of the PNS can be categorised into six cell types: (1) Satellite cells (STC) envelop neuronal cell bodies (soma) of the DRG and sympathetic and parasympathetic ganglia (109, 110) actively participate in the processing of sensory signals that enhances somatic activity (111). (2) Boundary cap cells (BCs) appear transiently at dorsal root entry zones (DREZ) and motor exit points (MEP) and function as gatekeepers between the motor neuron axons exiting the CNS and sensory afferent axons entering the central nervous system (CNS) (112). Additionally, BCs also contribute to populations of STC, Schwann cell precursors (SCPs), nociceptive neurons (113), thermoreceptive neurons (114), mature Schwann cells (115) and terminal glia of the skin (116). (3) Schwann cells are Integral to peripheral nerve development transitioning from neural crest stem cell (NCSC) to SCP, both phenotypes being migrating and proliferative. The SCP is dependent upon paracrine axonal signals to survive in order to generate immature Schwann cells (ISC). ISCs cease migration, develop autocrine survival signals and deposit basal lamina distinguishing themselves from the SCP. Just before birth and continuing postnatally, ISCs engage in radial sorting of late embryonic nerves segregating large diameter axons from those of smaller diameter. ISCs that form a 1:1 relationship with large axons, now termed pro-myelinating Schwann cells, will exit the cell cycle and form myelinating Schwann cells (MSC). Remaining small diameter axons will not be myelinated; instead, they are ensheathed by non-myelinating Schwann cells (NMSC) forming Remak fibres/bundles (reviewed in (109, 117-119)).

MSCs are renowned in the PNS but the less familiar NMSC are also integral to development and function of the PNS (120, 121) with the ability to form MSC (122). NMSC are harboured in diverse microenvironments to perform homeostatic functions in bone marrow (123, 124) or envelop the spiral ganglion neurons of the cochlea (125). Within NMSCs are the (4) Teloglia or Terminal Glia (TG) which are central to somatosensory innervation in the skin associated with mechanosensory

complexes such as lanceolate (126), Merkel, Ruffini, Pacinian and free nerve endings (127, 128), C-fibres (129, 130), and Meissner corpuscles (131, 132). TG are also present as peri-islet Schwann cells in the pancreas (133) and peri-synaptic Schwan cells at the neuromuscular junction (134, 135). (5) Enteric glia are also NMSC and are present throughout the ENS as mucosal or intramuscular enteric glia (136, 137). Lastly (6) Olfactory ensheathing cells (OEC) are specialized peripheral glia that share homology with Schwann cells (138) and are unique in that the OEC envelop from peripheral olfactory axons through to the olfactory bulb (139) located in the CNS.

4.2.4 Melanocyte lineage

NC derived pigment cells, or melanocytes, localise classically as cutaneous melanocytes in the skin epithelium and dermis or non-classically in non-cutaneous anatomical sites such as the eye (except retinal pigment epithelium), ear, heart, CNS meninges and adipose tissue (140, 141). Melanocytes have two distinct migratory pathways: At the trunk level, firstly, early delaminating NCCs proceed dorsoventrally between the neural tube and somites classically differentiating into neurons, glia and endoneurial fibroblasts (142, 143). Recent research has demonstrated that a subset of SCPs that lose contact with growing peripheral nerves, do not form glia and instead adopt a melanocyte fate (144) . Secondly, late migrating NCCs arise from the dorsal neural tube, accumulate in the 'migration staging area', receive early specification allowing migration dorsolaterally between the superficial ectoderm and dermomyotome to eventually colonise the skin (reviewed in (142, 145)). In populating the skin, late dorsolateral migrating melanoblasts form the first wave of colonising melanocytes whereas the early migrating dorsoventral SCP derived melanoblasts will form the second wave of melanocytes (146). Recently, mouse cranial melanocytes have also been identified as arising from two populations; initially from nerve associated SCP and later from a nerve independent source possibly differentiating directly from the NC (147).

4.2.5 DFT1 Immunohistochemical study

Our research documents for the first time the histomorphology and immunohistochemical expression of five strains of DFT1. We comprehensively employ 51 antibodies commonly used to discern neural crest derived Schwann cell and melanocyte lineages including growth, transcription and stem cell/self-renewal markers. We compare our immunohistochemical expression between strains and with previously published gene expression (4). Briefly, markers include; Schwann cell: MPZ, PRX, MBP, PMP22, PLP1, GFAP, GAP43 and MAG. Growth factors: NGFR, IGF2R, PDGFB and VEGF; Bungner Schwann cell: JUN, SHH and STAT3; Melanocyte markers: MITF, MLANA, TYR and PNL2; transcription factors: SOX10, SOX2, PAX3, TFAP2A and ERG2; and stem cell/self-renewal: EPCAM, CD44, PROM1, POU5F1 and NES. Immunohistochemical expression of myelin related proteins revealed a mixed SC phenotype consisting of precursor, immature, mature MSC and NMSC markers, characterising the various stages of Schwann cell development. The expression of JUN, SHH and STAT3 reveals the molecular signature of an activated repair program. The expression of growth factors IGFR2, BDNF and PDGFB indicate autocrine survival program activated by axonal loss. Essentially, melanocyte markers were negative for MLANA, TYR and MITF; however, unexpectedly, all cytogenetic strains expressed the melanocyte marker PNL2, suggesting that DFT1 is bipotent. Expression of NGFR, NES, SOX2, POU5F1, EPCAM, CD44, and PROM1 indicates a neural crest like-stem cell with self-renewal characteristics. Together, the phenotype would imply that DFT1 is a progenitor-like cell with Schwann cell, melanocyte and self-renewal characteristics.

4.3 Methods

4.3.1 Histochemisty

To provide excellent contrast against 3,3'-diaminobenzidine (DAB) stained primary antibodies PNL2, MLANA, TYR and MITF we used a modified 0.2 % Azure blue (Aldrich 86,105-7) pH 6.0 for 1 minute, differentiate in 95% ethanol 10 minutes, dehydrate clear and mount in CV mount (148, 149) turning brown melanin granules metachromatically green. We performed histochemical staining for melanin using well established histological methods; Schmorl's stain (ferricyanide to ferrocyanide, Prussian blue reaction) and Masson Fontana stain (reduction of ammoniacal silver to metallic silver, Argentaffin reaction) (150).

4.3.2 DFT1 morphology and immunohistochemical assessment

DFT1 Primary tumours, three each from strains 1-5, listed in table 1, were assessed by Haematoxylin and Eosin staining and immunohistochemically stained with primary antibodies listed in table 2. Microscopically, 10 by 10 high power fields for each DFT1 tumour strain were assessed semi quantitatively for expression of each antibody and the numerical average expressed as a percentage. Intensity of staining was also recorded as follows; negative (0), weak (1/+), moderate (2/++) and strong (3/+++). We present both percent expression and the intensity gradient averages of immunohistochemical staining as heat maps. We generated heat maps to measure differences in strain protein expression, using GraphPad Prism version 7.04, GraphPad Software, La Jolla California USA, www.graphpad.com.

Table 1: Primary tumour Tasmanian devils.

Strain	Devil	Microchip Identification	Laboratory accession	Age (years)	Sex (M/F) / weight (Kg)	Geographic location	Tumour location / Tumour size (cm)
S1	1	982009104719592	12/0820	4	F, 4.5	West pencil pine	Left lateral Upper lip, 2.5cm
S1	2	R00000000003005	12/1594	1	M, 3.2	Huon Valley	Rostral Lower Jaw, 8x5x2cm
S1	3	982000000122095	12/2095	2	F, 3.7	Upper Natone	Right upper lip/nose, 5x5x2
S1	16	982009104883696	10/1830	Adult	M, 7.2	Narawntapu Latrobe	Right face 4x4x3
S1	17	982009106165902	10/2449	Adult	F, 6.1	AHL Prospect	Right cheek 5x4x4
S1	18	982009104350416	10/1829	Adult	F, 5.4	Narawntapu Latrobe	Left lower lip, 8x8x3
S2	4	982009104751722	11/2824	4	F, 5.7	Parrawe Waratah	Right lateral lower jaw, 3x3x2
S2	5	982009106037874	12/4333	3	M, 7.9	Takone Wynyard	Right lateral lower jaw, 15x20
S2	6	982000123129847	13/0854	3	M, N/A	Takone Wynyard	Left lower jaw, 3x2x1
S2	7	982000190559724	12/3207	2	F, 4.5	Kempton	Right lower jaw incisor, 10x7x7
S2	19	982009106094088	10/1851	Adult	M, 10.1	Narawntapu Latrobe	Right cheek 6x6x5
S2	20	NC	10/0944	2	M, N/A	Mole Creek	Left face, 2x2
S2	21	M00000PT101692	10/1692	Adult	M, 5.3	Lake Leak	Right face 1x2
S3	8	982009106034139	11/0767	2	F, 6.1	Bangor Dunally	Whisker/skin area 5x5
S3	9	982000123122487	12/2320	2	M, 6.0	Sorrell Dunalley	Right cheek, very large.
S3	10	982000123208272	12/3045	2	F, 5.5	Bangor Dunally	Left cheek, 7x7x3
S3	22	982009105195643	10/0129	2	M, 9.3	Bangor Dunally	Left upper lip, 1x1x1

S3	23	982009104928037	10/2226	2	M, 9.1	Forestier Dunally	Inside mouth top lip, 10x9x6
S3	24	982009106543385	10/2222	1	F, 5.2	Sorrell Dunalley	Under chin 3x3x3
S4	11	982009106218282	11/4115	2	F, 4.6	AHL Prospect	Left upper lip, 4x4x2
S4	12	982009105830109	11/3426	1	F, 5.2	AHL Prospect	Right cheek, 2x2x2
S4	25	NC	06/2179	3	F, N/A	Freycinet Bicheno	Lower lip 4x4
S4	13	982009106392944	11/3178	2	F, 5.8	Freycinet Coles Bay	Left upper lip/nostril 0.5x0.5
S5	14	982009106144920	12/3084	2	F, 4.6	Takone Wynyard	Face/Lip 2x2x1
S5	15	982009106037874	12/1979	3	M, 10.7	Takone Yolla	Right cheek 0.5x0.5
S5	26	982009100367728	06/3549	2	F, N/A	Dunalley	Right Lip, 6x6
S5	27	NC	06/3519	1	F, N/A	Dunalley	Under chin 1x1
S5	28	982009105193063	07/2895	2	M, N/A	Dunalley	Lip, 1x1x1

Tasmanian devils 1-15 primary pilot study tumours. Devils 16-28 devils additional tumours. N/A = data not available. Adult = no age recorded but individual was an adult. NC = not microchipped.

Table 2: Immunohistochemistry antibodies applied to DFT1 S1-5 tissues.

Primary Antibody	**Gene Symbol**	**Clone/Poly Host**	**Manufacturer**	**Product code**	**Dilution**
Peripheral Myelin Protein 22	PMP22	Polyclonal Rabbit	Merck (Sigma-Aldrich)	SAB4502217	1:50
Myelin Associated Glycoprotein	MAG	Polyclonal Rabbit	Thermo Fisher Scientific	PA5-30087	1:50
Myelin Basic Protein	MBP	2H9 Mouse	Genetex	GTX60519	1:1500
Proteolypid Protein 1, PLP/DM20	PLP1				1:1000

Glial Fibrillary Acidic Protein	GFAP	Polyclonal Rabbit	Biocare Medical	CP040	1:100
Myelin Protein Zero, P0	MPZ	Polyclonal Rabbit	Merck Millipore	ABN363	1:2000
Periaxin	PRX	Polyclonal Rabbit	Merck (Sigma-Aldrich)	HPA001868	1:400
Growth Associated Protein 43	GAP43	B-5 Mouse	Santa Cruz Biotechnology	sc-17790	1:50
Laminin receptor, LAMR, Ribosomal Protein SA	RPSA	EPR8469 Rabbit	Abcam (Epitomics)	ab133645	1:200
Laminin		Rabbit Polyclonal	Thermo Fisher Scientific	RB-082-A0	1:50
Gap Junction Protein Beta 1, CX32, Connexin 32	GJB1	Polyclonal Rabbit	Merck (Sigma-Aldrich)	HPA010663	1:15
Nerve Growth Factor Receptor, $p75^{NTR}$,CD271	NGFR	Polyclonal Rabbit	Merck Millipore	07-476	1:150
S100 Calcium Binding Protein B	S100B	Polyclonal Rabbit	Agilent (Dako)	Z0311	1:1200
Vimentin	VIM	V9 Mouse	Agilent (Dako)	M0725	1:800
Enolase 2, Neuron Specific Enolase, NSE	ENO2	BBS/BC/VI-H14 Mouse	Agilent (Dako)	M0873	1:200
Insulin Like Growth Factor Receptor 2, M6PR	IGF2R	EPR6599 Rabbit	Abcam (Epitomics)	ab124767	1:300
Platelet Derived Growth Factor Subunit Beta	PDGFB	Y92 Rabbit	Abcam (Epitomics)	ab32570	1:50
Transforming Growth Factor Beta Receptor 2	TGFBR2	Polyclonal Rabbit	Abcam	ab216483	1:250
Vascular Endothelial Growth Factor Alpha, VEGF-A	VEGFA	EP1176Y Rabbit	Abcam (Epitomics)	ab52917	1:50
Tyrosinase	TYR	T311 Mouse	Agilent (Dako)	M3623	1:50

Anti-Melanoma (PNL2)		PNL2 Mouse	Thermo Fisher Scientific (Invitrogen)	18-0485	1:100
Melan-A, Mart-1	MLANA	A103,M2-7C10,M2-9E3	Thermo Fisher Scientific (Invitrogen)	18-7263	1:100
KIT Proto-oncogene Receptor Tyrosine Kinase, C-KIT, CD117	KIT	Polyclonal Rabbit	Agilent Dako	A4502	1:50
Melanogenisis (Micropthalmia) Associated Transcription Factor	MITF	C5+D5 Mouse	Thermo Fisher Scientific (Invitrogen)	18-0369	1:50
Early Growth Response 2, KROX20	EGR2	Polyclonal Rabbit	Abcam	ab43020	1:600
SRY-box 2	SOX2	EPR3131 Rabbit	Abcam (Epitomics)	ab92494	1:50
SRY-box 10	SOX10	EPR4007 Rabbit	Abcam (Epitomics)	ab155279	1:150
Paired box 3	PAX3	Polyclonal Rabbit	Abcam	ab180754	1:600
JUN Proto-oncogene AP-1 TF Subunit, c-JUN	JUN	E254 Rabbit	Abcam (Epitomics)	ab32137	1:50
Transcription Factor AP-2 Alpha, AP-2	TFAP2A	EPR2688(2) Rabbit	Abcam (Epitomics)	ab108311	1:50
Notch 1	NOTCH1	EP1238Y Rabbit	Abcam (Epitomics)	ab52627	1:50
Catenin Beta 1, Beta Catenin	CTNNB1	E247 Rabbit	Abcam	ab32572	1:50
Signal Transducer and Activator of Transcription 3	STAT3	9D8 Mouse	Abcam	ab1193652	1:2000
Nestin	NES	Polyclonal Rabbit	Genetex	GTX37606	1:50
Epithelial Cell Adhesion Molecule, EpCAM, CD326	EPCAM	EPR677(2) Rabbit	Abcam (Epitomics)	ab124825	1:150
Prominin 1, CD133	PROM1	Polyclonal Rabbit	St. Johns Laboratory	STJ20168	1:2000
CD44 Molecule	CD44	Polyclonal Rabbit	Abcam	ab190926	1:50
POU Class 5 Homebox 1, OCT4	POU5F1	EPR2054 Rabbit	Abcam	ab109183	1:100

Sonic Hedgehog	SHH	Polyclonal Rabbit	Biorbyt	Orb146711	1:500
Ubiquitin C-terminal Hydrolase L1, PGP9.5	UCHL1	31A3 Mouse	Biocare Medical	CM329	1:250
Neurofilament protein, NF	NEFL, NEFM, NEFH	FNP7, DA2, RdmO20.11 Mouse	ThermoFisher Scientific (Invitrogen)	18-0171Z	1:100
Calretanin	CALB2	CAL6 Mouse	Leica Biosystems (Novocastra)	NCL-L-CALRET-566	1:100
Cytokeratin, High Molecular Weight, CK		34βE12 Mouse	Agilent (Dako)		1:50
Brain Derived Neurotrophic Factor	BDNF	EPR1292 Rabbit	Abcam (Epitomics)	ab108319	1:2000
Neurotrophic Receptor Tyrosine Kinase 2, TRKB	NRTK2	EPR1294 Rabbit	Abcam (Epitomics)	ab134155	1:100
Cytokeratin, CK		AE1/AE3 Mouse	Agilent (Dako)	M3515	1:100
α-Smooth Muscle Antigen, SMA		1A4 Mouse	Agilent (Dako)	M0851	1:200
Muscle Specific Actin, MSA		SC28 Mouse	Leica Biosystems (Novocastra)	NCL-L-MSA-594	1:150
DEAD-Box Helicase 4, Vasa	DDX4	Polyclonal Rabbit	Merck (Sigma-Aldrich)	HPA037664	1:500
Y-Box Binding Protein 2	YBX2	Polyclonal Rabbit	Merck (Sigma-Aldrich)	HPA053904	1:200
Tumour Protein p53, P53	TP53	DO-7+BP53-12 Mouse	Thermo Fisher Scientific	MS-738	1:50
Proliferating cell nuclear antigen	PCNA	PC10 Mouse	Leica Biosystems (Novocastra)	NCL-PCNA	1:100

4.3.3 Statistical analysis

To compare the significance of percent expression between the strains for each antibody I performed two way ANOVA, followed by standalone comparison using Fisher's LSD test. The analysis was carried out using GraphPad Prism version 7.04, GraphPad Software, La Jolla California USA, www.graphpad.com.

4.3.4 Comparative analysis of gene to protein expression of DFT1 strains

Previously published DFT1 gene abundance data by Murchison et al. (4) in the supplementary materials is overlayed with our immunohistochemical expression of DFT1 strains and present graphically.

4.4 Results

Antibody percentage positive DFT1 cells in strains 1-5 cells are illustrated by heat map in figure 8 and the antibody intensity of staining of DFT1 positive cells in strains 1-5 are illustrated by heat map in figure 9 with average antibody percent expression and intensity of strains 1-5 shown in table 3. The antibody percentage of DFT1 positive cells in strains 1-5 (protein expression) were tabulated against the gene abundance data from Murchison et al. (4) in table 4 for comparative analysis of Schwann cell and melanocyte lineages, growth factors, transcription factors and multipotent/stem cell markers.

	% expression				
Antibodies	**S1**	**S2**	**S3**	**S4**	**S5**
PMP22	95	90	75	95	95
MAG	94	95	97	98	96
MBP	0	0	0	0	0
PLP1	88	87	90	90	91
GFAP	49	42	28	52	65
MPZ	22	31	51	48	50
PRX	96	97	98	96	98
GAP43	0	0	20	0	0
LAMA2	89	92	95	95	93
GJB1	85	87	90	89	86
NGFR	96	95	94	98	97
S100	50	56	51	39	35
VIM	98	99	97	97	98
NSE	90	89	85	91	95
IGFR2	99	98	98	99	96
PDGFB	93	70	85	82	85
TGFBR2	95	98	98	95	95
VEGFA	85	87	89	90	92
TYR	0	0	0	0	0
PNL2	8	47	12	96	10
MLANA	0	0	0	0	0
KIT	80	79	89	77	87
MITF	0	0	0	0	0
EGR2	80	78	50	68	91
SOX2	90	84	83	50	36
SOX10	86	80	86	86	83
PAX3	82	80	85	80	80
JUN	90	91	90	84	90
TFAP2A	83	87	85	89	82
NOTCH1	96	92	98	94	90
CTNNB1	80	78	82	86	89
STAT3	90	92	91	92	93
NES	91	92	96	79	88
EPCAM	94	96	95	96	97
PROM1	82	81	90	81	80
CD44	77	89	85	75	72
POU5F1	90	90	90	90	85
SHH	93	95	92	90	95
UCHL1	73	85	78	45	75
NF	0	0	0	0	0
CALB2	0	0	0	0	0

Legend	0	25	50	75	100

Figure 8: Antibody immunohistochemical percentage expression DFT1 strains 1-5.

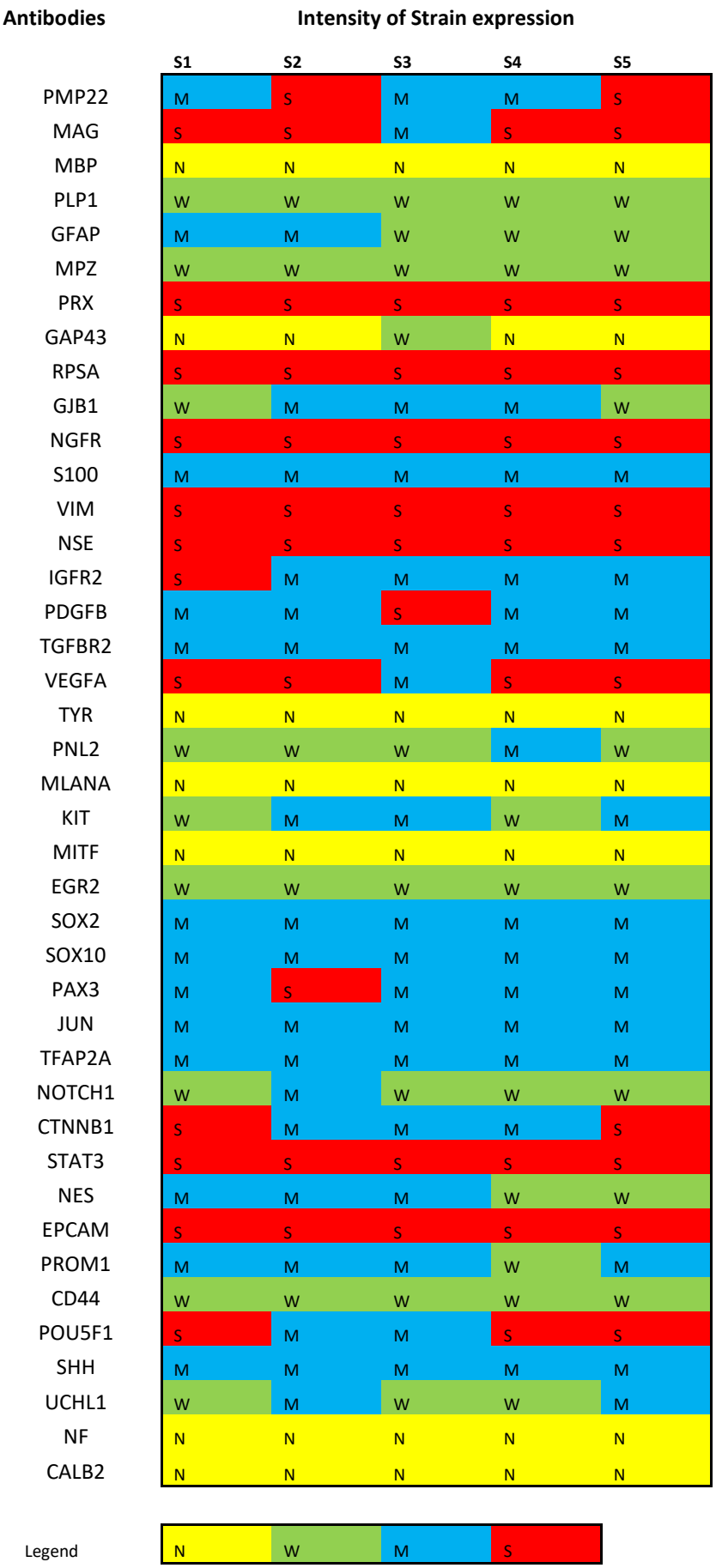

Figure 9: Antibody immunohistochemical intensity gradient DFT1 strains 1-5.

Table 3: **Antibody average percent and intensity of expression.**

Antibody	Ave % (S1-S5)	Strain Immunohistochemical Protein expression
PMP22	90	Moderate to strong cytoplasmic and membranous
MAG	96	Moderate to strong cytoplasmic and membranous
MBP	0	No expression was evident
PLP1	87	Weak cytoplasmic and membranous
GFAP	47	Weak to moderate cytoplasmic and membranous
MPZ	40	Weak cytoplasmic and membranous
PRX	97	Strong cytoplasmic, membranous, including nuclear
GAP43	20	Weak cytoplasmic and membranous, strain 3 only.
RPSA	93	RPSA strong cytoplasmic and membranous
GJB1	87	Weak to moderate cytoplasmic
NGFR	96	Strong cytoplasmic and membranous
S100	46	Moderate cytoplasmic and nuclear
VIM	99	Strong cytoplasmic and membranous
ENO2	90	Strong cytoplasmic
IGF2R	98	Moderate to strong cytoplasmic staining
PDGFB	83	Strong cytoplasmic and membranous
TGFBR2	96	Moderate cytoplasmic staining
VEGFA	88	Moderate to strong cytoplasmic
TYR	0	no expression was evident
PNL2	43	Granular cytoplasmic staining
MLANA	0	No expression was evident
KIT	82	Weak to moderate cytoplasmic
MITF	0	No expression was evident
EGR2	73	Weak nuclear
SOX2	60	Moderate nuclear
SOX10	84	Moderate nuclear
PAX3	81	Moderate to strong nuclear
JUN	89	Moderate nuclear
TFAP2A	85	Moderate nuclear
NOTCH1	94	Weak to moderate cytoplasmic
CTNNB1	83	Moderate to strong cytoplasmic and membranous
STAT3	92	Strong nuclear and some cytoplasmic
NES	89	Weak to moderate cytoplasmic
EPCAM	96	Strong cytoplasmic
PROM1	83	Weak to moderate cytoplasmic
CD44	80	Weak membranous
POU5F1	89	Moderate to strong nuclear
SHH	93	Moderate cytoplasmic
UCHL1	71	Weak to moderate cytoplasmic
NEFL/H	0	No expression was evident
CALB2	0	No expression was evident

Table 4: DFT1 gene abundance counts (cDNA) vs protein expression strains 1-5.

Antibody	Gene	Strain Immunohistochemical Protein expression and percentage
PMP22	83	Moderate to strong cytoplasmic and membranous (S1 95%, S2 90%, S3 75%, S4 95%, S5 95%)
MAG	8	Moderate to strong cytoplasmic and membranous (S1 94%, S2 95%, S3 97%, S4 98%, S5 96%)
MBP	47	no staining was observed
PLP1	67	Weak cytoplasmic and membranous (S1 88%, S2 87%, S3 90%, S4 90%, S5 91%)
GFAP	1	Weak to moderate cytoplasmic and membranous (S1 49%, S2 42%, S3 28%, S4 52%, S5 65%)
MPZ	283	Weak cytoplasmic and membranous (S1 22%, S2 31%, S3 51%, S4 48%, S5 50%)
PRX	279	Strong cytoplasmic, membranous, including nuclear (S1 96%, S2 97%, S3 98%, S4 96%, S5 98%)
GAP43	30	Weak cytoplasmic and membranous (S3 20 %)
LAMA2	25	RPSA strong cytoplasmic and membranous (S1 89%, S2 92%, S3 95%, S4 95%, S5 93%)
GJB1	1	Weak to moderate cytoplasmic (S1 85%, S2 87%, S3 90%, S4 89%, S5 86%)
NGFR	34	Strong cytoplasmic and membranous (S1 96%, S2 95%, S3 94%, S4 98%, S5 97%)
S100	N/A	Moderate cytoplasmic and nuclear (S1 50%, S2 56%, S3 51%, S4 39%, S5 35%)
VIM	303	Strong cytoplasmic and membranous (S1 98%, S2 99%, S3 97%, S4 97%, S5 98%)
ENO2	0	Strong cytoplasmic (S1 90%, S2 89%, S3 85%, S4 91%, S5 95%)
IGF2R	20	Moderate to strong cytoplasmic staining (S1 99%, S2 98%, S3 98%, S4 99%, S5 96%)
PDGFB	7	Strong cytoplasmic and membranous (S1 93%, S2 70%, S3 85%, S4 82%, S5 85%)
TGFBR2	13	Moderate cytoplasmic staining (S1 95%, S2 98%, S3 98%, S4 95%, S5 95%)
VEGFA	25	Moderate to strong cytoplasmic (S1 %, S2 %, S3 %, S4 %, S5 %)
TYR	0	no expression was evident
PNL2	N/A	Granular cytoplasmic staining (S1 8%, S2 47%, S3 12%, S4 96%, S5 10%)
MLANA	6	no expression was evident
KIT	19	Weak to moderate cytoplasmic (S1 80%, S2 79%, S3 89%, S4 77%, S5 87%)
MITF	3	no expression was evident
EGR2	9	Weak nuclear (S1 80%, S2 78%, S3 50%, S4 68%, S5 91%)
SOX2	27	Moderate nuclear (S1 90%, S2 84%, S3 83%, S4 50%, S5 36%)
SOX10	24	Moderate nuclear (S1 86%, S2 80%, S3 86%, S4 86%, S5 83%)
PAX3	3	Moderate to strong nuclear (S1 82%, S2 80%, S3 85%, S4 80%, S5 80%)
JUN	55	Moderate nuclear (S1 90%, S2 91%, S3 90%, S4 84%, S5 90%)
TFAP2A	7	Moderate nuclear (S1 83%, S2 87%, S3 85%, S4 89%, S5 82%)
NOTCH1	4	Weak to moderate cytoplasmic (S1 96%, S2 92%, S3 98%, S4 94%, S5 90%)
CTNNB1	60	Moderate to strong cytoplasmic and membranous (S1 80%, S2 78%, S3 82%, S4 86%, S5 89%)
STAT3	74	Strong nuclear and some cytoplasmic (S1 90%, S2 92%, S3 91%, S4 92%, S5 93%)
NES	N/A	Weak to moderate cytoplasmic (S1 91%, S2 92%, S3 96%, S4 79%, S5 88%)
EPCAM	8	Strong cytoplasmic (S1 94%, S2 96%, S3 95%, S4 96%, S5 97%)
PROM1	3	Weak to moderate cytoplasmic (S1 82%, S2 81%, S3 90%, S4 81%, S5 80%)
CD44	16	Weak membranous (S1 77%, S2 81%, S3 85%, S4 75%, S5 72%)
POU5F1	N/A	Moderate to strong nuclear (S1 90%, S2 90%, S3 90%, S4 90%, S5 85%)
SHH	14	Moderate cytoplasmic (S1 93%, S2 95%, S3 92%, S4 90%, S5 95%)
UCHL1	35	Weak to moderate cytoplasmic (S1 73%, S2 85%, S3 78%, S4 45%, S5 75%)
NEFL	7	no expression was evident
NEFLH	9	no expression was evident
CALB2	2	no expression was evident

N/A – Not available, S1-S5 = DFT1 Strains 1-5. Gene counts Murchison et al. 2010

4.4.1 DFT1 strains 1-5 histomorphology

Karyotypic description of DFT1 revealed that there are at least four major chromosomally distinct strains (variations) (46) with a rare fifth strain (DH, personal communication Anne-Maree Pearce unpublished data, DPIPWE). Conversely, a comprehensive histological description of DFT1 strains 1-5 have not been described until now. Representative photomicrographs of strain 1-5 are illustrated in figure 10.

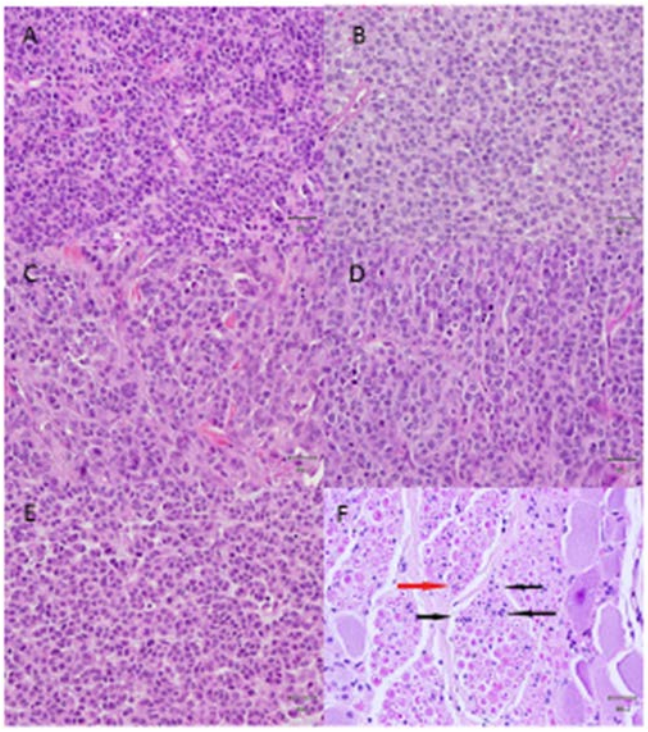

Figure 10: Histomorphology of DFT1 strains 1-5.

Representative Haematoxylin and Eosin stained DFT1 Strain 1 A, Strain 2 B, Strain 3 C, Strain 4 D, Strain 5 E. and normal Schwann cells F. Black arrow shows larger calibre nerve myelinated by Schwann cell and red arrows show small calibre myelinated and unmyelinated nerves enveloped by Remak Schwann cells. All micrographs are x40 magnification and scale bar represents 30 microns.

Strain 1

There is a densely cellular neoplasm effacing the dermis. The neoplasm consists of packets and cords of pleomorphic round to polygonal cells supported by fine fibrovascular stroma. These cells have indistinct cell borders, moderate eosinophilic cytoplasm and central oval nucleus, with fine stippled chromatin and prominent nucleolus or two nucleoli. There is a mitotic figure and low to moderate numbers of apoptotic cells. There is mild to moderate anisocytosis and anisokaryosis.

Strain 2

There is a densely cellular neoplasm effacing the dermis. The neoplasm consists of packets and cords of pleomorphic round to polygonal cells supported by fine fibrovascular stroma. These cells have indistinct cell borders, moderate amphiphilic cytoplasm and central oval nucleus, with fine stippled chromatin and prominent nucleolus or two nucleoli. There is a mitotic figure and low numbers of apoptotic cells. There is mild to moderate anisocytosis and anisokaryosis and mild nuclear moulding between low numbers of neighbouring cells.

Strain 3

There is a densely cellular neoplasm effacing the dermis. The neoplasm consists of packets and cords of pleomorphic round to polygonal cells supported by fine fibrovascular stroma. These cells have indistinct cell borders, moderate eosinophilic cytoplasm and central oval nucleus, with fine stippled chromatin and prominent nucleolus. There are 1-2 mitoses per HPF and low numbers of apoptotic cells. There is very mild anisocytosis and anisokaryosis.

Strain 4

There is a densely cellular neoplasm effacing the normal dermis, leaving only remnant collagen fibres. The neoplasm consists of packets and cords of pleomorphic round to polygonal cells supported by fine fibrovascular stroma. These cells have indistinct cell borders, moderate eosinophilic cytoplasm and central oval nucleus, with coarse chromatin and prominent nucleolus.

There are 1-2 mitoses per HPF and low to moderate numbers of apoptotic cells. There is very mild anisocytosis and anisokaryosis. Low numbers of neighbouring cells display nuclear moulding.

Strain 5

There is a densely cellular neoplasm effacing the dermis. The neoplasm consists of packets and cords of pleomorphic round to polygonal cells supported by fine fibrovascular stroma. These cells have indistinct cell borders, moderate eosinophilic cytoplasm and central oval nucleus, with coarse chromatin and nucleolus (which is present in most cells but not prominent). There are low to moderate numbers of apoptotic cells. There is very mild anisocytosis and anisokaryosis.

4.4.2 DFT1 histomorphology summary

In summary, all strains share similar microscopic architecture, round to polygonal cells forming packets supported by fine fibrovascular stroma. The cellular details of each strain are also similar, with the polygonal to round cells having indistinct cell borders, moderate eosinophilic cytoplasm and single central oval nucleus with prominent nucleolus. There is similar mild cell variation both within and across strains in chromatin patterns (varying from finely stippled, coarse to reticular), degree of anisokaryosis, anisocytosis and numbers of mitotic figures per high power field. For these reasons, discriminating between strain types is not possible, based on these histological characteristics on haematoxylin and eosin staining.

4.4.3 DFT1 strains 1-5 - Schwann cell lineage immunohistochemistry

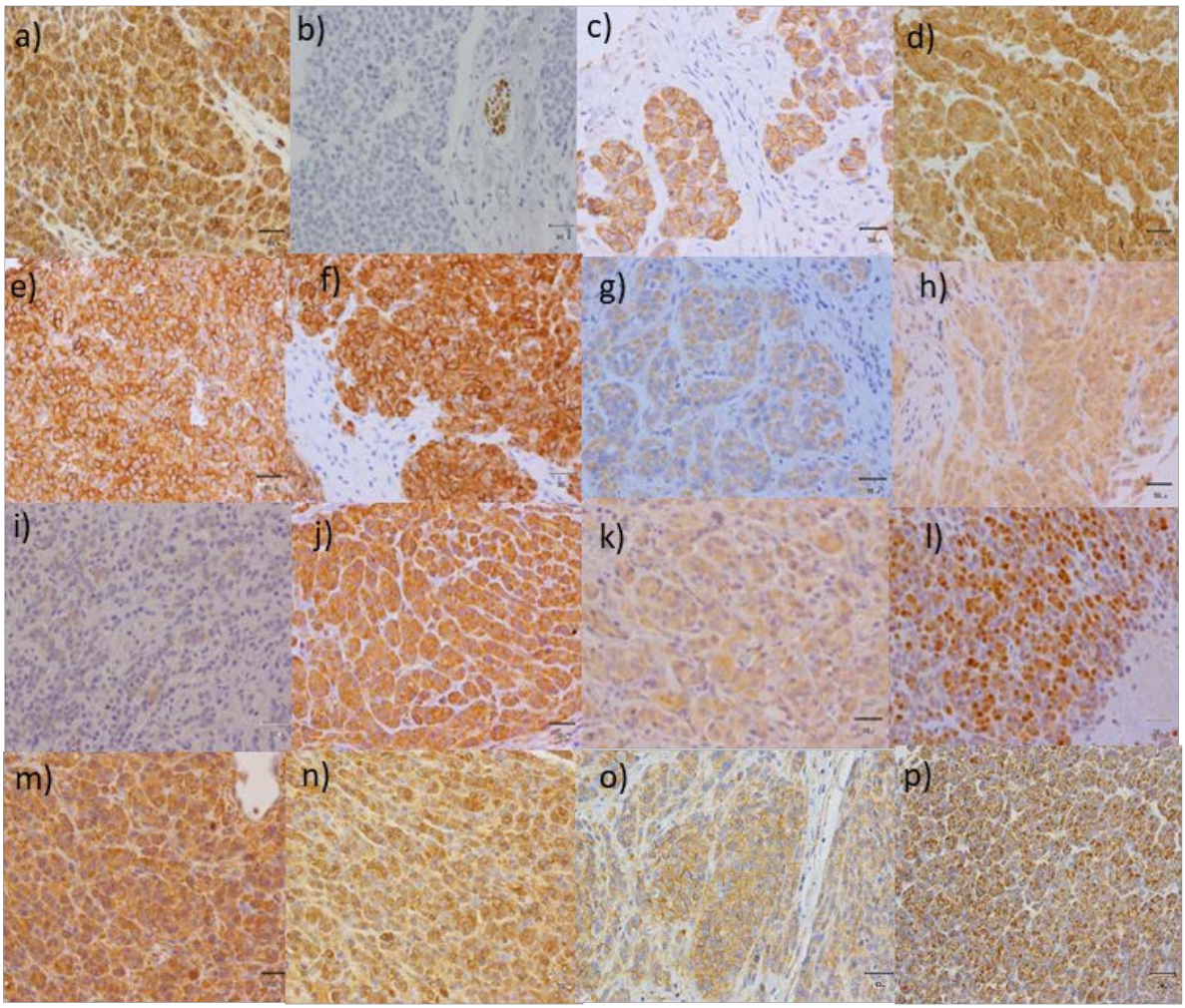

Figure 11. DFT1 strains 1-5 - Schwann cell lineage immunohistochemistry.

Representative photomicrographs: PMP22 Strain 1 **a**, MBP Strain 1 **b**, MPZ Strain 1 **c**, MAG Strain 2 **d**, NGFR Strain 2 **e**, PRX Strain 2 **f**, GFAP Strain 3 **g**, PLP1 Strain 3 **h**, GAP43 Strain 3 **i**, RPSA Strain 4 **j**, GJB1 Strain 3 **k**, S100 Strain 2 **l**, VIM Strain 1 **m**, NOTCH1 Strain 2 **n**, CTNNB1 Strain 1**o**, SHH Strain 1 **p**. All micrographs are x40 magnification and scale bar represents 30 microns.

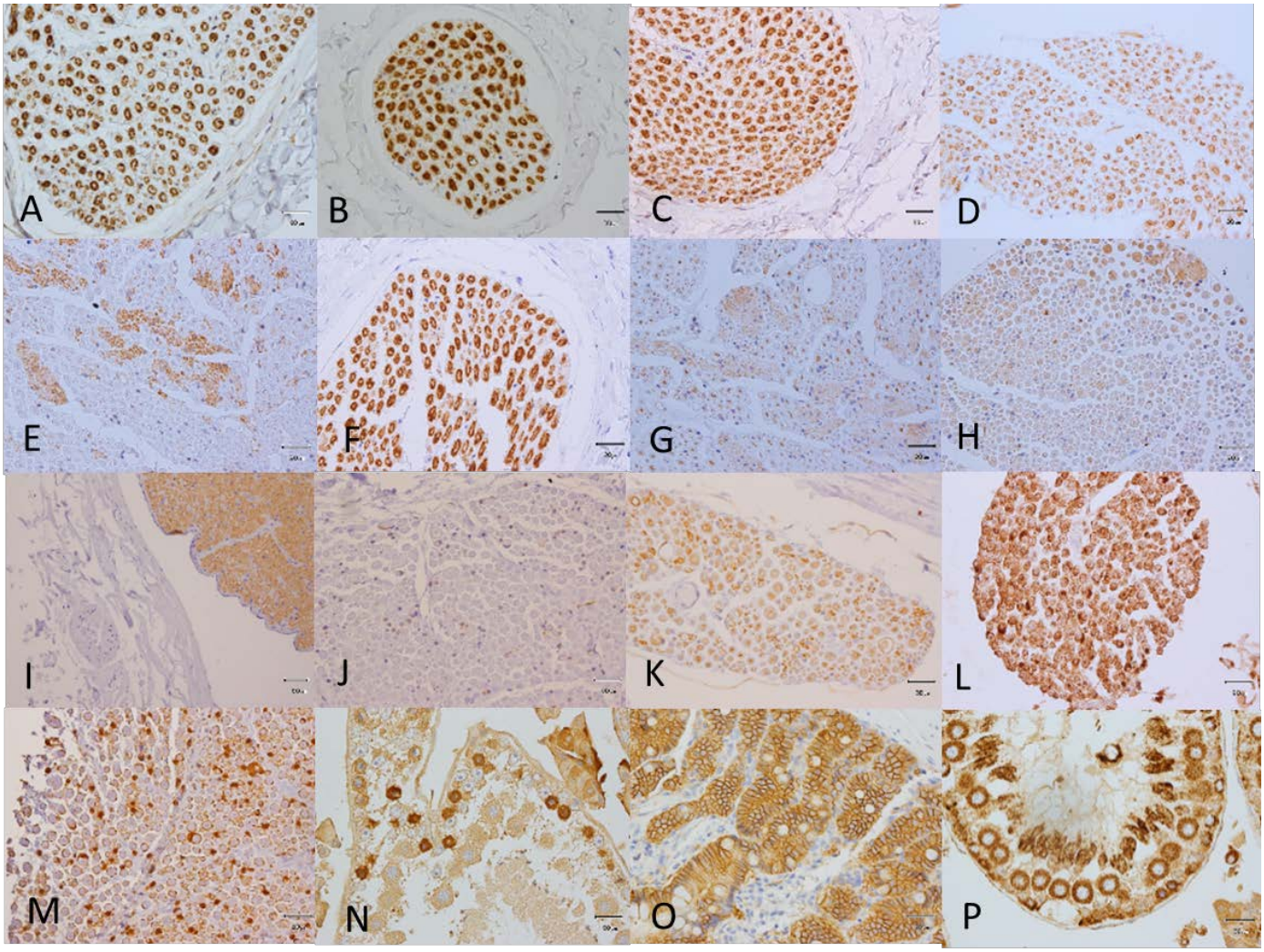

Figure 12: DFT1 strains 1-5 - Schwann cell lineage immunohistochemistry control tissue.

PMP22 **A** peripheral nerve, MBP **B** peripheral nerve, MPZ **C** peripheral nerve, MAG **D** peripheral nerve, NGFR **E** peripheral nerve non-myelinating Schwann cells, PRX **F** peripheral nerve, GFAP **G** peripheral nerve non-myelinating Schwann cells, PLP1 **H** peripheral nerve, GAP43 **I** optic nerve positive and adjacent peripheral nerve, RPSA **J** peripheral nerve, GJB1 **K** peripheral nerve, S100 **L** peripheral nerve, VIM **M** peripheral nerve, NOTCH1 **N** testis, CTNNB1 **O** intestine, SHH **P**, testis. All controls are Tasmanian devil tissues. All micrographs are x40 magnification and scale bar represents 30 microns

DFT1 strains 1-5 Schwann cell lineage immunohistochemical results documented in figures 8, 9 and table 3 demonstrates that most Schwann cell markers had similar expression and intensity of staining between strains with some exceptions noted. PMP22 (moderate to strong cytoplasmic and membranous S1 95%, S2 90%, S3 75%, S4 95%, S5 95%) demonstrated only 75 percent of cells in strain 3 were positive compared to other strains averaging 94%. MBP was not detected in any of

the strains however, as shown in micrograph figure 11b, MBP is clearly detectible in normal peripheral nerve but is absent in surrounding tumour cells. MPZ (weak cytoplasmic and membranous S1 22%, S2 31%, S3 51%, S4 48%, S5 50%), GFAP (weak to moderate cytoplasmic and membranous S1 49%, S2 42%, S3 28%, S4 52%, S5 65%) and S100 (moderate cytoplasmic and nuclear S1 50%, S2 56%, S3 51%, S4 39%, S5 35%) all demonstrated some variation in strain expression. Interestingly GAP43 was only expressed in strain 3 and therefore suggests that GAP43 may be an indicator of strain 3.

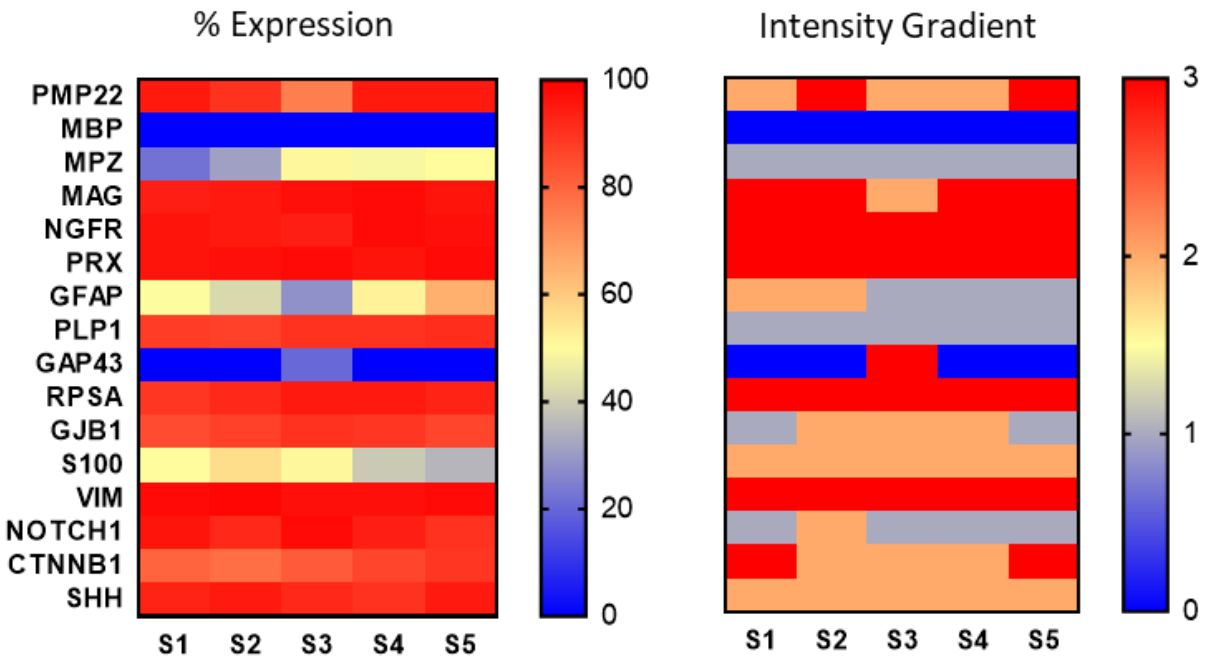

Figure 13: DFT1 strains 1-5 - Schwann cell lineage immunohistochemistry Heat maps.

Demonstration of percentage expression (0-100%) and intensity gradient of staining (0-3).

As described above, the heat maps in figure 13 illustrate varied percent expression by PMP22, MPZ, GFAP, and S100. GAP43 illustrates expression in strain 3 only and MBP is not expressed by any strain. There is some mild variation of staining intensity between strains noted.

Strain Variation (percent expression)																
Strains	PMP22	MBP	MPZ	MAG	NGFR	PRX	GFAP	PLP1	GAP43	RPSA	GJB1	S100	VIM	NOTCH1	CTNNB1	SHH
S1 vs. S2	NS	NS	NS	NS	NS	NS	NS	NS	NS	NS	NS	NS	NS	NS	NS	NS
S1 vs. S3	*	NS	**	NS	NS	NS	*	NS	*	NS	NS	NS	NS	NS	NS	NS
S1 vs. S4	NS	NS	*	NS	NS	NS	NS	NS	NS	NS	NS	NS	NS	NS	NS	NS
S1 vs. S5	NS	NS	**	NS	NS	NS	NS	NS	NS	NS	NS	NS	NS	NS	NS	NS
S2 vs. S3	NS	NS	*	NS	NS	NS	NS	NS	*	NS	NS	NS	NS	NS	NS	NS
S2 vs. S4	NS	NS	NS	NS	NS	NS	NS	NS	NS	NS	NS	NS	NS	NS	NS	NS
S2 vs. S5	NS	NS	NS	NS	NS	NS	*	NS	NS	NS	NS	*	NS	NS	NS	NS
S3 vs. S4	*	NS	NS	NS	NS	NS	*	NS	*	NS	NS	NS	NS	NS	NS	NS
S3 vs. S5	*	NS	NS	NS	NS	NS	***	NS	*	NS	NS	NS	NS	NS	NS	NS
S4 vs. S5	NS	NS	NS	NS	NS	NS	NS	NS	NS	NS	NS	NS	NS	NS	NS	NS

Devil strains number S1-S5. NS- non-significant *p<0.05, **p<0.01, ***p<0.001

Figure 14: DFT1 strains 1-5 - Schwann cell lineage immunohistochemistry strain variation.

Significance of percent expression between strains.

We compared the percentage expression of each of DFT1 strains 1-5 for each antibody for any significant differences (figure 14) finding *p<0.05 = PMP22 strain 1 vs 3, 3 vs 4, 3 vs 5. MPZ 1 vs 4, 2 vs 3. GFAP 1 vs 3, 2 vs 5, 3 vs 4. GAP43 1 vs 3, 2 vs 3, 3 vs 4 and 3 vs 5. S100 2 vs 5. **p<0.01 MPZ 1 vs 3 and 1 vs 5. ***p<0.001 GFAP 3 VS 5. There was no significant difference between other strains. These differences were also reflected in the heat maps.

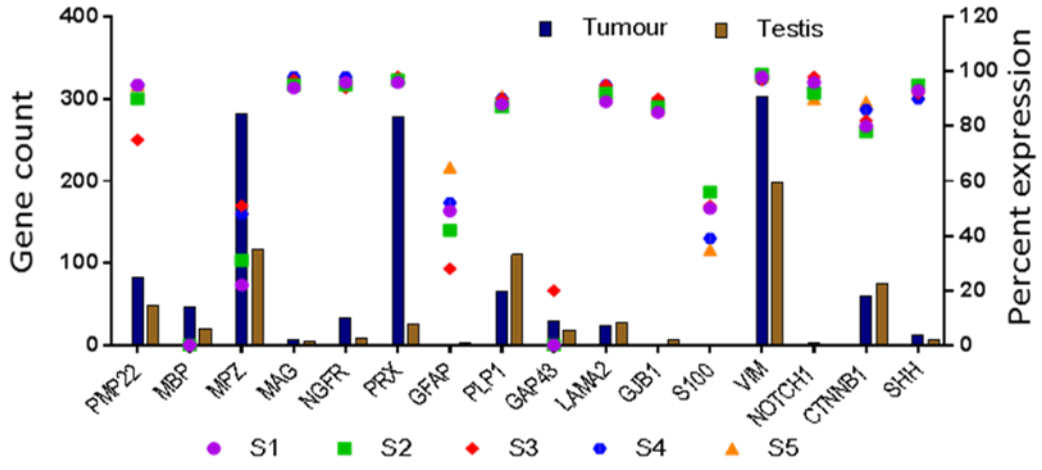

Figure 15: DFT1 strains 1-5 - Schwann cell lineage immunohistochemistry comparative analysis.

Graphical representation of gene counts vs protein expression.

Comparative analysis of gene counts and protein expression of Schwann cell lineage was compared in table 4 and graphically represented in figure 15. Active genes *PMP22*, *MBP*, *PLP1*, *MPZ*, *PRX*, *GAP43*, *LAMA2*, *NGFR*, *VIM*, *CTNNB1* and *SHH* have gene activity with corresponding protein expression except for *MBP* where protein expression is completely absent. Although *MPZ* gene activity is high, only 22%-50% of cells express MPZ weakly. *GAP43* gene activity was expressed only in strain 3 suggesting this marker may indeed be specific for strain 3. Further, the Tasmanian devil tumour used by Murchison et al. (4) to obtain the gene abundance data was actually strain 3 tumour (DH, personal communication, Elizabeth Murchison) correlating the two results but this does not exclude other stains at this stage. Low activity genes *MAG*, *GFAP*, *GJB1* and NOTCH1 showed MAG, GJB1 and NOTCH1 was expressed in most cells with GFAP expression ranging from 28% in strain 3 to 65% in strain 5.

4.4.4 DFT1 strains 1-5 - Schwann cell lineage growth factor immunohistochemistry

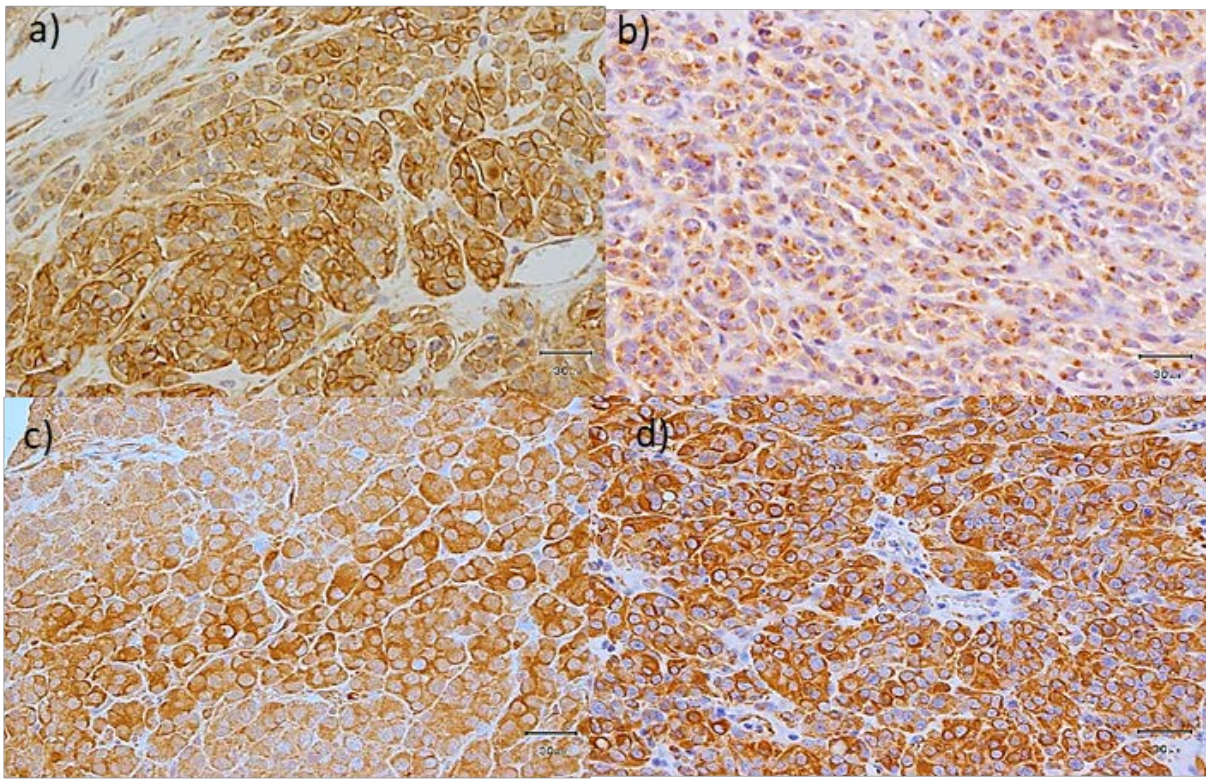

Figure 16: DFT1 strains 1-5 Schwann cell lineage growth factor immunohistochemistry.

Representative micrographs: PDGFB Strain 3 a, IGFR2 Strain 3 b, TGFBR2 Strain 1 c, VEGFA Strain 2 d. All micrographs are x40 magnification and scale bar represents 30 microns.

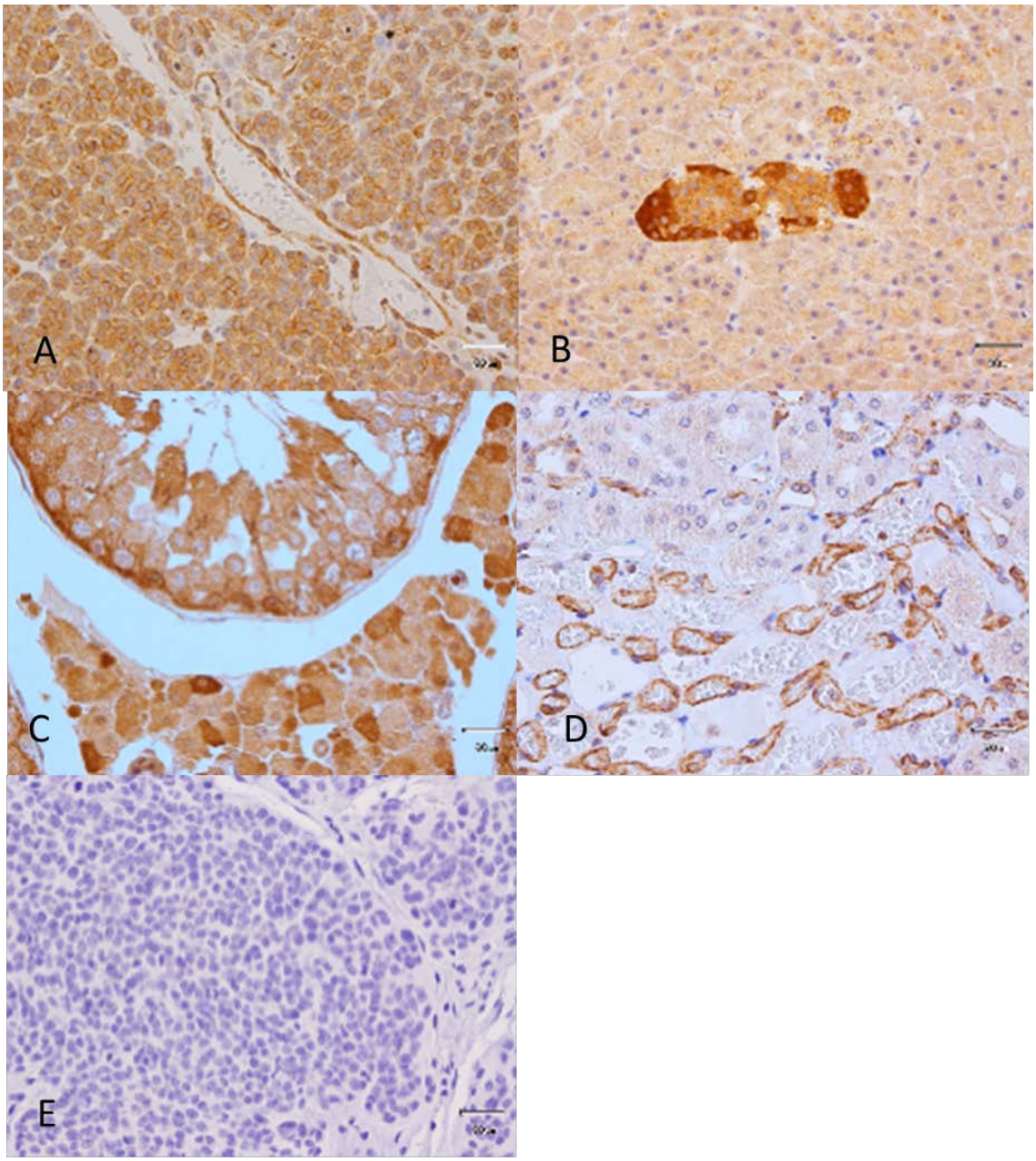

Figure 17: DFT1 strains 1-5 Schwann cell lineage growth factor immunohistochemistry control tissue.

PDGFB A intra tumoural blood vessel, IGFR2 B pancreatic islet, TGFBR2 C testis, VEGFA D kidney. All controls are Tasmanian devil tissues. All micrographs are x40 magnification and scale bar represents 30 microns.

Assessment of the immunohistochemical staining of Schwann cell lineage growth factor markers represented in figures 8, 9 and table 3 show that most growth factors had similar expression and intensity of staining with one noted exception. PDGFB (Strong cytoplasmic and membranous (S1

93%, S2 70%, S3 85%, S4 82%, S5 85%) which demonstrated increased positivity in strain 1 compared to other strains with strain 2 showing less positivity than the other strains.

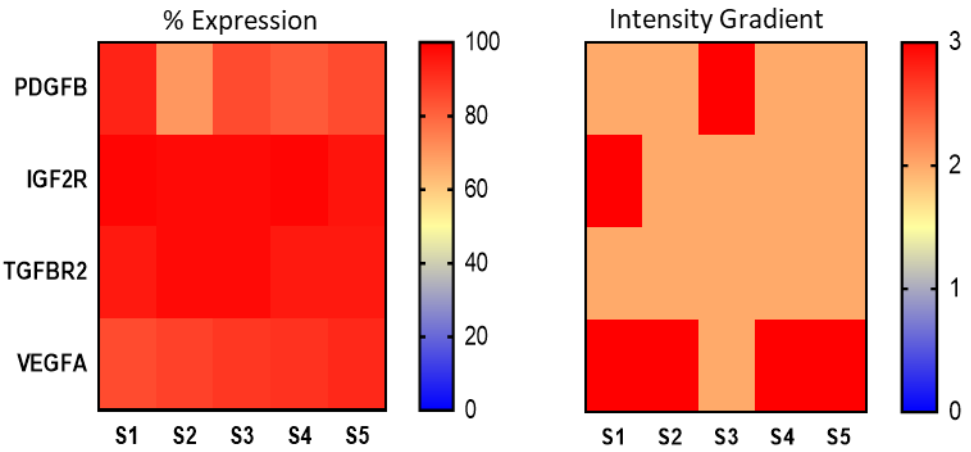

Figure 18: DFT1 strains 1-5 Schwann cell lineage growth factor immunohistochemistry heat maps.

Demonstrating percentage expression (0-100%) and Heat map intensity gradient of staining (0-3).

As described above in figure 18, the heat maps illustrate varied percent expression by PDGFB with some mild variation in staining intensity noticed.

Strain Variation (percent expression)				
Strains	PDGFB	IGF2R	TGFBR2	VEGFA
S1 vs. S2	**	NS	NS	NS
S1 vs. S3	NS	NS	NS	NS
S1 vs. S4	NS	NS	NS	NS
S1 vs. S5	NS	NS	NS	NS
S2 vs. S3	*	NS	NS	NS
S2 vs. S4	NS	NS	NS	NS
S2 vs. S5	*	NS	NS	NS
S3 vs. S4	NS	NS	NS	NS
S3 vs. S5	NS	NS	NS	NS
S4 vs. S5	NS	NS	NS	NS

Devil strains number S1-S5. NS- non-significant *p<0.05, **p<0.01, ***p<0.001

Figure 19: DFT1 strains 1-5 Schwann cell lineage growth factor immunohistochemistry strain variation.

Significance of percent expression between strains.

We compared the percentage expression of each of DFT1 strains 1-5 for each antibody for any significant differences (figure 19) finding *p<0.05 = PDGFRB strain 2 vs 3, 2 vs 5, 3 vs 5. **p<0.01 PDGFRB 1 vs 2. This difference was also reflected in the heat maps of figure 18. There was no significant difference between other strains.

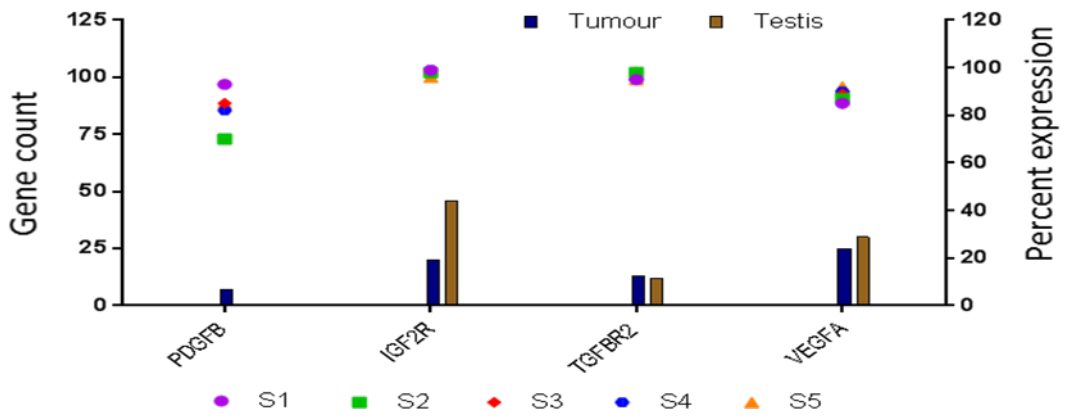

Figure 20: DFT1 strains 1-5 Schwann cell lineage growth factor immunohistochemistry comparative analysis.

Graphical representation of gene counts vs protein expression.

Comparative analysis of gene counts and protein expression of Schwann cell lineage growth factors was compared in table 4 and graphically represented in figure 20. Active genes *IGF2R*, *TGFBR2* and *VEGFA* have gene activity with corresponding protein expression. Gene activity for *PDGFB* was low but the majority of DFT1 cells expressed this protein.

4.4.5 DFT1 strains 1-5 Melanocyte lineage immunohistochemistry

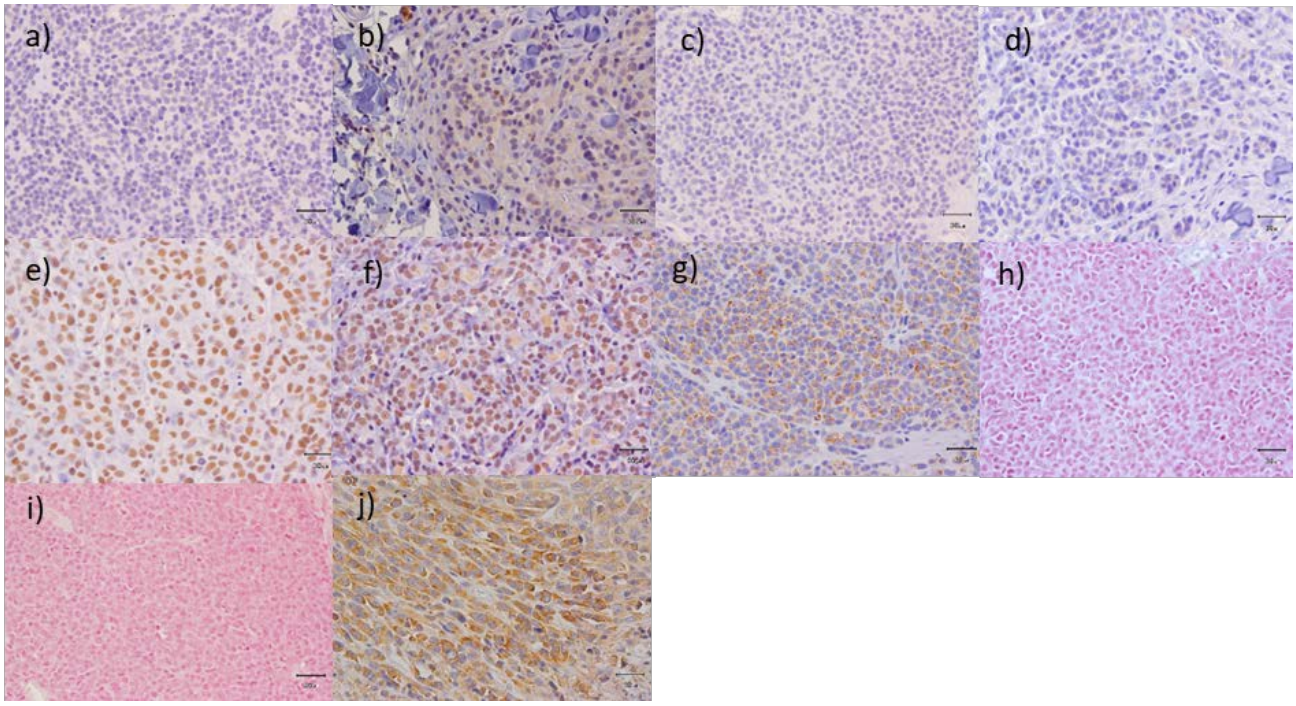

Figure 21: DFT1 strains 1-5 Melanocyte lineage immunohistochemistry.

Representative micrographs. MITF Strain 1 **a**, Occasional MITF nuclear positivity Strain 5 **b**, TYR Strain 1 **c**, occasional TYR cytoplasmic staining Strain 3 **d**, MLANA Strain 5 **e,** occasional MLANA cytoplasmic staining Strain 3 **f**, PNL2 Strain 4 **g**, Schmorl's stain Strain 4 **h**, Masson Fontana stain Strain 4 **i**, KIT Strain 3 **j**. All micrographs are x40 magnification and scale bar represents 30 microns.

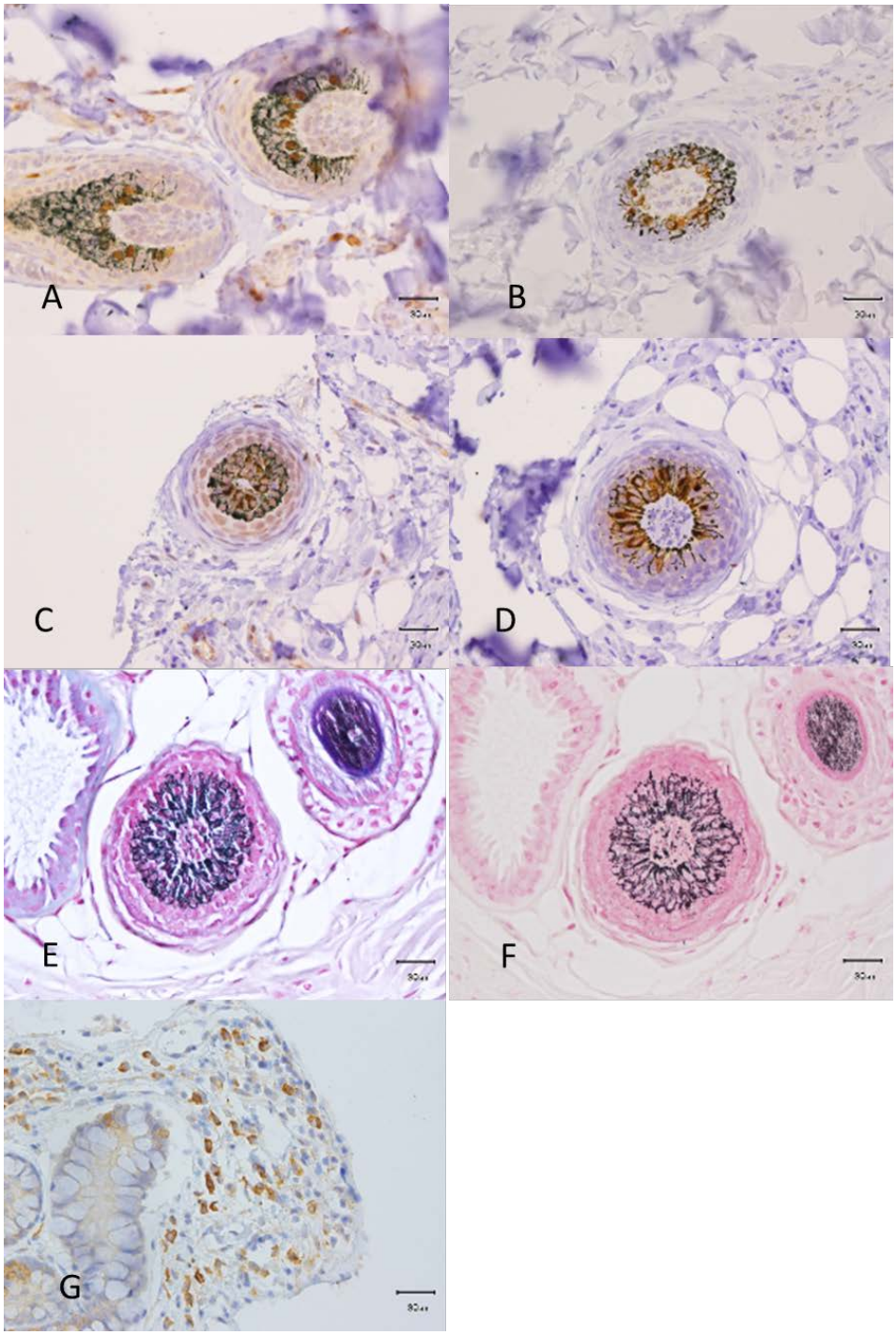

Figure 22: DFT1 strains 1-5 Melanocyte lineage immunohistochemistry control tissues.

MITF **A**, TYR B, MLANA **C,** PNL2 **D**, Schmorl's stain **E**, Masson Fontana stain **F**, KIT **G**. All controls are Tasmanian devil hair bulb tissues except for G which is intestinal mast cells. All micrographs are x40 magnification and scale bar represents 30 microns

DFT1 strains 1-5 melanocyte lineage immunohistochemical results documented in figures 8, 9 and table 3 demonstrates that Melanocyte lineage markers MITF, TYR and MLANA was not expressed

by DFT1 (figures 21a, c, e). However, on very intense screening of entire tumours very occasional isolated cells did show; MITF nuclear positivity figure 21b, TYR cytoplasmic staining figure 21d and cytoplasmic MLANA staining figure 21f. PNL2 figure 21G, demonstrated varied granular cytoplasmic staining of cells (8 % strain 1, 47 % strain 2, 12 % strain 3, 96 % strain 4 and 10 % strain 5). No expression was present for either the Schmorl's stain or Masson Fontana stain for melanin, as expected in this non-pigmented tumour.

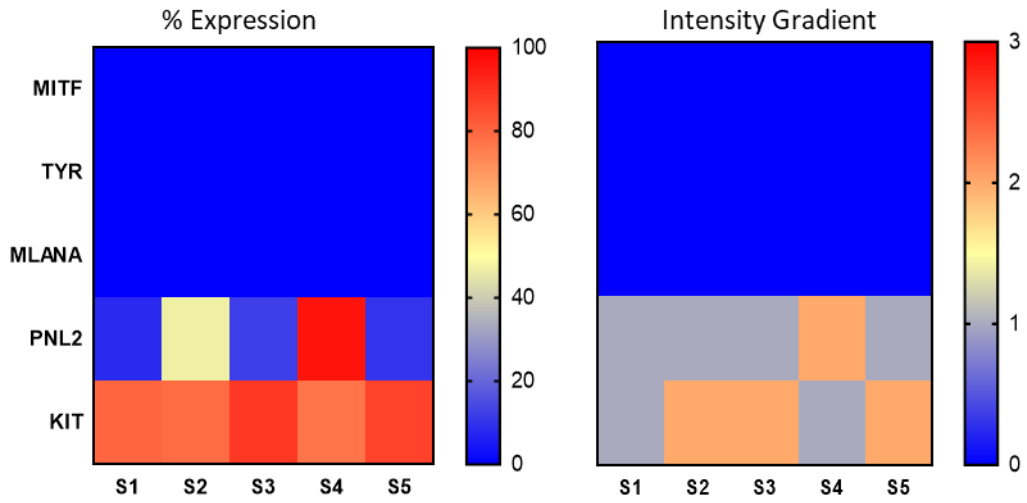

Figure 23: DFT1 strains 1-5 Melanocyte lineage immunohistochemistry heat maps.

Heat map Demonstrating percentage expression (0-100%) and intensity gradient of staining (0-3).

As described above in figure 23, the heat maps illustrate varied percent expression by PNL2 with some mild variation in staining intensity noticed. MITF, TYR and MLANA were essentially negative. Slight variation in intensity was noticed for KIT and PNL2.

Strain Variation (percent expression)					
Strains	**MITF**	**TYR**	**MLANA**	**PNL2**	**KIT**
S1 vs. S2	NS	NS	NS	NS	NS
S1 vs. S3	NS	NS	NS	NS	NS
S1 vs. S4	NS	NS	NS	**	NS
S1 vs. S5	NS	NS	NS	NS	NS
S2 vs. S3	NS	NS	NS	NS	NS
S2 vs. S4	NS	NS	NS	NS	NS
S2 vs. S5	NS	NS	NS	NS	NS
S3 vs. S4	NS	NS	NS	**	NS
S3 vs. S5	NS	NS	NS	NS	NS
S4 vs. S5	NS	NS	NS	**	NS

Devil strains number S1-S5. NS- non-significant *p<0.05, **p<0.01, ***p<0.001

Figure 24: DFT1 strains 1-5 Melanocyte lineage immunohistochemistry strain variation.

Percentage expression significant difference between DFT1 strains 1-5.

We compared the percentage expression of each of DFT1 strains 1-5 for each antibody for any significant differences (figure 24) finding **p<0.01 PNL2 1 vs 4, 3 vs 4, 4 vs 5. There was no significance difference between other strains.

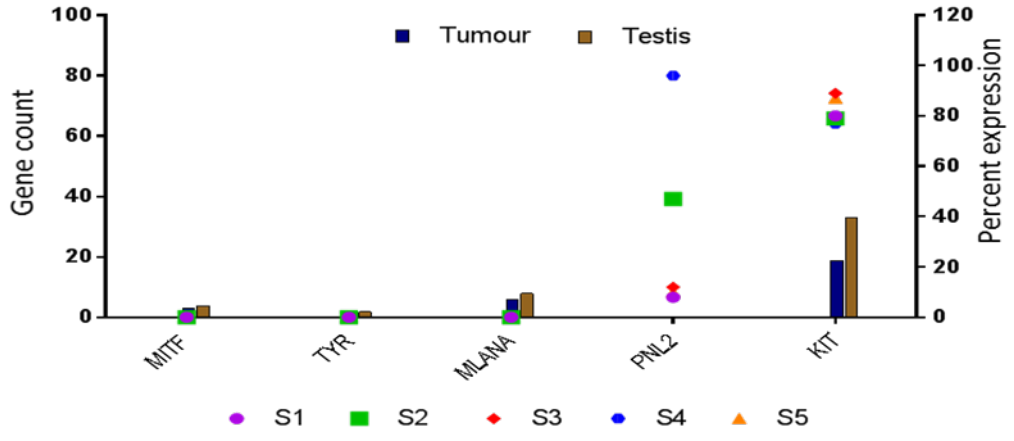

Figure 25: DFT1 strains 1-5 Melanocyte lineage immunohistochemistry comparative analysis.

Graphical representation of gene counts vs protein expression.

Comparative analysis of gene counts and protein expression of melanocyte lineage was compared in table 4 and graphically represented in figure 25 graphically. Activity was low or absent for genes *TYR*, *MLANA* and *MITF* with corresponding absence of cellular expression of these proteins in DFT1. *KIT* gene was active and was expressed in most DFT1 cells.

4.4.6 DFT1 strains 1-5 Schwann cell and Melanocyte lineage transcription factor immunohistochemistry

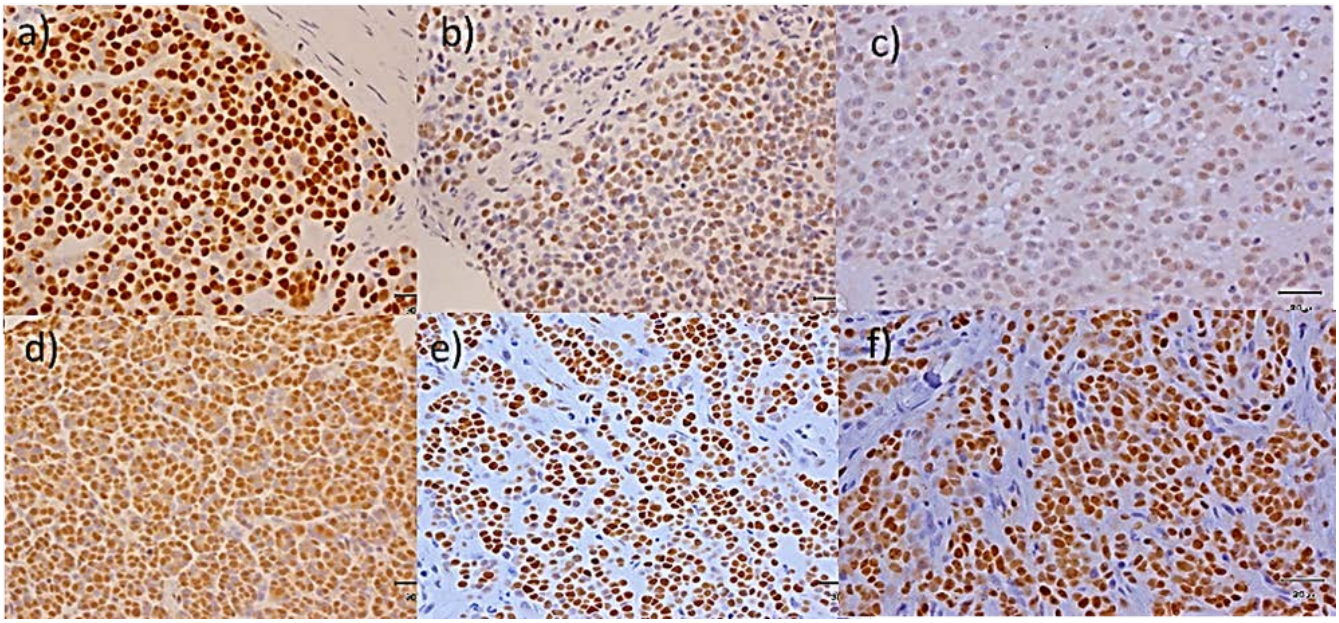

Figure 26: DFT1 strains 1-5 Schwann cell and Melanocyte lineage transcription factors immunohistochemistry.

Schwann cell and Melanocyte lineage transcription factor immunohistochemistry: SOX10 Strain 2 **a**. SOX2 Strain 2 **b**. EGR2 Strain 2 **c**. PAX3 Strain 3 **d**. JUN Strain 1 **e**. TFAP2A Strain 4 **f**. All micrographs are x40 magnification and scale bar represents 30 microns.

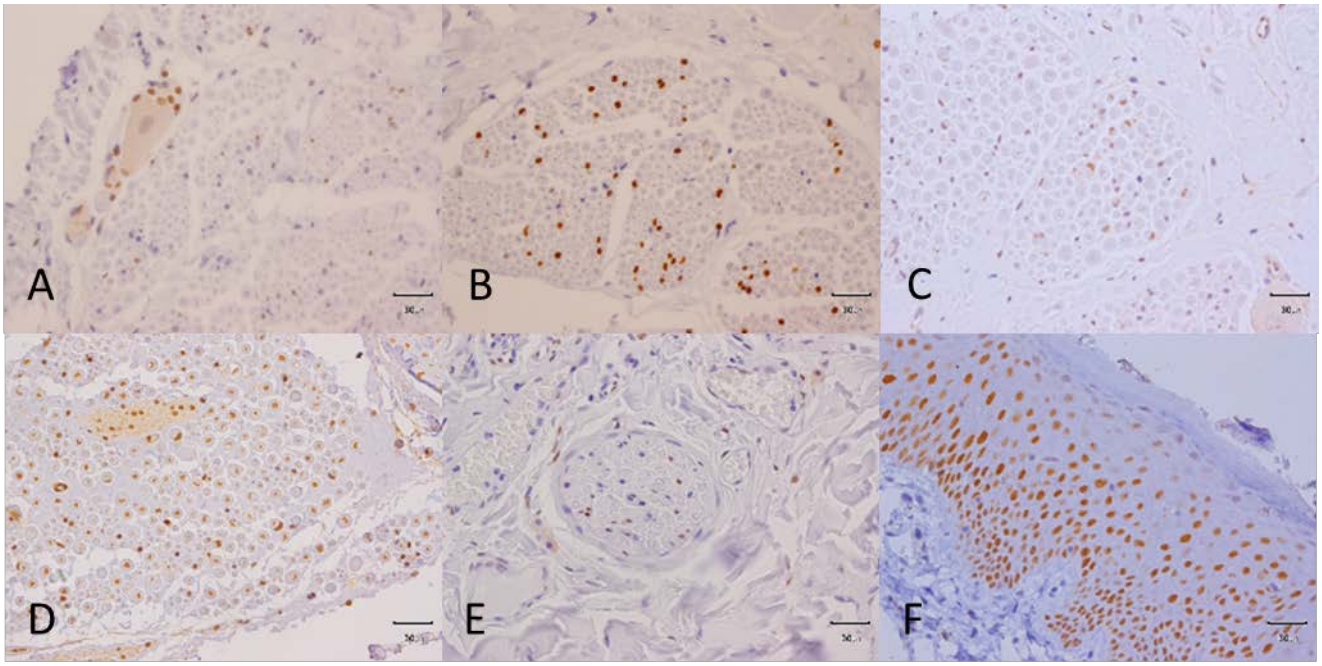

Figure 27: DFT1 strains 1-5 Schwann cell and Melanocyte lineage transcription factor immunohistochemistry control tissues.

Schwann cell and Melanocyte lineage transcription factor immunohistochemistry control tissues: SOX10 A. SOX2 B. EGR2 C, PAX3 D. JUN E. TFAP2A F. All controls are Tasmanian devil peripheral nerve tissues except for F, which is skin. All micrographs are x40 magnification and scale bar represents 30 microns.

DFT1 strains 1-5 Schwann cell and melanocyte lineage immunohistochemical results documented in figures 8, 9 and table 3 demonstrates that most Schwann cell and transcription factor markers had similar expression and intensity of staining between strains with two exceptions, as noted. SOX2 (moderate nuclear S1 90%, S2 84%, S3 83%, S4 50%, S5 36%) and ERG2 (weak nuclear S1 80%, S2 78%, S3 50%, S4 68%, S5 91%).

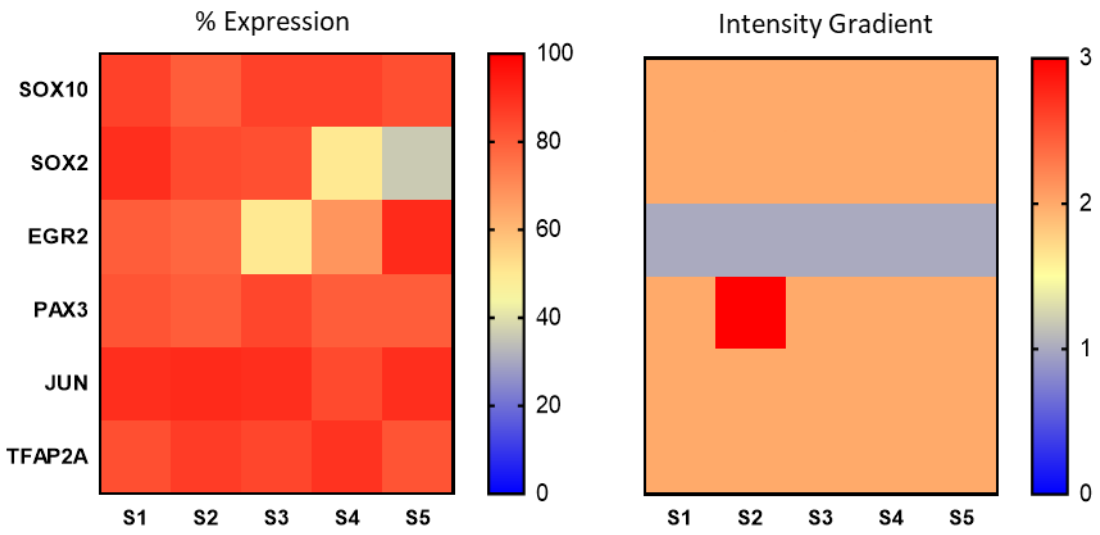

Figure 28: DFT1 strains 1-5 Schwann cell and Melanocyte lineage transcription factor immunohistochemistry Heat maps.

Demonstrating percentage expression (0-100%) and intensity gradient of staining (0-3).

As described above in figure 28 the heat maps illustrate varied percent expression by SOX2 and ERG2. There is some mild variation of staining intensity between strains noted.

Strain Variation (percent expression)

Strains	SOX10	SOX2	EGR2	PAX3	JUN	TFAP2A
S1 vs. S2	NS	NS	NS	NS	NS	NS
S1 vs. S3	NS	NS	NS	NS	NS	NS
S1 vs. S4	NS	*	NS	NS	NS	NS
S1 vs. S5	NS	**	NS	NS	NS	NS
S2 vs. S3	NS	NS	NS	NS	NS	NS
S2 vs. S4	NS	NS	NS	NS	NS	NS
S2 vs. S5	NS	*	NS	NS	NS	NS
S3 vs. S4	NS	NS	NS	NS	NS	NS
S3 vs. S5	NS	*	*	NS	NS	NS
S4 vs. S5	NS	NS	NS	NS	NS	NS

Devil strains number S1-S5. NS- non-significant *p<0.05, **p<0.01, ***p<0.001

Figure 29: DFT1 strains 1-5 Schwann cell and Melanocyte lineage transcription factor immunohistochemistry strain variation.

Percentage expression significant difference between strains.

We compared the percentage expression of each of DFT1 strains 1-5 for each antibody for any significant differences (figure 29) finding *p<0.05 = SOX2 strain 1 vs 4, 2 vs 5, 3 vs 5. ERG2 strain 3 vs 4. **p<0.01 SOX2 strain 1 vs 5. Evident here by a lower percentage of staining cells of strain 3 (50%) and strain 4 (34%). There was no significant difference between other strains.

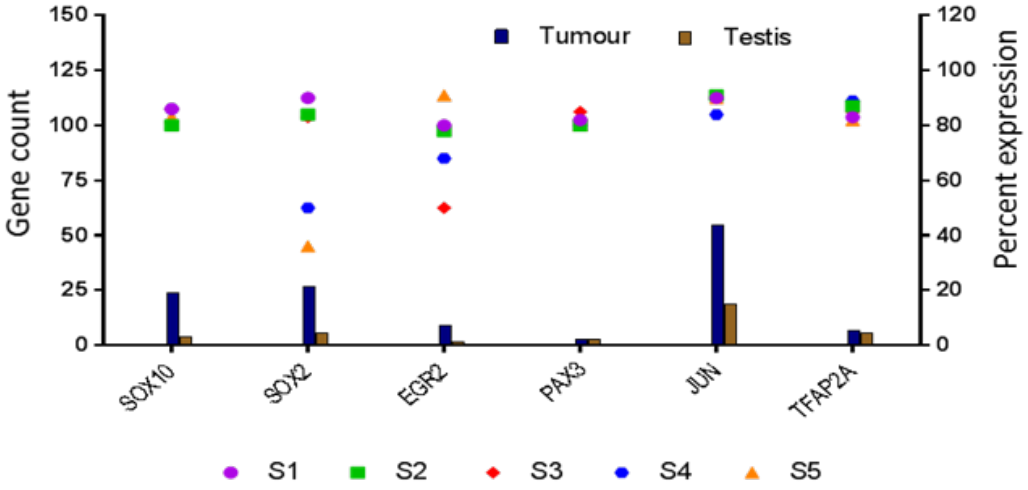

Figure 30: DFT1 strains 1-5 Schwann cell and Melanocyte lineage transcription factor immunohistochemistry comparative analysis.

Gene counts and protein expression of Transcription factors

Comparative analysis of gene counts and protein expression of Schwann cell and melanocyte lineage transcription factors (table 4) was compared graphically (figure 30). Active genes *SOX10*, *SOX2* and *JUN* show gene activity with corresponding protein expression. Low activity genes *EGR2*, *PAX3* and *TFAP2A* expressed these proteins moderately in most cells, although EGR2 weakly.

4.4.7 DFT1 strains 1-5 Stem cell and multipotency marker immunohistochemistry

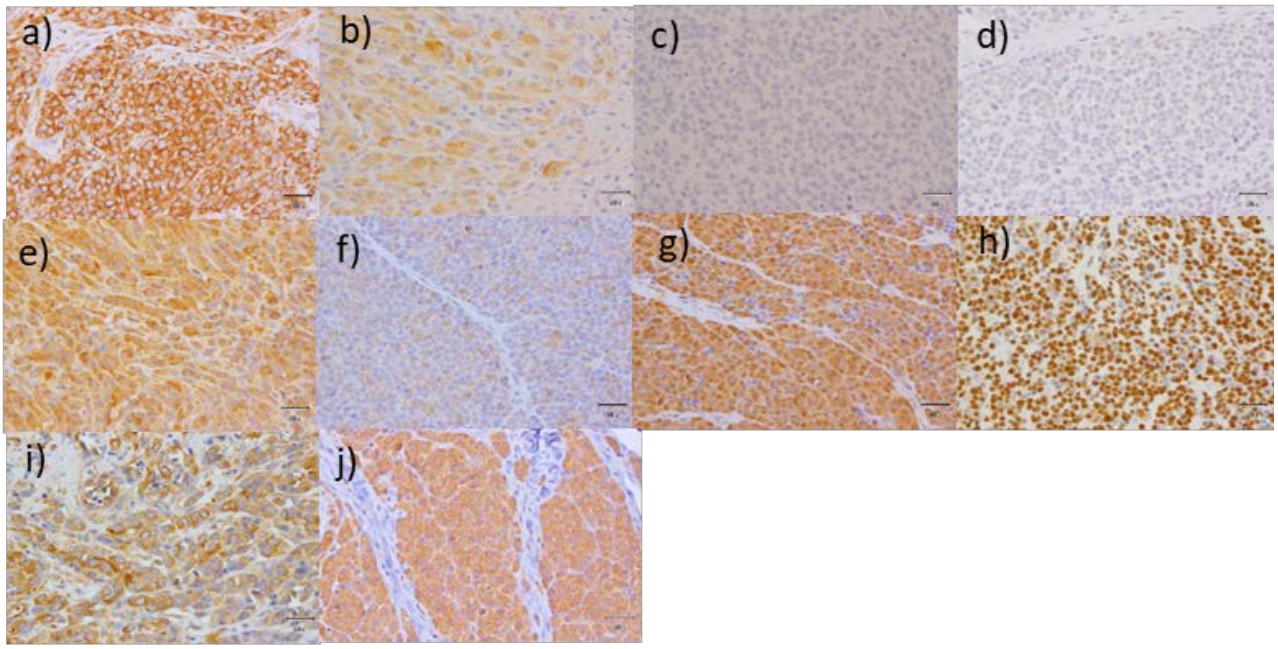

Figure 31: DFT1 strains 1-5 Stem cell and multipotency marker immunohistochemistry.

Representative micrographs. ENO2 Strain 3 a. UCHL1 Strain 3 b. CALB2 Strain 4 c. Neurofilament protein (pan-NEFL, NEFM, NEFH) Strain 2 d. PROM1 Strain 3 e. CD44 Strain 4 f. STAT3 Strain 4 g. POU5F1 Strain 2 h. NES Strain 3 i. EPCAM Strain 1 j. All micrographs are x40 magnification and scale bar represents 30 microns.

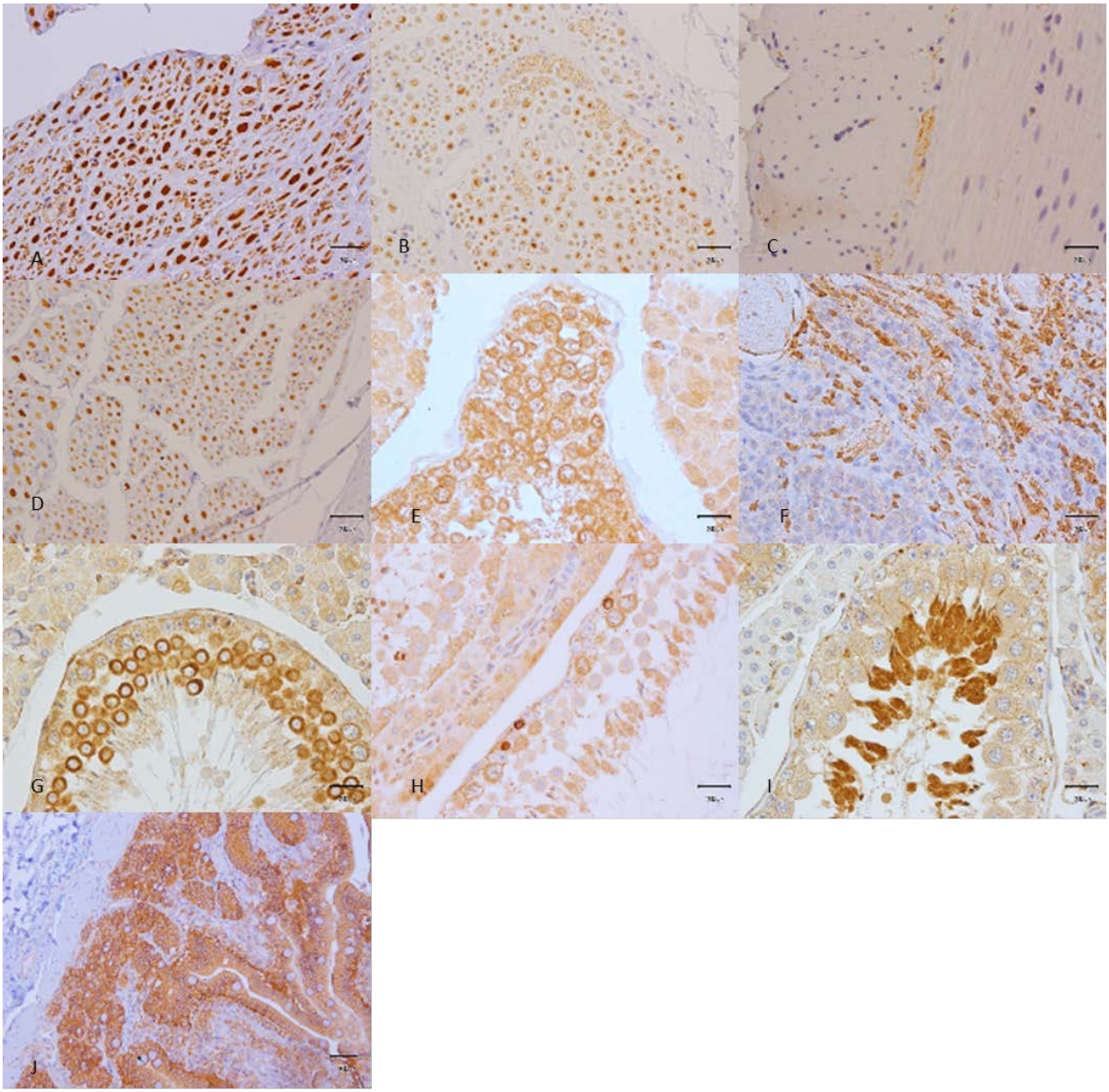

Figure 32: DFT1 strains 1-5 Stem cell and multipotency marker immunohistochemistry control tissues.

ENO2 **A** peripheral nerve. UCHL1 peripheral nerve **B**. CALB2 intestine **C**. NF (H/M/L) peripheral nerve **D**. PROM1 **E** testis. CD44 **F** lymph node. STAT3 **G** testis. POU5F1 **H** testis. NES **I** testis, EPCAM **J** intestine. All controls are Tasmanian devil tissues. All micrographs are x40 magnification and scale bar represents 30 microns.

Assessment of the immunohistochemical staining of stem cell and multipotency immunohistochemistry markers represented in figures 8, 9 and table 3 show that most growth factors had similar expression and intensity of staining with two exceptions. UCHL1 (weak to

moderate cytoplasmic S1 73%, S2 85%, S3 78%, S4 45%, S5 75%) demonstrates some expression between strains, particularly strain 4, with only 45% of cells positive. CD44 (weak membranous S1 77%, S2 81%, S3 85%, S4 75%, S5 72%) and NES (weak to moderate cytoplasmic (S1 91%, S2 92%, S3 96%, S4 79%, S5 88%) demonstrated minor expression between strains. CALB2 and NEFM/H was not expressed by DFT1.

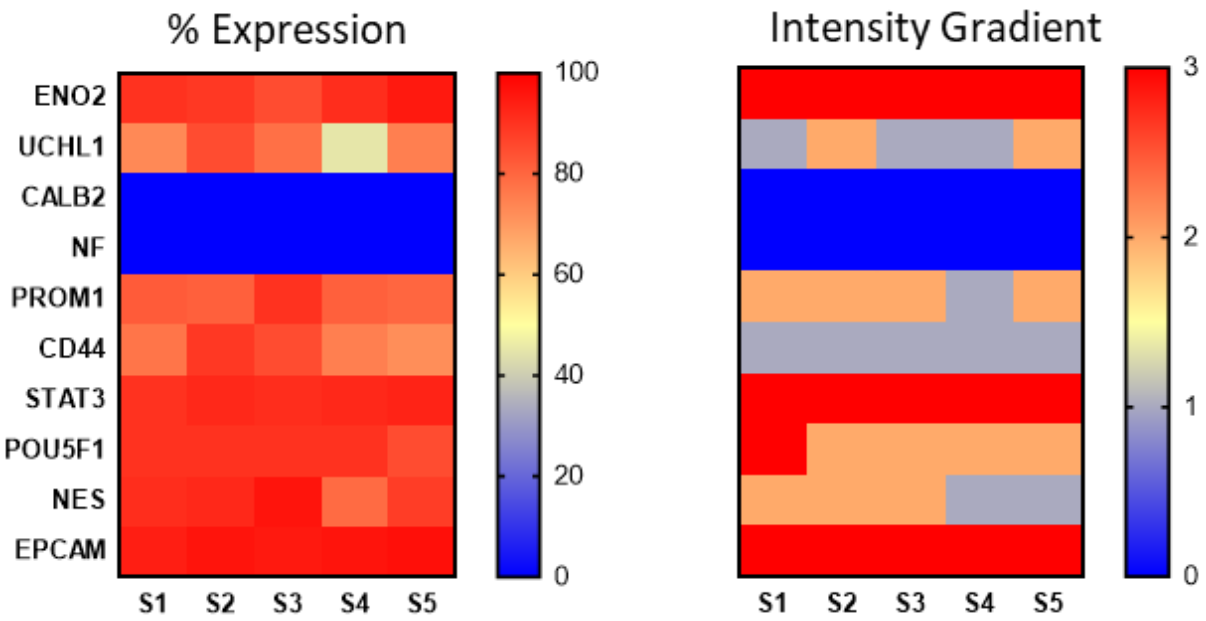

Figure 33: DFT1 strains 1-5 Stem cell and multipotency marker immunohistochemistry heat maps.

Percentage expression (0-100%) and heat map intensity gradient of staining (0-3).

Figure 33, UCHL1 shows obvious variation between strains whereas CD44 and NES show minor variation between strains

Strain Variation (percent expression)										
Strain	NSE	UCHL1	CALB2	NF	CD 133	CD44	STAT3	OCT4	NES	EPCAM
S1 vs. S2	NS	NS	NS	NS	NS	NS	NS	NS	NS	NS
S1 vs. S3	NS	NS	NS	NS	NS	NS	NS	NS	NS	NS
S1 vs. S4	NS	***	NS	NS	NS	NS	NS	NS	NS	NS
S1 vs. S5	NS	NS	NS	NS	NS	NS	NS	NS	NS	NS
S2 vs. S3	NS	NS	NS	NS	NS	NS	NS	NS	NS	NS
S2 vs. S4	NS	***	NS	NS	NS	NS	NS	NS	NS	NS
S2 vs. S5	NS	NS	NS	NS	NS	*	NS	NS	NS	NS
S3 vs. S4	NS	***	NS	NS	NS	NS	NS	NS	NS	NS
S3 vs. S5	NS	NS	NS	NS	NS	NS	NS	NS	*	NS
S4 vs. S5	NS	***	NS	NS	NS	NS	NS	NS	NS	NS

Devil strains number S1-S5. NS- non-significant *p<0.05, **p<0.01, ***p<0.001

Figure 34: DFT1 strains 1-5 Stem cell and multipotency marker immunohistochemistry strain variation.

Percentage expression significant difference between strains.

We compared the percentage expression of each of DFT1 strains 1-5 for each antibody for any significant differences (figure 34) finding *p<0.05 CD44 2 vs 5 and NES 3 vs 5, ***p<0.001 UCHL1 1 v 4, 2 v 4, 3 v 4, 4 v 5. Evident here by a lower percentage of staining cells by strain 4 (45%). There was no significant difference between other strains.

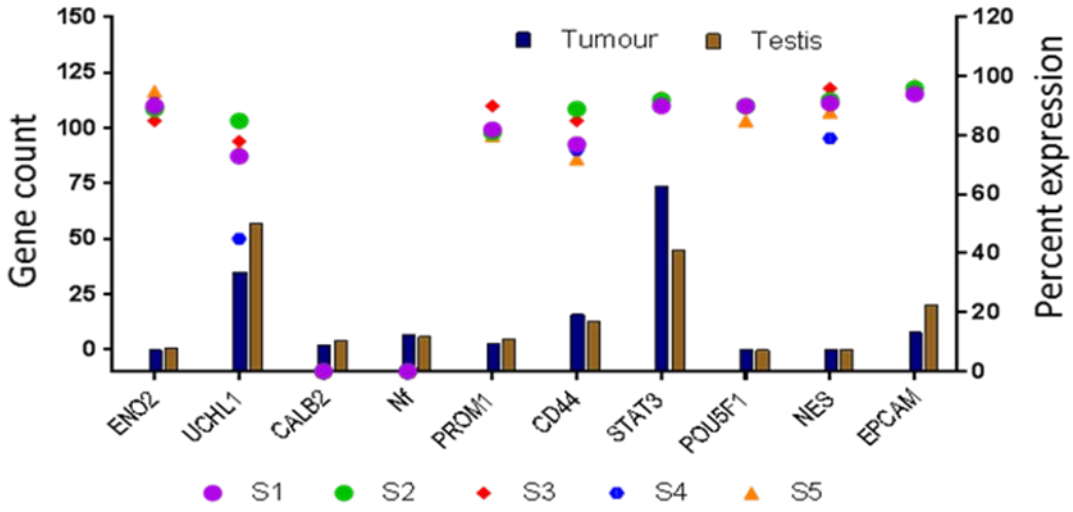

Figure 35: DFT1 strains 1-5 Stem cell and multipotency marker immunohistochemistry comparative analysis.

Gene counts and protein expression stem cell and multipotency markers. All micrographs are x40 magnification and scale bar represents 30 microns.

Comparative analysis of gene counts and protein expression of stem cell and multipotency markers (table 4) was compared graphically (figure 35). Active genes *STAT3*, *CD44* and *UCHL1* show corresponding protein expression. Low activity genes *ENO2*, *EPCAM* and *PROM1* showed protein expression in most DFT1 cells, whereas low activity genes *NEFL*, *NEFM* and *CALB2* were not expressed by DFT1.

4.5 Discussion

Phenotypically, DFT1 expresses both Schwann cell (precursor, immature, mature MSC and NMSC) and melanocyte marker PNL2, suggesting bipotency. The additional expression of Schwann cell autocrine survival factors and transdifferentiating Bungner Schwann cell (repair) markers typifies Schwann cell plasticity. The expression of markers of neural crest stem cells and self-renewal properties suggests DFT1 is a progenitor-like cell. Immunohistochemistry is able to regionalise expression of proteins providing information in addition to molecular gene and protein expression.

We compared Murchison's et al. gene abundance data with our immunohistochemical analysis for concordance finding that most of the active genes were translated into proteins, such as PRX. Several genes with very little activity translated into proteins readily detected by immunohistochemistry, such as MAG. Of particular note was the active *MBP* gene, its protein was not detected, indicating a translation anomaly. GAP43 was the only protein specifically expressed by only one strain, DFT1 strain 3. Gene expression is complex and messenger RNA (mRNA) and the synthesised protein are not always correlated (151). Non-coding RNAs (ncRNAs) such as transfer RNA (tRNA) and ribosomal RNA (rRNA) are key to translation; however the importance of small ncRNAs (sncRNAs) such as short interfering RNAs (siRNAs), microRNAs (miRNAs) and long ncRNAs (lncRNAs) in the regulation of protein translation has received much attention (152). The highly rearranged chromosomes of DFT1 adds yet another level of complexity because the translocation of genes within the stable karyotype will effect gene expression (4, 5, 19, 45, 46). Even though direct comparison of gene and protein expression is extremely difficult given ncRNA modifications, histone modifications, transcription factor binding and three dimensional folding (153, 154) we discuss our results relevant to Schwann cell and melanocyte lineage.

To encapsulate the diversity of these findings I will discuss DFT1 under the following headings;

4.5.1 Schwann cell/melanocyte GRN,
4.5.2 PNL2 antibody,
4.5.3 Bipotent Schwann cell/melanocyte lineage,
4.5.4 The Bungner (repair) Schwann cell,
4.5.5 Neural crest stem cells, multipotency and self-renewal,
4.5.6 Adult Skin and craniofacial stem cells,
4.5.7 DFT1: clonal evolution, cancer stem cell and plasticity models.

4.5.1 Schwann cell-melanocyte GRN and lineage markers

The GRN governing the formation and differentiation of the NC including specification of the Schwann cell and melanocyte lineages is complex, often signalling and transcription factors

appearing reiteratively during development [reviewed in (155-158)]. Briefly, forkhead box D3 (FOXD3) is expressed in most of the pre-migratory and migratory NC including neural and glial precursors but is down regulated in dorsolaterally migrating melanoblasts in aves (159-161) and mice (162) illustrating developmental segregation of the neural and melanocyte lineage (163, 164). The dorsolateral migrating melanoblasts express endothelin receptor type B (EDNRB) and receptor tyrosine kinase KIT responsive to their ligands endothelin B and KITL ligand respectively. While not essential for initial specification EDNRB is required for migration and proliferation and KIT, which is expressed by DFT1, is required for survival, migration and proliferation (165). Similarly, ventrally migrating SCP derived melanocytes also downregulate FOXD3, detach from the nerves and migrate to the ectoderm to differentiate (166). The suppression of MITF by FOXD3 prevents PAX3 from binding to the promoter in early stages until the downregulation of FOXD3 initiates lineage bifurcation of the neural/glial and melanocyte lineages (161). The canonical Wingless-type MMTV integration site family (WNT)/beta- catenin (CTNNB1) signalling pathway is instrumental in both melanocyte (167-171) and Schwann cell development (172-175). We found DFT1 expressed moderate to strong CTNNB1 staining, both membranous and cytoplasmic, however no obvious nuclear staining was apparent suggesting that translocation of CTNNB1 from the cytosol to the nucleus is not occurring. Central to the canonical WNT signalling is the CTNNB1 dependent pathway, however the canonical pathway now includes both WNT/TOR (mammalian target of rapamycin) and WNT/STOP (WNT dependent stabilisation of proteins), both of which are independent of CTNNB1. Both CTNNB1 dependent and independent pathways begin with WNT ligands binding to receptor Frizzled (FZD) and co-receptor low density lipoprotein related protein 5/6 (LRP5/6) where CTNNB1 is stabilised and prevented from proteosomal degradation by the 'destruction complex' as would be the case in the absence of WNT signals. The CTNNB1 dependent pathway allows CTNNB1 to accumulate in the cytoplasm prior to nuclear entry affecting transcription of downstream genes via the transcription factor 7/lymphoid enhancer binding

factor (TCF/LEF) transcription factor family. The CTNNB1 independent pathways differ after recruitment of the 'destruction complex' by upregulating mTOR which increases protein translation or the avoidance of ubiquitination of several other proteins, hence STOP, which peaks during mitosis. Non-canonical signalling does not involve CTNNB1 and transduces signals through FZD, ROR/RYK, G protein receptors to activate three main pathways; 1. WNT/planar cell polarity (PCP) also known as the WNT/c-Jun N-terminal kinase (JNK) 2. WNT/Ca^{2+} and 3. WNT/RTK (receptor tyrosine kinase) [reviewed in (176-179)]. In addition to CTNNB1 expression, DFT1 Gene expression reveals a number of receptors and proteins integral to WNT signalling including WNT3a, LRP6, R-spondin 3 (RSPO3), FZD2/3/8, LRP6 (4) often indicative of canonical signalling (180) but expected nuclear staining was not present. This suggests a number of scenarios; 1. CTNNB1 is at levels below our detection system. 2. More likely, CTNNB1 independent signalling through WNT/mTOR or WNT/STOP or non-canonical signalling through WNT/PCP, WNT/ Ca^{2+} or WNT/RTK signalling pathways. We have previously shown that YAP1/TAZ signalling is active in DFT1 (8), these co-activators of the Hippo pathway are activated by WNT/STOP or WNT/RTK (178). Hippo signalling can regulate CTNNB1 because YAP1/TAZ can bind to CTNNB1 thus inhibiting translocation to the nucleus (181), a plausible mechanism for nuclear absence of CTNNB1 in DFT1. We previously identified expression of ERBB3 by DFT1 (47) which can be transphosphorylated by receptor tyrosine kinase like orphan receptor 1 (ROR1) and subsequent activation of YAP1 target genes (182), highlighting crosstalk between ERBB3 and Hippo-YAP1 pathways. Our current research has also identified JUN, part of the non-canonical WNT/PCP pathway and therefore active in DFT1; we discuss JUN further in Schwann cell repair. We have identified possible WNT signalling pathways active in DFT1 but further research is required to tease out the intricacies including cross talk with TGFβ, SHH, IGF and Notch involved in maintenance and proliferation of cancer stem cells (CSCs) (177, 183).

Early melanocyte marker gene *MITF* (isoform M, specific for melanocytes) is the master regulator of melanocyte development and differentiation (184-187). The transactivation of MITF involves at least transcription factors PAX3, SOX10, both expressed by DFT1, and cAMP responsive element binding protein 1 (CREB1), In addition to WNT/CTNNB1/LEF1, to regulate transcription genes driving melanogenesis. As indicated above, without CTNNB1 translocation to the nucleus, transcription of melanocyte genes may be impaired. These include enzymes TYR, tyrosinase related protein 2/dopachrome tautomerase (DCT) and tyrosinase related protein 1 (TYRP1); and melanosomal proteins premelanosome protein/Pmel17/HMB45/gp100 (PMEL) and MLANA (188, 189). I found the clone used for PMEL was unsuccessful on devil tissue and therefore did not form part of the melanocyte panel, but this marker will be further examined in the future. TYR, MITF, MLANA were essentially negative although a very occasional positive cell was noticed during screening. This implies that the necessary melanocyte molecular machinery is present in DFT1. PNL2 was positive in all strains and we discuss its significance in detail below. Neuregulin 1 (NRG1)/Erb-B2 receptor tyrosine kinase 3 (ERBB3) signalling, while not essential for melanoblast formation, does suppress melanocyte differentiation and pigmentation, via depressed MITF, even in the presence of WNT3a, endothelin 3 (EDN3) and KIT ligand (steel factor, SCF/stem cell factor/KITLG) which strongly promote melanocyte differentiation (190). We first reported expression of ERBB3 by DFT1 (47) thus, ERBB3/NRG1 signalling is another possible mechanism for the suppression of MITF preventing differentiation. Critical to progression from SCP to MSC is the transition from reliance on nerve NRG1 to autocrine actors PDGF and IGF, Adameyko et al. found while both NRG1 and IGF1 led to cell survival, only IGF1 led to the development of MITF positive melanocytes indicating opposing effects of NRG1 and IGF1 on SC and melanocyte fate (144). DFT1s expression of IGFR2 and PDGFB suggests an autocrine survival network and its ERBB3 expression would be suppressive to melanocyte development, despite SOX1O and PAX3 expression. SOX2 was shown also to bind to MITF-m promoter repressing a melanocyte fate, and could reverse

melanocytes already specified, thus controls melanocyte differentiation from SCPs (147). The expression of SOX2 by DFT1 provides another regulatory pathway, in addition to NRG1, by which the melanocyte programs can be suppressed in the SCP. In Schwann cells, WNT/CTNNB1 is crucial in the lineage decision to become either MSC or NMSC during the process of radial sorting (191) which would be in keeping with DFT1s lack of nuclear expression. WNT/CTNNB1 signalling does not appear to promote the transformation of melanocytes from SCPs (192). SOX10, expressed by DFT1, is also required for glial fate, survival (193), developmental progression (194) and regulates the expression ERBB3 in NCCs and the developing SCs (195). Survival of SCPs is dependent on axonal paracrine signals from NRG1 and its receptor ERBB3 (117, 196), however, the transformation from SCP to immature SC induces secretion of a number of autocrine survival factor including IGF2, neurotrophin 3 (NT3) and PDGFB (109, 197). In addition to SOX10, a number of other transcription factors also regulate SC development, either positively towards myelination such as early growth response 2/KROX20 (ERG2) or the negative downregulation of myelination genes by SOX2, TFAP2A, JUN and PAX3 (109, 198). DFT1 expresses the transcription factors SOX2, TFAP2A and JUN that are responsible for the down regulation of myelination, further supported by the fact that DFT1 does not contain myelin (1) and reaffirmed by our results that DFT1 does not express MBP, a protein that is integral to myelin formation. NOTCH1 is essential for SCP transition to immature SC but equally NOTCH1, can also negatively regulate myelination (199), as NOTCH1 is expressed by DFT1 its role may therefore likely to be negative. The sequential differentiation from SCP to ISC to either MSC or NMSC is evident by differing marker expression of each cell type. Expression of the markers ERBB3, NGFR and SOX10 are common to NC, SCP and ISC with NGFR also expressed in NMSC. TFAP2A is expressed only in NC and SCPs. The expression of TFAP2A by DFT1 is very interesting as this indicates that DFT1 is in an undifferentiated state. Expression of MPZ, PMP22, PLP1, and GAP43 is common to SCP and ISC. As MPZ, PMP22 and PLP1 is expressed by DFT1 of particular importance is that MPZ and PMP22 are expressed at the early SCP and ISC

stages of development and not just in the mature myelinating phenotype. GFAP, S100 and the expression of laminin (forms basal lamina) first appears at the ISC stage. MSC continue to express MPZ, PMP22 and PLP1 with additional markers ERG2, MBP, MAG, PRX, GJB1 and S100. The NMSC expression includes markers GFAP, GAP43 and S100 in addition to NGFR (109, 117-119, 200). DFT1 does express all these markers indicating phenotypes from all developmental stages of SC. DFT1s expression of laminin and their integrin and dystroglycan receptors (DH, manuscript in preparation, figure 36N and 36O) is in keeping with the characteristic SC transition from SCP to ISC. Laminin 2, the major SC laminin consists of α2, β1, γ1 laminins and these were active in DFT1 transcriptome (β1 gene was not available) (4). We also tested the laminin marker RPSA, a non-integrin 36/67-kDa laminin receptor which was also strongly expressed both membranous and cytoplasmically by DFT1. RPSA is associated with cancer promoting adhesion, migration, metastasis and less tumour differentiation (201, 202). While the SC laminin-integrin-dystroglycan binding is well documented in literature (203-205), the expression of RPSA by SCs was not at all evident and may represent another significant SC antigen requiring further research. The only marker that was not expressed by DFT1 was MBP, a protein integral to compact myelin. This may be explained by the expression of PAX3, also expressed by DFT1, which has been shown to suppress MBP transcription (206). PRX is also generally associated with a myelinating phenotype so why is it strongly expressed by DFT1? The *PRX* gene encodes for two PRX isoforms, 147 KdA L-PRX and 16 kDa S-PRX both of which contain PDZ domains in their N terminus but are localised differently in myelinating Schwann cells, L-PRX localised to the plasma membrane and S-PRX diffusely throughout the cytoplasm. PRX is also expressed in the nucleus embryonically and is redistributed to the plasma membrane and further upregulated postnatally during myelination. (207-210). This is interesting because DFT1 does express PRX in the nucleus, the cytoplasm and the plasma membrane. PRX was first demonstrated to be expressed by DFT1 in 2010 (4, 20), the primary antibody used in those studies and by ourselves is a polyclonal rabbit and therefore, the

actual antigen is unknown. It is possible that the antibody will detect both L-PRX and S-PRX if the antigen/s encompassed the PDZ domain. It has also been shown that L-PRX and S-PRX do interact through the PDZ domain, which may affect the shuttling of L-PRX between the cytoplasm and the nucleus (211). Parkinson et al. demonstrated that PRX could be activated in SCPs by EGR2 in the absence of other early activation signals but importantly, there was also an ERG2 independent activation of PRX and ERG2 may not be responsible for activating the gene during normal development (212). DFT1 does not produce myelin and expresses EGR2 weakly thus an ERG2 independent activation may contribute some understanding as to why PRX expression is strongly expressed in DFT1.

4.5.2 Anti-melanocyte antibody PNL2

The monoclonal antibody PNL2, an anti-melanocyte antibody, has similar specificity but is a different antigen to MLANA and PMEL antibodies (213) having high specificity for melanocytes of the skin, oral mucosa and malignant melanoma. PNL2's exact immunogen is unknown although its antigen is present on a recombinant protein corresponding to the C-terminal of the subtype 2 of human somatostatin receptor (SSTR2) and yet, the antibody is unreactive with SSTR2. Extensive testing revealed that PNL2 was sensitive to melanocytes but it also stained granulocytes, melanotic schwannoma and perivascular epithelioid cell tumour (PEComa) family including clear cell sugar carcinoma (CCST), angiomyolipoma (AML) and lymphangioleiomyomatosis (LAM) (213). Interestingly, canine granulocytes are not stained by PNL2 (214, 215) and our results would indicate that Tasmanian devil granulocytes are also not stained by PNL2. It was suggested that PNL2 may cross react with a granulocyte epitope derived from a different gene than is recognised in melanocytes (216). Comparing DFT1 with cutaneous PECOMAs, DFT1 lacks MITF, and MLANA but expresses S100 and SOX10, two markers typically negative in PECOMA (217). Histochemically,

PECOMAs are often PAS positive for cytoplasmic glycogen whereas DFT1 has been shown to be negative for glycogen (1, 218) Somatostatin receptors are normally located on tissues of neuroendocrine origin and therefore it may not be surprising that malignant melanoma also expresses functional somatostatin receptors (219). In human studies, PNL2 has been compared with other melanocyte markers: PMEL, MLANA, TYR, MITF and S100, illustrating immunoreactivity of similar sensitivity (216, 220, 221) [reviewed in (222, 223). In veterinary pathology PNL2 staining of melanocytes and melanoma has been successfully applied to murine (224), porcine (225), equine (226), canine (214, 215, 227) and feline (228, 229) tissues with excellent sensitivity and specificity when compared to the melanocyte markers above. The data presented above illustrates PNL2s specificity for melanocytes and PECOMAs but how does this translate to DFT1? We know from electron microscopical studies that melanosome-like structures were not identified in DFT1 (1) and the expression of melanocytic markers by PECOMAs is due to the presence of pre-melanosomes (126). Our research suggests that PNL2 may be an early melanoblast antigen that is expressed before the pre-melanosomal stage and because MITF was negative in DFT1, suggests that activation of PNL2 may be independent of MITF. While not directly related to PNL2, Epstein et al. (230) found Tasmanian devils had evidence of a rapid evolutionary response to DFT1 and identified CD146 and a number of other genes as being from strongly selected genomic regions. As well as immune function, CD146 is a multifaceted molecule in functioning in foetal development, adhesion, angiogenesis, cancer and melanoma (231, 232). Interestingly, CD146, is also known as melanoma cell adhesion molecule (MCAM) and therefore I would be intrigued to determine if any relationship exists between PNL2 and MCAM, both being identified as melanoma antigens. In my future studies DFT1 would benefit also by the inclusion of other melanoma antigens such as PMEL or DCT that were not included in this study, to comprehensively encompass most melanocyte antigens.

4.5.3 The Bipotent Schwann cell/melanocyte progenitor

While our research confirms DFT1 has a SC phenotype, the unforeseen expression of PNL2 would appear somewhat contrary; however, it is conceivable that DFT1 is, more specifically, a bipotent Schwann cell/melanocyte progenitor. Following early reports of the appearance of melanocytes from spinal ganglia cultures (233), it was suggested that the appearance of melanocytes could represent a change in cell fate (234). Because the culture of 5 day old chick embryo DRG and peripheral nerve explants produced melanocytes, it was proposed that a bipotent precursor cell having both myelino/melano genesis potential was responsible (235, 236). The use of 12-O-tetradecanoylphorbol-18-acetate (TPA) on older chick embryo DRG as well as sympathetic ganglia and peripheral nerve was able to reverse developmental restriction of melanogenesis in peripheral nerve (237). The expression of melanoma-associated antigens on Schwann cells of traumatic neuroma and neurofibroma cell cultures reflects the common origins of SCs and melanocytes (238) and the identification of chick multipotent NCCs, differentiating into neurons, Schwann cells and melanocytes (239, 240) confirms such speculation. Clonal cultures of NC revealed a few melanocytes present in SC clones suggesting a bipotent precursor has survived after NC migration (241). TPA was shown to reverse the developmental restrictions trans-differentiating Schwann cell precursors into melanocytes and endogenous protein kinase C (PKC) activity may influence commitment of the bipotent Schwann cell/melanocyte progenitor to undergo melanogenesis (low PKC activity) or Schwann cell development (high PKC activity) (242). Basic fibroblast growth factor (bFGF) is also capable of reversing restriction of melanogenesis in early Schwann cell precursors (243) and the augmentation of bFGF by TPA also transdifferentiates SCPs into melanocytes (243, 244). The effects of retinoic acid testing on clonal cultures of cranial and trunk neural crest cells revealed that in addition to adrenergic and melanocyte differentiation, cultures also contained glial cells indicating pluripotency (245). EDN3 was found to promote proliferation and survival of

bipotent glial/melanocyte precursors including unipotent glial and melanocyte precursors. Avian embryonic epidermal melanocyte cultures exposed to EDN3 resulted in heterogeneous progeny consisting of melanocytes, cells expressing both melanocyte and glial markers and non-pigmented cells with only glial phenotype (246) showing reversal of the melanocyte program. EDN3 was shown to act not only on precursor cells but also on differentiated Schwann cells suggesting that it is able to reverse the differentiation program and induce melanogenesis (247). Purified glial cells responded to EDN3 enhancing survival and proliferation transitioning toward a melanocytic program, single cultures contained mixed progeny of glial, melanocyte and melanoblast cell types (248). In both CNC and TNC cultures, a repertoire from pluripotent glial (G) /neural (N) /melanocyte (M) /myofibroblast (F) to bipotent GM progenitor was evident, including self-renewal (249). As DFT1 expresses Schwann, melanocyte and self-renewal markers such as SOX2 and POU5F1 (discussed below) it implies that the DFT1 has activated a program reminiscent of early developmental stages. Experimental injury caused by cutting adult mouse sciatic nerve, particularly neurofibromatosis 1 (*Nf1*) mutant mice, induced pigmentation around the injury site. Further, nerve grafts from both wild type and *Nf1* mice into albino adult mice resulted in pigmentation, thus both experiments show melanocytes are derived from adult peripheral nerve and can be attributed to glial cells retaining the ability to form pigment within the wound environment (250). Murine embryonic and neonatal $KIT^{+}/CD45^{-}$ melanoblasts were shown to be multipotent giving rise to N, G and F in addition to M with self-renewal capability including GM type colonies (251). As with DFT1, the expression of KIT enhances survival, migration and proliferation but may be contributory to self-renewal also. Definitive evidence that the ventrally migrating SCP is the cellular origin of nerve derived melanocytes was confirmed by tracing experiments showing dermal and hair follicle melanocytes originated from SCPs associated with embryonic nerves innervating the skin in mice (144). Adameyko et al. also found by cutting the sciatic nerve, EGR2 positive pro-MSC and MSC retain the ability to form pigment at the site of

injury (144). NRG1/ERBB3 signalling appears critical to SC/melanocyte fate because in ERBB3 deficient mice there is a significant increase in melanocytes despite a decrease in SCPs and additionally, cultures of DRG and SCP showed NRG1 to be suppressive to melanocyte differentiation (144). As DFT1 expresses ERBB3 (47), it is possible that there is a suppressive effect accounting for the negativity of most of the melanocyte markers. Similar findings were reported in zebrafish; pigment cell precursors are associated with peripheral nerves and ganglia in post-embryonic development, additionally these precursors are absent in ERBB deficient mutants (252) and evidence of a stem cell population associated with DRG giving rise to ventromedial melanophores that migrate along nerves are also ERBB dependent (253) . Cultured human foreskin melanocytes dedifferentiated to Schwann-like cells that when transplanted into injured rat sciatic, behaved as Schwann cells closely associating with nerves and glia (254). Rare pigmentation in Schwann cell tumours is recognised in both melanotic schwannoma and pigmented neurofibroma (often associated with *Nf1)* which tend to be benign but have the potential to become malignant and are often positive for MLANA, TYR, PNL2 and PMEL (255, 256). In addition, neurofibroma associated with *Nf1* have been shown to contain NES positive progenitors, as does DFT1, which may represent alteration in self-renewal program potentially contributing to tumourigenicity. Melanocytic differentiation can also be present in non-pigmented diffuse neurofibromas (257). In veterinary tumours, a canine pigmented diffuse neurofibroma has also been recorded (258). An epithelioid malignant peripheral nerve sheath (EMPNST) tumour expressed PMEL showing melanocytic differentiation (259) which could be confused with a malignant melanoma with MPNST features (260). Divergent differentiation can also be exhibited by malignant melanoma and benign melanocytic naevi whereby Schwannian differentiation (often termed neurotization) is a feature. This is often expressed in spindle cell desmoplasic malignant melanoma/neurotrophic melanoma (261, 262). The experimental evidence cited above indicates that NC multipotent, bipotent and particularly the SCP have the molecular machinery to differentiate and/or

dedifferentiate into glia or melanocyte phenotypes during normal development or in disease. Although DFT1 is non-pigmented, the expression of PNL2 and SC markers provides evidence that the tumour is at least a bipotent progenitor-like cell.

4.5.4 The Bungner (Repair) Schwann cell

When peripheral nerve injury occurs phenotypically mature SCs dedifferentiate reprogramming from myelination to a progenitor-like phenotype that will support nerve survival and regeneration. These repair SCs or bridging SCs termed Bungner SCs (BSC) form regeneration tracks called bands of Bungner which function to direct axon ends to their targets (263-265). Quiescent intact SCs distal to nerve injury (dSC) dedifferentiate and down regulate myelination genes including EGR2, MPZ, MBP, MAG and PRX and upregulate early SC genes including JUN, NGFR, SOX2, GFAP, PAX3 and NCAM and simultaneously activating genes specifically related to repair including signal transducer and activator of transcription STAT3, SHH, glial derived neurotrophic factor (GDNF) and artemin. Our results show that DFT1 expresses STAT3, SHH, SOX2, NGFR, PAX3, GFAP and JUN, upregulated in the repair program with downregulation of EGR2, MPZ and MAG showing reduced expression, MBP was not expressed although PRX was still strongly expressed. The plasticity of MSC and NMSC (Remak), recapitulated by the BSC is often termed ‘dedifferentiation’ however, ‘reprogramming’ or ‘transdifferentiation’ more correctly describes the two distinct phenotypic states (263, 264, 266-268). Clements et al. found that when the repair program is activated, dedifferentiation was not simply a reversal of the SC development program because a stem-like state is created (pluripotency factors SOX2, POU5F1 and NANOG) and BSCs reduced their repair potential but increased proliferation and differentiation toward mesenchymal characteristics. A stem-like state is reflected in DFT1 as the tumour expresses SOX2, POU5F1 and NES. Additionally, the mesenchymal cell marker VIM, highly expressed in embryonic development and upregulated during nerve degeneration (269), it is also strongly expressed by DFT1. This describes a distinct

molecular difference that exists between BSC and dSC populations (265). Both the myelinating and repair programs can be active in Schwann cells for 3 days until there is significant downregulation of MPZ and ERG2 (270). Transcription factors, JUN and STAT3 and SOX2 are instrumental in nerve repair although they play different roles. JUN functions as a negative regulator of myelination thus supresses this program however, JUN is also an activator of the repair program and subsequent Wallerian degeneration (198, 263, 271). In the developing SC, JUN is low or absent in SCPs, upregulated in ISC and downregulated in MSC although it is detected in many NMSCs (266). It appears the primary role of JUN in SCs is during injury as inactivation of JUN in embryonic SCs, development proceeds normally (272). STAT3 has a duel role, it is crucial to long term autocrine survival (IGF, NT3 and PDGFB) and importantly, responsible for the maintenance of the BSC phenotype (273). DFT1 expresses IGFR2, PDGF, BDNF (DH, BDNF and its ligand TRKC results not presented, see figure 30A-D) and NGFR illustrating an active autocrine survival program, although with no axonal contact this is not surprising. Inactivation of STAT3 causes abnormal morphology of BSC and their regeneration tracks and fails to sustain repair markers such as JUN, SHH and BDNF. In SC development, STAT3 is detectable from SCP to adult SCs but does not appear significant in SC development, so it appears like JUN, STAT3s primary role in SCs is restricted to post injury BSCs (273). STAT3 also has important functions in various stem cells; outlined in the next section below. SOX2 is expressed by ISC, as is JUN, and is normally downregulated for myelination to occur, SOX2 is re-expressed in nerve injury and must once again be downregulated for re-myelination to occur during repair (268, 274). DFT1 expresses JUN, SOX2 and STAT3 all three transcription factors are re-expressed by SCs during nerve injury. Important to the repair program is the upregulation of a number of neurotrophic factors in addition to GDNF including BDNF, neurotrophin 3 (NT3), nerve growth factor (NGF), vascular endothelial growth factor (VEGF), NGFR, N- cadherin (CDH2), PDGFB and IGFR2 (197, 264, 266). This critical component of SC plasticity is demonstrated by DFT1s expression of IGF2, PDGFB, NGFR, and VEGFA. NRG1- III signalling is essential for myelination

however, during nerve regeneration SC derived secretion of NRG1- I and NRG1-II is prominent during the same time that axonal NRG1- III is lost (275-277). While SC derived NRG1-I and NRG1-II provides an autocrine loop their presence also has a negative regulatory effect on the myelination (278). Concomitant upregulation of the ERBB2/3 dimer upon nerve injury occurs (275, 276) where ERBB3 expression decreases one day after injury but Is strongly upregulated at day 7 post injury levels remaining elevated during regeneration (279, 280). I reported the expression of ERBB3 by DFT1 (47) and this would be in keeping with autocrine expression of NRG1 thus exerting a negative myelination signal. In addition, constitutive activation of NRG1/ERBB signalling has been associated with proliferation of neoplastic SCs in MPNST and neurofibromas (281) whereby sustained NRG1/ERBB expression may have occurred in DFT1 from nerve injury causing malignant transformation of a Bungner cell. Indeed, ERBB3 was also identified as a candidate gene for tumorigenesis in DFT1, where its mapping was rearranged with increased copy number (5) detected. MBP is also downregulated after injury and completely disappears during degenerating conditions (279), logically this could account for MBPs absence in DFT1. SHH, normally low or absent in ISCs, is controlled by JUN and is upregulated in SCs of injured nerves (263, 266, 271). SHH which is normally repressed in SCs by polcomb repressive complex 2 (PCR2), is also activated by demethylation of histone H3 lys27 (H3K27) upon nerve injury (282). SHH is also upregulated in damaged nerves facilitating nerve regeneration while its upregulation in SCs offers a neuroprotective effect as BDNF is also increased in cultured SCs (283, 284). VEGF has neurotrophic and mitogenic activity on both neurons and SCs enhancing survival, axonal outgrowth and proliferation of SCs (285). VEGF is upregulated in SCs secondary to nerve injury facilitating angiogenesis and oxygen delivery, macrophage recruitment for myelin degradation and axonal maintenance by SCs (286) similarly expressed by DFT1. Loss of contact between SCs and axons causes alteration to cytoskeletal antigens including upregulation of intermediate filaments VIM, GFAP, neurofilament (NEFM and NEFL) and laminin. VIM, otherwise normally restricted to the

outer ring of cytoplasm in MSCs; GFAP, normally only present in NMSC or immature myelinating SCs and laminin present on SCs from the ISC stage; all of whose activity intensifies maintaining SC alignment with neurotrophic molecules promoting axonal outgrowth (287). NEFM has been shown to be expressed in developing SCs and dedifferentiating Schwann cells during Wallerian degeneration along with VIM and both NEFL and NEFM mRNA are expressed during nerve repair (288, 289). DFT1 was essentially negative for neurofilament, although a very small focus showed occasional light cytoplasmic positivity (figure 36E), GFAP was expressed in approximately 50 percent of cells; however VIM and laminin (DH, data not presented, figure 36N and 36O) were strongly expressed in most. Of note is that pigmentation can occur at the site of peripheral nerve injury and repair. We outlined above how experimental injury caused by cutting adult mouse sciatic nerve induced pigmentation around the injury site (250). Similarly, Adameyko et al. suggests that EGR2 may restrict differentiation of SCPs into melanocytes but they still retain the ability to form pigment when challenged by loss of nerve contact in the repair microenvironment (144). The expression of PNL2 would indicate that DTT1 does retain some melanocyte antigens that become evident during reprogramming during injury or malignancy. Additionally, *Nf1* deficient mouse SCs at the wound site formed neurofibromas indicating that the wound changes from a normally tumour suppressive microenvironment to tumour conducive one (290). TGFβ is expressed by MSC as well as NMSC including SCPs, embryonic SCs and satellite SCs (291) and in developing nerves, it appears to modulate two opposing SC programs; death and proliferation. In the SC, TGFβ can block myelination in favor of a NMSC phenotype (292, 293) but in MPZ/PMP22 expressing multipotent progenitors TGFβ will produce mainly myofibroblasts or neurons depending on cell cluster size (294). TGFβ and NRG1 activate the JUN NH_2-terminal kinase (JNK)-JUN pathway in SCs necessary for apoptosis and proliferation. This can be suppressed by EGR2 upon myelination and cell death can be impeded by NRG1 and autocrine factors (295, 296). As SCs align with growing nerves TGFBR2 acts as a mitogen for those SCs associating with axons in a 1:1

ratio and NRG1 but superfluous non-associated SCs will apoptose (297). Recently, nerve injury was shown to upregulate TGFBR2 in the BSC, reprograming the cell to an invasive mesenchymal like cell type, promoting directional migration and thus nerve regeneration. These changes also indicate that transdifferentiation and activation of the repair program is more closely associated with ESCs than their immediate progenitors of the neural crest as cellular plasticity may be influenced by injury causing malignant transformation (265). Our results show DFT1 expresses TGFBR2 in the setting of a SC transdifferentiation phenotype including strong expression of mesenchymal marker VIM. Intriguingly, insights into cancer stem cells have revealed that the reprogramming of somatic cells may be contributory to some cancers (298), more specifically, concurrent induction of the Schwann cell repair program caused by cancer invasion of nerves guides cancer cells towards SCs where axonal guidance is a defining feature of BSCs during nerve outgrowth (299). We hypothesized that DFT1 may be a result of malignant transformation of the BSC and that facial injury, rich in whiskers and peripheral nerves, may provide the 'niche' microenvironment for successful transmission of DFT1. Comprehensively, our results show expression of specific markers upregulated in repair signalling; JUN, SHH, SOX2, STAT3, early SC lineage markers; TFAP2A, NGFR and autocrine survival factors such as BDNF, VEGF, IGFR2 and PDGFB. This scenario is true also for the inclusion of melanocyte markers because pigmentation can also occur at the site of nerve injury.

4.5.5 Neural Crest Stem Cells, Multipotency and Self-renewal

Recent publications have shown that nerve derived SCPs retain the ability to differentiate into pigment cells of the skin (144), endoneurial fibroblasts (143), parasympathetic neurons and ganglia (300, 301), enteric (302) and oesophageal neurons (303), mesenchymal stem cells producing dental pulp cells and odontoblasts (304) and chromaffin cells of the adrenal medulla (305), in addition to MSC and NMSC (109). Therefore, the SCP may represent multipotent NCSCs

capable of differentiation into a variety of cell types once considered to be only attributed to the embryonic NC (92). One property of all NC progenitors, from pluripotent to bipotent state, is the ability to yield glia illustrating their plasticity in response to various developmental signals (306) and the capacity of NCSC to self-renew has been recognised for some time. Stemple and Anderson et al. (307) isolated rat multipotent NCCs by their expression of NGFR and NES (both of which are expressed by DFT1) in culture these cells gave rise to not only G, N and others but also multipotent progeny, indicating the ability to self-renew. DFT1 also expresses NGFR and NES. Also evident was that self-renewal of the multipotent cells occurred by both symmetric and asymmetric cell divisions (307). Isolated $NGFR^+$ MPZ^- SCPs from rat foetal peripheral nerve, indistinguishable from NCSC invitro, generated both G and N when transplanted into chick embryos, indicating they self-renew in vivo and persist at least a week after NC migration (308). In $NGFR^+$ rat postmigratory DRG and differentiated NCSC cultures, multipotent progenitors expressing both MPZ and PMP22 gave rise to G, N and F. In this progenitor cell, MPZ and PMP22 mark glial cells long before myelination and PMP22 expression precedes neuronal differentiation (294), an important characteristic highlighted earlier because DFT1 expresses these proteins in an unmyelinated state. NCSCs isolated from rat sciatic nerve grafted into embryonic chick were able to differentiate into all types of peripheral glia and primarily parasympathetic neurons but in culture were able to differentiate into sympathetic neurons thus maintained multipotency and self-renewal (309). $NGFR^+$ isolated from adult rat gut were also multipotent containing G, N and F in cultures that self-renewed and were confirmed as NCSCs (310). Rat NCSCs from both sciatic nerve and gut, although both multipotent and give rise to G and N, displayed cell-intrinsic factors biasing sciatic nerve NCSC to form neuronal and gut NCSCs can acquire glial fates despite the presence of both lineage determination factors (311). Multipotent rat sciatic and gut NCSC colonies exposed to NRG1, BMP4 and Delta-Fc gave rise to different progeny either F and G (sciatic) or N and F (gut) indicates the complexity in peripheral nerve development (143). The reprogramming of cultured chick SCs

isolated from sciatic nerve to F in additional to G and GM, normally seen only in cephalic NCSC in vivo, highlights the potential of TNCs to recapitulate mesenchymal fate (312). CNC and TNC cultures showed that bipotent GM and GF progenitors behave like stem cells by self-renewal and production of restricted progeny (249). Melanocytes of embryonic quail skin were dedifferentiated in culture giving rise to multipotent cells (GMF, GM, MF) that were able to self-renew but this capability was enhanced when cultured in the presence of ET3 (313). Murine embryonic cells expressing $KIT^{+}/CD45^{-}$ were shown to be multipotent giving rise to N, G and F in addition to M with self-renewal capability including GM type colonies (251, 314). The same researchers also found that $SOX10^{+}/KIT^{+}$ and $SOX10^{+}/KIT^{-}$ are both multipotent, differentiating into G, M, N, including GM type colonies irrespective of KIT expression (315), suggesting that previously described dorsolateral migrating KIT^{+} and dorsoventral KIT^{-} migrating NCs is not strictly defined. Additionally, they also found that $SOX10^{+}/KIT^{+}$ present in the developing DRG and ear were also multipotent containing M colonies in addition to NG (316). Interestingly, KIT positivity occurred in about 10% of DRG cells identified as neurons (317). In vivo mouse experiments reveal that pre-migratory and migratory NCs are multipotent and the possibility of asymmetrical stem cell retention in the dorsal neural tube provides evidence of NCSCs in vivo (318). Cultured melanocyte spheres can be reprogrammed by NOTCH1 signalling to form functional induced NCSC, losing TYRP1 and PMEL, capable of self-renewal and differentiating into both mesenchymal and neural cell types expressing SMA, NEF and GFAP. These cells could also re-express melanocyte phenotype markers TYRP1 and PMEL including home to the basement membrane in a reconstructed skin context (319). As well as the upregulation if SHH in nerve injury, SHH is also required for survival of CNC and craniofacial development. SHH acts mainly on highly multipotent NC progenitors capable of differentiating into both neural and mesenchymal potential (G, M, F, N, chondrocytes C and osteocytes O), while positively influencing mesenchymal differentiation potential, SHH largely unaffected neural and melanocytic progenitors (320-322). Although crucial to embryonic

development or postnatal injury, the SHH pathway appears just as important in the progression of some cancers aberrantly expressing SHH. SHH can maintain stemness driving expression of genes such as *SOX2*, *POU5F1*, proliferation such as *IGF2R*, *VEGF* and *TP53* and cross talk with other pathways such as WNT, TGFβ, NOTCH and IGF shows the complexity of the SHH pathway (reviewed in (323-327), all of which are expressed by DFT1. Whether DFT1s signalling is canonical or non-canonical, autocrine or paracrine, is yet to be determined but key genes such as receptor patched (*PTCH1*), smoothened (*SMO*) and suppressor of fused (*SUFU*) appear activated (4). Interestingly SHH can regulate WNT signalling through SUFU which can supress nuclear levels of CTNNB1, perhaps another possible explanation for CTNNB1 absence in DFT1 (327). As part of our immunohistochemical profile, we included the common epithelial markers epithelial cell adhesion molecule (EPCAM) together with cytokeratin markers (pan) AE1/AE3 and high molecular weight 34Be12 (DH, data not presented, figure 36F and 36G). While AE1/AE3 and 34Be12 were negative, EPCAM/CD326 was expressed in all strains, a result quite unexpected as DFT1 is non-epithelial in origin. EPCAM is commonly used as a circulating tumour cell (CTC)/tumour initiating cell (TIC) marker of simple epithelia and a variety of epithelial carcinomas. EPCAM is not usually seen in tumours of mesodermal and ectodermal origin but it is also expressed by progenitor cells, normal and malignant stem cells, embryonic stem cells (328, 329), and neuroendocrine tumours (330). EPCAM is also expressed in early formation and assembly of the gonads (329) therefore we examined for the expression of a germ cell lineage using two commonly used antibodies; DEAD-box helicase 4 (DDX4) and Y-Box binding protein 2 (YBX2) both of which were negative (DH, data not presented, see figure 36J-M) demonstrating that DFT1 is not a germ cell neoplasm. Elevated EPCAM is experienced in human foetal tissues during morphogenesis and is co-expressed with pluripotency stem cell markers such as SOX2 and POU5F1 thus associated with self-renewal and maintenance of the undifferentiated state (331, 332). In mouse ESCs it was shown that EPCAM IS downregulated in early differentiation along with SOX2, POU5F1 and STAT3 however, in the

undifferentiated state the converse applies and while EPCAM is essential it is not sufficient to maintain pluripotency on its own (333). Expression of EPCAM by DFT1 would indicate that the tumour is in a relatively undifferentiated state. Further to this relationship reprogramming of fibroblasts using EPCAM, a potent stem cell marker, and its cleaved extracellular domain (EpEX) to activate the STAT3 – hypoxia inducible factor 2α (HIF2A/EPAS1) pathway for the production of induced pluripotent stem cells (iPSC) demonstrates a reprogramming trigger (334). IGF2 is instrumental in two SC programs; in embryonic development as SCP transition to immature SC and in repair following axonal loss and IGF2R is certainly expressed by DFT1. Increasing evidence shows that IGF2, as well as IGF1 is required by embryonic stem cells for self-renewal, pluripotency and cell survival and the same factors also help maintain the stem cell phenotype in cancer (335). Because EPCAM, SOX2, POU5F1 and STAT3 are expressed by DFT1, this would suggest that the self-renewal program is activated despite the tumour not being completely undifferentiated or an embryonic state. STAT3 has been identified as a key transcription factor that enables embryonic stem cells to self-renew and maintains their undifferentiated pluripotent state (336, 337). As well as normal stem cells STAT3 has also been reported to have an essential role in maintaining gene expression important to the CSC phenotype such as CD44 and PROM1/CD133 (338), SOX2 and NES (339). As STAT3 is a key transcription factor for self-renewal in stem cells and is crucial to activating the repair SC program, I surmise that SC trans-differentiation and stem cells share a similar function and perhaps should not be considered mutually exclusive. Interestingly, independent DFT1 researchers have also found STAT3 to be active in DFT1 (6). CD44 and PROM1 are often associated with CSCs so these markers were included on that premise. CD44 was expressed weakly by DFT1 in most of cells, primarily its role is bind hyaluronic acid and functions appear to be cell migration and adhesion. CD44 is expressed on haematopoietic, mesenchymal and adipose stem cells (340). CD44 co-localises with ERBB2-ERBB3 on the SC membrane during perinatal proliferation, crucial to heterodimerisation during NRG1 signalling (129). Although CD44-

EREBB co-localisation occurs in normal development, it is possible that a relationship still exists in malignancy. CD44 has also been detected in NMSCs of the neuromuscular junction (NMJ) (341) and in vestibular Schwannoma (*NF2*) (342). In cancer cells, CD44 can activate various pathways such as MAPK, Hippo [active in DFT (8)], CTNNB, TGFβ, PDGF and STAT3 (all demonstrated in this research) among others (343). CD44s is the smallest and standard isoform however, alternative splicing encodes larger isoforms referred to as CD44v and often these isoforms are expressed in cancer cells (344). Our CD44 antibody was N-terminal polyclonal rabbit and therefore it is not possible to determine any splice variants. We have shown that DFT1 expresses SC and melanocyte linage markers so we explored the possibility that DFT1 may be multipotent and utilised neuronal markers NSE, UCHL1, neurofilament, and CALB2. Strong ENO2 staining was consistent across all DFT1 strains, interesting because normally ENO2 stains central and peripheral neurons and neuroendocrine cells but not SCs (345, 346). This result appears contraindicative and erroneous. We previously identified ENO2, chromogranin A (CHGA) and Synaptophysin (SYN) positivity in DFT1 (2) supporting neuroendocrine differentiation. Neurosecretory granules were identified on electron microscopy (1) and even though CHGA and SYN monoclonal antibodies were negative in subsequent testing (DH, personal observation), together demonstrate neuroendocrine epitopes are present on DFT1. Recently, Furlan et al. provides conclusive evidence that chromaffin cells of the adrenal medulla originate from SCPs migrating along preganglionic nerves innervating the adrenal medulla (305). Chromaffin cells typically contain secretory granules, stain positive for CHGA, SYN and ENO2 however the general distinctive histomorphology 'Zellballen' and S100 positive sustentacular cells differs from DFT1 expression (347). Although pigmented paragangliomas and pheochromocytomas generally contain neuromelanin, they do not contain premelanosomes/melanosomes and are HMB45 negative (348-350), although others have reported that these features can be present (351-353). If we consider that the SCP can be the origin of melanocytes from dorsoventral migration, then melanocytic features are theoretically

possible. Instead of the neuroendocrine markers being aberrant in DFT1, it is conceivable that since SCPs are responsible for adrenal medulla chromaffin cells and melanocytes, the expression of ENO2 is not erroneous but appropriate for DFT1, and indeed possibly more specific than first thought (354). UCHL1 was also expressed by all strains and typically expressed by normal neural, neuroendocrine, melanocytes but not by SCs, however UCHL1 has been documented in a wide variety of tumours including neuroectodermal and mesenchymal (355), therefore its role is more complex that first thought. A study on mouse neural progenitor cells revealed that UCHL1 affected cell morphology of NES expressing neural precursors, however progenitors undergoing gliogenesis had little UCHL1 indicating UCHL1 supports neurogenesis (356). Normally SCs do not express UCHL1 but if a nerve is transected the denervated SC does have the ability to upregulate this protein and it has also been reported in nerve sheath tumours (357). In the developing enteric nervous system, UCHL1 can co-stain with NGFR glial precursors showing that UCHL1 is not necessarily specific for neural differentiation (358). These would indicate that neural differentiation cannot be categorically assured however, UCHL1 certainly has a role within progenitor cells during the early phases of neural/glial/melanocyte differentiation. In malignancy there is much to unravel as UCHL1 has been associated with CTNNB1, TP53 and JUN, all of which are expressed by DFT1, therefore UCHL1 may also be driven by other unknown factors (359). Neurofilament protein was essentially negative apart from a very occasional cytoplasmic expression perhaps suggestive of neural programming although this was not consistent feature. As previously mentioned it has been noted that loss of axonal contact can upregulate neurofilament in SCs. Because some SCPs undergo neurogenesis in the postnatal period, to provide CALB2 expressing neurons to the enteric nervous system (302) we tested DFT1s ability to express CALB2. All strains were negative for CALB2 but interestingly, apart from peripheral nerve staining this marker has found use in differentiating a Schwannoma from neurofibroma with positive staining being associated with Schwannomas (360, 361). As a general aside, I noticed that DFT1 had

nuclear expression of markers MLANA, SMA (DH data not presented, SMA figure 36H, negative MSA 36I,) and Desert Hedgehog (DH, data not presented) when the expected result is cytoplasmic. Taken on their own the nuclear expression would appear anomalous, a possible result of cross-reaction (human versus marsupial proteins) however, collectively it is conceivable that a progenitor cell, such as DFT1, may express these proteins aberrantly because the molecular machinery is intrinsic to the cell, but the expression is altered by malignant transformation. Signalling and maintenance of stem cells and self-renewal in normal as well as cancer cells involves a number of classic pathways such as WNT/β catenin, Hedgehog and Notch but in addition TGFβ, PI3K/ATK/mTOR, JAK/STAT and TP53 also contributes significantly to stemness (362-364). The intricacies of signalling are beyond our scope, but our current results have directly shown expression of CTNNB1, SHH, NOTCH1, TGFBR2, STAT3, TP53 (see below) and previously ERBB3 by DFT1, integral to the signalling pathways outlined above that maintain self-renewal in cancer or normal stem cells. Self-renewal and CSC markers were evident by DFT1s expression of markers SOX2, POU5F1, EPCAM, CD44 and CD133.

4.5.6 Adult skin and Craniofacial Ectomesenchymal stem cells

Craniofacial development requires embryonic CNC, the ectomesenchyme, to form both neural crest (neural, glial and melanocytes) and mesenchymal (skeletal, chondrocyte, connective tissues) derived tissues (322). Studies reveal that adult NCSCs reside in special craniofacial niches especially the oral region (365), including but not limited to stem cells of the palate (PNCSC), dental pulp (DPSC), skin (hair and whiskers) (366) fungiform papilla of the tongue (FPSC) (367) and oral mucosa stem cells (OMSC) (368) that are multipotent and have the ability to self-renew. The Tasmanian devil is notorious for challenging fellow devils while feeding or during mating, resulting in lacerations particularly around the facial region. Injuries to the lips and oral mucosa can also

occur as a result of feeding on large carcases, bone fragments and echidna spines and the number of injuries do not necessarily correlate to increased risk of acquiring DFT1 (64). Interestingly, tumours including the cheek, whisker pad, lip, gingiva, tongue, palate including loss of teeth (personal observations DH, GK,) involve the craniofacial niches mentioned above. Our research highlights that in addition to neural crest derived Schwann cells and melanocytes lineage markers, some are also expressed by several craniofacial stem cells. The discovery of rat PNCSCs as MSCs of possible lanceolate nerve endings that expressed NES, NGFR and S100 and pluripotency factors including SOX2 and POU5F1, are thought to arise because of their anatomical position and the injurious nature caused by mechanical stress, since sciatic nerve does not express these markers unless culture conditions mimic nerve injury (369). Subsequently, PNCSCs expressed GFAP (glia), neurofilament medium NEFM (neurons), SOX2, POU5F1 and PROM1 illustrating multipotency and self-renewal (370). The intermediate filament NES, recognised for its contribution to cellular structure has an additional role that is crucial to the survival and self-renewal of multipotent NCSCs (371). Mesenchymal DPSCs are self-renewing and retain the ability to be multipotent, including differentiation into glia and melanocytes, expressing NGFR, SOX10, NES, KIT, GFAP, MLANA, CD44 and PROM1 among others (372-374) and our research shows constant expression of these markers by DFT1 except for MLANA. The skin is home to several recognised stem cells; skin derived stem cells (SKPs) (375), epidermal neural crest stem cells (EPI-NCSC) (376) and hair follicle-associated (HAP) stem cells (377) including the bulge area in particular has identified NES positive pluripotent stem cell (378, 379). SKPs that occupy the hair and whisker papillae, are NES^{+} $NGFR^{-}$ $SOX10^{-}$ multipotent cells differentiating into neurons expressing NEFM, Schwann cells expressing GFAP, MBP, MPZ, S100 and NGFR and smooth muscle expressing SMA, additionally expression of PAX3, VIM and NSE also (380, 381). Additional research by Toma et al. found SKPs had low levels of NGFR differentiating into neurons, glia and smooth muscle cells (382). Cultured rodent vibrissial follicle papilla cells formed spheres with a similar profile but also expressed SOX10 and PAX3 but

did not express POU5F1 (383). Beirnaskie et al. found SKPs expressed SOX2 in the dermal sheath in addition to the dermal papilla, expressed CD44 and were also able to culture neural and mesodermal differentiated cells (384). EPI-NCSC are pluripotent NCSC found in the outer root sheath from the bulge to the matrix. Clonal cultures of bulge area explants from mouse whisker contained neurons, smooth muscle cells (SMA), rare Schwann cells (GFAP, S100) and melanocytes (early melanocyte marker/MelEM) (385). Human EPI-NCSCs (hEPI-NCSCs) bulge explants were shown to differentiate into osteocytes and melanocytes ($MITF^{+}$) and other cell types in secondary clones including self-renewal and pluripotency genes SOX2 and POU5F1 protein expression including SOX10, NGFR, NES, GFAP and SMA (386). Expansion of hEPI-NCSCs led to the expression of SOX10, EGR2, NGFR, MBP, GFAP, MPZ, 100B, VEGFA including JUN gene expression by manipulating SHH, WNT and TGFβ pathways in culture (387). Hair follicle-associated (HAP) stem cells, originally termed nestin-driven GFP (ND-GFP), are NES positive, cytokeratin 15 negative which can differentiate into neurons, glia, keratinocytes, smooth muscle cells and melanocytes (388, 389) isolated from the bulge area (390) but also migrate to the dermal papilla (391). These cells appear similar to EPI-NCSC. Identification of hair follicle stem cells (HFSC) in the bulge are of human scalp expressed NGFR, NES AND SOX10, spheres were multipotent differentiating into neural, melanocytes and smooth muscle cell types and able to self-renew expressing POU5F1 (392, 393). Glabrous dermal stem cells (DSC) isolated from human foreskin expressed NGFR, NES and POU5F1, neural crest characteristics, and were able to be differentiated into neurons (NEFM), smooth muscle cells (SMA), chondrocytes, adipocytes and melanocytes (MITF, DCT, S100, PMEL). The markers NGFR, SOX10, S100, SOX2 and PROM1 in dermal papilla are expressed by guard/awl/auchene hairs illustrating the heterogeneity of the dermal papilla (394). FPSCs express NGFR and are multipotent, as $NGFR^{+}$ NES^{+} spheres are able to be differentiated into neurons, glia, smooth muscle and keratinocytes (367). The isolation of NGFR and SOX10 positive human and mouse trunk skin was shown to be multipotent, giving rise to both neural (glia, melanocytes) and

non-neural lineages (smooth muscle, chondrocytes and adipocytes), are self-renewing and associated with the glial and melanocyte lineages, not from mesenchymal structures of the hair follicle (395). Finally, because oral tissue heals regeneratively, quickly and without scar tissue led to the discovery of OMSCs resident within the oral mucosa lamina propria (OMLP). Human buccal mucosal biopsies revealed a $CD44^{+}$ $CD45^{-}$ progenitor cell population that was self-renewing (SOX2, POU5F1 -RNA), multipotent by differentiated into both mesenchymal and neuronal lineages (NES, NOTCH1, SOX10, GFAP, NEFM, S100 and MBP in culture) (368). Human gingival and alveolar biopsies expressed NGFR, SOX2, POU5F1 but not NES and cell cultures expressing NGFR, SOX2, POU5F1, NES, β-3 Tubulin (TUBB3) and GFAP showing stem cell factors and multipotency (396). Of note was the OLMPs also secreted VEGF among other growth factor, a marker also expressed by DFT1. Human alveolar, labial and palatal mucosal biopsies revealed $CD44^{+}NES^{+}$ OMSCs that were multipotent expressing SMA, NSE, TUBB3 and GFAP and under culture conditions differentiating into neurons, glia, myocytes, adipocytes, chondrocytes and osteoblasts (397). Our results illustrate that a great number of markers expressed by adult stem cells of PNCSC, DPSC, skin (SKP, EPI-NCSC, HAP) FPSC and OMSC are expressed by DFT1. Our hypothesis that the niche microenvironment provided by the injured facial tissues would most likely include adult stem cells residing in the various facial and oral environs comprehensively outlined above and that DFT1 could also have its origins from these cell types.

4.5.7 DFT1: Clonal evolution, cancer stem cell and plasticity models

We have shown that DFT1 expresses markers commonly associated with stem cells and self-renewal, including, SOX2, POU5F1, NES, NGFR, CD44, PROM1 and EPCAM. The mere fact that the DFT1 is transmissible certainly poses a conceivable notion that DFT1 is CSC-like, a concept that other authors have also questioned (398, 399). Reliance on just cell markers alone is not sufficient to identify CSCs but if we consider additional evidence available from two separate research

findings, our results find corroboration. Firstly, a murine xenograft model for DFT1 showed conclusively that tumours grown in laboratory mice mimicked transmissible DFT1. Inoculation of DFT1 cell cultures into 17 non-obese diabetic/severe combined immunodeficiency (NOD/SCID) mice with all mice developing tumours (x-DFT1). In addition, 7 NOD/SCID mice were inoculated with viable cultures from x-DFT1, a second passage, with all mice once again producing tumours, suggesting self-renewal characteristics. All x-DFT1 tumours appeared histologically identical to the original DFT1 and the x-DFT1 karyotype was essentially similar to the pseudodiploid clone although an increase in the near triploid clone was observed. Neither immune competent BALB/c mice nor non-viable freeze/thaw tumour cells produced tumours. In this first study, because DFT1 cancer cells did initiate tumours in xenotransplantation, this does imply the presence of tumour initiating cells/CSC. However, the inoculated cell culture was not flow cytometry/FACS sorted for self-renewal/stem cell markers prior to transplantation, commonly performed as the gold standard for CSC identification (400). Additionally, the xenograft is not subject to any innate immune response in the immunocompromised mouse host and therefor the tumour microenvironment does not fully replicate tumour transmission in Tasmanian devils. The second study employed experimental transmission of DFT1 tumour cells (both tumour and cell culture) from a diseased Tasmanian devil into non-diseased Tasmanian devils successfully producing subcutaneous tumours that developed into classic DFT1 (3). This allograft (tumour and cell culture) when compared to the xenograft above, demonstrates Tasmanian devil tumour transmission and development insitu, simulating as close as possible, the wound microenvironment permissive to DFT1 transplantation. Two common theories employed to explain cancer heterogeneity are the stochastic/clonal evolution (CE) or the hierarchical /CSC models. The CE model originates from any cell, instability accumulates genetic mutations over time resulting in a subclone of selected equivalent tumourigenic traits driving tumour progression and heterogeneity. In contrast to CE, the CSC model states that within the tumour only a very small subpopulation of stem cells are able

to self-renew and differentiate to form a hierarchical tumour consisting of stem cells, intermediate progenitors and differentiated progeny (401, 402). Now CE and CSC are not mutually exclusive and an alternative model or the reversible cellular plasticity (RCP) model could amalgamate aspects of both CE and CSC models. This model considers intrinsic cell processes and microenvironmental stimuli that allow progenitor cancer cells to reacquire stem cell characteristics transforming between stem cell and differentiated state (401, 402). The concept of plasticity would theoretically allow less symmetrical division (two daughter cancer stem cells or two daughter cells that differentiate) because resultant from CSC asymmetric division (one daughter cancer cell and one daughter cell that differentiates) are progenitor cells that would be able to convert back to CSC, thus increasing the CSC pool (403). Normal stem cells divide by asymmetric cell division (two daughter cells, one with self-renewal stem cell fate the other with differentiated characteristics) but this is inefficient during development or in response to injury. Dynamic control in such situations is achieved by stem cells having the potential to divide symmetrically producing a pool of daughter cells with the same fate (two daughter stem cells or two daughter differentiated cells), allowing stem cells to add more or less daughter stem cells or differentiated cells balanced by developmental and environmental conditions (404). DFT1 is a clonal transmissible tumour and our results show that the majority of tumour cells express self-renewal and stem cell markers, a rather shallow hierarchy, which is in contrast to the expected small population of stem cells according to the CSC model. How does DFT1 align with these models? Our results suggest that there is a blend of CE, RCP and CSC features. DFT1 is certainly clonally evolved, arising from a highly plastic SC lineage located in a repair microenvironment, that seemingly encompasses RCP, imparting a selective advantage for a progenitor cell expressing self-renewal and stem cell markers. The CSC model appears less likely because DFT1 has a lack of hierarchy and we observed that the majority of cells in DFT1 express proliferating cell nuclear antigen (PCNA) (DH, manuscript in preparation, figure 36R-S) indicating cells are proliferative and not quiescent. Ultimately the cell of origin,

genetic mutations and how self-renewal, proliferation and differentiation programs are regulated will determine the tumours path (405). CSCs may derive from normal progenitor cells that reacquire the ability to self-renew during mutation but are not necessarily the result of a stem cell that has undergone carcinogenesis (406). It is also possible, and we think that this is the case for DFT1, that CE may select for stem-like traits within a cancer such as a progenitor that re-acquires self-renewal capabilities, without committing to the CSC model (400). One possible explanation to the high numbers of cells expressing stem cell features is that they are dividing by symmetric cell division, a function enhanced by loss of tumour suppressor protein 53 (TP53), causing a tumour population with clonal progeny all lacking TP53 regulation and subsequent loss of tumour heterogeneity (400). Additionally, loss of TP53 appears to impart a stem cell transcriptional signature enhancing self-renewal in a mammosphere culture system (407). We found consistent nuclear expression of TP53 by DFT1 (DH, manuscript in preparation, data not presented, figure 36P-Q) indicating dysfunction of the MDM2-TP53 autoregulatory feedback loop. Normally, TP53 levels are low due to its short half-life but stabilisation and accumulation occurs in response to DNA damage, usually cytoplasmic ubiquitination and degradation or nuclear repression of TP53 occurs mediated by MDM2 (408, 409). This correlates with recent chromosome mapping finding four copies of TP53, with two of those found on the marker chromosomes of DFT1, where function was likely to be affected (5). Interestingly we found no immunohistochemical expression of wild type TP53, however strong expression of TP53 antibody that contained both wild type and mutant TP53, indicating that TP53 has mutated in DFT1. CSC show downregulation of MHC molecules I, lacks MHC-II, and further downregulates antigen processing systems (410). Because DFT1 has been shown to lack expression of MHC-I and MHC-II molecules (43, 411), our results would reason that progenitor/self-renewal properties expressed by DFT1s would certainly contribute significantly to DFT1s MHC downregulation, immune evasion and therefore transmissibility.

A further note that offers a degree of complexity when comparing CE and CSC theories is the suggestion that DFT1 may have arisen from an extensive chromosomal rearrangement caused by a cataclysmic event known as chromothripsis, rather than an accumulation of genetic mutations (412). This occurs when chromosomes (single or several) or chromosomal segment shatters and re-joins by nonhomologous end-joining DNA repair mechanisms resulting in an extensive rearrangement of limited regions of the domain (413) and is postulated as a mechanism for clonal evolution (407).

4.5.8 Additional Immunohistochemistry

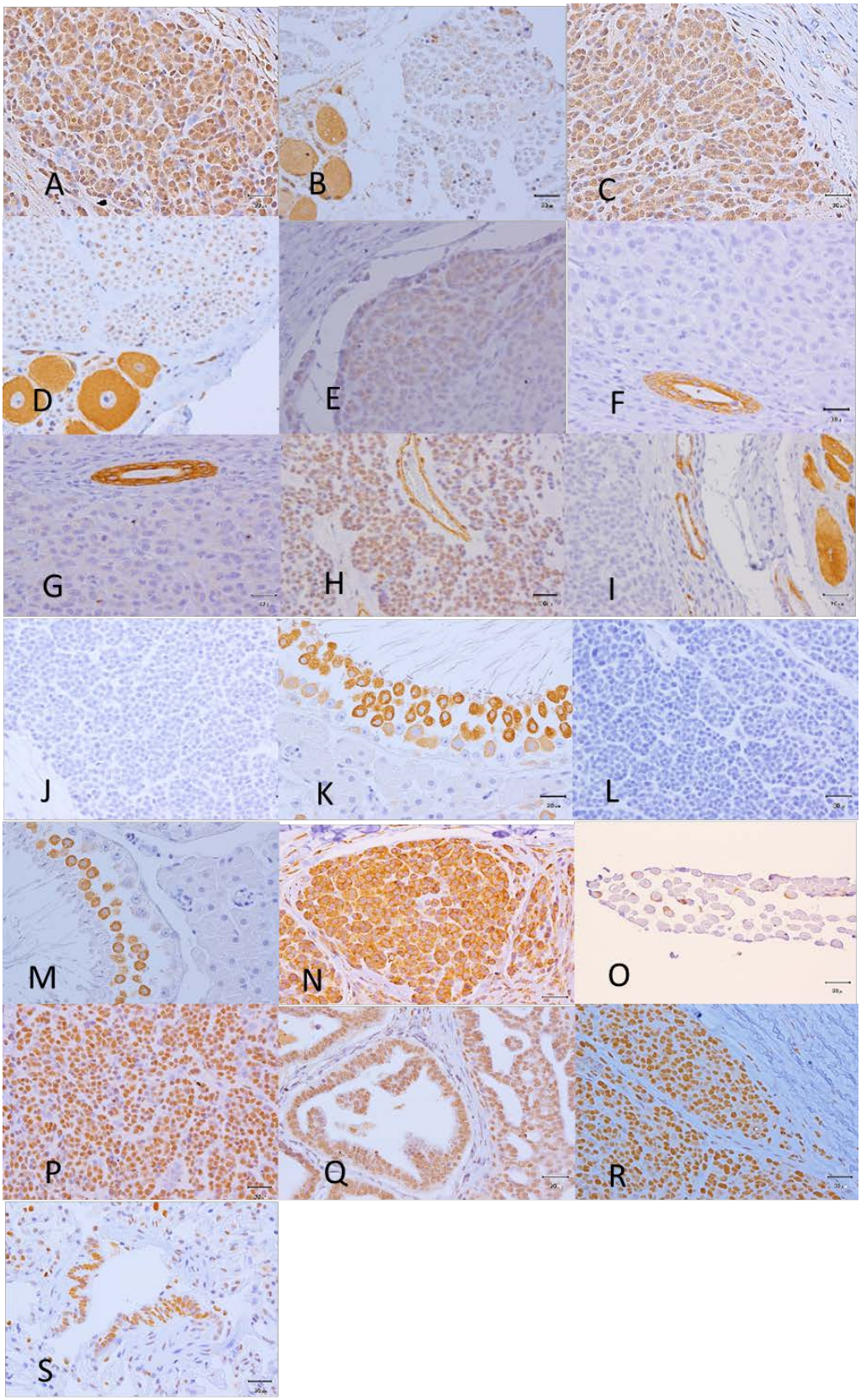

Figure 36: Additional immunohistochemistry.

DFT1 expressed moderate cytoplasmic staining of BDNF **A**, BDNF control peripheral nerve **B**, TRKB **C**. TRKB control peripheral nerve **D.** Very occasional isolated DFT1 cells did show cytoplasmic staining of Neurofilament protein (NEFL, NEFM, NEFH Pan) **E**. In ruling out epithelial origins of DFT1 we stained with pan cytokeratin AE1/AE3 which was not expressed, note internal positive control of hair shaft **F**. We also stained with high molecular weight cytokeratin 34Be12 which was also not expressed, note internal positive control of hair shaft **G**. We stained for SMA and although there is clearly no cytoplasmic staining there is however DFT1 often demonstrated light nuclear staining was present, note blood vessel internal positive control **H**. There is no expression of MSA by DFT1, note internal positive control blood vessel and skeletal muscle **I**. We included two markers often used to define germ cell lineage DDX4 **J**, testis control DDX4 **K** and YBX2 **L**, testis control YBX2 **M,** both of which were not expressed by DFT1. In addition to RPSA, laminin (α, β, γ) stained moderate to strong cytoplasmic and membranous **N**, laminin control peripheral nerve **O**. Moderate nuclear expression of TP53 was evident **P**, control adenocarcinoma TP53 **Q**. DFT1 expressed PCNA moderate to strong in the majority of cells **R**, control lung bronchial epithelium PCNA **S**. All controls are Tasmanian devil tissues. All micrographs are x40 magnification and scale bar represents 30 microns.

4.6 Conclusion

Our expressional results indicate six significant findings: 1. Histologically, strains 1-5 are very similar in appearance and difficult to differentiate on haematoxylin and eosin staining and for the most part share similar immunohistochemical expression. 2. The incredible SC plasticity is typified as many normal developmental stages of the Schwann cell lineage are represented including (TFAP2A) precursor, (PLP1) immature, (PRX) mature myelinating and (GFAP) non-myelinating Schwann cells however, no MBP is present. 3. The expression of growth factors IGFR2, BDNF, VEGF and PDGFRB indicates activated autocrine survival program from loss of axonal contact. 4. Expression of markers JUN, SHH and STAT3 that are specifically expressed by the Bungner Schwann cell suggests activation of the repair program. 5. Melanocyte markers were negative (MITF, MLANA, TYR), as predicted; however, unexpectedly, all DFT1 strains were positive for the melanocyte marker PNL2 suggesting a bipotent Schwann cell/melanocyte progenitor-like cell. 6.

The expression of SOX10, NGFR, NES, SOX2, POU5F1, EPCAM, CD44 and PROM1 indicates a NCSC/progenitor cell with self-renewal properties.

The extensive literature presented above certainly advocates the remarkable plasticity of NCSCs and the Schwann cell and melanocyte lineages derived from them. Our results find that DFT1 is a progenitor-like cell, bipotent with both SC and melanocyte features, expressing repair transcription and growth factors with the acquisition of NCSC self-renewal properties. We theorise that the facial wound and resultant nerve injury would provide a perfect microenvironment, a niche, containing trophic signals necessary for migration, survival, proliferation and self-renewal of DFT1. The wound environment would be conducive to the genetic selection of a NC progenitor with the molecular plasticity and MHC downregulation, causal to DFT1s clonal nature and transmissibility.

Chapter 2

5.0 ERBB3: A Potential Serum Biomarker for Early Detection and Therapeutic Target for Devil Facial Tumour 1 (DFT1)

Dane A. Hayes [1, 2, 3], Dale A. Kunde [3], Robyn L. Taylor [2, 4], Stephen B. Pyecroft [5], Sukhwinder Singh Sohal[3], Elizabeth T. Snow [3]

[1]Department of Primary Industries, Parks Water and Environment, Animal Health Laboratory, Launceston, Tasmania, Australia.

[2]Save the Tasmanian Devil Program, University of Tasmania, Hobart, Tasmania, Australia.

[3]School of Health Sciences, Faculty of Health, University of Tasmania, Launceston, Tasmania, Australia.

[4]Department of Primary Industries, Parks Water and Environment, Resource Management and Conservation, Hobart, Tasmania, Australia.

[5]School of Animal & Veterinary Sciences, Faculty of Science, University of Adelaide, Roseworthy Campus, Roseworthy, South Australia.

Funding: This research was funded by the Eric Guiler Tasmanian Devil Research grant through the University of Tasmanian and the Save the Tasmanian Devil Appeal (STDP) to DH http://www.tassiedevil.com.au/tasdevil.nsf and the Department of Primary Industries water and Environment (DPIPWE) for financial and in kind support.

Competing interests: The authors declared that there were no competing interests.

Corresponding author:

*E-mail: dane.hayes@dpipwe.tas.gov.au (DH)

5.1 Abstract

Devil Facial Tumour 1 (DFT1) is one of two transmissible neoplasms of Tasmanian devils (*Sarcophilus harrisii*) predominantly affecting their facial regions. DFT1's cellular origin is that of Schwann cell lineage where lesions are evident macroscopically late in the disease. Conversely, the pre-clinical timeframe from cellular transmission to appearance of DFT1 remains uncertain demonstrating the importance of an effective pre-clinical biomarker. We show that ERBB3, a marker expressed normally by the developing neural crest and Schwann cells, is immunohistohemically expressed by DFT1, therefore the potential of ERBB3 as a biomarker was explored. Under the hypothesis that serum ERBB3 levels may increase as DFT1 invades local and distant tissues our pilot study determined serum ERBB3 levels in normal Tasmanian devils and Tasmanian devils with DFT1. Compared to the baseline serum ERBB3 levels in unaffected Tasmanian devils, Tasmanian devils with DFT1 showed significant elevation of serum ERBB3 levels. Interestingly Tasmanian devils with cutaneous lymphoma (CL) also showed elevation of serum ERBB3 levels when compared to the baseline serum levels of Tasmanian devils without DFT1. Thus, elevated serum ERBB3 levels in otherwise healthy looking devils could predict possible DFT1 or CL in captive or wild devil populations and would have implications on the management, welfare and survival of Tasmanian devils. ERBB3 is also a therapeutic target and therefore the potential exists to consider modes of administration that may eradicate DFT1 from the wild.

5.2 Introduction

5.2.1 Receptor tyrosine Kinases

Receptor tyrosine kinases (RTK's) are transmembrane cell surface receptors possessing protein tyrosine kinase activity. That are essential regulators of development, cell cycle, migration, survival, proliferation, differentiation and to date 58 human RTK's have been identified, grouped into 20 subfamilies (414-416). Emerging is the concept that RTK's are part of a complex signalling network rather than a vertical linear pathway where cross talk between RTK's, plasma membrane and protein interaction domains, adaptor proteins, feed forward and feedback loops together synchronise a temperospatial signalling cascade allowing a dynamic cellular response to receptor activation. (Reviewed in (417-419).

5.2.2 ERBB family of Receptor tyrosine Kinases

The epidermal growth factor (EGF) family represents a complex group of type 1 transmembrane RTK's with differing ligands that are capable of receptor cross talk and lateral signalling that activates various pathways regulated to execute diverse cellular functions (420, 421). This family consists of four members (HER1-4) belonging to the ERBB lineage of proteins (Erbb1-4) where HER is derived from human epidermal growth factor, and ERBB derived from avian erythroblastosis oncogene, v-erbB, with each receptor numerically ascending 1-4. Collectively the human epidermal growth factor receptor gene family is designated *EGFR/ERBB1/HER1, ERBB2/HER2, ERBB3/HER3* and *ERBB4/HER4* (422). The extracellular domain (ECD) of the ERBB family members show high structural homology and consists of between 620-629 amino acids divided into four domains, I – IV. Domains I and III are leucine rich and interact with each other in an unstimulated state but also participate in ligand binding. Domains II and IV are cysteine rich and participate in

ERBB homo- and heterodimer complexes. Following the ECD is a single transmembrane segment of 19-25 amino acids and an intracellular portion of approximately 550 amino acids consisting of the juxtamembrane segment (~40 amino acids), protein kinase domain (~260 amino acids) and carboxyterminal tail (~232amino acids) (422-425). The EGF consists of 11 peptide growth factor members including transforming growth factor-alpha (TGFα), amphiregulin (AR), beta- cellulin (BTC), heparin binding EGF-like growth factor (HB-EGF), epiregulin (EPR), epigen (EPG), and the neuregulins (NRG1-6). Binding of the EGF results in a conformational change responsible for homo and/or heterodimerisation combinations (422, 426-429). The ligand binding changes the conformation of the ECD for all ERBB's except ERBB2 where the dimerization arm changes from a 'tethered' to "extended' to encourage dimer formation whereas ErbB2 remains in an extended conformation, reviewed in (430). Due to the presence of multiple p85 binding sites in its tyrosine kinase domain, ERBB3 efficiently activates the phoshatidylinositide 3-Kinase (PI3K) pathway (431) although the complex signalling network of ERBB receptors commonly activate the Ras- and Shc-mitogen activated protein kinase (MAPK) pathway and the phoshatidylinositide 3-Kinase (PI3K) pathway (432-435).

5.2.3 ERBB3

The importance of lateral signalling among ERBB's is no more apparent than with receptors Erbb2 and ERBB3 that must heterodimerise with other ERBB members to signal (432) as ERBB3 has a ligand but impaired tyrosine kinase activity (436) whereas ErbB2 has no know ligand (orphan receptor) but a functional kinase region (437). Although ERBB3 has long been considered impaired or termed a pseudo-kinase, Shi et al. (438) has determined that ERBB3 does have sufficient kinase activity, although substantially reduced. Not long after ERBB3's discovery and characterisation (439, 440), heregulin (neuregulin) was determined as its ligand (441) and the strong and preferred

dimer between ERBB2 and ERBB3 was soon recognised (442). Whilst the model of 'inactive monomer-active dimer' is long standing (443) researchers have provided new evidence of the intricacies of RTK signalling involving both extracellular and intracellular processes. How ERBB3 is able to activate other ERBB family members with its catalytically inactive domain has been elusive, Zhang (444) while studying the structure of EGFR described an allosteric mechanism termed an 'asymmetric dimer' providing the process. Essentially, ERBB3 functions as a cyclin-like activator only (C-lobe face) for other EGFR family members because its kinase domain (N-lobe face) is divergent and this concept of ERBB3 behaving as an "activator" despite being catalytically inactive has been supported by readily activating ERBB2 (445) and EGFR (446, 447). Similar to the cytoplasmic complexities the plasma membrane also holds intricacies of receptor positioning where ligand binding inducing dimerization is generally accepted there is evidence that some RTK's exist as oligomers (complexes of more than two receptors) or higher-order oligomerisation is required for activation (448). Unstimulated ERBB receptors have been shown to self-associate in oligomers that dissociate on NRG1 binding to allow heterodimers with ERBB2 (449) thus favouring ERBB2/ERBB3 heterodimerisation in the absence of homodimerisation (450). Although NRG1 binding destabilises ERBB3 oligomers, dimers are neither stabilised nor disrupted upon ligand binding indicating that two interfaces exist and that oligomers, dimers and monomers are either extended or closed in their conformation (451). Higher order and proxy phosphorylation appear to be integral to ERBB2/ERBB3 signalling (452) and that the ERBB3 formations may act as a scaffold for the assembly of signalling complexes (453). Recently, Steinkanmp (454) has suggested a modified model for ERBB3 signalling in addition to heterodimerisation and transphosphorylation, ERBB3 activated homodimers should also be competent for both transphosphorylation and phosphorylation of cytoplasmic partners leading to the development of a spatial stochastic model addressing the dynamics of ERBB3 homodimerisation and heterodimerisation with ERBB2 (455) by measures of diffusion, dimer-off rates, kinase activity and dephosphorylation. ERBB structure and

function has relied heavily on its crystallography (456), now new technologies such as fluorescence resonance energy transfer (FRET), single –particle tracking (SPT) and others are assisting researchers focusing on the dynamic regulation of signal transduction (448).

5.2.4 ERBB3 Endocytosis

Negative regulation and inactivation of ERBB receptors were thought to be similar to ERBB1, that is rapidly internalised in a clathrin mediated endocytosis (CME) destined for lysosomal degradation, although clathrin-independent endocytosis has been demonstrated (457, 458). However, in contrast it was found that ERBB2-4 appeared to be impaired and internalised very slowly (459-461) utilising pathways such as caveolin or micropinocytosis and clathrin-and caveolin independent pathways (462, 463). Unlike ERBB1, ERBB3 is degraded by proteasomes catalysed by the E3 ubiquitin ligase NRDP1 (Neuregulin Receptor Degradation Protein -1) (464) now known as RNF41 (Ring Finger 41, E3 Ubiquitin Protein Ligase) and that this protein acts as a regulator of steady-state ERBB3 receptor levels influencing NRG1 signalling (465-467). A recent study has shown that ERBB3 is endocytosed in the absence of added ligand in a clathrin-dependent manner, independently of its tyrosine phosphorylation state (468). The ligand induced down regulation of ERBB3 is further enhanced by USP8 (Ubiquitin Specific Peptidase -8) which stabilises RNF41 (467). Yen et al. (469) suggests that RNF41 is pivotal in ERBB3 regulation as RNF41 mediated degradation supresses cellular growth and motility and that loss of RNF41 may promote tumour progression in breast cancer. RNF41 has also been shown to associate with nascent forms of ERBB3 to accelerate its degradation involving the endoplasmic reticulum – associated degradation (ERAD) pathway as a mechanism of controlling steady state levels of ERBB3 (470). Recently Huang et al. (471) demonstrated that NEDD4 (Neural Cell Precursor Expressed, Developmentally Down-regulated 4, E3 Ubiquitin Protein Ligase) an E3 ligase also regulates ERBB3 as NEDD4 knockdown resulted in

increased expression of ERBB3 and tumour proliferation suggesting both NEDD4 and RNF41 interact with different domains to regulate ERBB3 levels. Mosesson et al. (472) suggests that defective internalisation, recycling and degradation of cell surface proteins and ligands is an emerging feature of cancer. Due to the oncogenic alterations of malignant cells aberrant function of E3 ubiquitin ligases such as NEDD4 enables degradation avoidance prolonging growth factor signalling and overexpression of receptors. Recently Shi et al. (473) suggested RNF41 mediated ERBB3 degradation could be beneficial in glioma therapy as overexpression of RNF41 decreased ERBB3 levels and suppressed glioma migration and invasion (A172 and U118 cell lines).

5.2.5 Nuclear localisation of ERBB3

Although the receptor ERBB3 is well known for its transmembrane exploits, nuclear detection of ERBB3 in certain cells suggests that nuclear- cytoplasmic shuttling can occur, although exactly how translocation occurs is yet to be defined. Nuclear expression has been observed in mammary epithelial cells and breast cancer (474), Schwann cells (475, 476), Prostate cancer (477-479), colorectal cancer , non-small cell lung cancer, head and neck Squamous cell carcinoma (480), colorectal cancer (481) and breast cancer (482). Recently an 80 kDa nuclear variant of ERBB3 receptor ($ERBB3_{80kDa}$) in a human lung adenocarcinoma cell line corresponding to the intracellular domain has been identified whose translocation occurs independently of NRG1 and is associated with cell proliferation activating the Cyclin D1 promotor (483). In contrast, full length ERBB3 (185 kDa) was found to translocate to the nucleus in a clathrin-independent pathway in breast cancer cell lines binding with STAT3 (signal transducer and activator of transcription 3) and STAT5, which are also associated with cell proliferation.

5.2.6 Secreted ERBB3

Shortly after ERBB3's discovery and characterisation (439, 440), Katoh et al. (484) identified a 1.4 kb transcript of ERBB3 (full length receptor is 6.2 kb) in gastric cancer cell lines due to alternative splicing of the *ERBB3* gene which encodes a secreted form of the receptor. Funayama et al. (485) reported that mRNA levels of this secreted form (sERBB3) were expressed 5-15 times higher in Squamous cell carcinoma cell lines than normal cell lines. However, the ratio of secreted ERBB3 type to the transmembrane ERBB3 type varied between cell lines suggesting that expression of secreted ERBB3 mRNA was regulated differently than transmembrane ERBB3 mRNA. Srinivasan et al. (486) found that the 1.4 kb transcript was also found intracellularly and predominantly as a glycosylated, disulphide-bonded dimer of 58kDa in breast and ovarian cancer cell lines as well as normal human tissues. Lee et al. (487) subsequently reported isolation of four novel alternative transcripts (1.6, 1.7, 2.1, and 2.3kb) from ovarian cancer cell lines all of which are truncated forms of the ligand binding domain and transfected fibroblast studies revealed three out of the four products are secreted proteins. Further studies by Lee et al. (488) found that the 2.1kb transcript also known as p85-SERB3, can bind to NRG1 with high affinity and can effectively block NRG1 binding the cell surface receptors thus inhibiting activation of heterodimers. The secreted isoform of ERBB3 identified as a bone metastasis factor (MDA-BF-1), corresponding to the 1.7 kb /p45 sERBB3 alternative transcript reported by Lee et al. (487, 488), was found by Vakar-Lopez et al. (489) to be highly expressed in the metastatic prostate carcinoma cells in both lymph node and bone. In addition MDA-BF-1 was also present in activated osteoblasts suggesting diverse functions in prostate cancer progression. Subsequently, the same secreted isoform (1.7 kb, p45-sERBB3, 45kDa, MDA-BF-1) was found in a series of prostate carcinoma investigations where it promotes osteonectin (490), detection in serum of patients with castration resistant prostate cancer with bone metastasis (491), present in serum as well as activated osteoblasts and prostate cancer cells

and interestingly in men without clinical prostate cancer raising questions of sERBB3 involvement in other cellular functions (492). As well as prostate, secreted ERBB3 has been indicated as an early marker of hepatocellular carcinoma (HCC) in patients with chronic hepatitis and cirrhosis by Hsieh et al. (493) They found that sERBB3 was present in interstitial fluid and these levels also correlated with those in sera although not associated with expression levels of ERBB3 in tissues. Recently, Takahashi et al. (494) demonstrated that sERBB3 has strong suppressive effects on NRG1 acting on cell surface molecules rather than the ligand and that the ERBB2/ERBB3 heterodimer is crucial for downstream signalling in MCF7 breast cancer cell lines.

5.2.7 ERBB3 in Schwann cell development

During development of the peripheral nervous system both myelinating and non-myelinating Schwann cells originate from the neural crest, initially migrating as multipotent cells that become fate restricted to Schwann cell lineage under trophic, mitogenic and axonal signalling influence. The sequential transition from Schwann cell precursor to immature Schwann cell and finally mature Schwann cell is under strict molecular signalling control resulting in two Schwann cell phenotypes emerging. Myelinating Schwann cells will form a 1:1 relationship with large calibre nerves whereupon a multilammelar myelin sheath or non-myelinating Schwann cells that envelop many small calibre nerves to form Remak bundles (reviewed in (109, 118, 119, 121, 264, 495-499). Meyer et al. (500) found that ERBB3 was expressed by developing Schwann cells and their precursors, was responsible for neuregulin-1 binding in the developing glial cells and that heterodimerisation occurs with a co-receptor ERBB2. Similar conclusions that ERBB3 was a receptor for neuregulin and that both ERBB3 and ERBB2 were able to be phosphorylated and that ERBB2 is able to mediate cellular transduction despite no known ligand (441, 501). The importance of neuregulin in early development became apparent when neuregulin mutant embryo mice

displayed multiple phenotypical changes in cells that express ERBB3 such as altered Schwann cell and ganglia development (500). Reithmacher et al. (502) found that mutant mice lacking ERBB3 formed motor and sensory neurons of the dorsal root ganglia but the great majority undergo cell death. Grinspan et al. (503) found that the normal programmed cell death of ERBB3/ERBB2 expressing pre-myelinating Schwann cells in neonatal rats was a consequence of competition for limited axonally derived neuregulin. This effectively limits the available pool of pre-myelinating Schwann cells to those with axonal contact and thus survival; however, apoptosis could be prevented if exogenous neuregulin was administered. Also noticed was that Schwann cell death was either reduced or absent in older animals following nerve transection compared to that of new born animals. Raabe etal. (504) found that neonatal rat cultured Schwann cells contain and secrete neuregulin which may act as a survival autocrine/paracrine or juxtacrine loop, while Cheng (505) also that rat postnatal Schwann cells secreted autocrine factors that suggested that Schwann cells switch form axonal survival signals to autocrine signals at around the time of birth, as would be required for peripheral nerve regeneration after injury. Realising that transection in postnatal nerves results in loss of axonal contact for Schwann cells but not their death Meier et al. (197) demonstrated that postnatal Schwann cells do indeed have an autocrine loop consisting of a number of growth factors such as insulin growth factor, platelet derived growth factor – BB and neurotrophin-3 ensuring their survival. Interestingly their research also found that the Schwann cell precursors did not have the same autocrine loop and their survival seems to depend on axonal signals. Li et al. (435) found that cultured neonatal rat Schwann cells demonstrated that the PI3K was essential for transducing both autocrine and neuregulin mediated survival signals. Meyer et al. (506) concluded that of the 3 isoforms of neuregulin -1 in mouse development, type I is expressed by tissues including cranial ganglia and governs, among others, neural crest derived neurons whereas type III is expressed in differentiating sensory and motor neurons and acts on Schwann cell precursors driving their initial development. In addition, Michaelov et al. (507) found

that neuregulin-1 type III overexpression in transgenic mice resulted in thicker myelin therefore, neuregulin-1 type III is involved in regulation of myelin thickness. Over the next decade researchers consolidate the importance of ERBB2 (508) and the ERBB3/neuregulin -1 signalling being crucial for growth, development and proliferation of Schwann cells and their axonal regulated radial sorting, ensheathment and myelination (196, 509-515). The adult peripheral nervous system requires maintenance when it is injured and the NRG1/ERBB system is crucial to its degeneration, regeneration and remyelination following nerve injury. Fricker et al. (516) found that Schwann cell proliferation, dedifferentiation, mobilisation of macrophages and myelin clean-up was not regulated by NRG1. However, NRG1 was required for target reinnervation, early phase of functional recovery and regulating remyelination but myelination fate was not absolutely dependent on NRG1. Ronchi et al. (279) demonstrated in rat median nerve one week after injury the expression of ERBB2/ERBB3 co-receptor is strongly upregulated and NRG type III was highly expressed and only switched off after axon regeneration illustrating the plasticity of the Schwann cell.

5.2.8 ERBB3 as a potential biomarker

ERBB2 and ERBB3 overexpression (439, 517, 518), cooperation in neoplastic transformation (431, 519-521) and loss of ERBB3 preventing the progressive transformation of ERBB2-over expressing tumours (522) reinforces ERBB3's pivotal role in ERBB signalling. Early studies revealed ERBB3 as a potential oncogene with overexpression due to possible increased transcription as no gene amplification was observed (523, 524) although recently oncogenic mutations have been reported (525) indicating either ERBB3 or its downstream components should represent a potential target for therapy (526).

ERBB3 is upregulated in a number of human cancers such breast, colon, gastric, ovarian and prostate (420, 527) but seldom reported in veterinary cancers (528-530) although it would appear the instrumental role that ERBB3 may play in some veterinary tumours is yet to be elucidated. DFT1's immunohistochemical expression of ERBB3 led us to postulate that excess extracellular domain (ECD) may circulate in the host's plasma and present itself as a possible candidate biomarker for DFT1. Literature reports five secreted alternative transcripts of ERBB3 present in serum or interstitial fluid (484, 487) which can be detected utilising ELISA methodology.

Our pilot study assessed serum ERBB3 for the first time in Tasmanian devils revealing that serum ERBB3 was substantially elevated in the serum of Tasmanian devils with DFT1 compared to those Tasmanian devils without DFT1. Interestingly, the inclusion of some Tasmanian devils with CL in our pilot study revealed that ERBB3 may also be a biomarker for this disease, although CL is clinically distinct from DFT1. We identify ERBB3 as a potential biomarker of DFT1 and highlight current literature supporting the therapeutic possibilities that can be directed towards ERBB3 overexpressing tumours that may be helpful in the elimination of DFT1 from the wild.

5.3 Methods

5.3.1 Tasmanian devil ERBB3 pilot study

A pilot study of thirty-five Tasmanian devils differing in age, sex and geographic location were selected and listed in table 5, to compare serum ERBB3 levels in clinically healthy Tasmanian devils (CHD), devils with DFT1 and those with CL. The Fifteen CHD'S included both adults (n=12) and clinically healthy juvenile Tasmanian devils (CHJD, n=3) 10 months of age. Adults included free range captive (n=5), captive (n=3) and wild devils (n=4). Clinically healthy adults either had no visible disease (ND, n=8) or had localised skin non-DFT1 dermatopathy (CHDD, n=4) consisting of two abscesses, a skin tag and localised dermatitis. Eight Tasmanian devils with clinical DFT1 and Twelve Tasmanian devils with CL. Tasmanian devils with CL were included in the study as a severe skin condition recognised clinically but very distinct from DFT1. All dermatopathies, DFT1 and CL were confirmed histologically by the Animal Health Laboratory, DPIPWE.

Table 5: Tasmanian devil pilot study individuals.

Devil	Microchip Identification	Laboratory accession	Age (years)	Sex (M/F)	Geographic location	Clinical status
1	982000190997443	13/3712	1	F	Freycinet [a]	CHD
2	982000123211124	13/3683	3	F	Freycinet [a]	CHD
3	982009104963600	13/3680	4	M	Freycinet [a]	CHD
4	982009104860765	13/3713	4	M	Freycinet [a]	CHD
5	982000123130282	13/3716	2	M	Freycinet [a]	CHD
6	982009105111670	09/4200	3	F	West Pencil Pine [b]	CHD
7	982009105849999	09/3957	2	M	Tullah [b]	CHD
8	985154000001063	09/1051	1	M	Cressy [c]	CHD
9	982009104269684	08/1805	2	M	Narawntapu [b]	CHDD
10	982009106039877	10/0156	2	M	Dunalley [b]	CHDD

11	982009104236464	08/0798	1	F	Taroona [c]	CHDD
12	982009104357109	09/2009	4	F	Fern Tree [c]	CHDD
13	985154000001151	09/0451	<1	M	Mt Pleasant [d]	CHJD
14	985154000001142	09/0449	<1	F	Mt Pleasant [d]	CHJD
15	985154000001130	09/0448	<1	M	Mt Pleasant [d]	CHJD
16	982009104841875	12/2065	6	F	West Pencil Pine [b]	DFT1
17	982009106034139	11/0767	2	F	Dunalley [b]	DFT1
18	982009104719592	12/0820	4	F	West Pencil Pine [b]	DFT1
19	982000000122095	12/2095	2	F	Upper Natone [b]	DFT1
20	982000123128645	11/3917	2	M	Hamilton [b]	DFT1
21	982000123216973	11/3918	1	F	Hamilton [b]	DFT1
22	982000123209814	11/4493	2	M	Waratah [b]	DFT1
23	000000000130406	13/0406	2	F	Mangalore [b]	DFT1
24	NC	11/0650	7	F	Mole Creek [c]	CL
25	985120016024404	11/4290	8	F	Mt Pleasant [c]	CL
26	982009106314654	10/4001	8	M	Taranna [c]	CL
27	982009106585887	10/3765	5	F	Calder [b]	CL
28	982009104789818	14/0034	6	F	Cressy [c]	CL
29	NC	08/4048	4	F	Circular Head [b]	CL
30	982009100786171	09/0402	6	F	Mt Pleasant [c]	CL
31	982009101694833	10/1013	6	F	Richmond [c]	CL
32	982009104910854	13/0518	6	F	Cressy [c]	CL
33	NC	09/3035	5	F	South Riana [b]	CL
34	NC	11/1615	6	F	Mole Creek [c]	CL
35	982009104873582	13/3714	4	F	Freycinet[a]	CL*

NC not microchipped, CHD clinically healthy devil, CHDD clinically healthy devil with dermatopathy, CHJD clinically healthy juvenile devil, DFT1 devil facial tumour 1, CL cutaneous lymphoma, [a] Free range enclosure, [b] Wild devil, [c] Captive devil, [d] captive juvenile, * no tissue diagnosis.

5.3.2 Tasmanian devil serum sample and collection

Bloods from Tasmanian devils (Table 5) were collected by wildlife veterinarians through jugular venepuncture, whilst the animals were restrained by a trained field officer. Ten millilitres of blood was collected in sterile serum separation tubes, stored on ice for transport to the laboratories, centrifuged and serum removed for archival storage at -20^{o}C.

Serum samples were retrieved from the frozen archive and thawed at room temperature immediately before analysis.

5.3.3 ERBB3 ELISA assay

Serum ERBB3 levels were measured using the RayBio anti-human ERBB3 ELISA Kit (Enzyme linked immunosorbent assay, ELH-ERBB3, RayBiotech Inc, GA, USA) according to manufacturer's instructions. Briefly, serum samples were diluted 1/5 in Assay Diluent A and 100 uL of standard or diluted sample were added in duplicate to wells of a 96 well assay plate and incubated for 24 hrs at 4^{o}C. The supernatant was removed and wells were washed 4 times with 300 uL of 1X wash solution using an Immunowash 1575 (BioRad Laboratories, CA, USA). One hundred microliters of prepared biotinylated anti-ERBB3 was added to each well and the assay plate incubated for 1 hour at room temperature. The assay plate was washed as described after which 100 uL of prepared HRP-streptavadin conjugate was added to each well and the assay plate incubated for 45 minutes at RT. The assay plate was again washed as described and 100 uL of TMP substrate was added and the plate incubated for 30 minutes at room temperature in the dark, after which 50 uL of stop reagent was added to each well. The absorbance of each well was measured at 450 nm using a Tecan Infinite M200 microplate reader (Tecan, Salzburg, AUT).

5.3.4 Data analysis

The ELISA standard curve was plotted using Prism v5 (GraphPad, CA, USA) and results for each serum interpolated and corrected for dilution. The significance of differences in serum ERBB3 between groups was determined using a Kruskal-Wallis test with Dunn's Multiple Comparison utilizing Prism v5 (GraphPad, CA, USA).

5.3.5 ERBB3 immunohistochemistry

Species	Gene ID	Peptide ID	Peptide length	% identity (Protein)	% coverage	Genomic location
Human (*Homo sapiens*)	ENSG00000065361	ENSP00000267101	1342 aa	82 %	98 %	12:56079857-56103505
Tasmanian devil (*Sarcophilus harrisii*)	ENSSHAG00000005870	ENSSHAP00000006754	1328 aa	83 %	99 %	GL861720.1:186836-237967

```
ENSP00000267101_Hsap/1-1342    MLGGTFLYWRGRRIQNKRAMRRYLERGESIEPLDPSEKANKVLARIFKETELRKLKVLGS
ENSSHAP00000006754_Shar/1-1328 ALLLTLLYLRGRKIQKKRAMRRYLERGESLEPLDPGEKANKVLARIFKETELRKLKVLGS
                                *  *:** ***:**:**************:******.************************

ENSP00000267101_Hsap/1-1342    GVFGTVHKGVWIPEGESIKIPVCIKVIEDKSGRQSFQAVTDHMLAIGSLDHAHIVRLLGL
ENSSHAP00000006754_Shar/1-1328 GVFGTVHKGIWIPEGESIKIPVCIKVIEDRSGRQSFQAVTDHMLAIGSLDHTHIVRLLGL
                               *********:*******************:**********************:*********

ENSP00000267101_Hsap/1-1342    CPGSSLQLVTQYLPLGSLLDHVRQHRGALGPQLLLNWGVQIAKGMYYLEEHGMVHRNLAA
ENSSHAP00000006754_Shar/1-1328 CPGSSLQLVTQFLPLGSVLDHVRQHRGALGPQLLLNWAVQIAKGMYYLEEHGMVHRNLAA
                               ***********:*****:******************.**********************

ENSP00000267101_Hsap/1-1342    RNVLLKSPSQVQVADFGVADLLPPDDKQLLYSEAKTPIKWMALESIHFGKYTHQSDVWSY
ENSSHAP00000006754_Shar/1-1328 RNVLLKSPSQVQVADFGVADLLPPDDKQLLHSEAKTPIKWMALESIHFGKYTHQSDVWSY
                               ******************************:*****************************

ENSP00000267101_Hsap/1-1342    GVTVWELMTFGAEPYAGLRLAEVPDLLEKGERLAQPQICTIDVYMVMVKCWMIDENIRPT
ENSSHAP00000006754_Shar/1-1328 GVTIWELMTFGDIPYKGLRLAEVPDLLEKGERLAQPQICTIDVYMVMVKCWMIDENIRPT
                               ***:*******  ** ********************************************
```

Figure 37: Human and Tasmanian devil sequence alignment for ERBB3.

Reference figure: Ensembl gene browser https://www.ensembl.org/

Monoclonal rabbit anti-human ERBB3 (Abcam, clone SP71, ab93739, internal region, depicted in figure 37 human Tasmanian devil ERBB3 sequence alignment below) was diluted 1:50 with antibody diluent (Dako, S0809) using standard immunohistochemical methodology outlined in section three.

5.4 Results

5.4.1 Histology and Immunohistochemistry

DFT1 histology (figure 38A) and Haematoxylin and Eosin demonstrates small round cells with indistinct cell membranes arranged in cords and packets. ERBB3 IHC on average revealed moderate to strong expression in 75% of cells in both primary and secondary DFT1 tumours in cytogenetically determined strains 1 to 5 of DFT1. Typical granular cytoplasmic expression (figure 38B) demonstrated by DFT1 strain 3 cells with small and large aggregates noted. Higher magnification (figure 38C) shows accumulation in and around vacuolar structures within the cytoplasm. In sections of devil skin and subcutaneous (figure 38E), peripheral nerve was seldom positive for ERBB3 (red arrow) in keeping with downregulation of ERBB3 in the adult in contrast to DFT1 ERBB3 expression (black arrow). ERBB3 expression was noted in Tasmanian devil lymphoid follicle (figure 38F) where cytoplasmic expression of ERBB3 is present in both T (germinal centre) and B (mantle) cells. Devils with CL were not included in the ERBB3 immunohistochemical staining. Trigeminal nerve section (figure 38I) showed ERBB3 expression in nerve bodies (black arrow) and occasional ERBB3 expression in the adaxonal area (red arrows) but generally, small myelinated nerves were negative. Positive control included devil bowel (figure 38G) which exhibited a similar expression pattern to human ERBB3 and negative controls DFT1 (figure 38D), bowel (figure 38H) and Trigeminal nerve (figure 38J). The monoclonal rabbit anti-human ERBB3 clone SP71 is a synthetic peptide corresponding to an internal sequence of Human ERBB3. Although the exact sequence is a proprietary secret ERBB3 sequence alignment between human and Tasmanian devil in this region has high homology (figure 37).

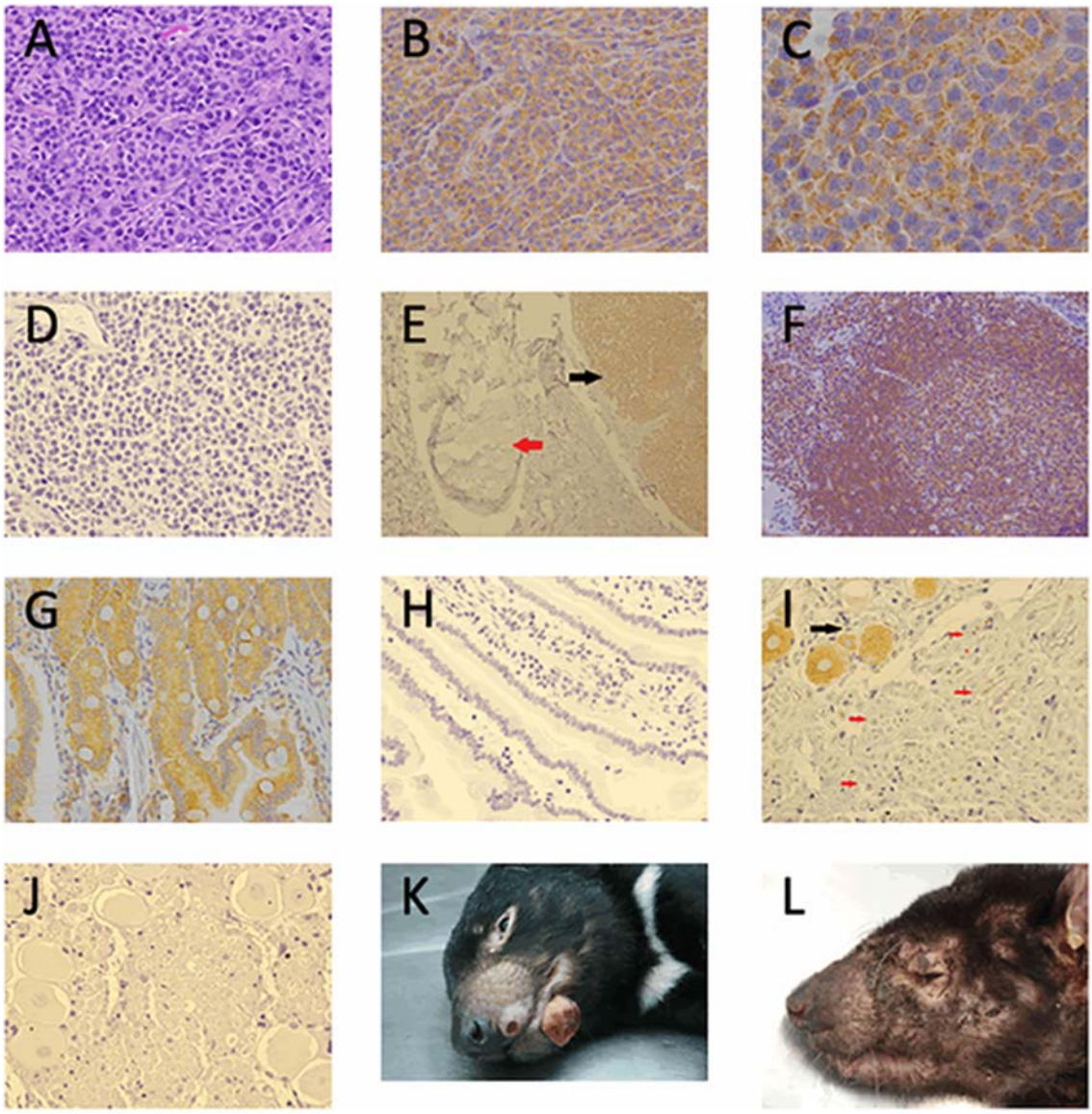

Figure 38: DFT1 staining and skin manifestation.

A Haematoxylin and Eosin stained DFT1 x40, **B** ERBB3 Immunohistochemical expression in DFT1 strain 3 x40, **C** ERBB3 immunohistochemical expression in DFT1 strain 3 x100, **D** DFT1 negative control, **E** Tasmanian devil skin and subcutis section with peripheral nerve (red arrow) and DFT1 (black arrow) x10, **F** Tasmanian devil lymph node ERBB3 expression lymphoid follicle x20, **G** Tasmanian devil bowel ERBB3 positive control x40, **H** ERBB3 IHC negative control bowel, **I** trigeminal nerve shows ERBB3 positive nerve body (black arrow) and occasional adaxonal ERBB3 positivity (red arrows) x40, **J** ERBB3 IHC negative control trigeminal nerve, **K** Tasmanian Devil gross appearance of DFT1. Photo credit: DPIPWE archive, **L** Tasmanian devil gross appearance cutaneous lymphoma. Photo credit DPIPWE archive.

5.4.2 Serum ERBB3 in Tasmanian devils

Serum ERBB3 levels are shown in Table 6 and graphically in figure 39. Serum ERBB3 in the Fifteen Tasmanian devils without neoplasia (devils 1-15 includes CHD, CHDD and CHJD) ranged from <30-663 pg/ml with a median of 32 pg/mL (30 – 220; interquartile range). Serum ERBB3 levels in the eight Tasmanian devils (devils 16-23) with clinical DFT1 ranged from 766-18,254 pg/ml with median of 3051 pg/mL (1060 – 10879; interquartile range. In the twelve Tasmanian devils with cutaneous lymphoma (devils 24-35) serum ERBB3 levels ranged from <30-20,021 pg/ml with a median of 1485 pg/mL (289 – 7901; interquartile range).

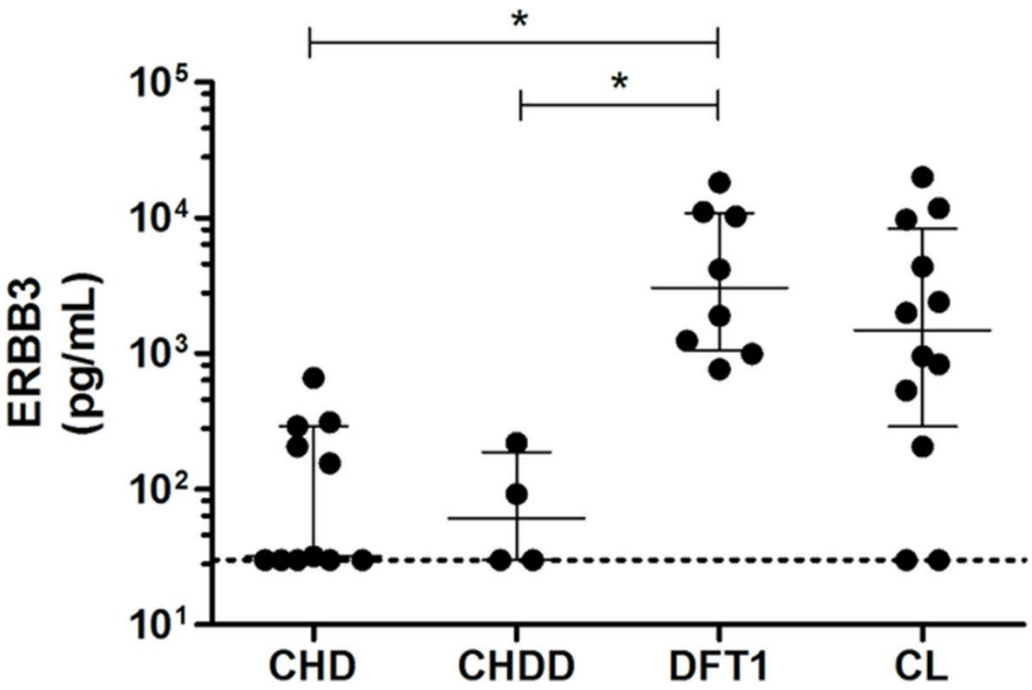

Figure 39: Serum ERBB3 levels in Tasmanian devils.

Serum ERBB3 levels were measured by ELISA in clinically healthy Tasmanian devils CHD (n=11), clinically healthy Tasmanian devils with dermatopathy CHDD (n=4), clinically diagnosed DFT1 (n=8) and those with cutaneous lymphoma CL (n=12). Horizontal dashed line indicates the limit of detection of the ELISA assay at 30 pg/mL. Results of individual devils are shown with the median and interquartile range identified by the whiskers. Significance testing using a Kruskal-Wallis test with Dunn's Multiple Comparison Testing shown with * representing $p < 0.05$.

5.6 Discussion

5.6.1 ERBB3 in devils without DFT1

Fifteen Tasmanian devils without neoplasia (twelve adults either wild caught, free range or from captive enclosures and three captive juveniles encompassing CHD, CHDD and CHJD) were studied with an average serum ERBB3 of 32 pg/ml. Collectively, CHD Tasmanian devils serum ERBB3 levels ranged from <30-663 pg/ml which could be considered representative of the reference range for Tasmanian devils. Wild caught devils 6 and 7 were unremarkable and had serum ERBB3 levels <30 pg/ml however devil 9 (220 pg/ml) and devil 10 (92 pg/ml) both recorded skin abscesses. The ERBB3 levels in the CHDD group (devils 9, 10, 11 and 12) ranged from <30-220 pg/ml all had a small isolated dermatopathy such as abscess (devil 9), pyogranuloma (devil 10), skin tag with associated inflammation (devil 11) and small focus of dermatitis (devil 12) all recorded a low serum ERBB3 levels of <92 pg/ml. The CHJD (devils 13, 14 and 15) approximately 10 months old had an unremarkable clinical history that indicated serum was collected for a health check only, reflected in the low serum ERBB3 level of <30 pg/ml.

Further assessment of data and clinical history (Table 6) revealed that four out of five Tasmanian devils from the Freycinet free range enclosure (devils 1-5) had higher serum ERBB3 ranging from 155-663 pg/ml compared to most other clinically healthy devils having serum ERBB3 levels <30 pg/ml. The Freycinet free range enclosure (FRE) consists of a 22 Hectare natural reserve that creates living conditions that are more similar to the wild than traditional captive conditions. The structure is fenced completely enclosing an insurance population of healthy devils with density capped to approximately one devil per hectare. This type of enclosure allows devils the opportunity to compete at feeding and breeding times and bite wounds are therefore common

(David Schaap, personal communication). In contrast, captive devils are housed in small enclosures that measure approximately 100 m^2 containing densities capped at one devil per 100 m^2.

Table 6: Tasmanian devil Serum ERBB3 and clinical history.

Devil	Serum Erbb3 pg/ml	Weight Kg	Serum transit day	clinical history	BCS, 0-5	DFT1 strain	DFT1 1° N° range, cm	Mets N°
1	155	N/A	1	CHD, NAD				
2	663	N/A	1	CHD, Localised alopecia				
3	207	OW	1	CHD, Multiple punctures				
4	313	N/A	1	CHD, Multiple punctures				
5	291	N/A	1	CHD, Multiple minor wounds				
6	<30	N/A	1	CHD, Few wounds, lactating				
7	<30	N/A	2	CHD, N/A				
8	<30	6	1	CHD, Great condition				
9	220	10.5	1	CHDD, Abscess/scab on face				
10	92	N/A	2	CHDD, Abscess left neck.				
11	<30	4.7	1	CHDD, Skin tag on left ear				
12	<30	N/A	1	CHDD, Dermatitis upper flank				
13	<30	4.2	1	CHJD, Health check				
14	32	3.4	1	CHJD, Health check				
15	<30	4.6	1	CHJD, Health check.				
16	18,254	N/A	1	DFT1, weak	2	2	2 (1.0-2.5)	3
17	999	6.1	3	DFT1, Reared 4 young	2	3	4 (1.0-1.5)	5
18	11,090	4.8	1	DFT1, Poor body condition	1-2	1	4 (2.0-3.0)	1

19	1903	3.7	1	DFT1, Emaciated disorientated	0	1	2 (1.6-5.2)	10
20	10,247	10	3	DFT1, Multiple lesions	3	2	4 (1.0-2.0)	2
21	1241	5	3	DFT1, Poor body condition	2.5	2	3 (1.0-1.5)	1
22	4198	9.3	4	DFT1, Advanced DFT1	2	4	7 (1.0-2.5)	0
23	766	N/A	1	DFT1, Emaciated	2	1	7 (1.0-4.7)	1
24	4383	6.7	1	CL, Generalised alopecia	N/A			
25	<30	8.2	1	CL, cutaneous plaques chest	N/A			
26	<30	8.0	1	CL, percutaneous plaque	N/A			
27	2008	5.9	1	CL, Skin lesions	N/A			
28	837	5.9	1	CL, Alopecia	Poor			
29	9703	5.3	1	CL, Generalised alopecia	Poor			
30	2403	8.2	1	CL, Alopecia ventrally	N/A			
31	536	7.4	1	CL, Alopecia left neck, pouch	N/A			
32	962	6.7	1	CL, Alopecia ventrally	N/A			
33	11,837	5.4	1	CL, Widespread alopecia	1-2			
34	207	5.7	1	CL, Multifocal dermatitis, cutaneous lump (acanthoma)	Poor			
35	20,021	N/A	1	CL, Multifocal alopecia	N/A			

N/A not available, NAD no abnormality detected, OW over weight, BCS - body condition score, DFT1 strain –cytogenetically determined strain, DFT1 1° N° – number and size of primary tumours recorded, Mets N° - number of metastasis recorded, CHD clinically healthy devil, CHDD clinically healthy devil with dermatopathy, CHJD clinically healthy juvenile devil, DFT1 devil facial tumour 1, CL cutaneous lymphoma

We noted that skin injuries were commonly recorded although no abnormality was noted for devil 1, alopecia bilaterally around the hind limbs and flank was present on one mother due to her 3 pouch young (devil 2) and multiple puncture wounds were present on the remainder (devils 3, 4 and 5). Given that these devils were otherwise clinically healthy it would suggest that skin wounds caused by biting may contribute to some elevation in the serum ERBB3 of Tasmanian devils. There is also the possibility that simply being a Tasmanian devil living in a free range enclosure as opposed to wild populations may in itself be contributory to elevation in serum ERBB3 due to more frequent devil-devil engagement. Our results indicate that Tasmanian devils without injuries or an isolated skin lesion have serum ERBB3 levels <30 pg/ml whereas Tasmanian devils with multiple injuries or large abscesses have serum ERBB3 levels ranging from 92-663 pg/ml. Together, these results suggest that cancer-free Tasmanian devils have a serum ERBB3 range of <30-663 pg/ml.

5.6.2 ERBB3 in devils with DFT1

All devils with DFT1 were wild caught and all subjected to field autopsy with most serum samples reaching the laboratory within one to three days. We assessed the available clinical history (Table 6) including animal weight, body condition score (BCS 1-5) where 1=emaciated, 2=moderately thin, 3=average, 4= good and 5=obese (Sarah Peck, personal communication), as well as number of primary and metastatic DFT1's and cytogenetic strain ensuring the consideration of any factors that may contribute to the ERBB3 range in DFT1 affected Tasmanian devils. No correlation was established between levels of ERBB3 and extent of DFT1 when comparing the number and size of primary DFT1 lesions and any metastatic disease (table 6). For example, the devil with the highest serum ERBB3 of 18,254 pg/ml (devil 16), had 2 primary lesions with 3 metastases whereas the lowest serum ERBB3 of 766 pg/ml (devil 23) had seven primary

DFT1 lesions and one metastasis. No correlation was established between serum ERBB3 levels and the BCS as most were low (BCS 1-2) with only one devil (devil 20) having a BCS of three out of five, indicating average body condition. Cytogenetic strain did not appear to correlate to serum ERBB3 levels and reflects the immunohistochemical findings that ERBB3 expression was present in all cytogenetic strains of DFT1. Our results indicate that Tasmanian devils with DFT1 have elevated serum ERBB3 levels compared to clinically healthy Tasmanian devils ranging from 766-18,254 pg/ml and that the extent of DFT1 does not readily correlate directly with the serum ERBB3 levels. Further investigations beyond the pilot study encompassing a larger study group of Tasmanian devils with advanced DFT1 and metastases would be necessary to establish any relationship with serum ERBB3 and the extent of DFT1.

5.6.3 ERBB3 in devils with cutaneous lymphoma

We included Tasmanian devils with cutaneous lymphoma (CL) in the study for two reasons. Firstly, they were non-DFT1 devils with a severe skin condition that can affect the facial regions and secondly, the disease presentation of alopecia, excoriation and thickened plaques is distinct from DFT1 (figs 38E and 38F). Our results revealed that some Tasmanian devils with CL had elevated serum ERBB3 levels, a result that was most unexpected. Although ERBB3 immunohistochemistry on Tasmanian devils with CL was beyond the scope of this research, ERBB3 Immunohistochemical staining of Tasmanian devil lymph node (fig. 38D) did reveal ERBB3 expression in the lymphoid follicle where cytoplasmic expression of ERBB3 is present in both T (germinal centre) and B (mantle) cells. CL devils were in the older age bracket ranging from 4-8 years where the maximum age of a wild devil would be considered 5-6 years (Sarah Peck, personal communication). Bodyweights ranging from 5.4-8.2 Kg compared to the mean weight of 6.6Kg for female and 8.3Kg for male (531) shows possible female underweight wild devils and overweight

captive devils. Age or weight did not appear to correlate with the broad range of serum ERBB3 of 30-20,021 pg/ml. interestingly, 11 of the 12 devils with CL were female. We noted that devils with widespread alopecia (devils 24, 29, 33 and 35), did exhibit increased serum ERBB3 levels ranging from 4383-20,021 pg/ml, suggesting that the severity of CL manifesting clinically as widespread alopecia may contribute to increased serum ERBB3 levels. Together, the elevated serum ERBB3 results in devils with CL is unlikely to cause confusion with DFT1 as CL tends to affects devils in the older age group and the clinical signs of CL are also distinct from DFT1 in established disease. Additionally, if elevated serum ERBB3 levels in Tasmanian devils indicative of CL could be established (pre-clinical) this would improve the healthy captive breeding populations of Tasmanian devils to ensure survival of the species by excluding these devils from this program.

5.6.4 Potential source of serum ERBB3

The capture and detection of antibody in our ELISA assay is selective for the extracellular domain (ECD) of transmembrane ERBB3 in serum or plasma, thus that ERBB3's ECD is cleaved and shed from the plasma membrane would be a natural assumption. In contrast the ERBB3 receptor is internalised, although very slowly, for negative regulation and inactivation (457-461) utilising pathways such as caveolin or micropinocytosis and clathrin-and caveolin independent pathways (462, 463). ERBB3 has also been shown to be endocytosed independent of phosphorylation and without ligand in clathrin-dependent manner (468). ERBB3 is degraded by proteasomes catalysed by two E3 ubiquitin ligases; NRDP1 (464), now known as RNF41 (465-467), and NEDD4 (471) that regulate steady-state ERBB3 levels influencing NRG1 signalling.

Defective internalisation, recycling and degradation of cell surface proteins and ligands is an emerging feature of cancer (472). It is therefore conceivable that DFT1 is subjected to the same dysregulation and inefficient degradation and recycling resulting in over expression of ERBB3

receptor at the plasma membrane and subsequent detectable levels of serum ERBB3. While dysregulated endocytosis, deregulation and recycling may theoretically account for excess ERBB3 ECD detectable in serum, secreted isoforms of ERBB3 must also be considered as an alternative explanation for the presence of excess ERBB3.

As well as functional transmembrane forms, secreted soluble forms of Epidermal Growth Factor Receptors have been well documented for ERBB1 (532-535), ERBB2 (536-539) and ERBB4 (540-542). Alternative transcripts for ERBB3 resulting in naturally occurring soluble truncated isoforms including a 1.4 kb transcript of ERBB3 in gastric cancer cell lines (484) and an additional four novel transcripts (1.6, 1.7, 2.1, and 2.3kb) from ovarian cancer cell lines (487) encouraged researchers to identify these secreted isoforms of ERBB3 in prostate (489-492), liver (493), breast (486, 494) and squamous cell carcinoma (485). ERBB3 isoforms have also been expressed intracellularly in breast cancer cell lines (486) as well as in the nucleus of Schwann cells (475, 476), prostate (477-479) and breast (474, 482). Secreted ERBB3 isoform p85 has been shown to inhibit the action of its ligand Neuregulin (488, 494), nuclear translocations act as co-transcriptional activators (480), possible post-translation modification and the tumour microenvironment are instructive to serum ERBB3 secretion from the cell (493) and functions yet to be determined.

The antigenic peptide used for this assay is located within the N-terminal domain of the full-length ERBB3 protein. Full length ERBB3 translates into a 180 kDa protein whereas ERBB3 transcripts, created by intron read through and alternative polyadenylation signals result in serum ERBB3 isoforms translating into various proteins ranging in size from 22-75 kDa (543). Secreted isoforms such as ERBB3-S (1.4kb, 140aa homologous to the N terminus and a 43aa unique carboxy terminal sequence) equates to approximately half of domain I, p50 (1.6kb, 351aa homologous to the N terminus and a 30aa unique carboxy terminal sequence) equates to domain I, II and some of domain III, p45 (1.7kb, 310aa homologous to the N terminus and a 2aa unique carboxy terminal sequence) equates to domain I, II and some of domain III, p85 (2.1kb, 519aa homologous to the N

terminus and a 24aa unique carboxy terminal sequence) equates to domain I, II,III and some of domain IV, p75 (2.3kb, 474aa homologous to the N terminus and a 41aa unique carboxy terminal sequence) equates to domain I, II and III (484, 487, 543) ERBB3 isoforms have been detected by a number of methods such as immunoprecipitation (486-488), immunohistochemistry (489) and ELISA (491-493). Isoforms that have been detected using ELISA assays include p45 sERBB3 utilising a capture antibody of sequence aa20-643 (detection antibody sequence was not recorded) (491, 492) and 40-50kDa secreted isoforms (possible p45/p50) utilising both capture and detection antibodies with a sequence aa20-643 (493). The Raybio ELISA kit utilised in our research uses a capture and detection antibody of sequence aa20-643 (personal communication Raybio) which accounts for most of the extracellular domain of ERBB3 and therefore would be able to capture and detect both truncated isoforms as well as the transmembrane ERBB3.

The correlation of serum levels with disease severity and progression would be the foundation of a good biomarker (493) as well; the expected biomarker should be in excess when compared to clinically healthy individuals (532) or possess additional qualities such as theranostic and tertiary prevention (535). The use of serum ERBB's as an indicator of human cancer appears useful however, its prognostic and theranostic value remains controversial and continued investigations will be required (485, 489-493, 532-542). The development of a diagnostic test for preclinical DFT1 would assist in the field operations if individuals could be identified before they become infectious (72), therefore application of serum ERBB3 as a diagnostic biomarker of DFT1 has great potential. The simplicity of the ELISA Serum ERBB3 methodology is easily incorporated into routine batch testing or rapid turnaround of results for urgent cases if required. Our research suggests that serum ERBB3 can be used as a biomarker for DFT1 and CL irrespective of transmembrane or truncated forms being detected in the serum of affected animals and therefore the potential of serum ERBB3 as a biomarker of early DFT1 detection should be explored.

5.6.5 ERBB3 and cancer

Overexpression of ERBB2 and ERBB3 had been documented early (439, 517, 518) but cooperation of both ERBB2 and ERBB3 in neoplastic transformation was recognised by Alimandi et al. (519) in mammary carcinoma cell lines, supported by additional research from Seigel et al. (520) Olayioye et al. (431) and Holbro et al. (521). As mentioned above ERBB3 was initially regarded as kinase deficient and that ERBB2, an orphan receptor, engage in heterodimerisation as a necessity for transactivation of the ERBB3 downstream signalling pathways PI3K and MAPK controlling gene expression, cell differentiation, proliferation, survival and apoptosis. Recently ERBB3 was confirmed as capable of allosterically activating other ERBB family members founding new interest in a receptor whose function was considered passive and clinical value greatly underestimated (reviewed in (544).

The normal spatial arrangement of RTK's is deregulated if both the cell polarity and cell-cell junctions are disturbed through loss of polarity and contact-dependent inhibition of proliferation due to gene amplification or overexpression in cancer. This deregulation can increases surface concentration and distribution, clustering and dimer formation and signalling (545). Yang et al. (546) found ERBB3 formed large clusters in breast cancer cell lines when treated with NRG. These complexes formed slowly and contained no visible clathrin structures consistent with slow internalisation. In addition, studies on Chinese hamster ovary cell line (CHO) revealed ERBB1-3 cluster individually implicating that segregation is a possible mechanism by which ERBB family members limit heterodimerisation. A similar finding by park et al. (547) utilising Aptamers demonstrated receptor clustering of ERBB3 in MCF7 breast cancer cell line, that ERBB3 are apparently segregated from ERBB2 in their resting state and that both ligand activated ERBB3 and

ERBB2 do not share the same topography as inactive ERBB3. A decreased level of spatial sequestration of ERBB3 in MCF7 (excess ERBB2) cells may then encourage heterodimerisation. Recently Littlefield et al. (548) studied the heterodimeric structure of EGFR/ERBB3 revealing ERBB3 an allosteric activator of EGFR, and further, that the ERBB3 mutations associated with cancer where the protein-protein interface is altered actually enhanced the allosteric potential.

Although ERBB3 is amplified or overexpressed in some cancers and oncogenic mutations had been reported, Jaiswal et al. (525) identified approximately 11% of colonic, 12% gastric, 1% of non-small cell lung cancer (NSCLC) adenocarcinoma and 1% of NSCLC (squamous) cancers had somatic mutations but their oncogenic activity was dependent on kinase active ERBB2. Most of the mutations identified clustered in the ECD region (eg V104) although some mapped to the kinase domain (EG Q809R) or intracellular domain of ERBB3. It was noted that most ECD mutations were oncogenic in the absence of ERBB3 ligand NRG1, but could be stimulated by addition of NRG1, in contrast G284R (ECD) and Q809R (KD) appeared to be less sensitive to ligand–mediated activation. Residues were mostly conserved across the orthologues indicating they may have a functional effect. Choi et al. (549) also found that the mutant V104 in exon 3 was also particularly related to gastric cancer and colorectal cancer and was not found in other cancers and an associated increased in the immunohistochemical expression of ERBB3 in the cancers with the mutation was observed. Gastric tumours that express ERBB2 and ERBB3 is a predictor of poor survival (550). Vaught et al. (522) showed that loss of ERBB3 prevents the progressive transformation of ERBB2 over expressing mouse model breast carcinomas suggesting that ERBB3 promotes tumour formation in the breast epithelium.

5.6.6 Schwann cell neoplasms

ERBB3 is crucial to the sequential transition from precursor to immature and finally mature Schwann cells where ERBB3 is down-regulated as myelination proceeds (495). The adult peripheral nervous system requires maintenance when injured and the NRG1/ERBB system is crucial to Schwann cell dedifferentiation, proliferation, and subsequent regeneration and remyelination where ERBB3 and NRG1 is upregulated and only switched off after axon regeneration illustrating the plasticity of the Schwann cell (279, 516, 551). Peripheral nerve sheath tumours [neurofibroma, malignant peripheral nerve sheath tumours (MPNST)] and schwannoma arise from the Schwann cell lineage and can be genetically characterised as Neurofibromas (either dermal or plexiform) and MPNST's [Neurofibromatosis 1 (NF1)], or Schwannomas [Neurofibromatosis 2 (NF2)], Schwannomatosis and Carney complex type 1. Although distinct characterisation of these complex diseases is possible, frequent overlapping features make diagnosis difficult and must also include other tumours with a Schwannian component such as Neuroblastic and Granular Cell Tumours [reviewed in (552-556)]. Veterinary Schwann cell neoplasms have been recorded (557-561) although ERBB3 expression in Schwann cell neoplasia has not previously been reported in veterinary literature. ERBB3 receptor has been expressed in human Schwann cell neoplasms including neurofibroma, MPNST, Schwannoma, neuroblastic (281, 562) and ganglioneuroma (GN) tumours (563). Interestingly, the down regulation of MHC class 1 and 2 molecules in a MPNST cell line (564) contrasting normal expression (565, 566) may indeed be similar to the MHC class 1 downregulation of DFT1 (43, 411, 567) resulting in defective antigen processing and presentation of the malignant Schwann cell neoplasm.

5.6.7 ERBB family targeting therapeutics

The ERBB3 receptor has been identified in tumours in early studies. ERBB3 mRNA was detected in breast cancer cell lines (439) and overexpression of the receptor protein demonstrated by immunohistochemistry (518) was positively associated with node metastasis but not on patient survival. A subsequent study of NSCLC found that high ERBB3 expression was associated with shorter survival times in advanced NSCLC (stage III and IV) with squamous cell carcinoma most frequently observed followed by adenocarcinoma and large cell carcinoma (568). Reschke et al. (524) showed that ERBB3 is upregulated in melanoma and its metastasis that correlated to decreased patient survival. Early studies reveal ERBB3 as a potential oncogene with overexpression due to possible increased transcription as no gene amplification was observed (523, 524) indicating either ERBB3 or its downstream components should represent a potential target for therapy (526). ERBB3 has long been considered kinase impaired (436) and therefore, therapeutically, it has not been considered a primary target, particularly in breast cancer. Tanner et al. (569) reported that ERBB3 expression was associated with decreased survival in ovarian cancer despite only a fraction of tumours expressing ERBB2 indicating the importance of ERBB3. The use of tyrosine kinase inhibitors (TKI's) such as gefitinib and erlotinib has been effective at inhibiting phosphorylation of ERBB1 and ERBB2 in breast tumours but not as effective in decreasing the advancement of the tumour due to communication with other ERBB family dimers, particularly transphosphorylation of ERBB3 and subsequent signalling through PI3K/AKT pathway (570). A multiscale modelling approach by Telesco et al. (571) to explore ERBB3 signalling and TKI resistance supported that ERBB3 was a weakly active kinase and this activity could be enough to induce AKT signalling and TKI resistance. to Liu et al. (572) recognised potency of the ERBB2/ERBB3 heterodimer and showed that ERBB3 modulates ERBB2 and tomoxifen resistance and siRNA decreased levels of ERBB3 restored tomoxifen sensitivity, again illustrating the

importance of ERBB3 as a target for therapy. The use of small interfering RNA (siRNA) proved successful by Sithanandam et al. (573) treating lung adenocarcinoma cells (H441, H1373 and A549) with siRNA directed at different regions of ERBB3 substantially suppressed expression of ERBB3. This raises the possibility of considering siRNA in a therapeutic approach. The central role that ERBB3 plays in ERBB2 amplified breast cancer was demonstrated by Lee-Hoeflich et al. (574) utilising siRNA/shRNA knockdown of ERBB3 in BT474M1 and MDA-MB-75 xenografts subjected to combined treatment of trastuzumab (humanised monoclonal antibody directed at a segment of the ECD of ERBB2) and pertuzumab (humanised monoclonal antibody directed at domain II dimerization arm of the ECD of ERBB2 blocking dimersiation of ERBB2/ERBB3) lead to sustained tumour growth inhibition. The evidence above reinforces the co-dependence of ERBB family members to compensate through lateral signalling allowing ERBB3 to escape drug therapy and persist signalling despite suppression of ERBB1 and ERBB2 beckons ERBB3 to be deemed a suitable biomarker(421) and certain candidate for therapeutic targeting. Sheng et al. (575) found in a subset of primary and ovarian cancer cell lines had an NRG1 activated ERBB3 autocrine loop although activation may be independent in some. Experimental procedures using RNA interference (RNAi) of multiple siRNA/shRNA of NRG1 or ERBB3 resulted in decrease in proliferation indicating that ERBB3 directed therapy must be further evaluated.

5.6.8 Cancer resistance: ERBB and other RTK families.

Recognition of other RTK families that may interact with the ERBB family supporting carcinogenesis and contributing to drug resistance must be considered in therapeutic approaches, particularly insulin-like growth factor 1 receptor (IGF1R) and hepatocyte growth factor receptor or c-MET (MET) (576). Protein-protein interactions have been observed between IGF1R and ERBB2 in trastuzumab resistant breast cancer sub cell line SKBR3 (577) and IGF1R, ERBB2 and ERBB3

heterodimerisation was found in trastuzumab resistant breast cancer subline pool2 (SKBR3 trastuzumab resistant subline) and HR20 subline (BT74 trastuzumab resistant subline) cells (578). In exploring resistance gefitinib and erlotinib, TKI's used to treat NSCLC, Engelman et al. (579) found firstly in CHO cells (normally do not express ERBB1/ERBB2/ERBB3) that coexpression of ERBB3 and MET resulted in increased phosphorylation of ERBB3 and secondly, in four of eight EGFR mutant NSCLC that showed amplification of MET. Yun et al. (580) also reported immunohistochemical staining and co-immunoprecipitation assays that dimers of ERBB3/MET and ERBB3/ERBB2 were present in human gastric cancers among other dimers illustrating crosstalk within RTK's. These articles communicate the necessity of drug regimens to include a wider application than just ERBB family of therapeutics to include RTK's such as IGF1R and MET in drug resistant tumours.

5.6.9 ERBB3 Therapeutics

Resistance to therapeutic agents such as TKI's (gefitinib and erlotinib - ERBB1 targeted and lapatininb - ERBB2 targeted) and monoclonal antibodies (cetuximab - ERBB1 targeted and trastuzumab and pertuzumab - ERBB2 targeted) has revealed escape mechanisms such as ERBB family crosstalk, cross talk with other RTK family members as well as up regulation of ERBB3 that contribute to ERBB1/2 resistance (581, 582). The large body of evidence illustrates the key role ERBB3 plays in various tumours prompting research into therapeutic options targeting ERBB3, particularly over the last decade [reviewed in (420, 527, 583-591)]. To date no FDA approved treatment has emerged specifically for ERBB3 although several agents are either in pre-clinical testing or clinical trials. Current therapeutic agents in pre-clinical stages or clinical trials have been reviewed in detail and are briefly outlined in Table 7.

Table 7: ERBB3 therapeutic agents cited in literature.

Name	Description	Target	Year	Current Clinical Trial status	Original Reference
α-HER3 ^{ECD}	Monoclonal antibody	ERBB3 ECD	2005	Pre-clinical	Van der Horst et al. (592)
BS-SCFV-ALM	Bispecific single-chain FV antibody	ERBB2/ERBB3	2008	Pre-clinical	Robinson et al. (593)
105.5 and 2D1D12	antibody	ERBB3	2008	Pre-clinical	Reschke et al. (524)
AMG 888 (U3-1287) Patritumab	Monoclonal antibody	ERBB3	2008	Phase 2	Treder et al. (594)
SNDX-275	Histone acetyltransferase and histone deacetylase inhibitor (HDACi)	ERBB2/ERBB3	2009	Phase 2	Huang et al. (595)
MM-121	Monoclonal antibody	ERBB3 ECD	2009	Phase 2	Schoeberl et al. (596, 597), Liles et al. (598)
AZD8931	Small molecule inhibitor	ERBB1/ERBB2/ ERBB3	2010	Phase 2	Hickinson et al. (599)
MEHD7945A (DL11) RG7597	Monoclonal antibody	EBRR1/ERBB3	2011	Phase 2	Schaefer et al. (600)
A3 and A4	Monoclonal antibody	ERBB3	2012	Pre-clinical	Belleudi et al. (601)
MM-111	Bispecific	ERBB2/ERBB3	2012	Phase 2	McDonagh et al. (602)
SL-175 and SL176	Surrobody	ERBB3	2012	Pre-clinical	Foreman et al. (603)
SGP1	Monoclonal antibody	ERBB3 ECD	2012	Pre-clinical	Blackburn et al. (604)

D1 and DIII (H4B-121 and 9F7-F11/16D3-C1)	Antibodies directed at domain I and III	ERBB3 ECD	2013	Pre-clinical	Lazrek et al. (605)
LJM716	Monoclonal antibody directed at domain II and IV	ERBB3 ECD	2013	Phase1/2	Garner et al. (606)
EV20	Monoclonal antibody	ERBB3 ECD	2013	Pre-clinical	Sala et al. (607)
RG7116	Monoclonal antibody	ERBB3 ECD	2013	Phase 1	Mirschberger (608)
EZN-3920	Locked nucleic acid based ERBB3 antisense oligonucleotide	ERBB3 RNA	2013		Wu et al. (609)
D1 and DIII (F4 and A5)	Antibodies directed at domain I and III	ERBB3 ECD	2014	Pre-clinical	D'Souza et al. (610)
D1,D2,D3	Peptide mimic and Vaccine	ERBB3 ECD	2014	Pre-clinical	Miller et al. (611)
MM-141	Tetravalent bispecific antibody	ERBB3 and IGF-R1	2014	Phase 2	Fitzgerald (612)
Sym013	Six Monoclonal antibodies	ERBB3, ERBB2, ERBB1	2014	Pre-clinical	Francis et al. (613)
REGN1400	Monoclonal antibody	ERBB3 ECD	2014	Phase 1	Zhang et al. (614)
GSK2849330	Monoclonal antibody	ERBB3 ECD	2014	Phase 1	Clarke et al (615)
NG33	Mouse monoclonal	ERBB3 ECD	2015	Pre-clinical	Gaborit et al. (616)
KTN3379	Monoclonal antibody	ERBB3 ECD	2015	Phase 1	Lee et al. (617)
AV-203	Monoclonal antibody	ERBB3 ECD	2015	Phase 1	Meetze et al. (618)
DVD Ig	bispecific duel variable domain immunoglobulin	ERBB1/ERBB3	2015	Pre-clinical	Gu et al.(619)
Perhexiline	Small molecule drug	ERBB3	2015	Pre-clinical	Ren et al. (620)

ECD= extracellular domain, Current clinical trial status= status at clinicaltrials.gov

5.6.10 ERBB3 as a therapeutic target

Despite evidence for multiple resistance mechanisms for existing therapeutic targeting of ERBB1/2 (570, 572, 573, 576-582, 621) numerous researchers have over the last decade explored the potential of ERBB3 as a therapeutic target [reviewed in (420, 527, 583-591)] using monoclonal antibodies (524, 592-594, 596, 597, 600-602, 604-608, 610, 612-619, 622-625), histone inhibitors (595), TKI (599), surrobodies (603), locked nucleic acid (LNA)-based ERBB3 antisense oligonucleotide (ASO) (609), peptide mimics and vaccine (611), anti-anginal drug (620) and disulphide disrupting agent (626), shown in table 7.

However, managing wildlife disease is considerably more difficult than human disease because of limited data, the effect of the disease on the host and the transmission of disease within a dynamic population makes it difficult to model (76). Previous efforts to eradicate DFT1 from wild populations by selective culling has proven unsuccessful because of the frequency-dependent transmission of DFT1 and the latency period (71, 72, 76). TKI's as a therapeutic approach may be limited due primarily to the early observation that kinase region of ERBB3 had substantialy reduced activity, however cancer immunotherapy broadly categorised as passive (including monoclonal antibodies, Cytokines, adoptive cell transfer) or active (including therapeutic cancer vaccine, immune checkpoint inhibitors) remains optimistic (627-632). Many of these successful human immunotherapeutics hold similar promise in veterinary medicine (633-635) however, drug administration to wild Tasmanian devils is very different from the clinical setting of human and companion animals and therefore treatments such as adoptive cell transfer would be difficult to implement. The fact that DFT1 expresses tumour associated antigens (TAA's)

such as ERBB3 invites the application of monoclonal antibodies and therapeutic cancer vaccines as prospective treatments. The passive administration of monoclonal antibodies to ERBB3 primarily focused on blocking receptor epitopes is still experimental (524, 592-594, 596, 597, 600-602, 604-608, 610, 612-619, 622-625) and any humanised anti-ERBB3 would certainly have to be become species specific (devil anti-ERBB3) to prevent adverse immunologic reactions (636). Very few monoclonal antibodies have been developed in veterinary oncology although two caninised antibodies anti-ERBB1 (637) and anti-CD20 (638) show promise. Therapeutic cancer vaccination modalities applicable to wildlife include antigen delivery vaccines that utilise inactivated cancer cells (autologous or allogenic) or peptide vaccines that mimic antigen sequences. Conclusive results using an inactivated cancer cell vaccine trial (allogenic DFT1 cell line) are eagerly awaited. Confidence that immunisation can be successful stems from research showing that Tasmanian devils have a competent immune system (26, 28, 411, 639) and can produce cytotoxic antibodies (31, 32). An alternative antigen presentation modality to cancer cell vaccine is a peptide vaccine, where single or multiple amino acid sequences (long or short) representing a defined antigen is combined with adjuvant to elicit an immune response (640). Development of just a single ERBB3 peptide vaccine can be found in the literature (611) however, peptide vaccines targeting ERBB1 (641, 642), ERBB2 (643-645) or both ERBB1/2 (646) including a monoclonal antibody against tyrosine related protein 1 (TRP-1) and altered peptide sequence to gp100 for mouse melanoma (647) all show promise. Overcoming self-tolerance is a major hurdle. One such strategy is the use of Xenoantigens, that is the exact same antigen but from a different species that has considerable sequence homology, differing only by several amino acids which appear to the host as altered epitopes or as “altered self” and therefore tolerance can be broken causing a T-cell response against the endogenous self-antigen (648). Veterinary xenogeneic vaccinations include a DNA plasmid vaccine encoding human Tyrosinase (TYR) (649) the only veterinary therapeutic tumour

vaccine licensed by the United States Department of Agriculture (USDA) for the use of oral and digital melanoma, now marketed as Oncept^{TM}.

Recent investigations reveal that the tumour microenvironment of metastatic DFT1 expressed PDL1 (programmed cell death 1 ligand 1/CD274/B7-H1) and DFT1 cell lines could upregulate PDL1 (650). Immune-suppressive tumour microenvironment created by tumour cells that escape 'immunoediting' allowing tumour growth and proliferation (651) where certain checkpoint pathways will be used advantageously by tumour cells to confer immune resistance (652). Hence, checkpoint blockades (monoclonal antibodies) targeting PDL1 and Cytotoxic T Lymphocyte Antigen 4 (CTLA-4) are now attractive therapeutical targets (653). Recent views consider cancer immunotherapy invaluable although a single treatment mode may be suitable for some cases, more combinatorial approach will be needed for others (654, 655).

Our research has highlighted ERBB3 as a potential therapeutic target although treatment of Tasmanian devils with DFT1 with therapeutic regimes such as chemotherapy and radiotherapy are impractical. However, a combinatorial approach using therapeutic cancer vaccines including inactivated allogenic DFT1 cancer vaccine, ERBB3 monoclonal antibody, ERBB3 Peptide or xenogeneic vaccine in combination with anti-immune checkpoint blockade therapy would be easier to implement in the field as well as providing a sustained immunological response against DFT1.

5.7 Conclusion

ERBB3 had previously avoided scrutiny due to its kinase inactivity; however, ERBB3 has been the subject of intense investigation over the past decade and is now recognised as a potent partner of the epidermal growth receptor family. ERBB3 upregulation during developmental, dedifferentiation and regenerative processes encapsulates the Schwann cell's inherent plasticity and imparts certain characteristics of malignant transformation advantageous to transmission of DFT1. Our pilot study has shown for the first time that ERBB3 is consistently expressed immunohistochemically and that ERBB3 is also elevated in the serum of Tasmanian devils with advanced DFT1 and cutaneous lymphoma. Therefore, our research indicates that serum ERBB3 has the potential to be employed as a biomarker of DFT1 or CL in Tasmanian devils to assist conservationists in the management and welfare of Tasmanian devils and species survival. The simplicity of the ELISA Serum ERBB3 methodology is easily incorporated into routine laboratory batch testing and equally applied to include rapid turnaround of results for urgent cases. Extension of this research is necessary to include greater numbers of healthy Tasmanian devils both with and without visible injuries, devils with large and small DFT1 lesions as well as pre-clinical DFT1. This will firmly establish the normal reference range for serum ERBB3 from which potential pre-clinical DFT1 may be identified. In addition, ERBB3 is now recognised as a therapeutic target and therefore the potential exists to consider modes of administration in addition to existing whole cell vaccination such as ERBB3 monoclonal antibody, peptide or xenogeneic vaccines including checkpoint inhibitors. A combinatorial immunotherapeutic approach will enhance cytotoxic destruction, provide long term immunity from DFT1 and therefore eradicate this transmissible tumour from the wild.

Chapter 3

6.0 A second Transmissible Tasmanian Devil facial Tumour – DFT2

6.1 introduction

The emergence of a second transmissible tumour is a completely unforeseen development in Tasmanian devil facial tumour research requiring immediate investigations to expose similar or different relationships to the original facial tumour, DFT1. As a result, I have collaborated with fellow Tasmanian devil researchers Ruth Pye, Max Stammnitz and Elizabeth Murchison providing histological and immunohistochemical support for their research papers. While DFT2 was not originally included in my candidature, DFT2 research is crucial to understanding transmissibility of both DFT1 and DFT2 and therefore, I have summarized our research below.

6.1.1 A second transmissible cancer in Tasmanian devils

The Channel area is a peninsula of approximately 550 km^2 south of Hobart, adjacent to the D'Entrecasteaux channel. DFTD was first detected in this area in 2012 and since that time, five cases out of twelve from that area have been identified as non-classical DFTD. Although the external appearance of facial tumours were indistinguishable to DFTD, the histomorphology was not consistent with typical pleomorphic small round cells forming distinct bundles, cords or packets of DFTD (1). Two interesting cases in 2014 were examined by our research team and reported by Pye et al. (7) and in contrast to DFTD, these cases had pleomorphic sheets containing amorphic, stellate and fusiform cell types with the distinct bundles, cords or packets characteristic of DFTD noticeably absent. Immunohistochemical staining was performed using Periaxin (figure 40), a Schwann cell marker, which is expressed by DFTD but was negative on these two unusual

facial tumours. At this early stage, the possibility that these two tumours either spontaneously arose from the hosts or they were derived from DFTD was still considered a possibility. Therefore, cytogenetic and genetic analysis was performed on these two tumours, three additional unusual tumours, as well as DFTD tumours from the Channel area.

As previously discussed, the distinctive DFTD karyotype has both chromosome two homologs absent, one of the chromosome 5 homologs absent, both X sex chromosomes absent and the presence of four abnormal marker chromosomes. In contrast to DFTDs karyotype, the unusual tumour's karyotype included additional material from chromosomes one, two and four, a deletion involving chromosome 5 and monosomy for chromosome six (figure 41). Both X and Y sex chromosomes were present. Of greatest significance was that all five tumours had the identical complex karyotype and therefore it was conceivable that they were derived from a single clone and for this reason we named the tumour DFT2, a second transmissible devil facial tumour. Previous investigations using fluorescent insitu hybridization had identified two X chromosome copies in DFT1 (19, 45) and further examination by Pye et al. (7) of 10 X chromosome variants all mapping to the X chromosome only, confirms that DFT1 carries two homologous X chromosomes and the tumour probably arose from a female devil originally. Because the DFT2 karyotype is completely different to DFT1, it carries a Y chromosome indicating the origin of DFT2 was from a male devil, and the fact that DFT2 is negative for Periaxin, together supports the conclusion that a single clonal origin of DFT1 and DFT2 is discordant. When the genotype of DFT1 and DFT2 were compared at nine polymorphic microsatellite loci, it was found that DFT1 tumours shared an identical genotype and DFT2 tumours also shared a different identical genotype which were both genetically distinct from the host's genotype. Additionally we identified that DFT2 has a different MHC class I genotype than DFT1 and that this genotype is also distinct from the hosts genotype, so like DFT1, DFT2 is not restricted to hosts with an identical genotype to the tumour. Together, our

study indicates that DFT2 is a transmissible tumour that is distinct from DFT1, however both are indistinguishable when observing facial tumours grossly. This discovery of DFT2 certainly provides some insight into the vulnerabilities of the Tasmanian devil given this is the second transmissible tumour in the species within twenty-two years, with DFT2 appearing as recently as 2014. No obvious shared DNA was identified between DFT2 and DFT1 leaving reduced genetic diversity contributing to the probability of these two transmissible tumours.

6.1.2 The Origins and Vulnerabilities of Two Transmissible Cancers in Tasmanian Devils

We further investigated and reported (8) on the functional and genetic characteristics of DFT1 and DFT2 in an attempt to elucidate any commonalities between the two transmissible tumours. Our panel of IHC (figure 43) showed similar characteristics with both DFT1 and DFT2, both being positive for S100, ENO2 and VIM and negative for SMA and CK. As previously reported, DFT1 is strongly positive for PRX (20) such that it is routinely used for a diagnostic marker; however, in contrast to DFT1, DFT2 is negative for PRX, providing an expressional distinction. Although the macroscopic appearance of the tumours might suggest that the cancer is from a comparable cell type, no expression of PRX and dissimilar histomorphology would suggest the tumours may be unrelated. Genotyping DFT1 and DFT2 at 320 nuclear polymorphic loci, and compared to previous data (84) found that DFT1 arose geographically in the North East of Tasmania Mt William area however, DFT2 arose in the south east Channel Peninsula area. Essentially, DFT1 and DFT2 appear to have emerged independently at separate locations. Investigation of exogenous pathogens such as viruses, mutational signatures and UV light in the genomes of DFT1, DFT2 and healthy devils did not provide any evidence of viral DNA, mutational signatures or UV light exposure (perhaps not surprising for a nocturnal marsupial). Identifying and annotating DFT1 and DFT2 founder individuals' inherited germline single-nucleotide variant (SNV) and small insertion and deletion

(indel) alleles to characterise any somatic mutations. SNVs and indels were detected in both DFT1 and DFT2 but none were confirmed in genes causative of cancer, however a DFT1 mutation in WWC family member 3 (*WWC3*) and a DFT2 mutation in multiple PDZ crumbs cell complex polarity complex component (*MPDZ*) genes may be early somatic mutations prior to clonal changes. Interestingly, both MPZD and WWC3 are purported to be negative regulators of YES associated protein 1 (*YAP1*) and WW domain containing transcription regulator 1 (*TAZ*) which are core effectors of the Hippo pathway. We performed immunohistochemistry for YAP1 and TAZ on DFT1 and DFT2 finding both cytoplasmic and nuclear expression illustrating these transcriptional co-activators are active shuttling between the cytoplasm and nucleus (Figure 43). This would suggest that the mutation in WWC3 and MPDZ genes may lead to ineffective regulation of YAP1 and TAZ. The insertion of the chromosome six homologue into the pericentric region of chromosome two, characteristic of DFT2, was shown by chromosome painting and FISH that chromosome six had a short telomere. Tasmanian devils have unusual telomeres characterized by extreme length dimorphism, a feature that is lost in DFT1 (52) and therefore, the possibility of unusual telomere length may predispose Tasmanian devils to the risk of chromosomal rearrangement (8). We tested copy number variants (CNVs) in DFT1 and DFT2, the majority of tumors being diploid. Among a number of findings was a gain in copy number of platelet derived growth factor α and β (PDGFA, PDGFB) in DFT2 and in some DFT1s extra-chromosomal DMs, correlated with strong immunohistochemical expression of both PDGFA and PDGFB in DFT1 and DFT2 (Figure 42). We also noted an increased copy number for Neuregulin-2 (NRG2) which is one ligand of ERBB3, which we have previously reported as expressing ERBB3 (47) with increased copy number (5). Interestingly, because DFT2 contains a Y chromosome it was noticed that of the now nine DFT2 tumours identified (85), seven were grafted into male hosts, one a female host and in the other female host the Y chromosome was not detected. It remains to be seen if female devil hosts provide DFT2 with some sort of immunological resistance. In wrapping up our research a number

of drugs were screened for the possibility of therapeutic agents. It was found that both DFT1 and DFT2 were sensitive to RTKs, particular DFT1 is sensitive to ERBB2 mediated Afatinib which is reassuring as our ERBB3 studies suggested a number of regimes that included the dimer ERBB2/ERBB3. DFT2 also showed sensitivity to Axitinib which is active against PDGFR and KIT which were both identified in this research, as described in chapter two of my thesis. In a recent publication Caldwell et al. (86) has found DFT2 expresses B2M and classical and non-classical MHC class I molecules which is contrary to DFT1 which has lost expression of MHC class I molecules. Results showed that expression of MHC class I alleles varied on DFT2 tumours with the highest expression of classic MHC-I allele also found present within host devils. This research by Caldwell et al. (86) suggests that loss of MHC is not necessary for tumour transmission because of varied expression; however, subclones may be selected upon transmission if they have downregulated MHC as the tumour encounters different devil's immune systems. It is predicted that DFT2 is likely to be losing MHC antigens already and this could lead to widespread transmission throughout the remaining fragile wild populations of Tasmanian devils, on the back of the decimation caused by DFT1.

6.2 Methods

6.2.1 Histology and immunohistochemistry

Standard histologic, immunohistochemical and photographic methods were used as outlined in chapter 3.0

6.2.2 Primary antibodies utilized for Immunohistochemistry

Primary antibodies PRX, PDGFRB, VIM, NSE, S100, SMA and CK have been outlined in table 2

Additionally, Polyclonal rabbit anti-human PDGFRA 1:800 (Cat#ab124392, Abcam, Cambridge, UK), Monoclonal mouse anti-human YAP1 1:100 (Cat#WH0010413M1, Sigma-Aldrich) and Polyclonal rabbit anti-human WWTR1/TAZ 1:100 (Cat#T4077, Sigma-Aldrich)

6.3 Results

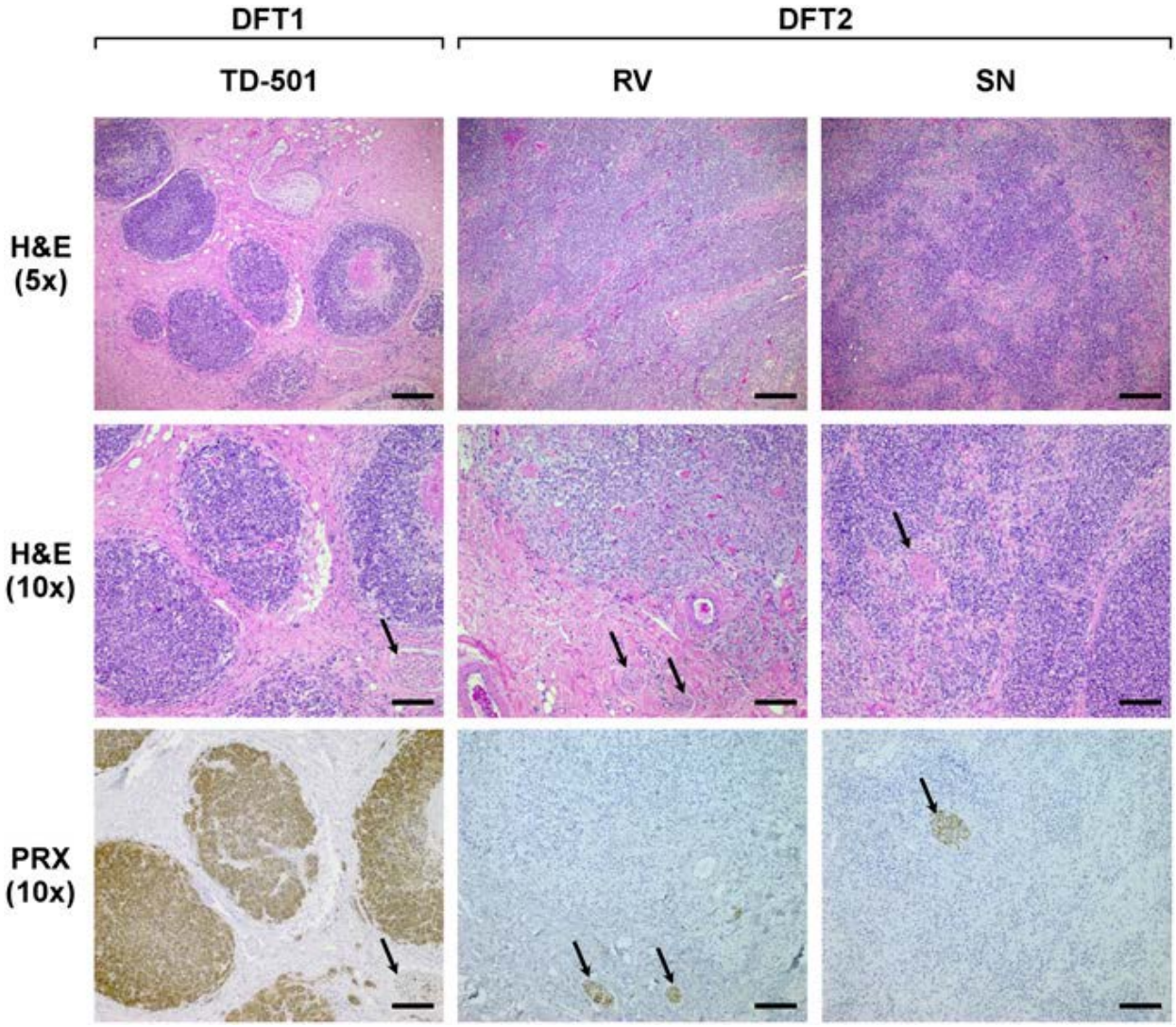

Figure 40: DFT2 tumours are histologically distinct from DFT1.

Representative images of H&E stained histological sections of DFT1 and DFT2 tumours (Upper and Middle). (Lower) Histological sections stained with DFT1 marker, PRX. Scale bars represent 200 µm (Upper) or 100 µm (Middle and Lower). Arrows indicate peripheral nerve bundles, which are positive for PRX. Figure reference: Figure 2 from Pye et al. 2016 (7) (appendix 5).

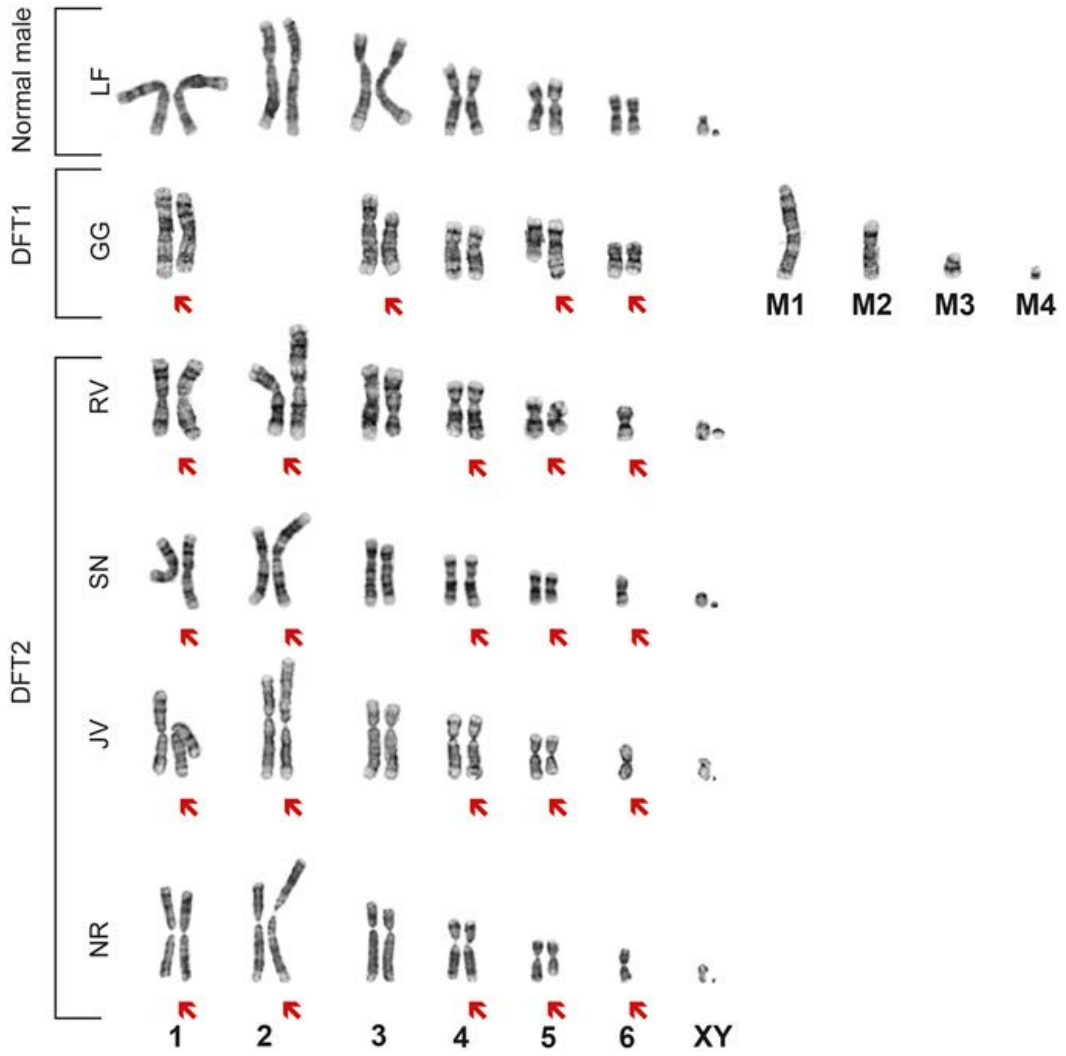

Figure 41: DFT2 tumours are cytogenetically distinct from DFT1.

Representative karyotypes of a normal male devil, a DFT1 tumour, and four DFT2 tumours. Red arrows indicate chromosomes carrying cytogenetic abnormalities. Four marker chromosomes found in DFT1 (9) are labelled M1 to M4. Figure reference: Figure 3 from Pye et al. (7) (appendix 5).

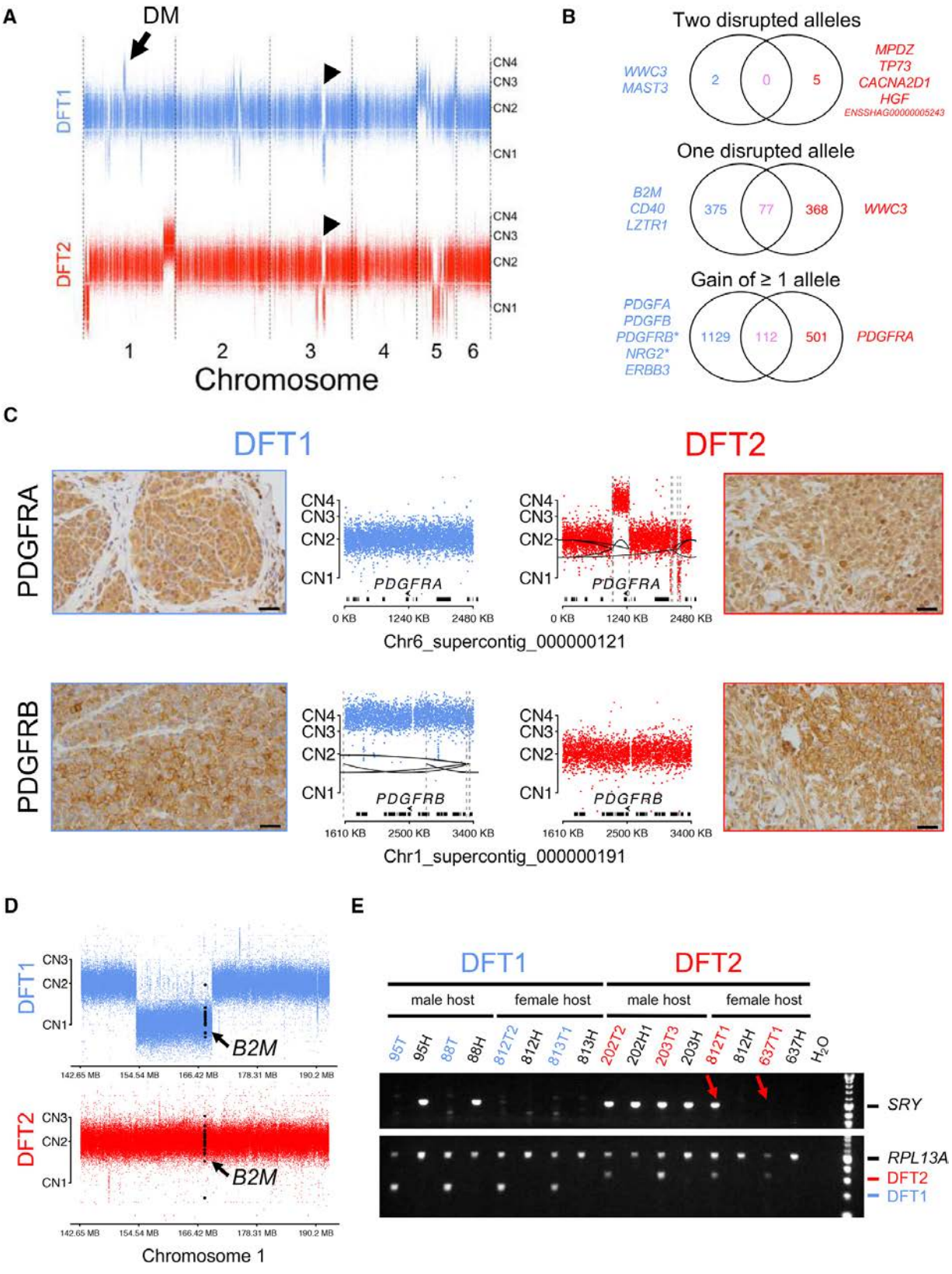

Figure 42: (C) Copy number and immunohistochemistry for PDGFRA and PDGFRB.

Reads mapping within 500 base pair genomic bins were counted and normalized; each dot represents log2R for a single bin, where R = (read count tumour)/(read count 203H). CN, copy number. Structural variants are represented by dashed gray lines connected by black lines. Genes are represented as black bars, and locations and orientations of PDGFRA and PDGFRB are shown. Brown stain reports expression,

counterstained with blue hematoxylin. Scale bar, 30 mm. Figure reference: Figure 4 Stammnitz et al. 2018 (8) (appendix 6)

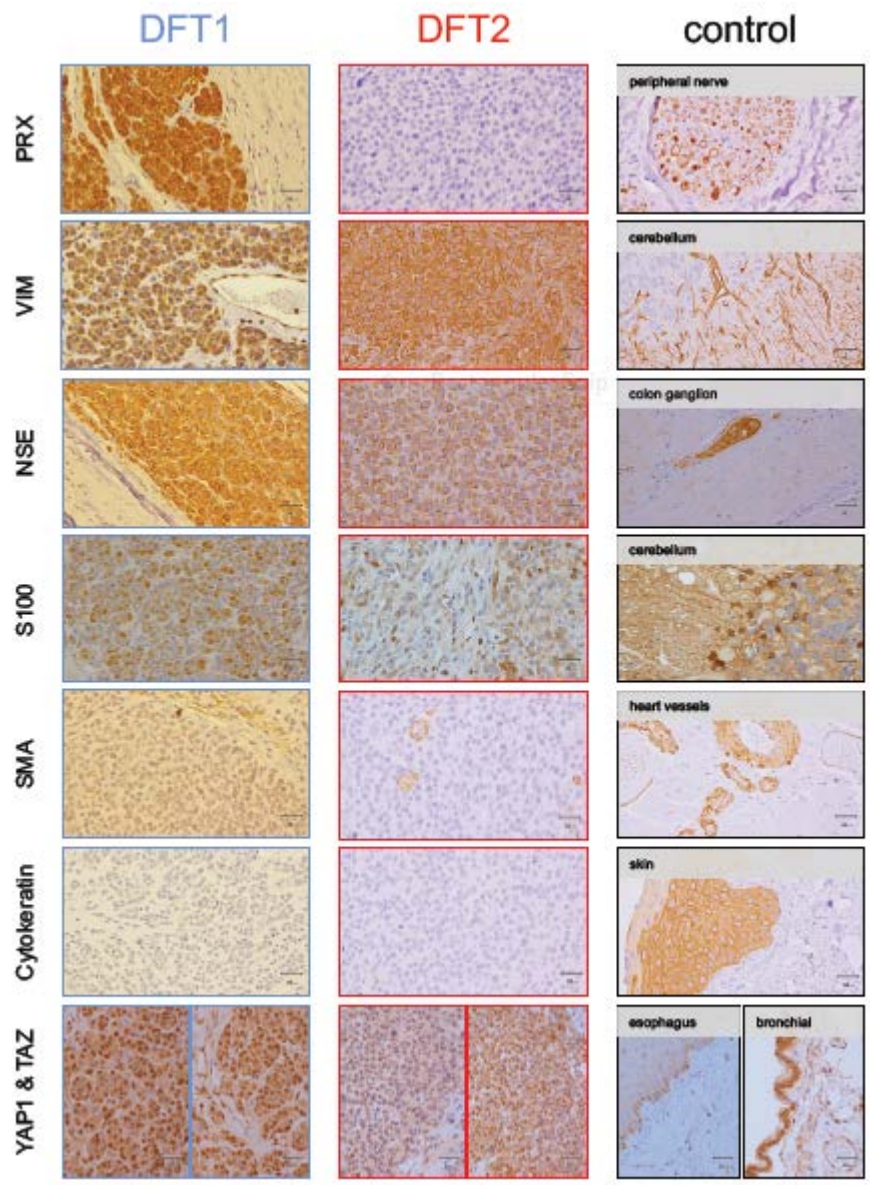

Figure 43*:* Immunohistological comparisons of DFT1 and DFT2

DFT1 (left), DFT2 (centre) and control (right) tissues stained with tissue lineage markers (Loh et al. 2006). PRX is included as a control (Pye et al., 2016 appendix 5). Scale bar, 30 µm. PRX, periaxin; VIM, vimentin; NSE, neural specific enolase; SMA, smooth muscle actin; YAP1 (bottom left panels), yes-associated protein 1; TAZ/WWTR1 (bottom right panels), transcriptional coactivator with PDZ-binding motif/WW domain-containing transcription regulator 1. Nuclear localization of YAP1 and TAZ/WWTR1 indicates dephosphorylated, active states of the proteins. Figure reference: Figure S1, related to Figure 1: Immunohistochemistry, Stammnitz et al. 2018 (appendix 6)

6.4 Discussion

The results and discussion are described in detail in the DFT2 Introduction 6.1, 6.1.1 and 6.1.2.

7.0 Final comments and future directions.

My research has comprehensively redefined the Immunophenotype of DFTD documenting the expression of 37 new and novel proteins not available in the current literature. My research expands on Schwann cell markers documented in current literature demonstrating the developmental stages of the Schwann cell lineage including precursor, immature, mature myelinating and non-myelinating Schwann cells. The expression of certain Schwann cell growth and transcription factors normally not expressed, suggests the activation of an autocrine repair program. Unexpectedly, my research demonstrated DFT1 expresses a melanocyte marker suggesting that DFT1 has divergent origins, a progenitor like cell with Schwann cell and melanocyte lineages with self-renewal characteristics. My research indicates that a progenitor-like state contributes to MHC down regulation, known in DFT1 cells, contributing to transmissibility of DFT1. I describe for the first time the histomorphology of the five strains of DFTD and extensively immunohistochemically stain these strains. I have described the expressional differences between strains and compared immunohistochemical expression with gene abundance data. The extensive literature presented above certainly advocates the remarkable plasticity of NCSCs and the Schwann cell and melanocyte lineages derived from them. Our results find that DFT1 is a progenitor-like cell, bipotent with both SC and melanocyte features, expressing repair transcription and growth factors with the acquisition of NCSC self-renewal properties. We theorise that the facial wound and resultant nerve injury would provide a perfect microenvironment, a niche, containing trophic signals necessary for migration, survival, proliferation and self-renewal of DFT1. The wound environment would be conducive to the genetic selection of a NC progenitor

with the molecular plasticity and MHC downregulation, causal to DFT1s clonal nature and transmissibility. I have prepared a manuscript ready for imminent submission of these research findings.

My research published the first description of the expression of ERBB3 by DFTD and measurement of ERBB3 as a possible early detection and therapeutic approach to tumour treatment. ERBB3 upregulation during developmental, dedifferentiation and regenerative processes encapsulates the Schwann cell's inherent plasticity and imparts certain characteristics of malignant transformation advantageous to transmission of DFT1. My pilot study has shown for the first time that ERBB3 is consistently expressed immunohistochemically and that ERBB3 is also elevated in the serum of Tasmanian devils with advanced DFT1. I also first reported that cutaneous lymphoma expresses ERBB3 in cutaneous lymphoma in Tasmanian devils, useful to the scientific community, both animal and human. Therefore, my research indicates that serum ERBB3 has the potential to be employed as a biomarker of DFT1 or CL in Tasmanian devils to assist conservationists in the management and welfare of Tasmanian devils and species survival. My research has devised a simple ELISA Serum ERBB3 methodology that is easily incorporated into routine laboratory batch testing, equally applied to include rapid turnaround of results for urgent cases.

My future directions include further studies on ERBB3, if determined by the STDP, extending this research is necessary to include greater numbers of healthy Tasmanian devils both with and without visible injuries, devils with large and small DFT1 lesions as well as pre-clinical DFT1. This will firmly establish the normal reference range for serum ERBB3 from which potential pre-clinical DFT1 may be identified. My research has specifically explored ERBB3, now recognised as a therapeutic target; therefore the potential exists to consider modes of administration. Additionally, quite a number of the unique proteins identified in my research can be targeted by

therapeutic monoclonal antibodies, another research project on its own. There will be ongoing research on DFT2 as directed by STDP, but monitoring any diffusion from the Channel Peninsula area as well as the pathobiology of both DFT1 and DFT2 will be a priority. From my current extensive research, I have a number of manuscripts in preparation including; DFT1 and the extracellular matrix, the latent period of DFT1 from exhaustive mining of the DPIPWE database and published articles and a tissue-microarray to further evaluate statistical analysis on strain expression patterns.

8.0 References

1. Loh R, Bergfeld J, Hayes D, O'Hara A, Pyecroft S, Raidal S, et al. The pathology of devil facial tumor disease (DFTD) in Tasmanian devils (Sarcophilus harrisii). Vet Pathol. 2006;43(6):890-5.

2. Loh R, Hayes D, Mahjoor A, O'Hara A, Pyecroft S, Raidal S. The immunohistochemical characterization of devil facial tumor disease (DFTD) in the Tasmanian Devil (Sarcophilus harrisii). Vet Pathol. 2006;43(6):896-903.

3. Pyecroft SB, Pearse AM, Loh R, Swift K, Belov K, Fox N, et al. Towards a case definition for devil facial tumour disease: What is it? EcoHealth. 2007;4(3):346-51.

4. Murchison EP, Tovar C, Hsu A, Bender HS, Kheradpour P, Rebbeck CA, et al. The Tasmanian Devil Transcriptome Reveals Schwann Cell Origins of a Clonally Transmissible Cancer. Science. 2010;327(5961):84-7.

5. Taylor RL, Zhang YR, Schoning JP, Deakin JE. Identification of candidate genes for devil facial tumour disease tumourigenesis. Sci Rep. 2017;7.

6. Kosack L, Wingelhofer B, Popa A, Vilagos B, Orlova A, Majek P, et al. The ERBB-STAT3 Axis Drives Tasmanian Devil Facial Tumor Disease. bioRxiv. 2018.

7. Pye RJ, Pemberton D, Tovar C, Tubio JMC, Dun KA, Fox S, et al. A second transmissible cancer in Tasmanian devils. Proc Natl Acad Sci U S A. 2016;113(2):374-9.

8. Stammnitz MR, Coorens THH, Gori KC, Hayes D, Fu BY, Wang JH, et al. The Origins and Vulnerabilities of Two Transmissible Cancers in Tasmanian Devils. Cancer Cell. 2018;33(4):607-+.

9. Guiler ER. Tasmanian devils in agriculture. Tasmanian Journal of Agriculture. 1970;41(2):134-&.

10. Munday BL. Marsupial disease. Proceedings No36 of Course for Veterinarians - Fauna. 1978:335-85.

11. Griner LA. Neoplasms in Tasmanian devils (Sarcophilus harrisii) J Natl Cancer Inst. 1979;62(3):589-95.

12. Canfield PJ, Hartley WJ, Reddacliff GL. Spontanious proliferations in Australian marsupials - A survey and review .2.Dasyurids and Bandicoots. J Comp Pathol. 1990;103(2):147-58.
13. Canfield PJ, Cunningham AA. Disease and mortality in Australasian marsupials held at London zoo, 1872-1972 J Zoo Wildl Med. 1993;24(2):158-67.
14. Ladds P. Pathology of Australian native wildlife. Ladds P, editor. Collingwood, Australia: CSIRO Publishing; 2009. 640 p.
15. Scheelings TF, Dobson EC, Hooper C. Cutaneous T-cell lymphoma in two captive Tasmanian devils (Sarcophilus harrisii) J Zoo Wildl Med. 2014;45(2):367-71.
16. Hawkins CE, Baars C, Hesterman H, Hocking GJ, Jones ME, Lazenby B, et al. Emerging disease and population decline of an island endemic, the Tasmanian devil Sarcophilus harrisii. Biol Conserv. 2006;131(2):307-24.
17. Chadwick B. Outbreak of facial tumours in Tasmanian devils. J Wildl Dis. 2003;39(4Supplement):7-8.
18. Pearse AM, Swift K. Transmission of devil facial-tumour disease - An uncanny similarity in the karyotype of these malignant tumours means that they could be infective. Nature. 2006;439(7076):549-.
19. Deakin JE, Bender HS, Pearse AM, Rens W, O'Brien PCM, Ferguson-Smith MA, et al. Genomic Restructuring in the Tasmanian Devil Facial Tumour: Chromosome Painting and Gene Mapping Provide Clues to Evolution of a Transmissible Tumour. PLoS Genet. 2012;8(2).
20. Tovar C, Obendorf D, Murchison EP, Papenfuss AT, Kreiss A, Woods GM. Tumor-Specific Diagnostic Marker for Transmissible Facial Tumors of Tasmanian Devils: Immunohistochemistry Studies. Vet Pathol. 2011;48(6):1195-203.
21. Woods GM, Kreiss A, Belov K, Siddle HV, Obendorf DL, Muller HK. The immune response of the Tasmanian Devil (Sarcophilus harrisii) and Devil Facial Tumour Disease. EcoHealth. 2007;4(3):338-45.
22. Kreiss A, Fox N, Bergfeld J, Quinn SJ, Pyecroft S, Woods GM. Assessment of cellular immune responses of healthy and diseased Tasmanian devils (Sarcophilus harrisii). Dev Comp Immunol. 2008;32(5):544-53.
23. Kreiss A, Wells B, Woods GM. The humoral immune response of the Tasmanian devil (Sarcophilus harrisii) against horse red blood cells. Vet Immunol Immunopathol. 2009;130(1-2):135-7.
24. Kreiss A, Obendorf DL, Hemsley S, Canfield PJ, Woods GM. A Histological and Immunohistochemical Analysis of Lymphoid Tissues of the Tasmanian Devil. Anat Rec. 2009;292(5):611-20.
25. Kreiss A, Cheng YY, Kimble F, Wells B, Donovan S, Belov K, et al. Allorecognition in the Tasmanian Devil (Sarcophilus harrisii), an Endangered Marsupial Species with Limited Genetic Diversity. PLoS One. 2011;6(7).
26. Brown GK, Kreiss A, Lyons AB, Woods GM. Natural Killer Cell Mediated Cytotoxic Responses in the Tasmanian Devil. PLoS One. 2011;6(9).
27. van der Kraan LE, Wong ESW, Lo N, Ujvari B, Belov K. Identification of natural killer cell receptor genes in the genome of the marsupial Tasmanian devil (Sarcophilus harrisii). Immunogenetics. 2013;65(1):25-35.
28. Howson LJ, Morris KM, Kobayashi T, Tovar C, Kreiss A, Papenfuss AT, et al. Identification of Dendritic Cells, B Cell and T Cell Subsets in Tasmanian Devil Lymphoid Tissue; Evidence for Poor Immune Cell Infiltration into Devil Facial Tumors. Anat Rec. 2014;297(5):925-38.
29. Cheng Y, Heasman K, Peck S, Peel E, Gooley RM, Papenfuss AT, et al. Significant decline in anticancer immune capacity during puberty in the Tasmanian devil. Sci Rep. 2017;7.
30. Kreiss A, Tovar C, Obendorf DL, Dun K, Woods GM. A Murine Xenograft Model for a Transmissible Cancer in Tasmanian Devils. Vet Pathol. 2011;48(2):475-81.
31. Kreiss A, Brown GK, Tovar C, Lyons AB, Woods GM. Evidence for induction of humoral and cytotoxic immune responses against devil facial tumor disease cells in Tasmanian devils (Sarcophilus harrisii) immunized with killed cell preparations. Vaccine. 2015;33(26):3016-25.
32. Pye R, Hamede R, Siddle HV, Caldwell A, Knowles GW, Swift K, et al. Demonstration of immune responses against devil facial tumour disease in wild Tasmanian devils. Biology Letters. 2016;12(10).
33. Tovar C, Pye RJ, Kreiss A, Cheng YY, Brown GK, Darby J, et al. Regression of devil facial tumour disease following immunotherapy in immunised Tasmanian devils. Sci Rep. 2017;7.

34. Pye R, Patchett A, McLennan E, Thomson R, Carver S, Fox S, et al. Immunization Strategies Producing a Humoral IgG Immune Response against Devil Facial Tumor Disease in the Majority of Tasmanian Devils Destined for Wild Release. Front Immunol. 2018;9.
35. Patchett AL, Darby JM, Tovar C, Lyons AB, Woods GM. The Immunomodulatory Small Molecule Imiquimod Induces Apoptosis in Devil Facial Tumour Cell Lines. PLoS One. 2016;11(12).
36. Siddle HV, Sanderson C, Belov K. Characterization of major histocompatibility complex class I and class II genes from the Tasmanian devil (Sarcophilus harrisii). Immunogenetics. 2007;59(9):753-60.
37. Siddle HV, Kreiss A, Eldridge MDB, Noonan E, Clarke CJ, Pyecroft S, et al. Transmission of a fatal clonal tumor by biting occurs due to depleted MHC diversity in a threatened carnivorous marsupial. Proc Natl Acad Sci U S A. 2007;104(41):16221-6.
38. Siddle HV, Marzec J, Cheng YY, Jones M, Belov K. MHC gene copy number variation in Tasmanian devils: implications for the spread of a contagious cancer. Proc R Soc B-Biol Sci. 2010;277(1690):2001-6.
39. Cheng YY, Belov K. Isolation and characterisation of 11 MHC-linked microsatellite loci in the Tasmanian devil (Sarcophilus harrisii). Conserv Genet Resour. 2012;4(2):463-5.
40. Lane A, Cheng YY, Wright B, Hamede R, Levan L, Jones M, et al. New Insights into the Role of MHC Diversity in Devil Facial Tumour Disease. PLoS One. 2012;7(6).
41. Cheng YY, Sanderson C, Jones M, Belov K. Low MHC class II diversity in the Tasmanian devil (Sarcophilus harrisii). Immunogenetics. 2012;64(7):525-33.
42. Cheng Y, Stuart A, Morris K, Taylor R, Siddle H, Deakin J, et al. Antigen-presenting genes and genomic copy number variations in the Tasmanian devil MHC. BMC Genomics. 2012;13.
43. Siddle HV, Kreiss A, Tovar C, Yuen CK, Cheng YY, Belov K, et al. Reversible epigenetic down-regulation of MHC molecules by devil facial tumour disease illustrates immune escape by a contagious cancer. Proc Natl Acad Sci U S A. 2013;110(13):5103-8.
44. Miller W, Hayes VM, Ratan A, Petersen DC, Wittekindt NE, Miller J, et al. Genetic diversity and population structure of the endangered marsupial Sarcophilus harrisii (Tasmanian devil). Proc Natl Acad Sci U S A. 2011;108(30):12348-53.
45. Murchison EP, Schulz-Trieglaff OB, Ning Z, Alexandrov LB, Bauer MJ, Fu B, et al. Genome sequencing and analysis of the tasmanian devil and its transmissible cancer. Cell. 2012;148(4):780-91.
46. Pearse AM, Swift K, Hodson P, Hua B, McCallum H, Pyecroft S, et al. Evolution in a transmissible cancer: a study of the chromosomal changes in devil facial tumor (DFT) as it spreads through the wild Tasmanian devil population. Cancer Genet. 2012;205(3):101-12.
47. Hayes DA, Kunde DA, Taylor RL, Pyecroft SB, Sohal SS, Snow ET. ERBB3: A potential serum biomarker for early detection and therapeutic target for devil facial tumour 1 (DFT1). PLoS One. 2017;12(6).
48. Ujvari B, Pearse A-M, Peck S, Harmsen C, Taylor R, Pyecroft S, et al. Evolution of a contagious cancer: epigenetic variation in Devil Facial Tumour Disease. Proc Biol Sci. 2013;280(1750):20121720.
49. Ingles ED, Deakin JE. Global DNA Methylation patterns on marsupial and devil facial tumour chromosomes. Mol Cytogenet. 2015;8.
50. Ujvari B, Pearse AM, Swift K, Hodson P, Hua B, Pyecroft S, et al. Anthropogenic selection enhances cancer evolution in Tasmanian devil tumours. Evol Appl. 2014;7(2):260-5.
51. Ujvari B, Pearse AM, Taylor R, Pyecroft S, Flanagan C, Gombert S, et al. Telomere Dynamics and Homeostasis in a Transmissible Cancer. PLoS One. 2012;7(8).
52. Bender HS, Murchison EP, Pickett HA, Deakin JE, Strong MA, Conlan C, et al. Extreme Telomere Length Dimorphism in the Tasmanian Devil and Related Marsupials Suggests Parental Control of Telomere Length. PLoS One. 2012;7(9).
53. Storfer A, Epstein B, Jones M, Micheletti S, Spear SF, Lachish S, et al. Landscape genetics of the Tasmanian devil: implications for spread of an infectious cancer. Conserv Genet. 2017;18(6):1287-97.
54. Bruniche-Olsen A, Burridge CP, Austin JJ, Jones ME. Disease induced changes in gene flow patterns among Tasmanian devil populations. Biol Conserv. 2013;165:69-78.
55. Wright B, Morris K, Grueber CE, Willet CE, Gooley R, Hogg CJ, et al. Development of a SNP-based assay for measuring genetic diversity in the Tasmanian devil insurance population. BMC Genomics. 2015;16.

56. Morris KM, Wright B, Grueber CE, Hogg C, Belov K. Lack of genetic diversity across diverse immune genes in an endangered mammal, the Tasmanian devil (Sarcophilus harrisii). Mol Ecol. 2015;24(15):3860-72.
57. Hendricks S, Epstein B, Schonfeld B, Wiench C, Hamede R, Jones M, et al. Conservation implications of limited genetic diversity and population structure in Tasmanian devils (Sarcophilus harrisii). Conserv Genet. 2017;18(4):977-82.
58. Bruniche-Olsen A, Jones ME, Austin JJ, Burridge CP, Holland BR. Extensive population decline in the Tasmanian devil predates European settlement and devil facial tumour disease. Biol Lett. 2014;10(11).
59. Lachish S, Jones M, McCallum H. The impact of disease on the survival and population growth rate of the Tasmanian devil. J Anim Ecol. 2007;76(5):926-36.
60. McCallum H, Tompkins DM, Jones M, Lachish S, Marvanek S, Lazenby B, et al. Distribution and impacts of Tasmanian devil facial tumor disease. EcoHealth. 2007;4(3):318-25.
61. Jones ME, Cockburn A, Hamede R, Hawkins C, Hesterman H, Lachish S, et al. Life-history change in disease-ravaged Tasmanian devil populations. Proc Natl Acad Sci U S A. 2008;105(29):10023-7.
62. McCallum H, Jones M, Hawkins C, Hamede R, Lachish S, Sinn DL, et al. Transmission dynamics of Tasmanian devil facial tumor disease may lead to disease-induced extinction. Ecology. 2009;90(12):3379-92.
63. Hamede R, Lachish S, Belov K, Woods G, Kreiss A, Pearse AM, et al. Reduced Effect of Tasmanian Devil Facial Tumor Disease at the Disease Front. Conserv Biol. 2012;26(1):124-34.
64. Hamede RK, McCallum H, Jones M. Biting injuries and transmission of Tasmanian devil facial tumour disease. J Anim Ecol. 2013;82(1):182-90.
65. Wells K, Hamede RK, Kerlin DH, Storfer A, Hohenlohe PA, Jones ME, et al. Infection of the fittest: devil facial tumour disease has greatest effect on individuals with highest reproductive output. Ecol Lett. 2017;20(6):770-8.
66. Hamede RK, Pearse AM, Swift K, Barmuta LA, Murchison EP, Jones ME. Transmissible cancer in Tasmanian devils: localized lineage replacement and host population response. Proc R Soc B-Biol Sci. 2015;282(1814):122-8.
67. Lazenby BT, Tobler MW, Brown WE, Hawkins CE, Hocking GJ, Hume F, et al. Density trends and demographic signals uncover the long-term impact of transmissible cancer in Tasmanian devils. J Appl Ecol. 2018;55(3):1368-79.
68. Grueber CE, Fox S, Belov K, Pemberton D, Hogg CJ. Landscape-level field data reveal broad-scale effects of a fatal, transmissible cancer on population ecology of the Tasmanian devil. Mamm Biol. 2018;91:41-5.
69. Siska V, Eriksson A, Mehlig B, Manica A. A metapopulation model of the spread of the Devil Facial Tumour Disease predicts the long term collapse of its host but not its extinction. bioRxiv. 2018.
70. Karu N, Wilson R, Hamede R, Jones M, Woods GM, Hilder EF, et al. Discovery of Biomarkers for Tasmanian Devil Cancer (DFTD) by Metabolic Profiling of Serum. J Proteome Res. 2016;15(10):3827-40.
71. Lachish S, McCallum H, Mann D, Pukk CE, Jones ME. Evaluation of Selective Culling of Infected Individuals to Control Tasmanian Devil Facial Tumor Disease. Conserv Biol. 2010;24(3):841-51.
72. Beeton N, McCallum H. Models predict that culling is not a feasible strategy to prevent extinction of Tasmanian devils from facial tumour disease. J Appl Ecol. 2011;48(6):1315-23.
73. Phalen DN, Frimberger A, Pyecroft S, Peck S, Harmsen C, Lola S, et al. Vincristine Chemotherapy Trials and Pharmacokinetics in Tasmanian Devils with Tasmanian Devil Facial Tumor Disease. PLoS One. 2013;8(6).
74. Phalen DN, Frimberger AE, Peck S, Pyecroft S, Harmsen C, Lola S, et al. Doxorubicin and carboplatin trials in Tasmanian devils (Sarcophilus harrisii) with Tasmanian devil facial tumor disease. Vet J. 2015;206(3):312-6.
75. Jones ME, Jarman PJ, Lees CM, Hesterman H, Hamede RK, Mooney NJ, et al. Conservation management of tasmanian devils in the context of an emerging, extinction-threatening disease: Devil facial tumor disease. EcoHealth. 2007;4(3):326-37.
76. McCallum H. Models for managing wildlife disease. Parasitology. 2016;143(7):805-20.

77. Hogg CJ, Ivy JA, Srb C, Hockley J, Lees C, Hibbard C, et al. Influence of genetic provenance and birth origin on productivity of the Tasmanian devil insurance population. Conserv Genet. 2015;16(6):1465-73.
78. Rogers T, Fox S, Pemberton D, Wise P. Sympathy for the devil: captive-management style did not influence survival, body-mass change or diet of Tasmanian devils 1 year after wild release. Wildl Res. 2016;43(7):544-52.
79. Thalmann S, Peck S, Wise P, Potts JM, Clarke J, Richley J. Translocation of a top-order carnivore: tracking the initial survival, spatial movement, home-range establishment and habitat use of Tasmanian devils on Maria Island. Aust Mammal. 2016;38(1):68-79.
80. McLennan EA, Gooley RM, Wise P, Belov K, Hogg CJ, Grueber CE. Pedigree reconstruction using molecular data reveals an early warning sign of gene diversity loss in an island population of Tasmanian devils (Sarcophilus harrisii). Conserv Genet. 2018;19(2):439-50.
81. Rout TM, Baker CM, Huxtable S, Wintle BA. Monitoring, imperfect detection, and risk optimization of a Tasmanian devil insurance population. Conserv Biol. 2018;32(2):267-75.
82. Grueber CE, Reid-Wainscoat EE, Fox S, Belov K, Shier DM, Hogg CJ, et al. Increasing generations in captivity is associated with increased vulnerability of Tasmanian devils to vehicle strike following release to the wild. Sci Rep. 2017;7(1):2161.
83. Hogg CJ, Grueber CE, Pemberton D, Fox S, Lee AV, Ivy JA, et al. "Devil Tools & Tech": A Synergy of Conservation Research and Management Practice. Conserv Lett. 2017;10(1):133-8.
84. Brüniche-Olsen A, Austin JJ, Jones ME, Holland BR, Burridge CP. Detecting Selection on Temporal and Spatial Scales: A Genomic Time-Series Assessment of Selective Responses to Devil Facial Tumor Disease. PLoS One. 2016;11(3):e0147875.
85. Kwon Y, Stammnitz MR, Wang J, Knowles GW, Pye RJ, Hamede R, et al. Tasman-PCR: A genetic diagnostic assay for Tasmanian devil facial tumour diseases. bioRxiv. 2018.
86. Caldwell A, Coleby R, Tovar C, Stammnitz MR, Kwon YM, Owen RS, et al. The newly-arisen Devil facial tumour disease 2 (DFT2) reveals a mechanism for the emergence of a contagious cancer. eLife. 2018;7.
87. Ramos-Vara JA. Technical aspects of immunohistochemistry. Vet Pathol. 2005;42(4):405-26.
88. Hall BK. The neural crest as a fourth germ layer and vertebrates as quadroblastic not triploblastic. Evol Dev. 2000;2(1):3-5.
89. Bronner ME, LeDouarin NM. Development and evolution of the neural crest: An overview. Dev Biol. 2012;366(1):2-9.
90. Theveneau E, Mayor R. Neural crest delamination and migration: From epithelium-to-mesenchyme transition to collective cell migration. Dev Biol. 2012;366(1):34-54.
91. Dupin E, Le Douarin NM. The Neural Crest, A Multifaceted Structure of the Vertebrates. Birth Defects Res Part C-Embryo Today-Rev. 2014;102(3):187-209.
92. Bronner ME, Simoes-Costa M. The Neural Crest Migrating into the Twenty-First Century. In: Wassarman PM, editor. Essays on Developmental Biology, Pt A. San Diego: Elsevier Academic Press Inc; 2016. p. 115-+.
93. Ferner K, Schultz JA, Zeller U. Comparative anatomy of neonates of the three major mammalian groups (monotremes, marsupials, placentals) and implications for the ancestral mammalian neonate morphotype. J Anat. 2017;231(6):798-822.
94. Frappell PB, MacFarlane PM. Development of the respiratory system in marsupials. Respir Physiol Neuro. 2006;154(1-2):252-67.
95. Smith KK. Craniofacial development in marsupial mammals: Developmental origins of evolutionary change. Dev Dyn. 2006;235(5):1181-93.
96. Smith KK. Early development of the neural plate, neural crest and facial region of marsupials. J Anat. 2001;199:121-31.
97. Vaglia JL, Smith KK. Early differentiation and migration of cranial neural crest in the opossum, Monodelphis domestica. Evol Dev. 2003;5(2):121-35.
98. Keyte AL, Smith KK. Developmental origins of precocial forelimbs in marsupial neonates. Development. 2010;137(24):4283-94.

99. Guiler E. Observations on the Tasmanian Devil, Sarcophilus harrisii (Marsupialia : Dasyuridae) II. Reproduction, breeding and growth of pouch young. Aust J Zool. 1970;18(1):63-70.
100. Etherington SJ, Hong IHK, Wong CJW, Stephens N, Warburton NM. Heterochronic neuromuscular junction development in an Australian marsupial (Macropus fuliginosus). J Zool. 2016;300(1):27-35.
101. Ashwell KWS. Timing of mammalian peripheral trigeminal system development relative to body size: A comparison of metatherians with rodents and monotremes. Somatosens Mot Res. 2015;32(3):187-99.
102. Ashwell KWS, Marotte LR, Cheng G. Development of the olfactory system in a wallaby (Macropus eugenii). Brain Behav Evol. 2008;71(3):216-30.
103. Schneider NY, Fletcher TP, Shaw G, Renfree MB. The olfactory system of the tammar wallaby is developed at birth and directs the neonate to its mother's pouch odours. Reproduction. 2009;138(5):849-57.
104. Hollis D, Lyne A. Innervation of vibrissa follicles in the marsupial Trichosurus vulpecula. Aust J Zool. 1974;22(3):263-76.
105. Gemmell RT, Peters B, Nelson J. Ultrastructural Identification of Merkel Cells Around The Mouth of The Newborn Marsupial. Anat Embryol. 1988;177(5):403-8.
106. Desmarais MJ, Beauregard F, Cabana T, Pflieger JF. Facial Mechanosensory Influence on Forelimb Movement in Newborn Opossums, Monodelphis domestica. PLoS One. 2016;11(2).
107. Lyne AG. Melanocyte Population in Skin During Development of Marsupial Trichosurus Vulpecula. Australian Journal of Biological Sciences. 1970;23(3):697-&.
108. Pralomkarn T, Nelson J, Gemmell RT. Post Natal Development of The Skin of The Marsupial Native Cat Dasyurus Hallucatus. . J Morphol. 1990;205(2):233-42.
109. Jessen KR, Mirsky R. The origin and development of glial cells in peripheral nerves. Nat Rev Neurosci. 2005;6(9):671-82.
110. Jacob C. Transcriptional control of neural crest specification into peripheral glia. Glia. 2015;63(11):1883-96.
111. Huang LYM, Gu YP, Chen Y. Communication between neuronal somata and satellite glial cells in sensory ganglia. Glia. 2013;61(10):1571-81.
112. Fontenas L, Kucenas S. Livin' On The Edge: glia shape nervous system transition zones. Curr Opin Neurobiol. 2017;47:44-51.
113. Maro GS, Vermeren M, Voiculescu O, Melton L, Cohen J, Charnay P, et al. Neural crest boundary cap cells constitute a source of neuronal and glial cells of the PNS. Nat Neurosci. 2004;7(9):930-8.
114. Hjerling-Leffler J, Marmigere F, Heglind M, Cederberg A, Koltzenburg M, Enerback S, et al. The boundary cap: a source of neural crest stem cells that generate multiple sensory neuron subtypes. Development. 2005;132(11):2623-32.
115. Aquino JB, Hjerling-Leffler J, Koltzenburg M, Edlund T, Villar MJ, Ernfors P. In vitro and in vivo differentiation of boundary cap neural crest stem cells into mature Schwann cells. Exp Neurol. 2006;198(2):438-49.
116. Gresset A, Coulpier F, Gerschenfeld G, Jourdon A, Matesic G, Richard L, et al. Boundary Caps Give Rise to Neurogenic Stem Cells and Terminal Glia in the Skin. Stem Cell Rep. 2015;5(2):278-90.
117. Jessen KR, Mirsky R. Signals that determine Schwann cell identity. J Anat. 2002;200(4):367-75.
118. Woodhoo A, Sommer L. Development of the Schwann Cell Lineage: From the Neural Crest to the Myelinated Nerve. Glia. 2008;56(14):1481-90.
119. Monk KR, Feltri ML, Taveggia C. New insights on schwann cell development. Glia. 2015;63(8):1376-93.
120. Harty BL, Monk KR. Unwrapping the unappreciated: recent progress in Remak Schwann cell biology. Curr Opin Neurobiol. 2017;47:131-7.
121. Griffin JW, Thompson WJ. Biology and Pathology of Nonmyelinating Schwann cells. Glia. 2008;56(14):1518-31.
122. Aguayo AJ, Charron L, Bray GM. Potential of Schwann Cells From Unmyelinated Nerves to produce Myelin - Quantitative Ultrasrtuctural and Radiographic Study. J Neurocytol. 1976;5(5):565-73.
123. Yamazaki S, Nakauchi H. Bone marrow Schwann cells induce hematopoietic stem cell hibernation. Int J Hematol. 2014;99(6):695-8.

124. Yamazaki S, Ema H, Karlsson G, Yamaguchi T, Miyoshi H, Shioda S, et al. Nonmyelinating Schwann Cells Maintain Hematopoietic Stem Cell Hibernation in the Bone Marrow Niche. Cell. 2011;147(5):1146-58.
125. Locher H, de Groot J, van Iperen L, Huisman MA, Frijns JHM, Lopes S. Distribution and Development of Peripheral Glial Cells in the Human Fetal Cochlea. PLoS One. 2014;9(1).
126. Fernandez-Flores A. Evidence on the neural crest origin of PEComas. Rom J Morphol Embryol. 2011;52(1):7-13.
127. Rosso G, Young P, Shahin V. Implications of Schwann Cells Biomechanics and Mechanosensitivity for Peripheral Nervous System Physiology and Pathophysiology. Front Molec Neurosci. 2017;10.
128. Verze P, Somma A, Imbimbo C, Mansueto G, Mirone V, Insabato L. Melanotic Schwannoma: A Case of Renal Origin. Clin Genitourin Cancer. 2014;12(1):E37-E41.
129. Sherman LS, Rizvi TA, Karyala S, Ratner N. CD44 enhances neuregulin signaling by Schwann cells. J Cell Biol. 2000;150(5):1071-83.
130. Furlan A, Adameyko I. Schwann cell precursor: a neural crest cell in disguise? Dev Biol. 2018. Epub 16 February 2018.
131. Zimmerman A, Bai L, Ginty DD. The gentle touch receptors of mammalian skin. Science. 2014;346(6212):950-4.
132. Sullivan KA, Kim B, Feldman EL. Insulin-Like Growth Factors in the Peripheral Nervous System. Endocrinology. 2008;149(12):5963-71.
133. Kim HJ, Jung CG, Jensen MA, Dukala D, Soliven B. Targeting of Myelin Protein Zero in a Spontaneous Autoimmune Polyneuropathy. J Immunol. 2008;181(12):8753-60.
134. Barik A, Li L, Sathyamurthy A, Xiong WC, Mei L. Schwann Cells in Neuromuscular Junction Formation and Maintenance. J Neurosci. 2016;36(38):9770-81.
135. Ko CP, Robitaille R. Perisynaptic Schwann Cells at the Neuromuscular Synapse: Adaptable, Multitasking Glial Cells. Cold Spring Harbor Perspect Biol. 2015;7(10).
136. Lousado L, Prazeres P, Andreotti JP, Paiva AE, Azevedo PO, Santos GSP, et al. Schwann cell precursors as a source for adrenal gland chromaffin cells. Cell Death Dis. 2017;8.
137. Boesmans W, Lasrado R, Vanden Berghe P, Pachnis V. Heterogeneity and Phenotypic Plasticity of Glial Cells in the Mammalian Enteric Nervous System. Glia. 2015;63(2):229-41.
138. Ulrich R, Imbschweiler I, Kalkuhl A, Lehmbecker A, Ziege S, Kegler K, et al. Transcriptional Profiling Predicts Overwhelming Homology of Schwann Cells, Olfactory Ensheathing Cells, and Schwann Cell-Like Glia. Glia. 2014;62(10):1559-81.
139. Barraud P, Seferiadis AA, Tyson LD, Zwart MF, Szabo-Rogers HL, Ruhrberg C, et al. Neural crest origin of olfactory ensheathing glia. Proc Natl Acad Sci U S A. 2010;107(49):21040-5.
140. Cichorek M, Wachulska M, Stasiewicz A. Heterogeneity of neural crest-derived melanocytes. Cent Eur J Biol. 2013;8(4):315-30.
141. Colombo S, Berlin, I. , Delmas, V. and Larue, L. Classical and Nonclassical Melanocytes in Vertebrates Ch2. In Melanins and Melanosomes: Biosynthesis, Biogenesis, Physiological and Pathological Functions. Editors J. Borovanský and P. A. Riley.: Wiley; 2011. p. 21-61. doi:10.1002/9783527636150.ch2.
142. Dupin E, Le Douarin NM. Development of melanocyte precursors from the vertebrate neural crest. Oncogene. 2003;22(20):3016-23.
143. Joseph NM, Mukouyama YS, Mosher JT, Jaegle M, Crone SA, Dormand EL, et al. Neural crest stem cells undergo multilineage differentiation in developing peripheral nerves to generate endoneurial fibroblasts in addition to Schwann cells. Development. 2004;131(22):5599-612.
144. Adameyko I, Lallemend F, Aquino JB, Pereira JA, Topilko P, Muller T, et al. Schwann Cell Precursors from Nerve Innervation Are a Cellular Origin of Melanocytes in Skin. Cell. 2009;139(2):366-79.
145. Erickson CA. From The Neural Crest to The Periphery - Control of Pigment Cell Migration and Lineage Segregation. . Pigm Cell Res. 1993;6(5):336-47.
146. Larue L, de Vuyst F, Delmas V. Modeling melanoblast development. Cell Mol Life Sci. 2013;70(6):1067-79.
147. Adameyko I, Lallemend F, Furlan A, Zinin N, Aranda S, Kitambi SS, et al. Sox2 and Mitf cross-regulatory interactions consolidate progenitor and melanocyte lineages in the cranial neural crest. Development. 2012;139(2):397-410.

148. Davis DA, Kurtz KA, Robinson RA. Ultrarapid staining for cutaneous melanoma: Study and protocol. Dermatol Surg. 2005;31(7):753-6.
149. Hillesheim PB, Slone S, Kelley D, Malone J, Bahrami S. An immunohistochemical comparison between MiTF and MART-1 with Azure blue counterstaining in the setting of solar lentigo and melanoma in situ. J Cutan Pathol. 2011;38(7):565-9.
150. Churukian. Charles J. Pigments and Minerals. Ch 14. Theory and Practice of Histological Techniques. Ed. Bancroft. J.D Gamble. M. 6th Ed. pg233-259. ISBN 978-0-443-10279-0. 2008.
151. Hoernes TP, Hüttenhofer A, Erlacher MD. mRNA modifications: Dynamic regulators of gene expression? RNA Biol. 2016;13(9):760-5.
152. Gomes AQ, Nolasco S, Soares H. Non-Coding RNAs: Multi-Tasking Molecules in the Cell. Int J Mol Sci. 2013;14(8):16010-39.
153. Roundtree IA, Evans ME, Pan T, He C. Dynamic RNA Modifications in Gene Expression Regulation. Cell. 2017;169(7):1187-200.
154. Gibcus JH, Dekker J. The context of gene expression regulation. F1000 Biol Rep. 2012;4:8.
155. Sauka-Spengler T, Bronner-Fraser M. A gene regulatory network orchestrates neural crest formation. Nat Rev Mol Cell Biol. 2008;9(7):557-68.
156. Rogers CD, Jayasena CS, Nie S, Bronner ME. Neural crest specification: tissues, signals, and transcription factors. Wiley Interdiscip Rev-Dev Biol. 2012;1(1):52-68.
157. Simoes-Costa M, Bronner ME. Establishing neural crest identity: a gene regulatory recipe. Development. 2015;142(2):242-57.
158. Martik ML, Bronner ME. Regulatory Logic Underlying Diversification of the Neural Crest. Trends Genet. 2017;33(10):715-27.
159. Erickson CA, Goins TL. Avian Neural Crest Cells Can Migrate in The Dorsolateral Path Only if They are Specified as Melanocytes. Development. 1995;121(3):915-24.
160. Kos R, Reedy MV, Johnson RL, Erickson CA. The winged-helix transcription factor FoxD3 is important for establishing the neural crest lineage and repressing melanogenesis in avian embryos. Development. 2001;128(8):1467-79.
161. Thomas AJ, Erickson CA. FOXD3 regulates the lineage switch between neural crest-derived glial cells and pigment cells by repressing MITF through a non-canonical mechanism. Development. 2009;136(11):1849-58.
162. Dottori M, Gross MK, Labosky P, Goulding M. The winged-helix transcription factor Foxd3 suppresses interneuron differentiation and promotes neural crest cell fate. Development. 2001;128(21):4127-38.
163. Krispin S, Nitzan E, Kassem Y, Kalcheim C. Evidence for a dynamic spatiotemporal fate map and early fate restrictions of premigratory avian neural crest. Development. 2010;137(4):585-95.
164. Nitzan E, Krispin S, Pfaltzgraff ER, Klar A, Labosky PA, Kalcheim C. A dynamic code of dorsal neural tube genes regulates the segregation between neurogenic and melanogenic neural crest cells. Development. 2013;140(11):2269-79.
165. Mort RL, Jackson IJ, Patton EE. The melanocyte lineage in development and disease. Development. 2015;142(4):620-32.
166. Nitzan E, Pfaltzgraff ER, Labosky PA, Kalcheim C. Neural crest and Schwann cell progenitor-derived melanocytes are two spatially segregated populations similarly regulated by Foxd3. Proc Natl Acad Sci U S A. 2013;110(31):12709-14.
167. Dorsky RI, Moon RT, Raible DW. Control of neural crest cell fate by the Wnt signalling pathway. Nature. 1998;396(6709):370-3.
168. Dorsky RI, Raible DW, Moon RT. Direct regulation of nacre, a zebrafish MITF homolog required for pigment cell formation, by the Wnt pathway. Genes Dev. 2000;14(2):158-62.
169. Jin EJ, Erickson CA, Takada S, Burrus LW. Wnt and BMP signaling govern lineage segregation of melanocytes in the avian embryo. Dev Biol. 2001;233(1):22-37.
170. Hari L, Brault V, Kleber M, Lee HY, Ille F, Leimeroth R, et al. Lineage-specific requirements of beta-catenin in neural crest development. J Cell Biol. 2002;159(5):867-80.
171. Larue L, Kumasaka M, Goding CR. beta-catenin in the melanocyte lineage. Pigm Cell Res. 2003;16(3):312-7.

172. Gess B, Halfter H, Kleffner I, Monje P, Athauda G, Wood PM, et al. Inhibition of N-cadherin and beta-catenin function reduces axon-induced Schwann cell proliferation. J Neurosci Res. 2008;86(4):797-812.
173. Lewallen KA, Shen YAA, De La Torre AR, Ng BK, Meijer D, Chan JR. Assessing the Role of the Cadherin/Catenin Complex at the Schwann Cell-Axon Interface and in the Initiation of Myelination. J Neurosci. 2011;31(8):3032-43.
174. Tawk M, Makoukji J, Belle M, Fonte C, Trousson A, Hawkins T, et al. Wnt/beta-Catenin Signaling Is an Essential and Direct Driver of Myelin Gene Expression and Myelinogenesis. J Neurosci. 2011;31(10):3729-42.
175. Grigoryan T, Stein S, Qi JJ, Wende H, Garratt AN, Nave KA, et al. Wnt/Rspondin/beta-catenin signals control axonal sorting and lineage progression in Schwann cell development. Proc Natl Acad Sci U S A. 2013;110(45):18174-9.
176. Acebron SP, Niehrs C. beta-Catenin-Independent Roles of Wnt/LRP6 Signaling. Trends Cell Biol. 2016;26(12):956-67.
177. Katoh M. Canonical and non-canonical WNT signaling in cancer stem cells and their niches: Cellular heterogeneity, omics reprogramming, targeted therapy and tumor plasticity (Review). Int J Oncol. 2017;51(5):1357-69.
178. Katoh M, Katoh M. Molecular genetics and targeted therapy of WNT-related human diseases. Int J Mol Med. 2017;40(3):587-606.
179. Oliva CA, Montecinos-Oliva C, Inestrosa NC. Wnt Signaling in the Central Nervous System: New Insights in Health and Disease. In progress in Molecular Biology and Translational Science. Editors Larrain, J. Olivares, G. San Diego: Elsevier Academic Press Inc; 2018. p. 81-130.
180. Kim K-A, Wagle M, Tran K, Zhan X, Dixon MA, Liu S, et al. R-Spondin Family Members Regulate the Wnt Pathway by a Common Mechanism. Mol Biol Cell. 2008;19(6):2588-96.
181. Imajo M, Miyatake K, Iimura A, Miyamoto A, Nishida E. A molecular mechanism that links Hippo signalling to the inhibition of Wnt/β-catenin signalling. EMBO J. 2012;31(5):1109-22.
182. Li C, Wang S, Xing Z, Lin A, Liang K, Song J, et al. A ROR1-HER3-LncRNA signaling axis modulates the Hippo-YAP pathway to regulate bone metastasis. Nat Cell Biol. 2017;19(2):106-19.
183. Shimobayashi M, Hall MN. Making new contacts: the mTOR network in metabolism and signalling crosstalk. Nat Rev Mol Cell Biol. 2014;15(3):155-62.
184. Goding CR. Mitf from neural crest to melanoma: signal transduction and transcription in the melanocyte lineage. Genes Dev. 2000;14(14):1712-28.
185. Takeda K, Yasumoto K, Takada R, Takada S, Watanabe K, Udono T, et al. Induction of melanocyte-specific microphthalmia-associated transcription factor by Wnt-3a. J Biol Chem. 2000;275(19):14013-6.
186. Shibahara S, Takeda K, Yasumoto K, Udono T, Watanabe K, Saito H, et al. Microphthalmia-associated transcription factor (MITF): Multiplicity in structure, function, and regulation. J Invest Dermatol Symp Proc. 2001;6(1):99-104.
187. Steingrimsson E, Copeland NG, Jenkins NA. Melanocytes and the Microphthalmia transcription factor network. Annu Rev Genet. 2004;38:365-411.
188. Vachtenheim J, Borovansky J. "Transcription physiology" of pigment formation in melanocytes: central role of MITF. Exp Dermatol. 2010;19(7):617-27.
189. Kawakami A, Fisher DE. The master role of microphthalmia-associated transcription factor in melanocyte and melanoma biology. Lab Invest. 2017;97(6):649-56.
190. Buac K, Xu M, Cronin J, Weeraratna AT, Hewitt SM, Pavan WJ. NRG1/ERBB3 signaling in melanocyte development and melanoma: inhibition of differentiation and promotion of proliferation. Pigment Cell Melanoma Res. 2009;22(6):773-84.
191. Grigoryan T, Birchmeier W. Molecular signaling mechanisms of axon-glia communication in the peripheral nervous system. BioEssays. 2015;37(5):502-13.
192. Hari L, Miescher I, Shakhova O, Suter U, Chin L, Taketo M, et al. Temporal control of neural crest lineage generation by Wnt/beta-catenin signaling. Development. 2012;139(12):2107-17.
193. Paratore C, Goerich DE, Suter U, Wegner M, Sommer L. Survival and glial fate acquisition of neural crest cells are regulated by an interplay between the transcription factor Sox10 and extrinsic combinatorial signaling. Development. 2001;128(20):3949-61.

194. Finzsch M, Schreiner S, Kichko T, Reeh P, Tamm ER, Bosl MR, et al. Sox10 is required for Schwann cell identity and progression beyond the immature Schwann cell stage. J Cell Biol. 2010;189(4):701-12.
195. Britsch S, Goerich DE, Riethmacher D, Peirano RI, Rossner M, Nave KA, et al. The transcription factor Sox10 is a key regulator of peripheral glial development. Genes Dev. 2001;15(1):66-78.
196. Birchmeier C, Nave KA. Neuregulin-1, a Key Axonal Signal that Drives Schwann Cell Growth and Differentiation. Glia. 2008;56(14):1491-7.
197. Meier C, Parmantier E, Brennan A, Mirsky R, Jessen KR. Developing Schwann cells acquire the ability to survive without axons by establishing an autocrine circuit involving insulin-like growth factor, neurotrophin-3, and platelet-derived growth factor-BB. J Neurosci. 1999;19(10):3847-59.
198. Parkinson DB, Bhaskaran A, Arthur-Farraj P, Noon LA, Woodhoo A, Lloyd AC, et al. c-Jun is a negative regulator of myelination. J Cell Biol. 2008;181(4):625-37.
199. Woodhoo A, Alonso MBD, Droggiti A, Turmaine M, D'Antonio M, Parkinson DB, et al. Notch controls embryonic Schwann cell differentiation, postnatal myelination and adult plasticity. Nat Neurosci. 2009;12(7):839-U46.
200. Mirsky R, Woodhoo A, Parkinson DB, Arthur-Farraj P, Bhaskaran A, Jessen KR. Novel signals controlling embryonic Schwann cell development, myelination and dedifferentiation. J Peripher Nerv Syst. 2008;13(2):122-35.
201. Nelson J, McFerran NV, Pivato G, Chambers E, Doherty C, Steele D, et al. The 67 kDa laminin receptor: structure, function and role in disease. Biosci Rep. 2008;28(1):33-48.
202. DiGiacomo V, Meruelo D. Looking into laminin receptor: critical discussion regarding the non-integrin 37/67-kDa laminin receptor/RPSA protein. Biol Rev. 2016;91(2):288-310.
203. Previtali SC, Nodari A, Taveggia C, Pardini C, Dina G, Villa A, et al. Expression of laminin receptors in Schwann cell differentiation: Evidence for distinct roles. J Neurosci. 2003;23(13):5520-30.
204. Feltri ML, Wrabetz L. Laminins and their receptors in Schwann cells and hereditary neuropathies. J Peripher Nerv Syst. 2005;10(2):128-43.
205. Chernousov MA, Yu WM, Chen ZL, Carey DJ, Strickland S. Regulation of Schwann Cell Function by the Extracellular Matrix. Glia. 2008;56(14):1498-507.
206. Kioussi C, Gross MK, Gruss P. PAX3 - A Paired Domain Gene as a Regulator in PNS Myelination. Neuron. 1995;15(3):553-62.
207. Gillespie CS, Sherman DL, Blair GE, Brophy PJ. Periaxin, a Novel Protein of Myelinating Schwann Cells with a Possible Role in Axonal Ensheathment. Neuron. 1994;12(3):497-508.
208. Scherer SS, Xu YT, Bannerman PGC, Sherman DL, Brophy PJ. Periaxin expression in myelinating Schwann cells: Modulation by axon-glial interactions and polarized localization during development. Development. 1995;121(12):4265-73.
209. Dytrych L, Sherman DL, Gillespie CS, Brophy PJ. Two PDZ Domain Proteins Encoded by the Murine Periaxin Gene Are the Result of Alternative Intron Retention and Are Differentially Targeted in Schwann Cells. J Biol Chem. 1998;273(10):5794-800.
210. Sherman DL, Brophy PJ. A Tripartite Nuclear Localization Signal in the PDZ-domain Protein L-periaxin. J Biol Chem. 2000;275(7):4537-40.
211. Yang YA, Shi YW. L-periaxin interacts with S-periaxin through its PDZ domain. Neurosci Lett. 2015;609:23-9.
212. Parkinson DB, Dickinson S, Bhaskaran A, Kinsella MT, Brophy PJ, Sherman DL, et al. Regulation of the myelin gene periaxin provides evidence for Krox-20-independent myelin-related signalling in Schwann cells. Mol Cell Neurosci. 2003;23(1):13-27.
213. Rochaix P, Lacroix-Triki M, Lamant L, Pichereaux C, Valmary S, Puente E, et al. PNL2, a new monoclonal antibody directed against a fixative-resistant melanocyte antigen. Mod Pathol. 2003;16(5):481-90.
214. Giudice C, Ceciliani F, Rondena M, Stefanello D, Grieco V. Immunohistochemical investigation of PNL2 reactivity of canine melanocytic neoplasms and comparison with Melan A. J Vet Diagn Invest. 2010;22(3):389-94.
215. Ramos-Vara JA, Miller MA. Immunohistochemical Identification of Canine Melanocytic Neoplasms With Antibodies to Melanocytic Antigen PNL2 and Tyrosinase: Comparison With Melan A. Vet Pathol. 2011;48(2):443-50.

216. Busam KJ, Kucukgol D, Sato E, Frosina D, Teruya-Feldstein J, Jungbluth AA. Immunohistochemical analysis of novel monoclonal antibody PNL2 and comparison with other melanocyte differentiation markers. Am J Surg Pathol. 2005;29(3):400-6.
217. Stuart LN, Tipton RG, DeWall MR, Parker DC, Stelton CD, Morrison AO, et al. Primary cutaneous perivascular epithelioid cell tumor (PEComa): Five new cases and review of the literature. J Cutan Pathol. 2017;44(8):713-21.
218. Thway K, Fisher C. PEComa: morphology and genetics of a complex tumor family. Ann Diagn Pathol. 2015;19(5):359-68.
219. Lum SS, Fletcher WS, O'Dorisio MS, Nance RW, Pommier RF, Caprara M. Distribution and functional significance of somatostatin receptors in malignant melanoma. World JSurg. 2001;25(4):407-12.
220. Morris LG, Wen YH, Nonaka D, DeLacure MD, Kutler DI, Huan YM, et al. PNL2 melanocytic marker in immunohistochemical evaluation of primary mucosal melanoma of the head and neck. Head Neck-J Sci Spec Head Neck. 2008;30(6):771-5.
221. Aung PP, Sarlomo-Rikala M, Lasota J, Lai JP, Wang ZF, Miettinen M. KBA62 and PNL2: 2 New Melanoma Markers-Immunohistochemical Analysis of 1563 Tumors Including Metastatic, Desmoplastic, and Mucosal Melanomas and Their Mimics. Am J Surg Pathol. 2012;36(2):265-72.
222. Ordonez NG. Value of melanocytic-associated immunohistochemical markers in the diagnosis of malignant melanoma: a review and update. Hum Pathol. 2014;45(2):191-205.
223. Pitcovski J, Shahar E, Aizenshtein E, Gorodetsky R. Melanoma antigens and related immunological markers. Crit Rev Oncol/Hematol. 2017;115:36-49.
224. Kurotaki T, Tomonari Y, Kanno T, Wako Y, Tsuchitani M. A novel immunohistochemical marker of normal and neoplastic melanocytes in formalin-fixed, paraffin-embedded tissues of albino rats. Vet Pathol. 2008;45(3):383-7.
225. Grossi AB, Hyttel P, Jensen HE, Leifsson PS. Porcine Melanotic Cutaneous Lesions and Lymph Nodes: Immunohistochemical Differentiation of Melanocytes and Melanophages. Vet Pathol. 2015;52(1):83-91.
226. Ramos-Vara JA, Frank CB, DuSold D, Miller MA. Immunohistochemical Expression of Melanocytic Antigen PNL2, Melan A, S100, and PGP 9.5 in Equine Melanocytic Neoplasms. Vet Pathol. 2014;51(1):161-6.
227. Smedley RC, Lamoureux J, Sledge DG, Kiupel M. Immunohistochemical Diagnosis of Canine Oral Amelanotic Melanocytic Neoplasms. Vet Pathol. 2011;48(1):32-40.
228. Wiggans KT, Reilly CM, Kass PH, Maggs DJ. Histologic and immunohistochemical predictors of clinical behavior for feline diffuse iris melanoma. Vet Ophthalmol. 2016;19:44-55.
229. Hirz M, Herden C. Cutaneous amelanotic signet-ring cell malignant melanoma with interspersed myofibroblastic differentiation in a young cat. J Vet Diagn Invest. 2016;28(4):429-35.
230. Epstein B, Jones M, Hamede R, Hendricks S, McCallum H, Murchison EP, et al. Rapid evolutionary response to a transmissible cancer in Tasmanian devils. Nat Commun. 2016;7.
231. Wang ZQ, Yan XY. CD146, a multi-functional molecule beyond adhesion. Cancer Lett. 2013;330(2):150-62.
232. Lei X, Guan C-W, Song Y, Wang H. The multifaceted role of CD146/MCAM in the promotion of melanoma progression. Cancer Cell Int. 2015;15(1):3-.
233. Peterson ER, Murray MR. Myelin Sheath Formation in Cultures of Avian Spinal Ganglia. Am J Anat. 1955;96(3):319-&.
234. Cowell LA, Weston JA. An analysis of melanogenesis in cultured chick embryo spinal ganglia. Dev Biol. 1970;22(4):670-97.
235. Nichols DH, Weston JA. Melanogenesis in Cultures of Peripheral Nevous Tissue 1. Origin and Prospective Fate of Cells Giving Rise to Melanocytes. Dev Biol. 1977;60(1):217-25.
236. Nichols DH, Kaplan RA, Weston JA. Melanogenesis in cultures of peripheral nervous tissue: II. Environmental factors determining the fate of pigment-forming cells. Dev Biol. 1977;60(1):226-37.
237. Ciment G, Glimelius B, Nelson DM, Weston JA. Reversal of a Developmental Restriction in Neural Crest-Derived Cells of Avian Embryos by a Phorbol Ester Drug Dev Biol. 1986;118(2):392-8.

238. Ross AH, Pleasure D, Sonnenfeld K, Atkinson B, Kreider B, Jackson DM, et al. Expression of melanoma-Associated Antigens by Normal and Neurofibroma Schwann Cells Cancer Res. 1986;46(11):5887-92.
239. Bronner-Fraser M, Fraser SE. Cell lineage analysis reveals multipotency of some avian neural crest cells. Nature. 1988;335:161.
240. Bronner-Fraser M, Fraser S. Developmental potential of avian trunk neural crest cells in situ. Neuron. 1989;3(6):755-66.
241. Dupin E, Baroffio A, Dulac C, Cameroncurry P, Ledouarin NM. Schwann Cell Differentiation in Clonal Cultures of the Neural crest, as Evidenced by the Anti-Schwann Cell Myelin protein Monoclonal Antibody Proc Natl Acad Sci U S A. 1990;87(3):1119-23.
242. Ciment G. The melanocyte/Schwann cell progenitor: A bipotent intermediate in the neural crest lineage. London: Gordon and Breach; 1990. 207-23 p.
243. Stocker KM, Sherman L, Rees S, Ciment G. Basic-FGF and TGF-beta-1 Influence Commitment to Melanogenesis in Neural Crest-Derived Cells of Avian Embryos. Development. 1991;111(2):635-45.
244. Sherman L, Stocker KM, Morrison R, Ciment G. Basic Fibroblast Growth Factor (BFGF) Acts Intracellularly to Cause the Transdifferentiation of Avian Neural Crest-Derived Schwann Cell Precursors into Melanocytes Development. 1993;118(4):1313-26.
245. Dupin E, Ledouarin NM. Retinoic Acid Promotes the Differentiation of Adronergic Cells and Melanocytes in Quail Neural Crest Cultures Dev Biol. 1995;168(2):529-48.
246. Dupin E, Glavieux C, Vaigot P, Le Douarin NM. Endothelin 3 induces the reversion of melanocytes to glia through a neural crest-derived glial-melanscytic progenitor. Proc Natl Acad Sci U S A. 2000;97(14):7882-7.
247. Nataf V, Le Douarin NM. Induction of melanogenesis by tetradecanoylphorbol-13 acetate and endothelin 3 in embryonic avian peripheral nerve cultures. Pigm Cell Res. 2000;13(3):172-8.
248. Dupin E, Real C, Glavieux-Pardanaud C, Vaigot P, Le Douarin NM. Reversal of developmental restrictions in neural crest lineages: Transition from Schwann cells to glial-melanocytic precursors in vitro. Proc Natl Acad Sci U S A. 2003;100(9):5229-33.
249. Trentin A, Glavieux-Pardanaud C, Le Douarin NM, Dupin E. Self-renewal capacity is a widespread property of various types of neural crest precursor cells. Proc Natl Acad Sci U S A. 2004;101(13):4495-500.
250. Rizvi TA, Huang Y, Sidani A, Atit R, Largaespada DA, Boissy RE, et al. A novel cytokine pathway suppresses glial cell melanogenesis after injury to adult nerve. J Neurosci. 2002;22(22):9831-40.
251. Motohashi T, Yamanaka K, Chiba K, Aoki H, Kunisada T. Unexpected Multipotency of Melanoblasts Isolated from Murine Skin. Stem Cells. 2009;27(4):888-97.
252. Budi EH, Patterson LB, Parichy DM. Post-Embryonic Nerve-Associated Precursors to Adult Pigment Cells: Genetic Requirements and Dynamics of Morphogenesis and Differentiation. PLoS genetics. 2011;7(5).
253. Dooley CM, Mongera A, Walderich B, Nüsslein-Volhard C. On the embryonic origin of adult melanophores: the role of ErbB and Kit signalling in establishing melanophore stem cells in zebrafish. Development. 2013;140(5):1003-13.
254. Chi GF, Kim DW, Jiang MH, Yoon KJ, Son Y. Schwann-like cells from human melanocytes and their fate in sciatic nerve injury. Neuroreport. 2011;22(12):603-8.
255. Van Raamsdonk CD, Deo M. Links between Schwann cells and melanocytes in development and disease. Pigment Cell Melanoma Res. 2013;26(5):634-45.
256. Schaffer JV, Chang MW, Kovich OI, Kamino H, Orlow SJ. Pigmented plexiform neurofibroma: Distinction from a large congenital melanocytic nevus. J Am Acad Dermatol. 2007;56(5):862-8.
257. Pizem J, Nicholson KM, Mraz J, Prieto VG. Melanocytic Differentiation Is Present in a Significant Proportion of Nonpigmented Diffuse Neurofibromas A Potential Diagnostic Pitfall. Am J Surg Pathol. 2013;37(8):1182-91.
258. Schoniger S, Summers BA. Localized, Plexiform, Diffuse, and Other Variants of Neurofibroma in 12 Dogs, 2 Horses, and a Chicken. Vet Pathol. 2009;46(5):904-15.
259. Rekhi B, Kosemehmetoglu K, Tezel GG, Dervisoglu S. Clinicopathologic features and immunohistochemical spectrum of 11 cases of epithelioid malignant peripheral nerve sheath tumors, including INI1/SMARCB1 results and BRAF V600E analysis. Apmis. 2017;125(8):679-89.

260. Cruz J, Reis JS, Lopes JM. Malignant peripheral nerve sheath tumour-like primary cutaneous malignant melanoma. J Clin Pathol. 2004;57(2):218-20.
261. Banerjee SS, Eyden B. Divergent differentiation in malignant melanomas: a review. Histopathology. 2008;52(2):119-29.
262. Reed JA, Finnerty B, Albino AP. Divergent cellular differentiation pathways during the invasive stage of cutaneous malignant melanoma progression. Am J Pathol. 1999;155(2):549-55.
263. Arthur-Farraj PJ, Latouche M, Wilton DK, Quintes S, Chabrol E, Banerjee A, et al. c-Jun Reprograms Schwann Cells of Injured Nerves to Generate a Repair Cell Essential for Regeneration. Neuron. 2012;75(4):633-47.
264. Jessen KR, Mirsky R, Lloyd AC. Schwann Cells: Development and Role in Nerve Repair. Cold Spring Harbor Perspect Biol. 2015;7(7).
265. Clements MP, Byrne E, Guerrero LFC, Cattin AL, Zakka L, Ashraf A, et al. The Wound Microenvironment Reprograms Schwann Cells to Invasive Mesenchymal-like Cells to Drive Peripheral Nerve Regeneration. Neuron. 2017;96(1):98-+.
266. Jessen KR, Mirsky R. The repair Schwann cell and its function in regenerating nerves. J Physiol-London. 2016;594(13):3521-31.
267. Gomez-Sanchez JA, Pilch KS, van der Lans M, Fazal SV, Benito C, Wagstaff LJ, et al. After Nerve Injury, Lineage Tracing Shows That Myelin and Remak Schwann Cells Elongate Extensively and Branch to Form Repair Schwann Cells, Which Shorten Radically on Remyelination. J Neurosci. 2017;37(37):9086-99.
268. Jessen KR, Mirsky R. Negative Regulation of Myelination: Relevance for Development, Injury, and Demyelinating Disease. Glia. 2008;56(14):1552-65.
269. Triolo D, Dina G, Taveggia C, Vaccari I, Porrello E, Rivellini C, et al. Vimentin regulates peripheral nerve myelination. Development. 2012;139(7):1359-67.
270. Arthur-Farraj PJ, Morgan CC, Adamowicz M, Gomez-Sanchez JA, Fazal SV, Beucher A, et al. Changes in the Coding and Non-coding Transcriptome and DNA Methylome that Define the Schwann Cell Repair Phenotype after Nerve Injury. Cell Reports. 2017;20(11):2719-34.
271. Fontana X, Hristova M, Da Costa C, Patodia S, Thei L, Makwana M, et al. c-Jun in Schwann cells promotes axonal regeneration and motoneuron survival via paracrine signaling. J Cell Biol. 2012;198(1):127-41.
272. Jessen KR, Mirsky R, Arthur-Farraj P. The Role of Cell Plasticity in Tissue Repair: Adaptive Cellular Reprogramming. Dev Cell. 2015;34(6):613-20.
273. Benito C, Davis CM, Gomez-Sanchez JA, Turmaine M, Meijer D, Poli V, et al. STAT3 Controls the Long-Term Survival and Phenotype of Repair Schwann Cells during Nerve Regeneration. J Neurosci. 2017;37(16):4255-69.
274. Roberts SL, Dun X-P, Doddrell RDS, Mindos T, Drake LK, Onaitis MW, et al. Sox2 expression in Schwann cells inhibits myelination in vivo and induces influx of macrophages to the nerve. Development (Cambridge, England). 2017;144(17):3114-25.
275. Carroll SL, Miller ML, Frohnert PW, Kim SS, Corbett JA. Expression of neuregulins and their putative receptors, ErbB2 and ErbB3, is induced during Wallerian degeneration. J Neurosci. 1997;17(5):1642-59.
276. Fricker FR, Bennett DLH. The role of neuregulin-1 in the response to nerve injury. Future neurology. 2011;6(6):809-22.
277. Stassart RM, Fledrich R, Velanac V, Brinkmann BG, Schwab MH, Meijer D, et al. A role for Schwann cell-derived neuregulin-1 in remyelination. Nat Neurosci. 2013;16(1):48-U76.
278. Eshed-Eisenbach Y, Gordon A, Sukhanov N, Peles E. Specific Inhibition of Secreted NRG1 Types I-II by Heparin Enhances Schwann Cell Myelination. Glia. 2016;64(7):1227-34.
279. Ronchi G, Haastert-Talini K, Fornasari BE, Perroteau I, Geuna S, Gambarotta G. The Neuregulin1/ErbB system is selectively regulated during peripheral nerve degeneration and regeneration. Eur J Neurosci. 2016;43(3):351-64.
280. Audisio C, Nicolino S, Scevola A, Tos P, Geuna S, Battiston B, et al. ErbB receptors modulation in different types of peripheral nerve regeneration. Neuroreport. 2008;19(16):1605-9.

281. Stonecypher MS, Byer SJ, Grizzle WE, Carroll SL. Activation of the neuregulin-1/ErbB signaling pathway promotes the proliferation of neoplastic Schwann cells in human malignant peripheral nerve sheath tumors. Oncogene. 2005;24(36):5589-605.
282. Ma KH, Hung HA, Svaren J. Epigenomic Regulation of Schwann Cell Reprogramming in Peripheral Nerve Injury. J Neurosci. 2016;36(35):9135-47.
283. Martinez JA, Kobayashi M, Krishnan A, Webber C, Christie K, Guo G, et al. Intrinsic facilitation of adult peripheral nerve regeneration by the Sonic hedgehog morphogen. Exp Neurol. 2015;271:493-505.
284. Hashimoto M, Ishii K, Nakamura Y, Watabe K, Kohsaka S, Akazawa C. Neuroprotective effect of sonic hedgehog up-regulated in Schwann cells following sciatic nerve injury. J Neurochem. 2008;107(4):918-27.
285. Sondell M, Lundborg G, Kanje M. Vascular endothelial growth factor has neurotrophic activity and stimulates axonal outgrowth, enhancing cell survival and Schwann cell proliferation in the peripheral nervous system. J Neurosci. 1999;19(14):5731-40.
286. Gupta R, Gray M, Chao T, Bear D, Modafferi E, Mozaffar T. Schwann cells upregulate vascular endothelial growth factor secondary to chronic nerve compression injury. Muscle & Nerve. 2005;31(4):452-60.
287. Neuberger TJ, Cornbrooks CJ. Transient Modulation of Schwann Cell Antigens after Peripheral Nerve Transection and Subsequent regeneration J Neurocytol. 1989;18(5):695-710.
288. Kelly BM, Gillespie CS, Sherman DL, Brophy PJ. Schwann Cells of the Myelin Forming Phenotype Express Neurofilament protein NF-M. J Cell Biol. 1992;118(2):397-410.
289. Fabrizi C, Kelly BM, Gillespie CS, Schlaepfer WW, Scherer SS, Brophy PJ. Transient expression of the neurofilament proteins NF-L and NF-M by Schwann cells is regulated by axonal contact. J Neurosci Res. 1997;50(2):291-9.
290. Ribeiro S, Napoli I, White IJ, Parrinello S, Flanagan AM, Suter U, et al. Injury Signals Cooperate with Nf1 Loss to Relieve the Tumor-Suppressive Environment of Adult Peripheral Nerve. Cell Reports. 2013;5(1):126-36.
291. Stewart HJS, Rougon G, Dong ZP, Dean C, Jessen KR, Mirsky R. TGF-beta s upregulate NCAM and L1 expression in cultured Schwann cells, suppress cyclic AMP-induced expression of O4 and galactocerebroside, and are widely expressed in cells of the Schwann cell lineage in vivo. Glia. 1995;15(4):419-36.
292. Guenard V, Gwynn LA, Wood PM. Transforming Growth factor-beta Blocks Myelination but not Ensheathment of Axons by Schwann Cells In-Vitro J Neurosci. 1995;15(1):419-28.
293. Einheber S, Hannocks MJ, Metz CN, Rifkin DB, Salzer JL. Transforming Growth factor-beta-1 regulates Axon-Schwann Cell Interactions J Cell Biol. 1995;129(2):443-58.
294. Hagedorn L, Suter U, Sommer L. P0 and PMP22 mark a multipotent neural crest-derived cell type that displays community effects in response to TGF-beta family factors. Development. 1999;126(17):3781-94.
295. Parkinson DB, Dong Z, Bunting H, Whitfield J, Meier C, Marie H, et al. Transforming Growth Factor β (TGFβ) Mediates Schwann Cell Death In Vitro and In Vivo: Examination of c-Jun Activation, Interactions with Survival Signals, and the Relationship of TGFβ-Mediated Death to Schwann Cell Differentiation. The Journal of Neuroscience. 2001;21(21):8572-85.
296. Parkinson DB, Bhaskaran A, Droggiti A, Dickinson S, D'Antonio M, Mirsky R, et al. Krox-20 inhibits Jun-NH(2)-terminal kinase/c-Jun to control Schwann cell proliferation and death. J Cell Biol. 2004;164(3):385-94.
297. D'Antonio M, Droggiti A, Feltri ML, Roes J, Wrabetz L, Mirsky R, et al. TGF beta type II receptor signaling controls Schwann cell death and proliferation in developing nerves. J Neurosci. 2006;26(33):8417-27.
298. Friedmann-Morvinski D, Verma IM. Dedifferentiation and reprogramming: origins of cancer stem cells. EMBO Rep. 2014;15(3):244-53.
299. Deborde S, Wong RJ. How Schwann cells facilitate cancer progression in nerves. Cell Mol Life Sci. 2017;74(24):4405-20.

300. Dyachuk V, Furlan A, Shahidi MK, Giovenco M, Kaukua N, Konstantinidou C, et al. Parasympathetic neurons originate from nerve-associated peripheral glial progenitors. Science. 2014;345(6192):82-7.
301. Espinosa-Medina I, Outin E, Picard CA, Chettouh Z, Dymecki S, Consalez GG, et al. Parasympathetic ganglia derive from Schwann cell precursors. Science. 2014;345(6192):87-90.
302. Uesaka T, Nagashimada M, Enomoto H. Neuronal Differentiation in Schwann Cell Lineage Underlies Postnatal Neurogenesis in the Enteric Nervous System. J Neurosci. 2015;35(27):9879-88.
303. Espinosa-Medina I, Jevans B, Boismoreau F, Chettouh Z, Enomoto H, Muller T, et al. Dual origin of enteric neurons in vagal Schwann cell precursors and the sympathetic neural crest. Proc Natl Acad Sci U S A. 2017;114(45):11980-5.
304. Kaukua N, Shahidi MK, Konstantinidou C, Dyachuk V, Kaucka M, Furlan A, et al. Glial origin of mesenchymal stem cells in a tooth model system. Nature. 2014;513(7519):551-4.
305. Furlan A, Dyachuk V, Kastriti ME, Calvo-Enrique L, Abdo H, Hadjab S, et al. Multipotent peripheral glial cells generate neuroendocrine cells of the adrenal medulla. Science. 2017;357(6346).
306. Le Douarin NM, Creuzet S, Couly G, Dupin E. Neural crest cell plasticity and its limits. Development. 2004;131(19):4637-50.
307. Stemple DL, Anderson DJ. Isolation of a stem-cell for neurons and glia from the mammalian neural crest. Cell. 1992;71(6):973-85.
308. Morrison SJ, White PM, Zock C, Anderson DJ. Prospective identification, isolation by flow cytometry, and in vivo self-renewal of multipotent mammalian neural crest stem cells. Cell. 1999;96(5):737-49.
309. White PM, Morrison SJ, Orimoto K, Kubu CJ, Verdi JM, Anderson DJ. Neural crest stem cells undergo cell-intrinsic developmental changes in sensitivity to instructive differentiation signals. Neuron. 2001;29(1):57-71.
310. Kruger GM, Mosher JT, Bixby S, Joseph N, Iwashita T, Morrison SJ. Neural crest stem cells persist in the adult gut but undergo changes in self-renewal, neuronal subtype potential, and factor responsiveness. Neuron. 2002;35(4):657-69.
311. Bixby S, Kruger GM, Mosher JT, Joseph NM, Morrison SJ. Cell-intrinsic differences between stem cells from different regions of the peripheral nervous system regulate the generation of neural diversity. Neuron. 2002;35(4):643-56.
312. Real C, Glavieux-Pardanaud C, Vaigot P, Le Douarin N, Dupin E. The instability of the neural crest phenotypes: Schwann cells can differentiate into myofibroblasts. Int J Dev Biol. 2005;49(2-3):151-9.
313. Real C, Glavieux-Pardanaud C, Le Douarin NM, Dupin E. Clonally cultured differentiated pigment cells can dedifferentiate and generate multipotent progenitors with self-renewing potential. Dev Biol. 2006;300(2):656-69.
314. Motohashi T, Aoki H, Chiba K, Yoshimura N, Kunisada T. Multipotent cell fate of neural crest-like cells derived from embryonic stem cells. Stem Cells. 2007;25(2):402-10.
315. Motohashi T, Yamanaka K, Chiba K, Miyajima K, Aoki H, Hirobe T, et al. Neural Crest Cells Retain Their Capability for Multipotential Differentiation Even After Lineage-Restricted Stages. Dev Dyn. 2011;240(7):1681-93.
316. Motohashi T, Kitagawa D, Watanabe N, Wakaoka T, Kunisada T. Neural Crest-Derived Cells Sustain Their Multipotency Even After Entry Into Their Target Tissues. Dev Dyn. 2014;243(3):368-80.
317. Hirata T, Morii E, Morimoto M, Kasugai T, Tsujimura T, Hirota S, et al. Stem cell factor induces outgrowth of c-kit-positive neurites and supports the survival of c-kit-positive neurons in dorsal root ganglia of mouse embryos. Development. 1993;119(1):49-56.
318. Baggiolini A, Varum S, Mateos JM, Bettosini D, John N, Bonalli M, et al. Premigratory and Migratory Neural Crest Cells Are Multipotent In Vivo. Cell Stem Cell. 2015;16(3):314-22.
319. Zabierowski SE, Baubet V, Himes B, Li L, Fukunaga-Kalabis M, Patel S, et al. Direct reprogramming of melanocytes to neural crest stem-like cells by one defined factor. Stem cells (Dayton, Ohio). 2011;29(11):1752-62.
320. Calloni GW, Glavieux-Pardanaud C, Le Douarin NM, Dupin E. Sonic Hedgehog promotes the development of multipotent neural crest progenitors endowed with both mesenchymal and neural potentials. Proc Natl Acad Sci U S A. 2007;104(50):19879-84.

321. Calloni GW, Le Douarin NM, Dupin E. High frequency of cephalic neural crest cells shows coexistence of neurogenic, melanogenic, and osteogenic differentiation capacities. Proc Natl Acad Sci U S A. 2009;106(22):8947-52.
322. Dupin E, Calloni GW, Le Douarin NM. The cephalic neural crest of amniote vertebrates is composed of a large majority of precursors endowed with neural, melanocytic, chondrogenic and osteogenic potentialities. Cell Cycle. 2010;9(2):238-49.
323. Merchant A, Matsui W. Targeting Hedgehog - a Cancer Stem Cell Pathway. Clin Cancer Res. 2010;16(12):3130-40.
324. Milla LA, Gonzalez-Ramirez CN, Palma V. Sonic Hedgehog in cancer stem cells: a novel link with autophagy. Biol Res. 2012;45(3):223-30.
325. Cochrane CR, Szczepny A, Watkins DN, Cain JE. Hedgehog Signaling in the Maintenance of Cancer Stem Cells. Cancers. 2015;7(3):1554-85.
326. Hanna A, Shevde LA. Hedgehog signaling: modulation of cancer properies and tumor mircroenvironment. Mol Cancer. 2016;15.
327. Carballo GB, Honorato JR, de Lopes GPF, Spohr T. A highlight on Sonic hedgehog pathway. Cell Commun Signal. 2018;16.
328. Gires O, Stoecklein NH. Dynamic EpCAM expression on circulating and disseminating tumor cells: causes and consequences. Cell Mol Life Sci. 2014;71(22):4393-402.
329. Dolle L, Theise ND, Schmelzer E, Boulter L, Gires O, van Grunsven LA. EpCAM and the biology of hepatic stem/progenitor cells. Am J Physiol-Gastroint Liver Physiol. 2015;308(4):G233-G50.
330. Khan MS, Tsigani T, Rashid M, Rabouhans JS, Yu D, Tu VL, et al. Circulating Tumor Cells and EpCAM Expression in Neuroendocrine Tumors. Clin Cancer Res. 2011;17(2):337-45.
331. Schnell U, Cirulli V, Giepmans BNG. EpCAM: Structure and function in health and disease. Biochim Biophys Acta-Biomembr. 2013;1828(8):1989-2001.
332. Ng VY, Ang SN, Chan JX, Choo ABH. Characterization of Epithelial Cell Adhesion Molecule as a Surface Marker on Undifferentiated Human Embryonic Stem Cells. Stem Cells. 2010;28(1):29-35.
333. Gonzalez B, Denzel S, Mack B, Conrad M, Gires O. EpCAM Is Involved in Maintenance of the Murine Embryonic Stem Cell Phenotype. Stem Cells. 2009;27(8):1782-91.
334. Kuan II, Liang K-H, Wang Y-P, Kuo T-W, Meir Y-JJ, Wu SC-Y, et al. EpEX/EpCAM and Oct4 or Klf4 alone are sufficient to generate induced pluripotent stem cells through STAT3 and HIF2α. Sci Rep. 2017;7:41852.
335. Malaguarnera R, Belfiore A. The emerging role of insulin and insulin-like growth factor signaling in cancer stem cells. Front Endocrinol. 2014;5.
336. Niwa H, Burdon T, Chambers I, Smith A. Self-renewal of pluripotent embryonic stem cells is mediated via activation of STAT3. Genes Dev. 1998;12(13):2048-60.
337. Matsuda T, Nakamura T, Nakao K, Arai T, Katsuki M, Heike T, et al. STAT3 activation is sufficient to maintain an undifferentiated state of mouse embryonic stem cells. EMBO J. 1999;18(15):4261-9.
338. Galoczova M, Coates P, Vojtesek B. STAT3, stem cells, cancer stem cells and p63. Cell Mol Biol Lett. 2018;23:12.
339. Foshay KM, Gallicano GI. Regulation of Sox2 by STAT3 initiates commitment to the neural precursor cell fate. Stem Cells Dev. 2008;17(2):269-78.
340. Kim WT, Ryu CJ. Cancer stem cell surface markers on normal stem cells. BMB Rep. 2017;50(6):285-98.
341. Gorlewicz A, Wlodarczyk J, Wilczek E, Gawlak M, Cabaj A, Majczynski H, et al. CD44 is expressed in non-myelinating Schwann cells of the adult rat, and may play a role in neurodegeneration-induced glial plasticity at the neuromuscular junction. Neurobiol Dis. 2009;34(2):245-58.
342. Sherman L, Jacoby LB, Lampe J, Pelton P, Aguzzi A, Herrlich P, et al. CD44 expression is aberrant in benign Schwann cell tumors possessing mutations in the neurofibromatosis type 2, but not type 1, gene. Cancer Res. 1997;57(21):4889-97.
343. Chen C, Zhao SJ, Karnad A, Freeman JW. The biology and role of CD44 in cancer progression: therapeutic implications. J Hematol Oncol. 2018;11.
344. Ponta H, Sherman L, Herrlich PA. CD44: From adhesion molecules to signalling regulators. Nat Rev Mol Cell Biol. 2003;4(1):33-45.

345. Schmechel D, Marangos PJ, Brightman M. Neurone-specific enolase is a molecular marker for peripheral and central neuroendocrine cells. Nature. 1978;276:834.
346. Kirino T, Brightman M, Oertel W, Schmechel D, Marangos P. Neuron-specific enolase as an index of neuronal regeneration and reinnervation. J Neurosci. 1983;3(5):915-23.
347. Tischler AS, deKrijger RR. Pathology of pheochromocytoma and paraganglioma. Endocr-Relat Cancer. 2015;22(4):T123-T33.
348. Kakkar A, Kaur K, Kumar T, Cherian LB, Kaushal R, Sharma MC, et al. Pigmented Pheochromocytoma: an Unusual Variant of a Common Tumor. Endocr Pathol. 2016;27(1):42-5.
349. Zhao L, Luo J, Zhang HL, Da JP. Pigmented paraganglioma of the kidney: a case report. Diagn Pathol. 2012;7.
350. Bellezza G, Giansanti M, Cavaliere A, Sidoni A. Pigmented "Black" Pheochromocytoma of the Adrenal Gland: A Case Report and Review of the Literature. Arch Pathol Lab Med. 2004;128(10):e125-e8.
351. Maison N, Korpershoek E, Eisenhofer G, Robledo M, de Krijger R, Beuschlein F. Somatic RET mutation in a patient with pigmented adrenal pheochromocytoma. Endocrinol Diabetes & Metab Case Rep. 2016;2016:150117.
352. Chetty R, Clark SP, Taylor DA. Pigmented Pheochromocytomas of the Adrenal Medulla Hum Pathol. 1993;24(4):420-3.
353. Unger PD, Hoffman K, Thung SN, Pertsemlides D, Wolfe D, Kaneko M. HMB-45 Reactivity in Adrenal Pheochromocytomas Arch Pathol Lab Med. 1992;116(2):151-3.
354. Mjones P, Sagatun L, Nordrum IS, Waldum HL. Neuron-Specific Enolase as an Immunohistochemical Marker Is Better Than Its Reputation. J Histochem Cytochem. 2017;65(12):687-703.
355. Campbell LK, Thomas JR, Lamps LW, Smoller BR, Folpe AL. Protein gene product 9.5 (PGP 9.5) is not a specific marker of neural and nerve sheath tumors: An immunohistochemical study of 95 mesenchymal neoplasms. Mod Pathol. 2003;16(10):963-9.
356. Sakurai M, Ayukawa K, Setsuie R, Nishikawa K, Hara Y, Ohashi H, et al. Ubiquitin C-terminal hydrolase L1 regulates the morphology of neural progenitor cells and modulates their differentiation. J Cell Sci. 2006;119(1):162-71.
357. Friedrich R, Holstein A, Middendorff R, Davidoff M. Vascular Wall Cells Contribute to Tumourigenesis in Cutaneous Neurofibromas of Patients with Neurofibromatosis Type 1. A Comparative Histological, Ultrastructural and Immunohistochemical Study. Anticancer Res. 2012;32(5):2139-58.
358. Sidebotham EL, Woodward MN, Kenny SE, Lloyd DA, Vaillant CR, Edgar DH. Assessment of protein gene product 9.5 as a marker of neural crest-derived precursor cells in the developing enteric nervous system. Pediatr Surg Int. 2001;17(4):304-7.
359. Fang Y, Shen XZ. Ubiquitin carboxyl-terminal hydrolases: involvement in cancer progression and clinical implications. Cancer Metastasis Rev. 2017;36(4):669-82.
360. Park JY, Park H, Park NJ, Park JS, Sung HJ, Lee SS. Use of Calretinin, CD56, and CD34 for Differential Diagnosis of Schwannoma and Neurofibroma. Korean J Pathol. 2011;45(1):30-5.
361. Fine SW, McClain SA, Li M. Immunohistochemical Staining for Calretinin Is Useful for Differentiating Schwannomas From Neurofibromas. Am J Clin Pathol. 2004;122(4):552-9.
362. Islam F, Gopalan V, Smith RA, Lam AKY. Translational potential of cancer stem cells: A review of the detection of cancer stem cells and their roles in cancer recurrence and cancer treatment. Exp Cell Res. 2015;335(1):135-47.
363. Singh AK, Arya RK, Maheshwari S, Singh A, Meena S, Pandey P, et al. Tumor heterogeneity and cancer stem cell paradigm: Updates in concept, controversies and clinical relevance. International Journal of Cancer. 2015;136(9):1991-2000.
364. de Souza VB, Schenka AA. Cancer Stem and Progenitor-Like Cells as Pharmacological Targets in Breast Cancer Treatment. Breast Cancer : Basic and Clinical Research. 2015;9(Suppl 2):45-55.
365. Silva LB, Neto APDS, Pacheco RGP, Júnior SA, de Menezes RF, Carneiro VSM, et al. The Promising Applications of Stem Cells in the Oral Region: Literature Review. Open Dent J. 2016;10:227-35.
366. Kaltschmidt B, Kaltschmidt C, Widera D. Adult Craniofacial Stem Cells: Sources and Relation to the Neural Crest. Stem Cell Rev. 2012;8(3):658-71.

367. Mii S, Amoh Y, Katsuoka K, Hoffman RM. Comparison of Nestin-Expressing Multipotent Stem Cells in the Tongue Fungiform Papilla and Vibrissa Hair Follicle. J Cell Biochem. 2014;115(6):1070-6.
368. Davies LC, Locke M, Webb RDJ, Roberts JT, Langley M, Thomas DW, et al. A Multipotent Neural Crest-Derived Progenitor Cell Population Is Resident Within the Oral Mucosa Lamina Propria. Stem Cells Dev. 2010;19(6):819-30.
369. Widera D, Heimann P, Zander C, Imielski Y, Heidbreder M, Heilemann M, et al. Schwann Cells Can Be Reprogrammed to Multipotency by Culture. Stem Cells Dev. 2011;20(12):2053-64.
370. Widera D, Zander C, Heidbreder M, Kasperek Y, Noll T, Seitz O, et al. Adult Palatum as a Novel Source of Neural Crest-Related Stem Cells. Stem Cells. 2009;27(8):1899-910.
371. Park D, Xiang AP, Mao FF, Zhang L, Di CG, Liu XM, et al. Nestin Is Required for the Proper Self-Renewal of Neural Stem Cells. Stem Cells. 2010;28(12):2162-71.
372. Gronthos S, Brahim J, Li W, Fisher LW, Cherman N, Boyde A, et al. Stem cell properties of human dental pulp stem cells. J Dent Res. 2002;81(8):531-5.
373. Stevens A, Zuliani T, Olejnik C, Leroy H, Obriot H, Kerr-Conte J, et al. Human Dental Pulp Stem Cells Differentiate into Neural Crest-Derived Melanocytes and Have Label-Retaining and Sphere-Forming Abilities. Stem Cells Dev. 2008;17(6):1175-84.
374. Al-Zer H, Apel C, Heiland M, Friedrich RE, Jung O, Kroeger N, et al. Enrichment and Schwann Cell Differentiation of Neural Crest-derived Dental Pulp Stem Cells. In Vivo. 2015;29(3):319-26.
375. Fernandes KJL, Toma JG, Miller FD. Multipotent skin-derived precursors: adult neural crest-related precursors with therapeutic potential. Philos Trans R Soc B-Biol Sci. 2008;363(1489):185-98.
376. Sieber-Blum M, Hu YF. Epidermal Neural Crest Stem Cells (EPI-NCSC) and Pluripotency. Stem Cell Rev. 2008;4(4):256-60.
377. Amoh Y, Hoffman RM. Hair follicle-associated-pluripotent (HAP) stem cells. Cell Cycle. 2017;16(22):2169-75.
378. Mignone JL, Roig-Lopez JL, Fedtsova N, Schones DE, Manganas LN, Maletic-Savatic M, et al. Neural potential of a stem cell population in the hair follicle. Cell Cycle. 2007;6(17):2161-70.
379. Ma MS, Czepiel M, Krause T, Schafer KH, Boddeke E, Copray S. Generation of Induced Pluripotent Stem Cells from Hair Follicle Bulge Neural Crest Stem Cells. Cell Reprogramm. 2014;16(5):307-13.
380. Toma JG, Akhavan M, Fernandes KJL, Barnabe-Heider F, Sadikot A, Kaplan DR, et al. Isolation of multipotent adult stem cells from the dermis of mammalian skin. Nat Cell Biol. 2001;3(9):778-84.
381. Fernandes KJL, McKenzie IA, Mill P, Smith KM, Akhavan M, Barnabe-Heider F, et al. A dermal niche for multipotent adult skin-derived precursor cells. Nat Cell Biol. 2004;6(11):1082-U16.
382. Toma JG, McKenzie IA, Bagli D, Miller FD. Isolation and characterization of multipotent skin-derived precursors from human skin. Stem Cells. 2005;23(6):727-37.
383. Hunt DPJ, Morris PN, Sterling J, Anderson JA, Joannides A, Jahoda C, et al. A highly enriched niche of precursor cells with neuronal and glial potential within the hair follicle dermal papilla of adult skin. Stem Cells. 2008;26(1):163-72.
384. Biernaskie J, Paris M, Morozova O, Fagan BM, Marra M, Pevny L, et al. SKPs Derive from Hair Follicle Precursors and Exhibit Properties of Adult Dermal Stem Cells. Cell Stem Cell. 2009;5(6):610-23.
385. Sieber-Blum M, Grim M, Hu YF, Szeder V. Pluripotent neural crest stem cells in the adult hair follicle. Dev Dyn. 2004;231(2):258-69.
386. Clewes O, Narytnyk A, Gillinder KR, Loughney AD, Murdoch AP, Sieber-Blum M. Human Epidermal Neural Crest Stem Cells (hEPI-NCSC)—Characterization and Directed Differentiation into Osteocytes and Melanocytes. Stem Cell Reviews and Reports. 2011;7(4):799-814.
387. Sakaue M, Sieber-Blum M. Human epidermal neural crest stem cells as a source of Schwann cells. Development. 2015;142(18):3188-97.
388. Amoh Y, Li L, Katsuoka K, Penman S, Hoffman RM. Multipotent nestin-positive, keratin-negative hair-follicle bulge stem cells can form neurons. Proc Natl Acad Sci U S A. 2005;102(15):5530-4.
389. Amoh Y, Li LN, Campillo R, Kawahara K, Katsuoka K, Penman S, et al. Implanted hair follicle stem cells form Schwann cells that support repair of severed peripheral nerves. Proc Natl Acad Sci U S A. 2005;102(49):17734-8.

390. Liu F, Uchugonova A, Kimura H, Zhang CS, Zhao M, Zhang L, et al. The bulge area is the major hair follicle source of nestin-expressing pluripotent stem cells which can repair the spinal cord compared to the dermal papilla. Cell Cycle. 2011;10(5):830-9.
391. Uchugonova A, Duong J, Zhang N, Konig K, Hoffman RM. The Bulge Area Is the Origin of Nestin-Expressing Pluripotent Stem Cells of the Hair Follicle. J Cell Biochem. 2011;112(8):2046-50.
392. Yu H, Fang D, Kumar SM, Li L, Nguyen TK, Acs G, et al. Isolation of a Novel Population of Multipotent Adult Stem Cells from Human Hair Follicles. The American Journal of Pathology. 2006;168(6):1879-88.
393. Yu H, Kumar SM, Kossenkov AV, Showe L, Xu XW. Stem Cells with Neural Crest Characteristics Derived from the Bulge Region of Cultured Human Hair Follicles. J Invest Dermatol. 2010;130(5):1227-36.
394. Driskell RR, Giangreco A, Jensen KB, Mulder KW, Watt FM. Sox2-positive dermal papilla cells specify hair follicle type in mammalian epidermis. Development. 2009;136(16):2815-23.
395. Wong CE, Paratore C, Dours-Zimmermann MT, Rochat A, Pietri T, Suter U, et al. Neural crest-derived cells with stem cell features can be traced back to multiple lineages in the adult skin. J Cell Biol. 2006;175(6):1005-15.
396. Marynka-Kalmani K, Treves S, Yafee M, Rachima H, Gafni Y, Cohen MA, et al. The Lamina Propria of Adult Human Oral Mucosa Harbors a Novel Stem Cell Population. Stem Cells. 2010;28(5):984-95.
397. Abe S, Yamaguchi S, Sato Y, Harada K. Sphere-Derived Multipotent Progenitor Cells Obtained From Human Oral Mucosa Are Enriched in Neural Crest Cells. Stem Cells Transl Med. 2016;5(1):117-28.
398. O'Neill ID. Concise Review: Transmissible Animal Tumors as Models of the Cancer Stem-Cell Process. Stem Cells. 2011;29(12):1909-14.
399. Ujvari B, Piddington L, Pearse A-M, Peck S, Harmsen C, Taylor R, et al. Devil Facial Tumor Disease, A Potential Model of the Cancer Stem-Cell Process? JVet. 2015;1(1):6.
400. van Niekerk G, Davids LM, Hattingh SM, Engelbrecht AM. Cancer stem cells: A product of clonal evolution? Int J Cancer. 2017;140(5):993-9.
401. Rich JN. Cancer stem cells: understanding tumor hierarchy and heterogeneity. Medicine. 2016;95.
402. Cabrera MC, Hollingsworth RE, Hurt EM. Cancer stem cell plasticity and tumor hierarchy. World J Stem Cells. 2015;7(1):27-36.
403. Plaks V, Kong NW, Werb Z. The Cancer Stem Cell Niche: How Essential Is the Niche in Regulating Stemness of Tumor Cells? Cell Stem Cell. 2015;16(3):225-38.
404. Morrison SJ, Kimble J. Asymmetric and symmetric stem-cell divisions in development and cancer. Nature. 2006;441(7097):1068-74.
405. Shackleton M, Quintana E, Fearon ER, Morrison SJ. Heterogeneity in Cancer: Cancer Stem Cells versus Clonal Evolution. Cell. 2009;138(5):822-9.
406. Fulawka L, Donizy P, Halon A. Cancer stem cells - the current status of an old concept: literature review and clinical approaches. Biol Res. 2014;47.
407. Greaves M, Maley CC. Clonal evolution in cancer. Nature. 2012;481(7381):306-13.
408. Yu ZK, Geyer RK, Maki CG. MDM2-dependent ubiquitination of nuclear and cytoplasmic P53. Oncogene. 2000;19(51):5892-7.
409. O'Keefe K, Li HP, Zhang YP. Nucleocytoplasmic shuttling of p53 is essential for MDM2-mediated cytoplasmic degradation but not ubiquitination. Mol Cell Biol. 2003;23(18):6396-405.
410. Codony-Servat J, Rosell R. Cancer stem cells and immunoresistance: clinical implications and solutions. Transl Lung Cancer Res. 2015;4(6):689-703.
411. Woods GM, Howson LJ, Brown GK, Tovar C, Kreiss A, Corcoran LM, et al. Immunology of a Transmissible Cancer Spreading among Tasmanian Devils. J Immunol. 2015;195(1):23-9.
412. Deakin JE. Marsupial Genome Sequences: Providing Insight into Evolution and Disease. Scientifica. 2012;2012:543176.
413. Deakin JE, Belov K. A Comparative Genomics Approach to Understanding Transmissible Cancer in Tasmanian Devils. In Annual Review of Genomics and Human Genetics. Editors Chakravarti, A. Green, E. Palo Alto: Annual Reviews; 2012. p. 207-22.
414. Schlessinger J. Cell signaling by receptor tyrosine kinases. Cell. 2000;103(2):211-25.
415. Blume-Jensen P, Hunter T. Oncogenic kinase signalling. Nature. 2001;411(6835):355-65.

416. Lemmon MA, Schlessinger J. Cell Signaling by Receptor Tyrosine Kinases. Cell. 2010;141(7):1117-34.
417. Pawson T, Nash P. Assembly of cell regulatory systems through protein interaction domains. Science. 2003;300(5618):445-52.
418. Volinsky N, Kholodenko BN. Complexity of Receptor Tyrosine Kinase Signal Processing. Cold Spring Harbor Perspect Biol. 2013;5(8).
419. Delos Santos RC, Garay C, Antonescu CN. Charming neighborhoods on the cell surface: Plasma membrane microdomains regulate receptor tyrosine kinase signaling. Cell Signal. 2015;27(10):1963-76.
420. Sithanandam G, Anderson LM. The ERBB3 receptor in cancer and cancer gene therapy. Cancer Gene Ther. 2008;15(7):413-48.
421. Hsieh AC, Moasser MM. Targeting HER proteins in cancer therapy and the role of the non-target HER3. Br J Cancer. 2007;97(4):453-7.
422. Roskoski R. The ErbB/HER family of protein-tyrosine kinases and cancer. Pharmacol Res. 2014;79:34-74.
423. Carrasco-Garcia E, Saceda M, Martinez-Lacaci I. Role of receptor tyrosine kinases and their ligands in glioblastoma. Cells. 2014;3(2):199-235.
424. Burgess AW, Cho HS, Eigenbrot C, Ferguson KM, Garrett TPJ, Leahy DJ, et al. An open-and-shut case? Recent insights into the activation of EGF/ErbB receptors. Mol Cell. 2003;12(3):541-52.
425. Lemmon MA. Ligand-induced ErbB receptor dimerization. Exp Cell Res. 2009;315(4):638-48.
426. Wilson KJ, Gilmore JL, Foley J, Lemmon MA, Riese DJ. Functional selectivity of EGF family peptide growth factors: Implications for cancer. Pharmacol Ther. 2009;122(1):1-8.
427. Falls DL. Neuregulins: functions, forms, and signaling strategies. Exp Cell Res. 2003;284(1):14-30.
428. Montero JC, Rodriguez-Barrueco R, Ocana A, Diaz-Rodriguez E, Esparis-Ogando A, Pandiella A. Neuregulins and cancer. Clin Cancer Res. 2008;14(11):3237-41.
429. Mei L, Nave KA. Neuregulin-ERBB Signaling in the Nervous System and Neuropsychiatric Diseases. Neuron. 2014;83(1):27-49.
430. Carraway KL, Kozloski GA. Conformational changes in receptor tyrosine kinase signaling: an ErbB garden of delights. F1000 biology reports. 2009;1:72.
431. Olayioye MA, Neve RM, Lane HA, Hynes NE. The ErbB signaling network: receptor heterodimerization in development and cancer. Embo J. 2000;19(13):3159-67.
432. Yarden Y, Sliwkowski MX. Untangling the ErbB signalling network. Nat Rev Mol Cell Biol. 2001;2(2):127-37.
433. Citri A, Yarden Y. EGF-ERBB signalling: towards the systems level. Nat Rev Mol Cell Biol. 2006;7(7):505-16.
434. Warren CM, Landgraf R. Signaling through ERBB receptors: Multiple layers of diversity and control. Cell Signal. 2006;18(7):923-33.
435. Li YW, Tennekoon GI, Birnbaum M, Marchionni MA, Rutkowski JL. Neuregulin signaling through a PI3K/Akt/Bad pathway in Schwann cell survival. Mol Cell Neurosci. 2001;17(4):761-7.
436. Guy PM, Platko JV, Cantley LC, Cerione RA, Carraway KL. Insect cell-expressed P180(ERBB3) possesses an impaired tyrosine kinase-activity Proc Natl Acad Sci U S A. 1994;91(17):8132-6.
437. Klapper LN, Glathe S, Vaisman N, Hynes NE, Andrews GC, Sela M, et al. The ErbB-2/HER2 oncoprotein of human carcinomas may function solely as a shared coreceptor for multiple stroma-derived growth factors. Proc Natl Acad Sci U S A. 1999;96(9):4995-5000.
438. Shi FM, Telesco SE, Liu YT, Radhakrishnan R, Lemmon MA. ErbB3/HER3 intracellular domain is competent to bind ATP and catalyze autophosphorylation. Proc Natl Acad Sci U S A. 2010;107(17):7692-7.
439. Kraus MH, Issing W, Miki T, Popescu NC, Aaronson SA. Isolation and characterization of ERBB3, a 3rd member of the ERBB/epidemal growth factor receptor family: Evidence for overexpression in a subset of human mammary tumours. Proc Natl Acad Sci U S A. 1989;86(23):9193-7.
440. Plowman GD, Whitney GS, Neubauer MG, Green JM, McDonald VL, Todaro GJ, et al. Molecular Cloning and Expression of an Additional Epidermal Growth Factor Receptor Related Gene Proc Natl Acad Sci U S A. 1990;87(13):4905-9.
441. Carraway KL, Sliwkowski MX, Akita R, Platko JV, Guy PM, Nuijens A, et al. The ERBB3 Gene Product is a Receptor for Heregulin J Biol Chem. 1994;269(19):14303-6.

442. Tzahar E, Waterman H, Chen XM, Levkowitz G, Karunagaran D, Lavi S, et al. A hierarchical network of interreceptor interactions determines signal transduction by neu differentiation factor/neuregulin and epidermal growth factor. Mol Cell Biol. 1996;16(10):5276-87.
443. Lemmon MA, Schlessinger J, Ferguson KM. The EGFR Family: Not So Prototypical Receptor Tyrosine Kinases. Cold Spring Harbor Perspect Biol. 2014;6(4).
444. Zhang XW, Gureasko J, Shen K, Cole PA, Kuriyan J. An allosteric mechanism for activation of the kinase domain of epidermal growth factor receptor. Cell. 2006;125(6):1137-49.
445. Monsey J, Shen W, Schlesinger P, Bose R. Her4 and Her2/neu Tyrosine Kinase Domains Dimerize and Activate in a Reconstituted in Vitro System. J Biol Chem. 2010;285(10):7035-44.
446. Littlefield P, Moasser MM, Jura N. An ATP-Competitive Inhibitor Modulates the Allosteric Function of the HER3 Pseudokinase. Chem Biol. 2014;21(4):453-8.
447. Jura N, Shan YB, Cao XX, Shaw DE, Kuriyan J. Structural analysis of the catalytically inactive kinase domain of the human EGF receptor 3. Proc Natl Acad Sci U S A. 2009;106(51):21608-13.
448. Valley CC, Lidke KA, Lidke DS. The Spatiotemporal Organization of ErbB Receptors: Insights from Microscopy. Cold Spring Harbor Perspect Biol. 2014;6(2).
449. Landgraf R, Eisenberg D. Heregulin reverses the oligomerization of HER3. Biochemistry. 2000;39(29):8503-11.
450. Berger MB, Mendrola JM, Lemmon MA. ErbB3/HER3 does not homodimerize upon neuregulin binding at the cell surface. FEBS Lett. 2004;569(1-3):332-6.
451. Kani K, Warren CM, Kaddis CS, Loo JA, Landgraf R. Oligomers of ERBB3 have two distinct interfaces that differ in their sensitivity to disruption by heregulin. J Biol Chem. 2005;280(9):8238-47.
452. Zhang Q, Park E, Kani K, Landgraf R. Functional isolation of activated and unilaterally phosphorylated heterodimers of ERBB2 and ERBB3 as scaffolds in ligand-dependent signaling. Proc Natl Acad Sci U S A. 2012;109(33):13237-42.
453. Macdonald-Obermann JL, Adak S, Landgraf R, Piwnica-Worms D, Pike LJ. Dynamic Analysis of the Epidermal Growth Factor (EGF) Receptor-ErbB2-ErbB3 Protein Network by Luciferase Fragment Complementation Imaging. J Biol Chem. 2013;288(42):30773-84.
454. Steinkamp MP, Low-Nam ST, Yang SJ, Lidke KA, Lidke DS, Wilson BS. erbB3 Is an Active Tyrosine Kinase Capable of Homo- and Heterointeractions. Mol Cell Biol. 2014;34(6):965-77.
455. McCabe Pryor M, Steinkamp MP, Halasz AM, Chen Y, Yang S, Smith MS, et al. Orchestration of ErbB3 signaling through heterointeractions and homointeractions. Mol Biol Cell. 2015;26(22):4109-23.
456. Cho HS, Leahy DJ. Structure of the extracellular region of HER3 reveals an interdomain tether. Science. 2002;297(5585):1330-3.
457. Roepstorff K, Grovdal L, Grandal M, Lerdrup M, van Deurs B. Endocytic downregulation of ErbB receptors: mechanisms and relevance in cancer. Histochem Cell Biol. 2008;129(5):563-78.
458. Sorkin A, Goh LK. Endocytosis and intracellular trafficking of ErbBs. Exp Cell Res. 2009;315(4):683-96.
459. Waterman H, Sabanai I, Geiger B, Yarden Y. Alternative intracellular routing of ErbB receptors may determine signaling potency. J Biol Chem. 1998;273(22):13819-27.
460. Waterman H, Yarden Y. Molecular mechanisms underlying endocytosis and sorting of ErbB receptor tyrosine kinases. FEBS Lett. 2001;490(3):142-52.
461. Baulida J, Kraus MH, Alimandi M, DiFiore PP, Carpenter G. All ErbB receptors other than the epidermal growth factor receptor are endocytosis impaired. J Biol Chem. 1996;271(9):5251-7.
462. Mayor S, Pagano RE. Pathways of clathrin-independent endocytosis. Nat Rev Mol Cell Biol. 2007;8(8):603-12.
463. Le Roy C, Wrana JL. Clathrin- and non-clathrin-mediated endocytic regulation of cell signalling. Nat Rev Mol Cell Biol. 2005;6(2):112-26.
464. Qiu XB, Goldberg AL. Nrdpl/FLRF is a ubiquitin ligase promoting ubiquitination and degradation of the epidermal growth factor receptor family member, ErbB3. Proc Natl Acad Sci U S A. 2002;99(23):14843-8.
465. Diamonti AJ, Guy PM, Ivanof C, Wong K, Sweeney C, Carraway KL. An RBCC protein implicated in maintenance of steady-state neuregulin receptor levels. Proc Natl Acad Sci U S A. 2002;99(5):2866-71.

466. Bouyain S, Leahy DJ. Structure-based mutagenesis of the substrate-recognition domain of Nrdp1/FLRF identifies the binding site for the receptor tyrosine kinase ErbB3. Protein Sci. 2007;16(4):654-61.
467. Cao ZW, Wu XL, Yen L, Sweeney C, Carraway KL. Neuregulin-induced ErbB3 downregulation is mediated by a protein stability cascade involving the E3 ubiquitin ligase Nrdp1. Mol Cell Biol. 2007;27(6):2180-8.
468. Sak MM, Breen K, Ronning SB, Pedersen NM, Bertelsen V, Stang E, et al. The oncoprotein ErbB3 is endocytosed in the absence of added ligand in a clathrin-dependent manner. Carcinogenesis. 2012;33(5):1031-9.
469. Yen L, Cao ZW, Wu XL, Ingalla ERQ, Baron C, Young LJT, et al. Loss of Nrdp1 enhances ErbB2/ErbB3-dependent breast tumor cell growth. Cancer Res. 2006;66(23):11279-86.
470. Fry WHD, Simion C, Sweeney C, Carraway KL. Quantity Control of the ErbB3 Receptor Tyrosine Kinase at the Endoplasmic Reticulum. Mol Cell Biol. 2011;31(14):3009-18.
471. Huang Z, Choi BK, Mujoo K, Fan X, Fa M, Mukherjee S, et al. The E3 ubiquitin ligase NEDD4 negatively regulates HER3/ErbB3 level and signaling. Oncogene. 2015;34(9):1105-15.
472. Mosesson Y, Mills GB, Yarden Y. Derailed endocytosis: an emerging feature of cancer. Nat Rev Cancer. 2008;8(11):835-50.
473. Shi HL, Gong H, Cao K, Zou SS, Zhu BX, Bao HM, et al. Nrdp1-mediated ErbB3 degradation inhibits glioma cell migration and invasion by reducing cytoplasmic localization of p27(Kip1). J Neuro-Oncol. 2015;124(3):357-64.
474. Offterdinger M, Schofer C, Weipoltshammer K, Grunt TW. c-erbB-3: a nuclear protein in mammary epithelial cells. J Cell Biol. 2002;157(6):929-39.
475. Raabe TD, Deadwyler G, Varga JW, Devries GH. Localization of neuregulin Isoforms and erbB receptors in myelinating glial cells. Glia. 2004;45(2):197-207.
476. Adilakshmi T, Ness-Myers J, Madrid-Aliste C, Fiser A, Tapinos N. A Nuclear Variant of ErbB3 Receptor Tyrosine Kinase Regulates Ezrin Distribution and Schwann Cell Myelination. J Neurosci. 2011;31(13):5106-19.
477. Koumakpayi IH, Diallo JS, Le Page C, Lessard L, Gleave M, Begin LR, et al. Expression and nuclear localization of ErbB3 in prostate cancer. Clin Cancer Res. 2006;12(9):2730-7.
478. Cheng CJ, Ye XC, Vakar-Lopez F, Kim J, Tu SM, Chen DT, et al. Bone microenvironment and androgen status modulate subcellular localization of ErbB3 in prostate cancer cells. Mol Cancer Res. 2007;5(7):675-84.
479. Koumakpayi IH, Le Page C, Delvoye N, Saad F, Mes-Masson AM. Macropinocytosis Inhibitors and Arf6 Regulate ErbB3 Nuclear Localization in Prostate Cancer Cells. Mol Carcinog. 2011;50(11):901-12.
480. Brand TM, Iida M, Luthar N, Wleklinski MJ, Starr MM, Wheeler DL. Mapping C-Terminal Transactivation Domains of the Nuclear HER Family Receptor Tyrosine Kinase HER3. PLoS One. 2013;8(8).
481. Mitsui K, Yonezawa M, Tatsuguchi A, Shinji S, Gudis K, Tanaka S, et al. Localization of phosphorylated ErbB1-4 and heregulin in colorectal cancer. BMC Cancer. 2014;14.
482. Reif R, Adawy A, Vartak N, Schroder J, Gunther G, Ghallab A, et al. Activated ErbB3 Translocates to the Nucleus via Clathrin-independent Endocytosis, Which Is Associated with Proliferating Cells. J Biol Chem. 2016;291(8):3837-47.
483. Andrique L, Fauvin D, El Maassarani M, Colasson H, Vannier B, Seite P. ErbB3(80) (kDa), a nuclear variant of the ErbB3 receptor, binds to the Cyclin D1 promoter to activate cell proliferation but is negatively controlled by p14(ARF). Cell Signal. 2012;24(5):1074-85.
484. Katoh M, Yazaki Y, Sugimura T, Terada M. c-erbb3 gene encodes secreted as well as transmembrane receptor tyrosine kinase Biochem Biophys Res Commun. 1993;192(3):1189-97.
485. Funayama T, Nakanishi T, Takahashi K, Taniguchi S, Takigawa M, Matsumura T. Overexpression of c-erbB-3 in various stages of human squamous cell carcinomas. Oncology. 1998;55(2):161-7.
486. Srinivasan R, Leverton KE, Sheldon H, Hurst HC, Sarraf C, Gullick WJ. Intracellular expression of the truncated extracellular domain of c-erbB-3/HER3. Cell Signal. 2001;13(5):321-30.
487. Lee H, Maihle NJ. Isolation and characterization of four alternate c-erbB3 transcripts expressed in ovarian carcinoma-derived cell lines and normal human tissues. Oncogene. 1998;16(25):3243-52.

488. Lee H, Akita RW, Sliwkowski MX, Maihle NJ. A naturally occurring secreted human ErbB3 receptor isoform inhibits heregulin-stimulated activation of ErbB2, ErbB3, and ErbB4. Cancer Res. 2001;61(11):4467-73.
489. Vakar-Lopez F, Cheng CJ, Kim J, Shi GG, Troncoso P, Tu SM, et al. Up-regulation of MDA-BF-1, a secreted isoform of ErbB3, in metastatic prostate cancer cells and activated osteoblasts in bone marrow. J Pathol. 2004;203(2):688-95.
490. Chen NY, Ye XC, Chu K, Navone NM, Sage EH, Yu-Lee LY, et al. A secreted isoform of ErbB3 promotes osteonectin expression in bone and enhances the invasiveness of prostate cancer cells. Cancer Res. 2007;67(14):6544-8.
491. Lin SH, Cheng CJ, Lee YC, Ye X, Tsai WW, Kim J, et al. A 45-kDa ErbB3 secreted by prostate cancer cells promotes bone formation. Oncogene. 2008;27(39):5195-203.
492. Lin SH, Lee YC, Choueiri MB, Wen SJ, Mathew P, Ye XC, et al. Soluble ErbB3 levels in bone marrow and plasma of men with prostate cancer. Clin Cancer Res. 2008;14(12):3729-36.
493. Hsieh SY, He JR, Yu MC, Lee WC, Chen TC, Lo SJ, et al. Secreted ERBB3 Isoforms Are Serum Markers for Early Hepatoma in Patients with Chronic Hepatitis and Cirrhosis. J Proteome Res. 2011;10(10):4715-24.
494. Takahashi M, Hasegawa Y, Ikeda Y, Wada Y, Tajiri M, Ariki S, et al. Suppression of Heregulin beta Signaling by the Single N-Glycan Deletion Mutant of Soluble ErbB3 Protein. J Biol Chem. 2013;288(46):32910-21.
495. Mirsky R, Jessen KR. The neurobiology of Schwann cells. Brain Pathol. 1999;9(2):293-311.
496. Svaren J, Meijer D. The Molecular Machinery of Myelin Gene Transcription in Schwann Cells. Glia. 2008;56(14):1541-51.
497. Taveggia C, Feltri ML, Wrabetz L. Signals to promote myelin formation and repair. Nat Rev Neurol. 2010;6(5):276-87.
498. Nave KA, Werner HB. Myelination of the Nervous System: Mechanisms and Functions. In Annual Review of Cell and Developmental Biology. Editors Schekman, R.Lehmann, R. Palo Alto: Annual Reviews; 2014. p. 503-33.
499. Salzer JL. Schwann Cell Myelination. Cold Spring Harbor Perspect Biol. 2015;7(8).
500. Meyer D, Birchmeier C. Multiple Essential Functions of Neuregulin in Development. Nature. 1995;378(6555):386-90.
501. Levi ADO, Bunge RP, Lofgren JA, Meima L, Hefti F, Nikolics K, et al. The Influence of Heregulins on Human Schwann Cell Proliferation J Neurosci. 1995;15(2):1329-40.
502. Riethmacher D, SonnenbergRiethmacher E, Brinkmann V, Yamaai T, Lewin GR, Birchmeier C. Severe neuropathies in mice with targeted mutations in the ErbB3 receptor. Nature. 1997;389(6652):725-30.
503. Grinspan JB, Marchionni MA, Reeves M, Coulaloglou M, Scherer SS. Axonal interactions regulate Schwann cell apoptosis in developing peripheral nerve: Neuregulin receptors and the role of neuregulins. J Neurosci. 1996;16(19):6107-18.
504. Raabe TD, Clive DR, Neuberger TJ, Wen D, DeVries GH. Cultured neonatal Schwann cells contain and secrete neuregulins. J Neurosci Res. 1996;46(2):263-70.
505. Cheng LL, Esch FS, Marchionni MA, Mudge AW. Control of Schwann cell survival and proliferation: autocrine factors and neuregulins. Mol Cell Neurosci. 1998;12(3):141-56.
506. Meyer D, Yamaai T, Garratt A, RiethmacherSonnenberg E, Kane D, Theill LE, et al. Isoform-specific expression and function of neuregulin. Development. 1997;124(18):3575-86.
507. Michailov GV, Sereda MW, Brinkmann BG, Fischer TM, Haug B, Birchmeier C, et al. Axonal neuregulin-1 regulates myelin sheath thickness. Science. 2004;304(5671):700-3.
508. Garratt AN, Voiculescu O, Topilko P, Charnay P, Birchmeier C. A dual role of erbB2 in myelination and in expansion of the Schwann cell precursor pool. J Cell Biol. 2000;148(5):1035-46.
509. Taveggia C, Zanazzi G, Petrylak A, Yano H, Rosenbluth J, Einheber S, et al. Neuregulin-1 type III determines the ensheathment fate of axons. Neuron. 2005;47(5):681-94.
510. Navel KA, Salzer JL. Axonal regulation of myelination by neuregulin 1. Curr Opin Neurobiol. 2006;16(5):492-500.

511. Chen S, Velardez MO, Warot X, Yu ZX, Miller SJ, Cros D, et al. Neuregulin 1-erbB signaling is necessary for normal myelination and sensory function. J Neurosci. 2006;26(12):3079-86.
512. Syed N, Reddy K, Yang DP, Taveggia C, Salzer JL, Maurel P, et al. Soluble Neuregulin-1 Has Bifunctional, Concentration-Dependent Effects on Schwann Cell Myelination. J Neurosci. 2010;30(17):6122-31.
513. Newbern J, Birchmeier C. Nrg1/ErbB signaling networks in Schwann cell development and myelination. Semin Cell Dev Biol. 2010;21(9):922-8.
514. Heermann S, Schmucker J, Hinz U, Rickmann M, Unterbarnscheidt T, Schwab MH, et al. Neuregulin 1 Type III/ErbB Signaling Is Crucial for Schwann Cell Colonization of Sympathetic Axons. PLoS One. 2011;6(12).
515. Raphael AR, Lyons DA, Talbot WS. ErbB Signaling Has a Role in Radial Sorting Independent of Schwann Cell Number. Glia. 2011;59(7):1047-55.
516. Fricker FR, Antunes-Martins A, Galino J, Paramsothy R, La Russa F, Perkins J, et al. Axonal neuregulin 1 is a rate limiting but not essential factor for nerve remyelination. Brain. 2013;136:2279-97.
517. Yarden Y, Peles E. Biochemical analysis of the ligand for the Neu oncogene receptor Biochemistry. 1991;30(14):3543-50.
518. Lemoine NR, Barnes DM, Hollywood DP, Hughes CM, Smith P, Dublin E, et al. Expression of the ERBB3 gene product in breast cancer Br J Cancer. 1992;66(6):1116-21.
519. Alimandi M, Romano A, Curia MC, Muraro R, Fedi P, Aaronson SA, et al. Cooperative signalling of ERBB3 and ERBB2 in neoplastic transformation and human mammary carcinomas Oncogene. 1995;10(9):1813-21.
520. Siegel PM, Ryan ED, Cardiff RD, Muller WJ. Elevated expression of activated forms of Neu/ErbB-2 and ErbB-3 are involved in the induction of mammary tumors in transgenic mice: implications for human breast cancer. Embo J. 1999;18(8):2149-64.
521. Holbro T, Civenni G, Hynes NE. The ErbB receptors and their role in cancer progression. Exp Cell Res. 2003;284(1):99-110.
522. Vaught DB, Stanford JC, Young C, Hicks DJ, Wheeler F, Rinehart C, et al. HER3 Is Required for HER2-Induced Preneoplastic Changes to the Breast Epithelium and Tumor Formation. Cancer Res. 2012;72(10):2672-82.
523. Rajkumar T, Gullick WJ. The type 1 growth factor receptors in human breast cancer Breast Cancer Res Treat. 1994;29(1):3-9.
524. Reschke M, Mihic-Probst D, van der Horst EH, Knyazev P, Wild PJ, Hutterer M, et al. HER3 is a determinant for poor prognosis in melanoma. Clin Cancer Res. 2008;14(16):5188-97.
525. Jaiswal BS, Kljavin NM, Stawiski EW, Chan E, Parikh C, Durinck S, et al. Oncogenic ERBB3 Mutations in Human Cancers. Cancer Cell. 2013;23(5):603-17.
526. Gullick WJ. The c-erb/HER3 receptor in human cancer. Cancer Surv. 1996;27:339-49.
527. Jiang N, Saba NF, Chen ZG. Advances in Targeting HER3 as an Anticancer Therapy. Chemotherapy research and practice. 2012;2012:817304.
528. Kim JH, Im KS, Kim NH, Yhee JY, Nho WG, Sur JH. Expression of HER-2 and nuclear localization of HER-3 protein in canine mammary tumors: Histopathological and immunohistochemical study. Vet J. 2011;189(3):318-22.
529. Doster AR, Yhee JY, Kim JH, Im KS, Sur JH. CDX-2 and HER-3 Expression in Canine Gastric and Colorectal Adenocarcinomas. J Comp Pathol. 2011;145(1):12-9.
530. Matsuyama S, Nakamura M, Yonezawa K, Shimada T, Ohashi F, Takamori Y, et al. Expression patterns of the erbB subfamily mRNA in canine benign and malignant mammary tumors. J Vet Med Sci. 2001;63(9):949-54.
531. Peck S, Corkrey R, Hamede R, Jones M, Canfield P. Hematologic and serum biochemical reference intervals for wild Tasmanian devils (Sarcophilus harrisii). Vet Clin Pathol. 2015;44(4):519-29.
532. Maramotti S, Paci M, Manzotti G, Rapicetta C, Gugnoni M, Galeone C, et al. Soluble Epidermal Growth Factor Receptors (sEGFRs) in Cancer: Biological Aspects and Clinical Relevance. Int J Mol Sci. 2016;17(4).

533. Baron AT, Cora EM, Lafky JM, Boardman CH, Buenafe MC, Rademaker A, et al. Soluble epidermal growth factor receptor (sEGFR/sErbB1) as a potential risk, screening, and diagnostic serum biomarker of epithelial ovarian cancer. Cancer Epidemiol Biomarkers Prev. 2003;12(2):103-13.
534. Pitteri SJ, Amon LM, Buson TB, Zhang YZ, Johnson MM, Chin A, et al. Detection of Elevated Plasma Levels of Epidermal Growth Factor Receptor Before Breast Cancer Diagnosis among Hormone Therapy Users. Cancer Res. 2010;70(21):8598-606.
535. Baron AT, Wilken JA, Haggstrom DE, Goodrich ST, Maihle NJ. Clinical implementation of soluble EGFR (sEGFR) as a theragnostic serum biomarker of breast, lung and ovarian cancer. IDrugs. 2009;12(5):302-8.
536. Baric M, Kulic A, Sirotkovic-Skerlev M, Plavetic ND, Vidovic M, Horvatic-Herceg G, et al. Circulating Her-2/Neu Extracellular Domain in Breast Cancer Patients-Correlation with Prognosis and Clinicopathological Parameters Including Steroid Receptor, Her-2/Neu Receptor Coexpression. Pathol Oncol Res. 2015;21(3):589-95.
537. Lam L, McAndrew N, Yee M, Fu T, Tchou JC, Zhang HT. Challenges in the clinical utility of the serum test for HER2 ECD. Biochim Biophys Acta-Rev Cancer. 2012;1826(1):199-208.
538. Siampanopoulou M, Galaktidou G, Dimasis N, Gotzamani-Psarrakou A. Profiling serum HER-2/NEU in prostate cancer. Hippokratia. 2013;17(2):108-12.
539. Carney WP. The emerging role of monitoring serum HER-2/neu oncoprotein levels in women with metastatic breast cancer. Lab Med. 2003;34(1):58-64.
540. Rio C, Buxbaum JD, Peschon JJ, Corfas G. Tumor necrosis factor-alpha-converting enzyme is required for cleavage of erbB4/HER4. J Biol Chem. 2000;275(14):10379-87.
541. Feng SM, Sartor CI, Hunter D, Zhou H, Yang XH, Caskey LS, et al. The HER4 cytoplasmic domain, but not its c terminus, inhibits mammary cell proliferation. Mol Endocrinol. 2007;21(8):1861-76.
542. Feng SM, Muraoka-Cook RS, Hunter D, Sandahl MA, Caskey LS, Miyazawa K, et al. The E3 Ubiquitin Ligase WWP1 Selectively Targets HER4 and Its Proteolytically Derived Signaling Isoforms for Degradation. Mol Cell Biol. 2009;29(3):892-906.
543. Maihle NJ, Lee H. Soluble ErbB3 methods of detection and antibodies United States patent and Trade Mark Office. 2010;Patent number US 7,744,882(June 29, 2010):1-39 [cited 14th July 2016) available from: http://patft.uspto.gov/netacgi/nph-Parser?Sect1=PTO1&Sect2=HITOFF&d=PALL&p=1&u=%2Fnetahtml%2FPTO%2Fsrchnum.htm&r=1&f=G&l=50&s1=7,744,882.PN.&OS=PN/7,744,882&RS=PN/7,744,882.
544. Li Q, Yuan ZY, Cao BW. The function of human epidermal growth factor receptor-3 and its role in tumors. Oncol Rep. 2013;30(6):2563-70.
545. Casaletto JB, McClatchey AI. Spatial regulation of receptor tyrosine kinases in development and cancer. Nat Rev Cancer. 2012;12(6):386-99.
546. Yang S, Raymond-Stintz MA, Ying W, Zhang J, Lidke DS, Steinberg SL, et al. Mapping ErbB receptors on breast cancer cell membranes during signal transduction. J Cell Sci. 2007;120(16):2763-73.
547. Park E, Baron R, Landgraf R. Higher-Order Association States of Cellular ERBB3 Probed with Photo-Cross-Linkable Aptamers. Biochemistry. 2008;47(46):11992-2005.
548. Littlefield P, Liu LJ, Mysore V, Shan YB, Shaw DE, Jura N. Structural analysis of the EGFR/HER3 heterodimer reveals the molecular basis for activating HER3 mutations. Sci Signal. 2014;7(354).
549. Choi MR, An CH, Chung YJ, Choi YJ, Yoo NJ, Lee SH. Mutational and expressional analysis of ERBB3 gene in common solid cancers. Apmis. 2014;122(12):1207-12.
550. Begnami MD, Fukuda E, Fregnani J, Nonogaki S, Montagnini AL, da Costa WL, et al. Prognostic Implications of Altered Human Epidermal Growth Factor Receptors (HERs) in Gastric Carcinomas: HER2 and HER3 Are Predictors of Poor Outcome. J Clin Oncol. 2011;29(22):3030-6.
551. Fricker FR, Lago N, Balarajah S, Tsantoulas C, Tanna S, Zhu N, et al. Axonally Derived Neuregulin-1 Is Required for Remyelination and Regeneration after Nerve Injury in Adulthood. J Neurosci. 2011;31(9):3225-33.
552. Carroll SL. Molecular mechanisms promoting the pathogenesis of Schwann cell neoplasms. Acta Neuropathol. 2012;123(3):321-48.

553. Rodriguez FJ, Stratakis CA, Evans DG. Genetic predisposition to peripheral nerve neoplasia: diagnostic criteria and pathogenesis of neurofibromatoses, Carney complex, and related syndromes. Acta Neuropathol. 2012;123(3):349-67.
554. Rodriguez FJ, Folpe AL, Giannini C, Perry A. Pathology of peripheral nerve sheath tumors: diagnostic overview and update on selected diagnostic problems. Acta Neuropathol. 2012;123(3):295-319.
555. Akahane K, Kato K, Ogiso S, Sakaguchi K, Hashimoto M, Ishikawa A, et al. Malignant granular cell tumor of the breast: case report and literature review. Beast Cancer. 2015;22(3):317-23.
556. Bourdeaut F, Ribeiro A, Paris R, Pierron G, Couturier J, Peuchmaur M, et al. In neuroblastic tumours, Schwann cells do not harbour the genetic alterations of neuroblasts but may nevertheless share the same clonal origin. Oncogene. 2008;27(21):3066-71.
557. Omi K, Kitano Y, Agawa H, Kadota K. An immunohistochemical study of peripheral neuroblastoma, ganglioneuroblastoma, anaplastic ganglioglioma, schwannoma and neurofibroma in cattle J Comp Pathol. 1994;111(1):1-14.
558. Kagawa Y, Hirayama K, Tagami M, Tsunoda N, Yoshino T, Matsui T, et al. Immunohistochemical analysis of equine pulmonary granular cell tumours. J Comp Pathol. 2001;124(2-3):122-7.
559. Chijiwa K, Uchida K, Tateyama S. Immunohistochemical evaluation of canine peripheral nerve sheath tumors and other soft tissue sarcomas. Vet Pathol. 2004;41(4):307-18.
560. Schoniger S, Valentine BA, Fernandez CJ, Summers BA. Cutaneous Schwannomas in 22 Horses. Vet Pathol. 2011;48(2):433-42.
561. Duke FD, Teixeira LBC, Galle LE, Green N, Dubielzig RR. Malignant Uveal Schwannoma With Peripheral Nerve Extension in a 12-Week-Old Color-Dilute Labrador Retriever. Vet Pathol. 2015;52(1):181-5.
562. Izycka-Swieszewska E, Wozniak A, Drozynska E, Kot J, Grajkowska W, Klepacka T, et al. Expression and significance of HER family receptors in neuroblastic tumors. Clin Exp Metastasis. 2011;28(3):271-82.
563. Wilzen A, Krona C, Sveinbjornsson B, Kristiansson E, Dalevi D, Ora I, et al. ERBB3 is a marker of a ganglioneuroblastoma/ganglioneuroma-like expression profile in neuroblastic tumours. Mol Cancer. 2013;12.
564. Lee PR, Cohen JE, Fields RD. Immune system evasion by peripheral nerve sheath tumor. Neurosci Lett. 2006;397(1-2):126-9.
565. Horste GMZ, Hu W, Hartung HP, Lehmann HC, Kieseier BC. The immunocompetence of Schwann cells. Muscle & Nerve. 2008;37(1):3-13.
566. Tzekova N, Heinen A, Kury P. Molecules Involved in the Crosstalk Between Immune- and Peripheral Nerve Schwann Cells. J Clin Immunol. 2014;34:S86-S104.
567. Siddle HV, Kaufman J. Immunology of naturally transmissible tumours. Immunology. 2015;144(1):11-20.
568. Yi ES, Harclerode D, Gondo M, Stephenson M, Brown RW, Younes M, et al. High c-erbB-3 protein expression is associated with shorter survival in advanced non-small cell lung carcinomas. Mod Pathol. 1997;10(2):142-8.
569. Tanner B, Hasenclever D, Stern K, Schormann W, Bezler M, Hermes M, et al. ErbB-3 predicts survival in ovarian cancer. J Clin Oncol. 2006;24(26):4317-23.
570. Sergina NV, Rausch M, Wang DH, Blair J, Hann B, Shokat KM, et al. Escape from HER-family tyrosine kinase inhibitor therapy by the kinase-inactive HER3. Nature. 2007;445(7126):437-41.
571. Telesco SE, Shih AJ, Jia F, Radhakrishnan R. A multiscale modeling approach to investigate molecular mechanisms of pseudokinase activation and drug resistance in the HER3/ErbB3 receptor tyrosine kinase signaling network. Mol Biosyst. 2011;7(6):2066-80.
572. Liu BL, Ordonez-Ercan D, Fan ZY, Edgerton SM, Yang XH, Thor AD. Downregulation of erbB3 abrogates erbB2-mediated tamoxifen resistance in breast cancer cells. Int J Cancer. 2007;120(9):1874-82.
573. Sithanandam G, Fornwald LW, Fields J, Anderson LM. Inactivation of ErbB3 by siRNA promotes apoptosis and attenuates growth and invasiveness of human lung adenocarcinoma cell line A549. Oncogene. 2005;24(11):1847-59.
574. Lee-Hoeflich ST, Crocker L, Yao E, Pham T, Munroe X, Hoeflich KP, et al. A central role for HER3 in HER2-amplified breast cancer: implications for targeted therapy. Cancer Res. 2008;68(14):5878-87.

575. Sheng Q, Liu XG, Fleming E, Yuan K, Piao HY, Chen JY, et al. An Activated ErbB3/NRG1 Autocrine Loop Supports In Vivo Proliferation in Ovarian Cancer Cells. Cancer Cell. 2010;17(3):298-310.
576. Stern DF. ERBB3/HER3 and ERBB2/HER2 duet in mammary development and breast cancer. J Mammary Gland Biol Neoplasia. 2008;13(2):215-23.
577. Nahta R. Deciphering the role of insulin-like growth factor-I receptor in trastuzumab resistance. Chemotherapy research and practice. 2012;2012:648965.
578. Huang XP, Gao LZ, Wang SL, McManaman JL, Thor AD, Yang XH, et al. Heterotrimerization of the Growth Factor Receptors erbB2, erbB3, and Insulin-like Growth Factor-I Receptor in Breast Cancer Cells Resistant to Herceptin. Cancer Res. 2010;70(3):1204-14.
579. Engelman JA, Zejnullahu K, Mitsudomi T, Song YC, Hyland C, Park JO, et al. MET amplification leads to gefitinib resistance in lung cancer by activating ERBB3 signaling. Science. 2007;316(5827):1039-43.
580. Yun C, Gang L, Gu RM, Xu W, Ming XZ, Chen HQ. Essential role of Her3 in two signaling transduction patterns: Her2/Her3 and MET/Her3 in proliferation of human gastric cancer. Mol Carcinog. 2015;54(12):1700-9.
581. Wang XC, Batty KM, Crowe PJ, Goldstein D, Yang JL. The potential of panHER inhibition in cancer. Front Oncol. 2015;5.
582. Dey N, Williams C, Leyland-Jones B, De P. A critical role for HER3 in HER2-amplified and non-amplified breast cancers: function of a kinase-dead RTK. Am J Transl Res. 2015;7(4):733-50.
583. Hamburger AW. The role of ErbB3 and its binding partners in breast cancer progression and resistance to hormone and tyrosine kinase directed therapies. J Mammary Gland Biol Neoplasia. 2008;13(2):225-33.
584. Tinoco G, Warsch S, Gluck S, Avancha K, Montero AJ. Treating Breast Cancer in the 21st Century: Emerging Biological Therapies. J Cancer. 2013;4(2):117-32.
585. Baselga J, Swain SM. Novel anticancer targets: revisiting ERBB2 and discovering ERBB3. Nat Rev Cancer. 2009;9(7):463-75.
586. Kruser TJ, Wheeler DL. Mechanisms of resistance to HER family targeting antibodies. Exp Cell Res. 2010;316(7):1083-100.
587. Aurisicchio L, Marra E, Roscilli G, Mancini R, Ciliberto G. The promise of anti-ErbB3 monoclonals as new cancer therapeutics. Oncotarget. 2012;3(8):744-58.
588. Kol A, van Scheltinga A, Timmer-Bosscha H, Lamberts LE, Bensch F, de Vries EGE, et al. HER3, serious partner in crime Therapeutic approaches and potential biomarkers for effect of HER3-targeting. Pharmacol Ther. 2014;143(1):1-11.
589. Ma J, Lyu H, Huang JC, Liu BL. Targeting of erbB3 receptor to overcome resistance in cancer treatment. Mol Cancer. 2014;13.
590. Lee Y, Ma J, Lyu H, Huang JC, Kim A, Liu BL. Role of erbB3 receptors in cancer therapeutic resistance. Acta Biochim Biophys Sin. 2014;46(3):190-8.
591. Zhang N, Chang Y, Rios A, An Z. HER3/ErbB3, an emerging cancer therapeutic target. Acta Biochim Biophys Sin. 2016;48(1):39-48.
592. van der Horst EH, Murgia M, Treder M, Ullrich A. Anti-HER-3 MAbs inhibit HER-3-mediated signaling in breast cancer cell lines resistant to anti-HER-2 antibodies. International Journal of Cancer. 2005;115(4):519-27.
593. Robinson MK, Hodge KM, Horak E, Sundberg AL, Russeva M, Shaller CC, et al. Targeting ErbB2 and ErbB3 with a bispecific single-chain Fv enhances targeting selectivity and induces a therapeutic effect in vitro. Br J Cancer. 2008;99(9):1415-25.
594. Treder M, Ogbagabriel S, Moor R, Schulze-Horsel U, Hettmann T, Rothe M, et al. Fully human anti-HER3 mAb U3-1287 (AMG 888) demonstrates unique in vitro and in vivo activities versus other HER family inhibitors in NSCLC models. EJC Suppl. 2008;6(12):99-.
595. Huang XP, Gao LZ, Wang SL, Lee CK, Ordentlich P, Liu BL. HDAC Inhibitor SNDX-275 Induces Apoptosis in erbB2-Overexpressing Breast Cancer Cells via Down-regulation of erbB3 Expression. Cancer Res. 2009;69(21):8403-11.
596. Schoeberl B, Faber AC, Li DN, Liang MC, Crosby K, Onsum M, et al. An ErbB3 Antibody, MM-121, Is Active in Cancers with Ligand-Dependent Activation. Cancer Res. 2010;70(6):2485-94.

597. Schoeberl B, Pace EA, Fitzgerald JB, Harms BD, Xu LH, Nie L, et al. Therapeutically Targeting ErbB3: A Key Node in Ligand-Induced Activation of the ErbB Receptor-PI3K Axis. Sci Signal. 2009;2(77).
598. Liles JS, Arnoletti JP, Kossenkov AV, Mikhaylina A, Frost AR, Kulesza P, et al. Targeting ErbB3-mediated stromal-epithelial interactions in pancreatic ductal adenocarcinoma. Br J Cancer. 2011;105(4):523-33.
599. Hickinson DM, Klinowska T, Speake G, Vincent J, Trigwell C, Anderton J, et al. AZD8931, an Equipotent, Reversible Inhibitor of Signaling by Epidermal Growth Factor Receptor, ERBB2 (HER2), and ERBB3: A Unique Agent for Simultaneous ERBB Receptor Blockade in Cancer. Clin Cancer Res. 2010;16(4):1159-69.
600. Schaefer G, Haber L, Crocker LM, Shia S, Shao L, Dowbenko D, et al. A Two-in-One Antibody against HER3 and EGFR Has Superior Inhibitory Activity Compared with Monospecific Antibodies. Cancer Cell. 2011;20(4):472-86.
601. Belleudi F, Marra E, Mazzetta F, Fattore L, Giovagnoli MR, Mancini R, et al. Monoclonal antibody-induced ErbB3 receptor internalization and degradation inhibits growth and migration of human melanoma cells. Cell Cycle. 2012;11(7):1455-67.
602. McDonagh CF, Huhalov A, Harms BD, Adams S, Paragas V, Oyama S, et al. Antitumor Activity of a Novel Bispecific Antibody That Targets the ErbB2/ErbB3 Oncogenic Unit and Inhibits Heregulin-Induced Activation of ErbB3. Mol Cancer Ther. 2012;11(3):582-93.
603. Foreman PK, Gore M, Kobel PA, Xu L, Yee H, Hannum C, et al. ErbB3 Inhibitory Surrobodies Inhibit Tumor Cell Proliferation In Vitro and In Vivo. Mol Cancer Ther. 2012;11(7):1411-20.
604. Blackburn E, Zona S, Murphy ML, Brown IR, Chan SKW, Gullick WJ. A monoclonal antibody to the human HER3 receptor inhibits Neuregulin 1-beta binding and co-operates with Herceptin in inhibiting the growth of breast cancer derived cell lines. Breast Cancer Res Treat. 2012;134(1):53-9.
605. Lazrek Y, Dubreuil O, Garambois V, Gaborit N, Larbouret C, Le Clorennec C, et al. Anti-HER3 Domain 1 and 3 Antibodies Reduce Tumor Growth by Hindering HER2/HER3 Dimerization and AKT-Induced MDM2, XIAP, and Fox01 Phosphorylation. Neoplasia. 2013;15(3):335-+.
606. Garner AP, Bialucha CU, Sprague ER, Garrett JT, Sheng Q, Li SR, et al. An Antibody That Locks HER3 in the Inactive Conformation Inhibits Tumor Growth Driven by HER2 or Neuregulin. Cancer Res. 2013;73(19):6024-35.
607. Sala G, Rapposelli IG, Ghasemi R, Piccolo E, Traini S, Capone E, et al. EV20, a Novel Anti-ErbB-3 Humanized Antibody, Promotes ErbB-3 Down-Regulation and Inhibits Tumor Growth In Vivo. Transl Oncol. 2013;6(6):676-U293.
608. Mirschberger C, Schiller CB, Schraml M, Dimoudis N, Friess T, Gerdes CA, et al. RG7116, a Therapeutic Antibody That Binds the Inactive HER3 Receptor and Is Optimized for Immune Effector Activation. Cancer Res. 2013;73(16):5183-94.
609. Wu YM, Zhang YX, Wang ML, Li Q, Qu ZX, Shi V, et al. Downregulation of HER3 by a Novel Antisense Oligonucleotide, EZN-3920, Improves the Antitumor Activity of EGFR and HER2 Tyrosine Kinase Inhibitors in Animal Models. Mol Cancer Ther. 2013;12(4):427-37.
610. D'Souza JW, Reddy S, Goldsmith LE, Shchaveleva I, Marks JD, Litwin S, et al. Combining Anti-ERBB3 Antibodies Specific for Domain I and Domain III Enhances the Anti-Tumor Activity over the Individual Monoclonal Antibodies. PLoS One. 2014;9(11).
611. Miller MJ, Foy KC, Overholser JP, Nahta R, Kaumaya PTP. HER-3 peptide vaccines/mimics: Combined therapy with IGF-1R, HER-2, and HER-1 peptides induces synergistic antitumor effects against breast and pancreatic cancer cells. OncoImmunology. 2014;3(11).
612. Fitzgerald JB, Johnson BW, Baum J, Adams S, Iadevaia S, Tang J, et al. MM-141, an IGF-IR- and ErbB3-Directed Bispecific Antibody, Overcomes Network Adaptations That Limit Activity of IGF-IR Inhibitors. Mol Cancer Ther. 2014;13(2):410-25.
613. Francis D, Huang S, Werner L, Lantto J, Horak ID, Kragh M, et al. Sym013, novel pan-HER monoclonal antibody mixture, augments radiation response in human lung and head and neck tumors. Cancer Res. 2014;74(19).
614. Zhang L, Castanaro C, Luan B, Yang K, Fan LF, Fairhurst JL, et al. ERBB3/HER2 Signaling Promotes Resistance to EGFR Blockade in Head and Neck and Colorectal Cancer Models. Mol Cancer Ther. 2014;13(5):1345-55.

615. Clarke N, Hopson C, Hahn A, Sully K, Germaschewski F, Yates J, et al. Preclinical pharmacologic characterization of GSK2849330, a monoclonal AccretaMab (R) antibody with optimized ADCC and CDC activity directed against HER3. Eur J Cancer. 2014;50:98-9.
616. Gaborit N, Abdul-Hai A, Mancini M, Lindzen M, Lavi S, Leitner O, et al. Examination of HER3 targeting in cancer using monoclonal antibodies. Proc Natl Acad Sci U S A. 2015;112(3):839-44.
617. Lee S, Greenlee EB, Amick JR, Ligon GF, Lillquist JS, Natoli EJ, et al. Inhibition of ErbB3 by a monoclonal antibody that locks the extracellular domain in an inactive configuration. Proc Natl Acad Sci U S A. 2015;112(43):13225-30.
618. Meetze K, Vincent S, Tyler S, Mazsa EK, Delpero AR, Bottega S, et al. Neuregulin 1 Expression Is a Predictive Biomarker for Response to AV-203, an ERBB3 Inhibitory Antibody, in Human Tumor Models. Clin Cancer Res. 2015;21(5):1106-14.
619. Gu JM, Yang JS, Chang Q, Liu ZH, Ghayur T, Gu JJ. Identification of Anti-EGFR and Anti-ErbB3 Dual Variable Domains Immunoglobulin (DVD-Ig) Proteins with Unique Activities. PLoS One. 2015;10(5).
620. Ren X-R, Wang J, Osada T, Mook RA, Jr., Morse MA, Barak LS, et al. Perhexiline promotes HER3 ablation through receptor internalization and inhibits tumor growth. Breast cancer research : BCR. 2015;17(1):528.
621. Amin DN, Sergina N, Lim L, Goga A, Moasser MM. HER3 signalling is regulated through a multitude of redundant mechanisms in HER2-driven tumour cells. Biochem J. 2012;447:417-25.
622. Huang JC, Wang SL, Lyu H, Cai B, Yang XH, Wang JX, et al. The anti-erbB3 antibody MM-121/SAR256212 in combination with trastuzumab exerts potent antitumor activity against trastuzumab-resistant breast cancer cells. Mol Cancer. 2013;12.
623. Huang S, Li CR, Armstrong EA, Peet CR, Saker J, Amler LC, et al. Dual Targeting of EGFR and HER3 with MEHD7945A Overcomes Acquired Resistance to EGFR Inhibitors and Radiation. Cancer Res. 2013;73(2):824-33.
624. Rajkumar T, Gullick WJ. A monoclonal antibody to the human c-erbb3 protein stimulates the anchorage independent growth of breast cancer cell lines Br J Cancer. 1994;70(3):459-65.
625. Garrett JT, Sutton CR, Kurupi R, Bialucha CU, Ettenberg SA, Collins SD, et al. Combination of Antibody That Inhibits Ligand-Independent HER3 Dimerization and a p110 alpha Inhibitor Potently Blocks PI3K Signaling and Growth of HER2+ Breast Cancers. Cancer Res. 2013;73(19):6013-23.
626. Ferreira RB, Law ME, Jahn SC, Davis BJ, Heldermon CD, Reinhard M, et al. Novel agents that downregulate EGFR, HER2, and HER3 in parallel. Oncotarget. 2015;6(12):10445-59.
627. Aurisicchio L, Ciliberto G. Genetic cancer vaccines: current status and perspectives. Expert Opin Biol Ther. 2012;12(8):1043-58.
628. Guo CQ, Manjili MH, Subjeck JR, Sarkar D, Fisher PB, Wang XY. Therapeutic Cancer Vaccines: Past, Present, and Future. In: Tew KD, Fisher PB, editors. Advances in Cancer Research, Vol 119. San Diego: Elsevier Academic Press Inc; 2013. p. 421-75.
629. Melero I, Gaudemack G, Gerritsen W, Huber C, Parmiani G, Scholl S, et al. Therapeutic vaccines for cancer: an overview of clinical trials. Nat Rev Clin Oncol. 2014;11(9):509-24.
630. Melief CJM, van Hall T, Arens R, Ossendorp F, van der Burg SH. Therapeutic cancer vaccines. J Clin Invest. 2015;125(9):3401-12.
631. Papaioannou NE, Beniata OV, Vitsos P, Tsitsilonis O, Samara P. Harnessing the immune system to improve cancer therapy. Ann Transl Med. 2016;4(14).
632. Kazemi T, Younesi V, Jadidi-Niaragh F, Yousefi M. Immunotherapeutic approaches for cancer therapy: An updated review. Artif Cell Nanomed Biotechnol. 2016;44(3):769-79.
633. Anderson K, Modiano J. Progress in Adaptive Immunotherapy for Cancer in Companion Animals: Success on the Path to a Cure. Veterinary Sciences. 2015;2(4):363.
634. Bergman PJ. Immunotherapy in Veterinary Oncology. Vet Clin N Am-Small Anim Pract. 2014;44(5):925-+.
635. Regan D, Guth A, Coy J, Dow S. Cancer immunotherapy in veterinary medicine: Current options and new developments. Vet J 2016;207:20-8.
636. Fazekas J, Furdos I, Singer J, Jensen-Jarolim E. Why man's best friend, the dog, could also benefit from an anti-HER-2 vaccine. Oncol Lett. 2016;12(4):2271-6.

637. Singer J, Fazekas J, Wang W, Weichselbaumer M, Matz M, Mader A, et al. Generation of a Canine Anti-EGFR (ErbB-1) Antibody for Passive Immunotherapy in Dog Cancer Patients. Mol Cancer Ther. 2014;13(7):1777-90.
638. Ito D, Brewer S, Modiano JF, Beall MJ. Development of a novel anti-canine CD20 monoclonal antibody with diagnostic and therapeutic potential. Leuk Lymphoma. 2015;56(1):219-25.
639. Pinfold TL, Brown GK, Bettiol SS, Woods GM. Mouse Model of Devil Facial Tumour Disease Establishes That an Effective Immune Response Can be Generated Against the Cancer Cells. Front Immunol. 2014;5:251.
640. Slingluff CL. The Present and Future of Peptide Vaccines for Cancer Single or Multiple, Long or Short, Alone or in Combination? Cancer J. 2011;17(5):343-50.
641. Foy KC, Wygle RM, Miller MJ, Overholser JP, Bekaii-Saab T, Kaumaya PTP. Peptide Vaccines and Peptidomimetics of EGFR (HER-1) Ligand Binding Domain Inhibit Cancer Cell Growth In Vitro and In Vivo. J Immunol. 2013;191(1):217-27.
642. Overholser J, Ambegaokar KH, Eze SM, Sanabria-Figueroa E, Nahta R, Bekaii-Saab T, et al. Anti-Tumor Effects of Peptide Therapeutic and Peptide Vaccine Antibody Co-targeting HER-1 and HER-2 in Esophageal Cancer (EC) and HER-1 and IGF-1R in Triple-Negative Breast Cancer (TNBC). Vaccines. 2015;3(3):519-43.
643. Allen SD, Garrett JT, Rawale SV, Jones AL, Phillips G, Forni G, et al. Peptide vaccines of the HER-2/neu dimerization loop are effective in inhibiting mammary tumor growth in vivo. J Immunol. 2007;179(1):472-82.
644. Gil EY, Jo UH, Lee HJ, Kang J, Seo JH, Lee ES, et al. Vaccination with ErbB-2 peptides prevents cancer stem cell expansion and suppresses the development of spontaneous tumors in MMTV-PyMT transgenic mice. Breast Cancer Res Treat. 2014;147(1):69-80.
645. Clifton GT, Peoples GE, Mittendorf EA. The development and use of the E75 (HER2 369-377) peptide vaccine. Future Oncol. 2016;12(11):1321-9.
646. Kaumaya PTP. A paradigm shift: Cancer therapy with peptide-based B-cell epitopes and peptide immunotherapeutics targeting multiple solid tumor types: Emerging concepts and validation of combination immunotherapy. Human Vaccines Immunother. 2015;11(6):1368-86.
647. Ly LV, Sluijter M, van der Burg SH, Jager MJ, van Hall T. Effective Cooperation of Monoclonal Antibody and Peptide Vaccine for the Treatment of Mouse Melanoma. J Immunol. 2013;190(1):489-96.
648. Cavallo F, Aurisicchio L, Mancini R, Ciliberto G. Xenogene vaccination in the therapy of cancer. Expert Opin Biol Ther. 2014;14(10):1427-42.
649. Bergman PJ, Camps-Palau MA, McKnight JA, Leibman NF, Craft DM, Leung C, et al. Development of a xenogeneic DNA vaccine program for canine malignant melanoma at the Animal Medical Center. Vaccine. 2006;24(21):4582-5.
650. Flies A, Woods G, Lyons AB, Hayball J. B7-H1 (PD-L1) is expressed in the Tasmanian devil facial tumor microenvironment and is strongly upregulated in response to IFN-gamma. Eur J Immunol. 2016;46:1095-.
651. Muenst S, Laubli H, Soysal SD, Zippelius A, Tzankov A, Hoeller S. The immune system and cancer evasion strategies: therapeutic concepts. J Intern Med. 2016;279(6):541-62.
652. Pardoll DM. The blockade of immune checkpoints in cancer immunotherapy. Nat Rev Cancer. 2012;12(4):252-64.
653. Topalian SL, Drake CG, Pardoll DM. Immune Checkpoint Blockade: A Common Denominator Approach to Cancer Therapy. Cancer Cell. 2015;27(4):450-61.
654. Chen DS, Mellman I. Oncology Meets Immunology: The Cancer-Immunity Cycle. Immunity. 2013;39(1):1-10.
655. van der Burg SH, Arens R, Ossendorp F, van Hall T, Melief AJM. Vaccines for established cancer: overcoming the challenges posed by immune evasion. Nat Rev Cancer. 2016;16(4):219-33.

9.0 Appendices

Appendix 1 has been removed for copyright or proprietary reasons.

It is: Loh, R., Bergfeld, J., Hayes, D., O'Hara, A., et al., 2006. The pathology of devil facial tumor disease (DFTD) in Tasmanian devils (Sarcophilus harrisii), Vet Pathol., 43(6), 890-5.
doi: 10.1354/vp.43-6-890

Appendix 2 has been removed for copyright or proprietary reasons.

It is: Loh, R., Hayes, D., Mahjoor, A., O'Hara, A., et al., 2006. The immunohistochemical characterization of devil facial tumor disease (DFTD) in the Tasmanian Devil (Sarcophilus harrisii), Vet Pathol, 43(6), 896-903.
doi: 10.1354/vp.43-6-896

Appendix 3 has been removed for copyright or proprietary reasons.

It is: Pyecroft, S. B., Pearse, A. M., Loh, R., Swift, K., Belov, K., Fox, N., et al. 2007. Towards a case definition for devil facial tumour disease: What is it?, Ecohealth, 4(3), 346-51.
doi: 10.1007/s10393-007-0126-0

PLOS ONE

RESEARCH ARTICLE

ERBB3: A potential serum biomarker for early detection and therapeutic target for devil facial tumour 1 (DFT1)

Dane A. Hayes[1,2,3]*, Dale A. Kunde[3], Robyn L. Taylor[2,4], Stephen B. Pyecroft[5], Sukhwinder Singh Sohal[3], Elizabeth T. Snow[3]

1 Department of Primary Industries, Parks Water and Environment, Animal Health Laboratory, Launceston, Tasmania, Australia, **2** Save the Tasmanian Devil Program, University of Tasmania, Hobart, Tasmania, Australia, **3** School of Health Sciences, Faculty of Health, University of Tasmania, Launceston, Tasmania, Australia, **4** Department of Primary Industries, Parks Water and Environment, Resource Management and Conservation, Hobart, Tasmania, Australia, **5** School of Animal & Veterinary Sciences, Faculty of Science, University of Adelaide, Roseworthy Campus, Roseworthy, South Australia

* dane.hayes@dpipwe.tas.gov.au

OPEN ACCESS

Citation: Hayes DA, Kunde DA, Taylor RL, Pyecroft SB, Sohal SS, Snow ET (2017) ERBB3: A potential serum biomarker for early detection and therapeutic target for devil facial tumour 1 (DFT1). PLoS ONE 12(6): e0177919. https://doi.org/10.1371/journal.pone.0177919

Editor: Aamir Ahmad, University of South Alabama Mitchell Cancer Institute, UNITED STATES

Received: December 12, 2016

Accepted: May 5, 2017

Published: June 7, 2017

Data Availability Statement: All relevant data are within the paper.

Funding: This research was funded by the Dr Eric Guiler Tasmanian Devil Research grant through the University of Tasmanian and the Save the Tasmanian Devil Appeal (STDP) to DH and SS http://www.tassiedevil.com.au/tasdevil.nsf. The Department of Primary Industries water and Environment (DPIPWE) and the University of Adelaide provided financial and in kind support.

Abstract

Devil Facial Tumour 1 (DFT1) is one of two transmissible neoplasms of Tasmanian devils (*Sarcophilus harrisii*) predominantly affecting their facial regions. DFT1's cellular origin is that of Schwann cell lineage where lesions are evident macroscopically late in the disease. Conversely, the pre-clinical timeframe from cellular transmission to appearance of DFT1 remains uncertain demonstrating the importance of an effective pre-clinical biomarker. We show that ERBB3, a marker expressed normally by the developing neural crest and Schwann cells, is immunohistohemically expressed by DFT1, therefore the potential of ERBB3 as a biomarker was explored. Under the hypothesis that serum ERBB3 levels may increase as DFT1 invades local and distant tissues our pilot study determined serum ERBB3 levels in normal Tasmanian devils and Tasmanian devils with DFT1. Compared to the baseline serum ERBB3 levels in unaffected Tasmanian devils, Tasmanian devils with DFT1 showed significant elevation of serum ERBB3 levels. Interestingly Tasmanian devils with cutaneous lymphoma (CL) also showed elevation of serum ERBB3 levels when compared to the baseline serum levels of Tasmanian devils without DFT1. Thus, elevated serum ERBB3 levels in otherwise healthy looking devils could predict possible DFT1 or CL in captive or wild devil populations and would have implications on the management, welfare and survival of Tasmanian devils. ERBB3 is also a therapeutic target and therefore the potential exists to consider modes of administration that may eradicate DFT1 from the wild.

Introduction

The Tasmanian devil (*Sarcophilus harrisii*) belongs to the Dasyuridae family, it is a carnivorous marsupial that is extinct on mainland Australia and now found only on the island of Tasmania. Superficial dermal cutaneous lesions of wild Tasmanian devils can be found commonly in the form of skin sores [1] and neoplasia [2]. Spontaneous neoplasms in captive Tasmanian devils

Competing interests: The authors have declared that no competing interests exist.

including squamous cell carcinoma of the lip and gingiva, dermal lymphosarcoma [3], trichoepithelioma, papilloma and keratoacanthoma [4] and a single devil with multiple unrelated tumours involving internal organs in combination with skin [5] have been recorded, suggestive of potential metastasis. Similar observations were made while reviewing Dasyurid archival material at the Australian Registry of Wildlife Health [6] and recently, two captive female devils with pruritus and dermatitis were diagnosed with cutaneous T-cell lymphoma [7]. None of the recorded neoplastic superficial lesions found in captive or wild Tasmanian devils appeared to mimic the firm, flattened centrally ulcerated soft tissue lesions of DFT1 affected Tasmanian devils [8].

Although the first evidence of DFT1 in wild populations occurred in 1996 when several Tasmanian devils were photographed by Christo Baars in the north east of the state with facial lesions. However, a tissue diagnosis was not obtained until 2001 [9]. Review of Tasmanian devil archival slides submitted to the Animal Health Laboratory, DPIPWE, revealed a single case in 1997 that was consistent with DFT1 [8, 10]. An emerging disease was finally recognised in 2003 [10] and subsequent investigations revealed the tumour to be a transmissible allograft being transferred from devil to devil via biting [11] with tumours tending to be located on the face, lips and oral mucosa [8].The timeframe of the pre-clinical stage of DFTD1 remains largely undetermined with observations ranging from 2–13 months [9, 12–15] but as little as 1 month has been recorded (Author unpublished observation, laboratory records, DPIPWE). Immunohistochemical examination of DFT1 suggested a possible undifferentiated neuroendocrine tumour [16, 17] although subsequent molecular testing lead to the conclusion that DFT1 is of Schwann cell origin [18]. Down-regulation mechanisms causing absence of major histocompatibility complex (MHC) class 1 cell surface antigens is a major contributing factor allowing the DFT1 allograft to evade the host devil's immune system without rejection [19–21]. Further cytogenetic and molecular techniques have identified four karyotypic strains that are differentiated by a small number of identifiable rearrangements [22, 23]. As a consequence of this cancer, wild populations of the Tasmanian devil have been significantly reduced in Tasmania where the possibility of extinction either locally within 10–15 years [24, 25] or completely within 25–35 years [25] has been predicted. The impedance of this 2007 dire prediction includes the adaption of wild Tasmanian devils to their life history change by precocial sexual maturity [26] and through a strong collaborative scientific research and conservation management framework devised by the Save the Tasmanian Devil Program (STDP) [27]. A second transmissible tumour in Tasmanian devils, devil facial tumour 2 (DFT2), distinct from DFT1 has recently been reported [28] suggesting that the species may well be prone to transmissible cancers, increasing the urgency of biomarker identification and therapeutic intervention.

ERBB3 is expressed in early embryonal development and plays an integral role in the development of the neural crest and Schwann cells [29] regulating pathways that execute diverse cellular functions including development, cell cycle, migration, survival, proliferation and differentiation [30–34]. ERBB3 is a member of the Epidermal Growth Factor (EGF) family representing a complex group of type 1 transmembrane receptor tyrosine kinase (RTK) with differing ligands. The EGF family consists of four members and collectively the human epidermal growth factor receptor gene family members are designated *EGFR/ERBB1/HER1*, *ERBB2/HER2*, *ERBB3/HER3* and *ERBB4/HER4* [35]. The extracellular domain (ECD) of ERBB receptors has high structural homology although they bind selectively within a group of 11 peptide growth factor members that includes Neuregulin 1 and 2 (NRG1/NRG2) both ERBB3 ligands. [35–39]. Although the complex signalling network of ERBB receptors commonly activate the mitogen activated protein kinase (MAPK) pathway and the phosphatidylinositide 3-Kinase (PI3K) pathway [40–43], ERBB3 efficiently activates the PI3K pathway [44] due to the presence of multiple p85 binding sites in its tyrosine kinase domain.

Lateral signalling among ERBB's is no more apparent than with receptors ERBB2 and ERBB3 that must heterodimerise with other ERBB members to signal [40] as ERBB3 has a ligand but impaired tyrosine kinase activity [45] and ERBB2 has no known ligand (orphan receptor) but a functional kinase region [46]. Although ERBB3 has long been considered impaired or termed a pseudo-kinase, it does have sufficient, although substantially reduced [47], kinase activity. How ERBB3 is able to activate other ERBB family members with its weak catalytic domain remained elusive until an allosteric mechanism termed an 'asymmetric dimer' enabling trans-autophosphorylation was discovered [48].

ERBB2 and ERBB3 overexpression [49–51], cooperation in neoplastic transformation [44, 52–54] and loss of ERBB3 preventing the progressive transformation of ERBB2-over expressing tumours [55] reinforces ERBB3's pivotal role in ERBB signalling. Early studies revealed ERBB3 as a potential oncogene with overexpression due to possible increased transcription as no gene amplification was observed [56, 57] although recently oncogenic mutations have been reported [58] indicating either ERBB3 or its downstream components should represent a potential target for therapy [59].

ERBB3 is upregulated in a number of human cancers such breast, colon, gastric, ovarian and prostate [33, 60] but seldom reported in veterinary cancers [61–63] although it would appear the instrumental role that ERBB3 may play in some veterinary tumours is yet to be elucidated. DFT1's immunohistochemical expression of ERBB3 led us to postulate that excess extracellular domain (ECD) may circulate in the host's plasma and present itself as a possible candidate biomarker for DFT1. Literature reports five secreted alternative transcripts of ERBB3 present in serum or interstitial fluid [64, 65] which can be detected utilising ELISA methodology.

Our pilot study assessed serum ERBB3 for the for the first time in Tasmanian devils revealing that serum ERBB3 was substantially elevated in the serum of Tasmanian devils with DFT1 compared to those Tasmanian devils without DFT1. Interestingly, the inclusion of some Tasmanian devils with CL in our pilot study revealed that ERBB3 may also be a biomarker for this DFT1, although CL is clinically distinct from DFT1. We identify ERBB3 as a potential biomarker of DFT1 and highlight current literature supporting the therapeutic possibilities that can be directed towards ERBB3 overexpressing tumours that may be helpful in the elimination of DFT1 from the wild.

Materials and methods

Animal ethics statement

Serum and paraffin embedded tissue samples were collected by veterinary staff for the Save the Tasmanian Devil Program (STDP) http://www.tassiedevil.com.au/tasdevil.nsf encompassing health checks, field trapping trips, or autopsy due to animal welfare reasons. All samples were accessed from the Animal Health Laboratory archive and did not require ethics approval.

Tasmanian devil ERBB3 pilot study

A pilot study of thirty-five Tasmanian devils differing in age, sex and geographic location were selected (Table 1) to compare serum ERBB3 levels in clinically healthy Tasmanian devils (CHD), devils with DFT1 and those with CL. The Fifteen CHD'S included both adults (n = 12) and clinically healthy juvenile Tasmanian devils (CHJD, n = 3) 10 months of age. Adults included free range captive (n = 5), captive (n = 3) and wild devils (n = 4). Clinically healthy adults either had no visible disease (ND, n = 8) or had localised skin non-DFT1 dermatopathy (CHDD, n = 4) consisting of two abscesses, a skin tag and localised dermatitis. Eight Tasmanian devils with clinical DFT1 and Twelve Tasmanian devils with CL. Tasmanian devils with

Table 1. Tasmanian devil pilot study individuals.

Devil	Microchip Identification	Laboratory accession	Age (years)	Sex (M/F)	Geographic location	Clinical status
1	982000190997443	13/3712	1	F	Freycinet [a]	CHD
2	982000123211124	13/3683	3	F	Freycinet [a]	CHD
3	982009104963600	13/3680	4	M	Freycinet [a]	CHD
4	982009104860765	13/3713	4	M	Freycinet [a]	CHD
5	982000123130282	13/3716	2	M	Freycinet [a]	CHD
6	982009105111670	09/4200	3	F	West Pencil Pine [b]	CHD
7	982009105849999	09/3957	2	M	Tullah [b]	CHD
8	985154000001063	09/1051	1	M	Cressy [c]	CHD
9	982009104269684	08/1805	2	M	Narawntapu [b]	CHDD
10	982009106039877	10/0156	2	M	Dunalley [b]	CHDD
11	982009104236464	08/0798	1	F	Taroona [c]	CHDD
12	982009104357109	09/2009	4	F	Fern Tree [c]	CHDD
13	985154000001151	09/0451	<1	M	Mt Pleasant [d]	CHJD
14	985154000001142	09/0449	<1	F	Mt Pleasant [d]	CHJD
15	985154000001130	09/0448	<1	M	Mt Pleasant [d]	CHJD
16	982009104841875	12/2065	6	F	West Pencil Pine [b]	DFT1
17	982009106034139	11/0767	2	F	Dunalley [b]	DFT1
18	982009104719592	12/0820	4	F	West Pencil Pine [b]	DFT1
19	982000000122095	12/2095	2	F	Upper Natone [b]	DFT1
20	982000123128645	11/3917	2	M	Hamilton [b]	DFT1
21	982000123216973	11/3918	1	F	Hamilton [b]	DFT1
22	982000123209814	11/4493	2	M	Waratah [b]	DFT1
23	000000000130406	13/0406	2	F	Mangalore [b]	DFT1
24	NC	11/0650	7	F	Mole Creek [c]	CL
25	985120016024404	11/4290	8	F	Mt Pleasant [c]	CL
26	982009106314654	10/4001	8	M	Taranna [c]	CL
27	982009106585887	10/3765	5	F	Calder [b]	CL
28	982009104789818	14/0034	6	F	Cressy [c]	CL
29	NC	08/4048	4	F	Circular Head [b]	CL
30	982009100786171	09/0402	6	F	Mt Pleasant [c]	CL
31	982009101694833	10/1013	6	F	Richmond [c]	CL
32	982009104910854	13/0518	6	F	Cressy [c]	CL
33	NC	09/3035	5	F	South Riana [b]	CL
34	NC	11/1615	6	F	Mole Creek [c]	CL
35	982009104873582	13/3714	4	F	Freycinet[a]	CL*

NC not microchipped, CHD clinically healthy devil, CHDD clinically healthy devil with dermatopathy, CHJD clinically healthy juvenile devil, DFT1 devil facial tumour 1, CL cutaneous lymphoma

[a] Free range enclosure

[b] Wild devil

[c] Captive devil

[d] captive juvenile

* no tissue diagnosis.

https://doi.org/10.1371/journal.pone.0177919.t001

CL were included in the study as a severe skin condition recognised clinically but very distinct from DFT1. All dermatopathies, DFT1 and CL were confirmed histologically by the Animal Health Laboratory.

Tasmanian devil serum sample and collection

Blood samples from Tasmanian devils (Table 1) were collected by wildlife veterinarians through jugular venepuncture, whilst the animals were restrained by a trained field officer. Ten millilitres of blood was collected in sterile serum separation tubes, stored on ice for transport to the laboratories, centrifuged and serum removed for archival storage at -20°C. Serum samples were retrieved from the frozen archive and thawed at room temperature immediately before analysis.

Histology

Tasmanian Devil tissues were fixed in 10% Neutral Buffered Formaldehyde (Confix, ACFC, Australian Biostain, Traralgon, Victoria, Australia) for 24 hours and selected tissues were cassetted and processed overnight using a standard 15 hour overnight procedure in the TP1050 tissue processor (Leica Microsystems, Wetzlar, Germany). Tissues were orientated on the EG1160 (Leica), embedded in paraffin wax (Surgipath Paraplast, 39601006, Leica) and sectioned at 3 microns using Leica RM2245 microtome and adhered to microscope slides (Menzel Glaser, Braunschweig, Germany) for 20 minutes at 60°C. Sections were deparaffinised, rehydrated and stained using Jung autostainer XL (Leica) for Haematoxylin (Harris' Haematoxylin, AHHNA, Australian Biostain) and Eosin, dehydrated cleared and mounted in CV Mount (Leica, 046430011).

Immunohistochemistry

Archival Tasmanian devil tissues and tumours were sectioned at 3 microns, floated onto Superfrost plus slides (Menzel Glaser) and subjected to standard deparaffinisation and rehydration techniques using an automated stainer (Leica). Antigen retrieval in tissue sections was conducted in citrate buffer at pH 6.0 (Reveal Decloaker, Biocare Medical, California, USA) at 120°C for 8 minutes using a Pascal pressure chamber (Dako, Glostrup, Denmark) then cooled to 20°C. Endogenous peroxidase activity was quenched using 3% hydrogen peroxide (Ajax Finechem, Sydney, Australia, 260) in methanol (Ajax, 723) for 30 minutes. Detection of primary antibodies was achieved using Mach1 Universal HRP-Polymer detection kit (Biocare Medical, California, USA, M1U539GL10). Protein block (Background Sniper BS966L10) was applied for 20 minutes prior to application of primary antibodies. Monoclonal rabbit anti-human ERBB3 (Abcam, clone SP71, ab93739, internal region) was diluted 1:50 with antibody diluent (Dako, S0809) and applied to both devil tumour and normal devil control tissues at room temperature for 30 minutes. Negative control was omission of primary antibody with buffer substitution. Universal HRP-polymer was applied for 30 minutes (MRH538L10) followed by 1 drop of Betazoid DAB Chromogen 3,3 Diaminobenzidine (BDB900G) in 1ml of substrate buffer (DB900) applied for 4 minutes. Tris buffered saline (Biocare Medical, TWB945) was used to rinse between all steps. Slides were rinsed, stained with Carazzi's Haematoxylin for 5 minutes, washed for 3 minute in tap water, dehydrated, cleared and mounted in CV mount. Sections were viewed under light microscopy using Olympus BX41 (Olympus corporation, Tokyo, Japan) and selected areas were photographed using an Olympus digital camera (DP20).

ERBB3 ELISA assay

Serum ERBB3 levels were measured using the RayBio anti-human ERBB3 ELISA Kit (ELH-ERBB3, RayBiotech Inc, GA, USA) according to manufacturer's instructions. Briefly, serum samples were diluted 1/5 in Assay Diluent A and 100 uL of standard or diluted sample

were added in duplicate to wells of a 96 well assay plate and incubated for 24 hrs at 4°C. The supernatant was removed and wells were washed 4 times with 300 uL of 1X wash solution using an Immunowash 1575 (BioRad Laboratories, CA, USA). One hundred microliters of prepared biotinylated anti-ERBB3 was added to each well and the assay plate incubated for 1 hour at room temperature. The assay plate was washed as described after which 100 uL of prepared HRP-streptavadin conjugate was added to each well and the assay plate incubated for 45 minutes at RT. The assay plate was again washed as described and 100 uL of TMP substrate was added and the plate incubated for 30 minutes at room temperature in the dark, after which 50 uL of stop reagent was added to each well. The absorbance of each well was measured at 450 nm using a Tecan Infinite M200 microplate reader (Tecan, Salzburg, AUT).

Data analysis

The ELISA standard curve was plotted using Prism v5 (GraphPad, CA, USA) and results for each serum interpolated and corrected for dilution. The significance of differences in serum ERBB3 between groups was determined using a Kruskal-Wallis test with Dunn's Multiple Comparison utilizing Prism v5 (GraphPad, CA, USA).

Results

Histology and Immunohistochemstry

DFT1 histology (Fig 1A) and Haematoxylin and Eosin demonstrates small round cells with indistinct cell membranes arranged in cords and packets. ERBB3 IHC on average revealed moderate to strong expression in 75% of cells in both primary and secondary DFT1 tumours in cytogenetically determined strains 1 to 5 of DFT1. Typical granular cytoplasmic expression (Fig 1B) demonstrated by DFT1 strain 3 cells with small and large aggregates noted. Higher magnification (Fig 1C) shows accumulation in and around vacuolar structures within the cytoplasm. In sections of devil skin and subcutous (Fig 1E), peripheral nerve was seldom positive for ERBB3 (red arrow) in keeping with downregulation of ERBB3 in the adult in contrast to DFT1 ERBB3 expression (black arrow). ERBB3 expression was noted in Tasmanian devil lymphoid follicle (Fig 1F) where cytoplasmic expression of ERBB3 is present in both T (germinal centre) and B (mantle) cells. Devils with CL were not included in the ERBB3 immunohistochemical staining. Trigeminal nerve section (Fig 1I) showed ERBB3 expression in nerve bodies (black arrow) and occasional ERBB3 expression in the adaxonal area (red arrows) but generally small myelinated nerves were negative. Positive control included devil bowel (Fig 1G) which exhibited a similar expression pattern to human ERBB3 and negative controls DFT1 (Fig 1D), bowel (Fig 1H) and Trigeminal nerve (Fig 1J). The monoclonal rabbit anti-human ERBB3 clone SP71 is a synthetic peptide corresponding to an internal sequence of Human ERBB3. Although the exact sequence is a proprietary secret ERBB3 sequence alignment between Human and Tasmanian devil in this region has high homology (S1 Fig. ERBB3 Orthologue protein alignment).

Serum ERBB3 in Tasmanian devils

Serum ERBB3 levels are shown in Table 2 and graphically in Fig 2. Serum ERBB3 in the Fifteen Tasmanian devils without neoplasia (devils 1–15 includes CHD,CHDD and CHJD) ranged from <30–663 pg/ml with a median of 32 pg/mL (30–220; interquartile range). Serum ERBB3 levels in the eight Tasmanian devils (devils 16–23) with clinical DFT1 ranged from 766–18,254 pg/ml with median of 3051 pg/mL (1060–10879; interquartile range. In the twelve Tasmanian devils with cutaneous lymphoma (devils 24–35) serum ERBB3 levels ranged from <30–20,021 pg/ml with a median of 1485 pg/mL (289–7901; interquartile range).

Discussion

ERBB3 in devils without DFT1

Fifteen Tasmanian devils without neoplasia (twelve adults either wild caught, free range or captive enclosures and three captive juveniles encompassing CHD, CHDD and CHJD) were studied with an average serum ERBB3 of 32 pg/ml. Collectively, CHD Tasmanian devils serum ERBB3 levels ranged from <30–663 pg/ml which could be considered representative of the reference range for Tasmanian devils. Wild caught devils 6 and 7 were unremarkable and had serum ERBB3 levels <30 pg/ml however devil 9 (220 pg/ml) and devil 10 (92 pg/ml) both recorded skin abscesses. The ERBB3 levels in the CHDD group (devils 9, 10, 11 and 12) ranged from <30–220 pg/ml all had a small isolated dermatopathy such as abscess (devil 9), pyogranuloma (devil 10), skin tag with associated inflammation (devil 11) and small focus of dermatitis (devil 12) all recorded a low serum ERBB3 levels of <92 pg/ml. The CHJD (devils 13, 14 and 15) approximately 10 months old had an unremarkable clinical history that indicated serum was collected for a health check only, reflected in the low serum ERBB3 level of <30 pg/ml.

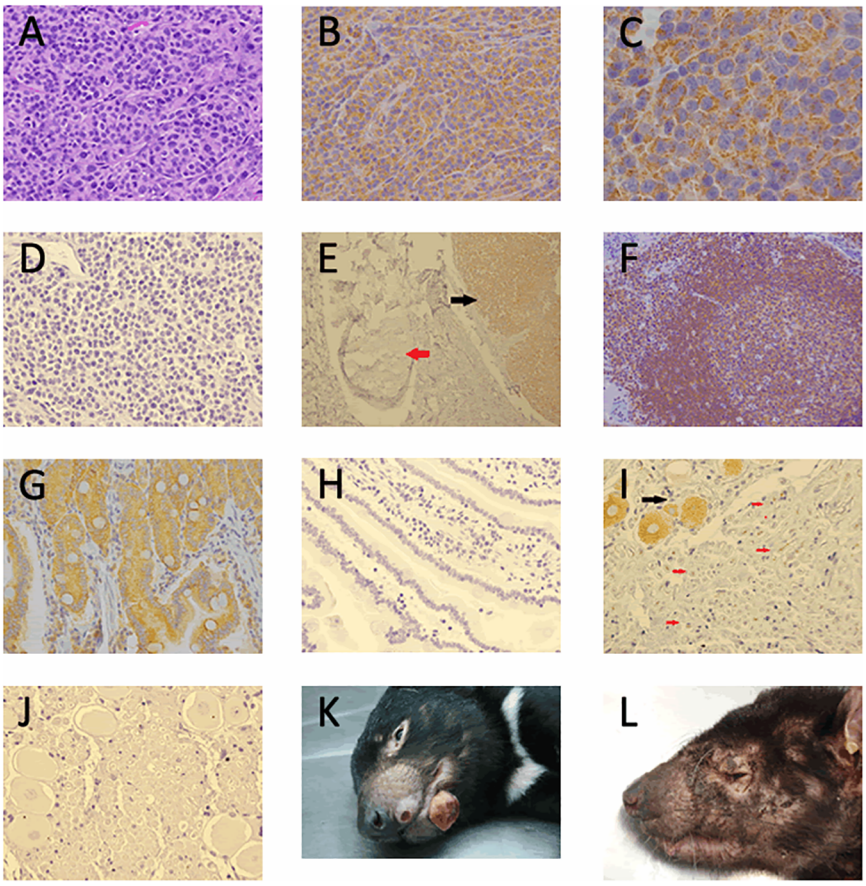

Fig 1. DFT1 staining and skin manifestation. (A) Haematoxylin and Eosin stained DFT1 x40, (**B)** ERBB3 Immunohistochemical expression in DFT1 strain 3 x40, (**C)** ERBB3 immunohistochemical expression in DFT1 strain 3 x100, (**D)** DFT1 negative control, (**E)** Tasmanian devil skin and subcutis section with peripheral nerve (red arrow) and DFT1 (black arrow) x10, **(F)** Tasmanian devil lymph node ERBB3 expression lymphoid follicle x20, (**G)** Tasmanian devil bowel ERBB3 positive control x40, (**H)** ERBB3 IHC negative control bowel, (**I)** trigeminal nerve shows ERBB3 positive nerve body (black arrow) and occasional adaxonal ERBB3 positivity (red arrows) x40, (**J)** ERBB3 IHC negative control trigeminal nerve, (**K)** Tasmanian Devil gross appearance of DFT1. Photo credit: DPIPWE archive, (**L)** Tasmanian devil gross appearance cutaneous lymphoma. Photo credit DPIPWE archive.

https://doi.org/10.1371/journal.pone.0177919.g001

Table 2. Tasmanian devil serum ERBB3 and clinical history.

Devil	Serum Erbb3 (pg/ml)	Weight (Kg)	Serum transit (days)	clinical history	BCS (0–5)	DFT1 strain	DFT1 1° N° (range cm)	Mets N°
1	155	N/A	1	CHD, NAD				
2	663	N/A	1	CHD, Localised alopecia				
3	207	OW	1	CHD, Multiple punctures				
4	313	N/A	1	CHD, Multiple punctures				
5	291	N/A	1	CHD, Multiple minor wounds				
6	<30	N/A	1	CHD, Few wounds, lactating				
7	<30	N/A	2	CHD, N/A				
8	<30	6	1	CHD, Great condition				
9	220	10.5	1	CHDD, Abscess/scab on face				
10	92	N/A	2	CHDD, Abscess left neck.				
11	<30	4.7	1	CHDD, Skin tag on left ear				
12	<30	N/A	1	CHDD, Dermatitis upper flank				
13	<30	4.2	1	CHJD, Health check				
14	32	3.4	1	CHJD, Health check				
15	<30	4.6	1	CHJD, Health check.				
16	18,254	N/A	1	DFT1, weak	2	2	2 (1.0–2.5)	3
17	999	6.1	3	DFT1, Reared 4 young	2	3	4 (1.0–1.5)	5
18	11,090	4.8	1	DFT1, Poor body condition	1–2	1	4 (2.0–3.0)	1
19	1903	3.7	1	DFT1, Emaciated disorientated	0	1	2 (1.6–5.2)	10
20	10,247	10	3	DFT1, Multiple lesions	3	2	4 (1.0–2.0)	2
21	1241	5	3	DFT1, Poor body condition	2.5	2	3 (1.0–1.5)	1
22	4198	9.3	4	DFT1, Advanced DFT1	2	4	7 (1.0–2.5)	0
23	766	N/A	1	DFT1, Emaciated	2	1	7 (1.0–4.7)	1
24	4383	6.7	1	CL, Generalised alopecia	N/A			
25	<30	8.2	1	CL, cutaneous plaques chest	N/A			
26	<30	8.0	1	CL, percutaneous plaque	N/A			
27	2008	5.9	1	CL, Skin lesions	N/A			
28	837	5.9	1	CL, Alopecia	Poor			
29	9703	5.3	1	CL, Generalised alopecia	Poor			
30	2403	8.2	1	CL, Alopecia ventrally	N/A			
31	536	7.4	1	CL, Alopecia left neck, pouch	N/A			
32	962	6.7	1	CL, Alopecia ventrally	N/A			
33	11,837	5.4	1	CL, Widespread alopecia	1–2			
34	207	5.7	1	CL, Multifocal dermatitis, cutaneous lump (acanthoma)	Poor			
35	20,021	N/A	1	CL, Multifocal alopecia	N/A			

N/A not available, NAD no abnormality detected, OW over weight, BCS—body condition score, DFT1 strain–cytogenetically determined strain, DFT1 1° No–number and size of primary tumours recorded, Mets No—number of metastasis recorded, CHD clinically healthy devil, CHDD clinically healthy devil with dermatopathy, CHJD clinically healthy juvenile devil, DFT1 devil facial tumour 1, CL cutaneous lymphoma

https://doi.org/10.1371/journal.pone.0177919.t002

Further assessment of data and clinical history (Table 2) revealed that four out of five Tasmanian devils from the Freycinet free range enclosure (devils 1–5) had higher serum ERBB3 ranging from 155–663 pg/ml compared to most other clinically healthy devils having serum ERBB3 levels <30 pg/ml. The Freycinet free range enclosure (FRE) consists of a 22 Hectare natural reserve that creates living conditions that are more similar to the wild than traditional captive conditions. The structure is fenced completely enclosing an insurance population of

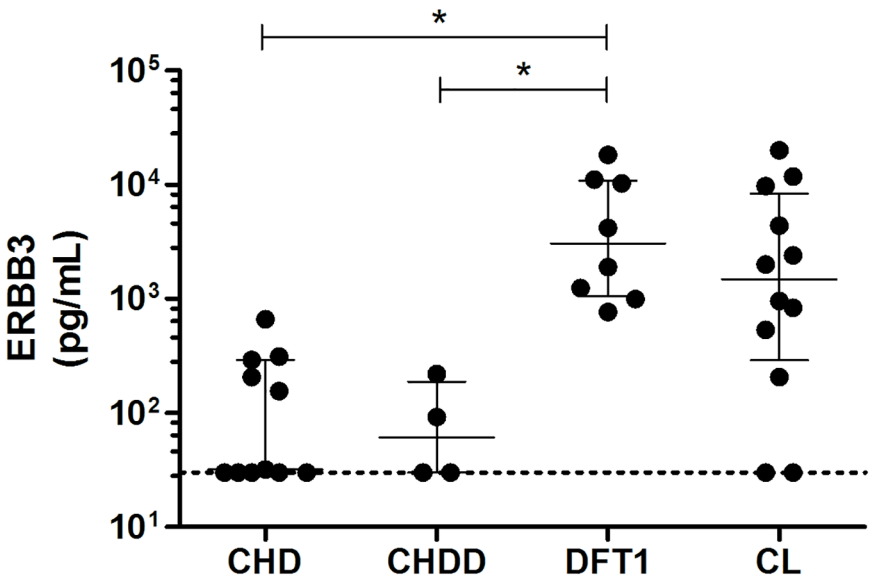

Fig 2. Serum ERBB3 levels in Tasmanian devils. Serum ERBB3 levels were measured by ELISA in clinically healthy Tasmanian devils CHD (n = 11), clinically healthy Tasmanian devils with dermatopathy CHDD (n = 4), clinically diagnosed DFT1 (n = 8) and those with cutaneous lymphoma CL (n = 12). Horizontal dashed line indicates the limit of detection of the ELISA assay at 30 pg/mL. Results of individual devils are shown with the median and interquartile range identified by the whiskers. Significance testing using a Kruskal-Wallis test with Dunn's Multiple Comparison Testing shown with * representing $p < 0.05$.

https://doi.org/10.1371/journal.pone.0177919.g002

healthy devils with density caped to approximately one devil per hectare. This type of enclosure allows devils the opportunity to compete at feeding and breeding times and bite wounds are therefore common (David Schaap, personal communication). In contrast, captive devils are housed in small enclosures that measure approximately 100 m^2 containing capped at one devil per 100 m^2.

We noted that skin injuries were commonly recorded although no abnormality was noted for devil 1, alopecia bilaterally around the hind limbs and flank was present on one mother due to her 3 pouch young (devil 2) and multiple puncture wounds were present on the remainder (devils 3, 4 and 5). Given that these devils were otherwise clinically healthy it would suggest that skin wounds caused by biting may contribute to some elevation in the serum ERBB3 of Tasmanian devils. There is also the possibility that simply being a Tasmanian devil living in a free range enclosure as opposed to wild populations may in itself be contributory to elevation in serum ERBB3 due to more frequent devil-devil engagement. Our results indicate that Tasmanian devils without injuries or an isolated skin lesion have serum ERBB3 levels <30 pg/ml whereas Tasmanian devils with multiple injuries or large abscesses have serum ERBB3 levels ranging from 92–663 pg/ml. Together, these results suggest that cancer-free Tasmanian devils have a serum ERBB3 range of <30–663 pg/ml.

ERBB3 in devils with DFT1

All devils with DFT1 were wild caught and all subjected to field autopsy with most serum samples reaching the laboratory within one to three days. We assessed the available clinical history (Table 2) including animal weight, body condition score (BCS 1–5) where 1 = emaciated, 2 = moderately thin, 3 = average, 4 = good and 5 = obese (Sarah Peck, personal communication), number of primary and metastatic DFT1's and cytogenetic strain ensuring the consideration of any factors that may contribute to the ERBB3 range in DFT1 affected Tasmanian

devils. No correlation was established between levels of ERBB3 and extent of DFT1 when comparing the number and size of primary DFT1 lesions and any metastatic disease (see Table 2). For example, the devil with the highest serum ERBB3 of 18,254 pg/ml (devil 16), had 2 primary lesions with 3 metastases whereas the lowest serum ERBB3 of 766 pg/ml (devil 23) had seven primary DFT1 lesions and one metastasis. No correlation was established between serum ERBB3 levels and the BCS as most were low (BCS 1–2) with only one devil (devil 20) having a BCS of three out of five, indicating average body condition. Cytogenetic strain did not appear to correlate to serum ERBB3 levels and reflects the immunohistochemical findings that ERBB3 expression was present in all cytogenetic strains of DFT1. Our results indicate that Tasmanian devils with DFT1 have elevated serum ERBB3 levels compared to clinically healthy Tasmanian devils ranging from 766–18,254 pg/ml and that the extent of DFT1 does not readily correlate directly with the serum ERBB3 levels. Further investigations beyond the pilot study encompassing a larger study group of Tasmanian devils with advanced DFT1 and metastases would be necessary to establish any relationship with serum ERBB3 and the extent of DFT1.

ERBB3 in devils with cutaneous lymphoma

We included Tasmanian devils with cutaneous lymphoma (CL) in the study for two reasons. Firstly, they were non-DFT1 devils with a severe skin condition that can affect the facial regions and secondly, the disease presentation of alopecia, excoriation and thickened plaques is distinct from DFT1 (Fig 1E and 1F). Our results revealed that some Tasmanian devils with CL had elevated serum ERBB3 levels, a result that was most unexpected. Although ERBB3 immunohistochemistry on Tasmanian devils with CL was beyond the scope of this research, ERBB3 Immunohistochemical staining of Tasmanian devil lymph node (Fig 1D) did reveal ERBB3 expression in the lymphoid follicle where cytoplasmic expression of ERBB3 is present in both T (germinal centre) and B (mantle) cells. CL devils were in the older age bracket ranging from 4–8 years where the maximum age of a wild devil would be considered 5–6 years (Sarah Peck, personal communication). Bodyweights ranging from 5.4–8.2 Kg compared to the mean weight of 6.6Kg for female and 8.3Kg for male [66] shows possible female underweight wild devils and overweight captive devils. Age or weight did not appear to correlate to the broad range of serum ERBB3 of 30–20,021 pg/ml. Interestingly, 11 of the 12 devils with CL were female. We noted that devils with widespread alopecia (devils 24, 29, 33 and 35), did exhibit increased serum ERBB3 levels ranging from 4383–20,021 pg/ml, suggesting that the severity of CL manifesting clinically as widespread alopecia may contribute to increased serum ERBB3 levels. Together, the elevated serum ERBB3 results in devils with CL is unlikely to cause confusion with DFT1 as CL tends to affects devils in the older age group and the clinical signs of CL are also distinct from DFT1 in established disease. Additionally, if elevated serum ERBB3 levels in Tasmanian devils indicative of CL could be established (pre-clinical) this would improve the healthy captive breeding populations of Tasmanian devils to ensure survival of the species by excluding these devils from this program.

Potential source of serum ERBB3

The capture and detection of antibody in our ELISA assay is selective for the extracellular domain (ECD) of transmembrane ERBB3 in serum or plasma, thus ERBB3's ECD is cleaved and shed from the plasma membrane would be a natural assumption. In contrast the ERBB3 receptor is internalised, although very slowly, for negative regulation and inactivation [67–71] utilising pathways such as caveolin or micropinocytosis and clathrin-and caveolin independent pathways [72, 73]. ERBB3 has also been shown to be endocytosed independent of phosphorylation and without ligand in clathrin-dependent manner [74]. ERBB3 is degraded by

proteasomes catalysed by two E3 ubiquitin ligases; NRDP1 (Neuregulin Receptor Degradation Protein -1) [75], now known as RNF41 (Ring Finger 41, E3 Ubiquitin Protein Ligase) [76–78], and NEDD4 (Neural Cell Precursor Expressed, Developmentally Down-regulated 4, E3 Ubiquitin Protein Ligase) [79] that regulate steady-state ERBB3 levels influencing NRG1 signalling.

Defective internalisation, recycling and degradation of cell surface proteins and ligands is an emerging feature of cancer [80]. It is therefore conceivable that DFT1 is subjected to the same dysregulation and inefficient degradation and recycling resulting in over expression of ERBB3 receptor at the plasma membrane and subsequent detectable levels of serum ERBB3. While dysregulated endocytosis, deregulation and recycling may theoretically account for excess ERBB3 ECD detectable in serum, secreted isoforms of ERBB3 must also be considered as an alternative explanation for the presence of excess ERBB3.

As well as functional transmembrane forms, secreted soluble forms of Epidermal Growth Factor Receptors have been well documented for ERBB1 [81–84], ERBB2 [85–88] and ERBB4 [89–91]. Alternative transcripts for ERBB3 resulting in naturally occurring soluble truncated isoforms including a 1.4 kb transcript of ERBB3 in gastric cancer cell lines [64] and an additional four novel transcripts (1.6, 1.7, 2.1, and 2.3kb) from ovarian cancer cell lines [65] encouraged researchers to identify these secreted isoforms of ERBB3 in Prostate [92–95], liver [96], breast [97, 98] and squamous cell carcinoma [99]. ERBB3 isoforms have also been expressed intracellularly in breast cancer cell lines [97] as well as in the nucleus of Schwann cells [100, 101], prostate [102–104] and breast [105, 106]. Secreted ERBB3 isoform p85 has been shown to inhibit the action of its ligand Neuregulin [98, 107], nuclear translocations act as co-transcriptional activators [108], possible post-translation modification and the tumour micro-environment are instructive to serum ERBB3 secretion from the cell [96] and functions yet to be determined.

The antigenic peptide used for this assay is located within the N-terminal domain of the full length ERBB3 protein. Full length ERBB3 translates into a 180 kDa protein whereas ERBB3 transcripts, created by intron read through and alternative polyadenylation signals result in serum ERBB3 isoforms translating into various proteins ranging in size from 22–75 kDa [109]. Secreted isoforms such as ERBB3-S (1.4kb, 140aa homologous to the N terminus and a 43aa unique carboxy terminal sequence) equates to approximately half of domain I, p50 (1.6kb, 351aa homologous to the N terminus and a 30aa unique carboxy terminal sequence) equates to domain I, II and some of domain III, p45 (1.7kb, 310aa homologous to the N terminus and a 2aa unique carboxy terminal sequence) equates to domain I, II and some of domain III, p85 (2.1kb, 519aa homologous to the N terminus and a 24aa unique carboxy terminal sequence) equates to domain I, II,III and some of domain IV, p75 (2.3kb, 474aa homologous to the N terminus and a 41aa unique carboxy terminal sequence) equates to domain I, II and III [64, 65, 109] ERBB3 isoforms have been detected by a number of methods such as immunoprecipitation [65, 97, 107], immunohistochemistry [92] and ELISA [94–96]. Isoforms that have been detected using ELISA assays include p45 sERBB3 utilising a capture antibody of sequence aa20-643 (detection antibody sequence was not recorded) [94, 95] and 40-50kDa secreted isoforms (possible p45/p50) utilising both capture and detection antibodies with a sequence aa20-643 [96]. The Raybio ELISA kit utilised in our research uses a capture and detection antibody of sequence aa20-643 (personal communication Raybio) which accounts for most of the extracellular domain of ERBB3 and therefore would be able to capture and detect both truncated isoforms as well as the transmembrane ERBB3.

The correlation of serum levels with disease severity and progression would be the foundation of a good biomarker [96] as well; the expected biomarker should be in excess when compared to clinically healthy individuals [81] or possess additional qualities such as theranostic and tertiary prevention [84]. The use of serum ERBB's as an indicator of human cancer

appears useful however, its prognostic and theranostic value remains controversial and continued investigations will be required [81–96, 99]. The development of a diagnostic test for preclinical DFT1 would assist in the field operations if individuals could be identified before they become infectious[110], therefore application of serum ERBB3 as a diagnostic biomarker of DFT1 has great potential. The simplicity of the ELISA Serum ERBB3 methodology is easily incorporated into routine batch testing or rapid turnaround of results for urgent cases if required. Our research suggests that serum ERBB3 can be used as a biomarker for DFT1 and CL irrespective of transmembrane or truncated forms being detected in the serum of affected animals and therefore the potential of serum ERBB3 as a biomarker of early DFT1 detection should be explored.

Schwann cell neoplasms

ERBB3 is crucial to the sequential transition from precursor to immature and finally mature Schwann cells where ERBB3 is down-regulated as myelination proceeds [111]. The adult peripheral nervous system requires maintenance when injured and the NRG1/ERBB system is crucial to Schwann cell dedifferentiation, proliferation, and subsequent regeneration and remyelination where ERBB3 and NRG1 is upregulated and only switched off after axon regeneration illustrating the plasticity of the Schwann cell [112–114]. Peripheral nerve sheath tumours [neurofibroma, malignant peripheral nerve sheath tumours (MPNST)] and schwannoma arise from the Schwann cell lineage and can be genetically characterised as Neurofibromas (either dermal or plexiform) and MPNST's [Neurofibromatosis 1 (NF1)], or Schwannomas [Neurofibromatosis 2 (NF2)], Schwannomatosis and Carney complex type 1. Although distinct characterisation of these complex diseases is possible, frequent overlapping features make diagnosis difficult and must also include other tumours with a Schwannian component such as Neuroblastic and Granular Cell Tumours [reviewed in [115–119]]. Veterinary Schwann cell neoplasms have been recorded [120–124] although ERBB3 expression in Schwann cell neoplasia has not previously been reported in veterinary literature. ERBB3 receptor has been expressed in human Schwann cell neoplasms including neurofibroma, MPNST, Schwannoma, neuroblastic [125, 126] and ganglioneuroma (GN) tumours [127]. Interestingly, the down regulation of MHC class 1 and 2 molecules in a MPNST cell line [128] contrasting normal expression [129, 130] may indeed be similar to the MHC class 1 downregulation of DFT1 [19–21] resulting in defective antigen processing and presentation of the malignant Schwann cell neoplasm.

ERBB3 as a therapeutic target

Despite evidence for multiple resistance mechanisms for existing therapeutic targeting of ERBB1/2 [131–141] numerous researchers have over the last decade explored the potential of ERBB3 as a therapeutic target [reviewed in [33, 60, 142–150]] using monoclonal antibodies [57, 151–176], histone inhibitors [177], TKI [178], surrobodies [179], locked nucleic acid (LNA)-based ERBB3 antisense oligonucleotide (ASO) [180], peptide mimics and vaccine [181], anti-anginal drug [182] and disulphide disrupting agent [183].

However, managing wildlife disease is considerably more difficult than human disease because of limited data, the effect of the disease on the host and the transmission of disease within a dynamic population makes it difficult to model [184]. Previous efforts to eradicate DFT1 from wild populations by selective culling has proven unsuccessful because of the frequency-dependent transmission of DFT1 and the latency period [110, 184, 185]. TKI's as a therapeutic approach may be limited due primarlily to the early observation that kinase region of ERBB3 had substantialy reduced activity, however cancer immunotherapy broadly categorised as passive (including monoclonal antibodies, Cytokines, adoptive cell transfer) or active

(including therapeutic cancer vaccine, immune checkpoint inhibitors) remains optimistic [186–191]. Many of these successful human immunotherapeutics do hold similar promise in veterinary medicine [192–194] however, drug administration to wild Tasmanian devils is very different from the clinical setting of human and companion animals and therefore treatments such as adoptive cell transfer would be difficult to implement. The fact that DFT1 expresses tumour associated antigens (TAA's) such as ERBB3 invites the application of monoclonal antibodies and therapeutic cancer vaccines as prospective treatments. The passive administration of monoclonal antibodies to ERBB3 primarily focused on blocking receptor epitopes are still experimental [57, 151–176] and any humanised anti-ERBB3 would certainly have to be become species specific (devil anti-ERBB3) to prevent adverse immunologic reactions [195]. Very few monoclonal antibodies have been developed in veterinary oncology although two caninised antibodies anti-ERBB1 [196] and anti-CD20 [197] show promise. Therapeutic cancer vaccination modalities applicable to wildlife include antigen delivery vaccines that utilise inactivated cancer cells (autologous or allogenic) or peptide vaccines that mimic antigen sequences. Results using an inactivated cancer cell vaccine trial (allogenic DFT1 cell line) are eagerly awaited (http://www.utas.edu.au/news/2015/10/16/19-world-first-trial-of-tasmanian-devil-vaccine-begins-in-the-wild/). Confidence that immunisation can be successful stems from research showing that Tasmanian devils have a competent immune system [21, 198–200] and can produce cytotoxic antibodies [14, 201]. An alternative antigen presentation modality to cancer cell vaccine is a peptide vaccine, where single or multiple amino acid sequences (long or short) representing a defined antigen is combined with adjuvant to elicit an immune response [202]. Development of just a single ERBB3 peptide vaccine can be found in the literature [181] however, peptide vaccines targeting ERBB1 [203, 204], ERBB2 [205–207] or both ERBB1/2 [208] including monoclonal antibody against tyrosine related protein 1 (TRP-1) and altered peptide sequence to gp100 for mouse melanoma [209] all show promise. Overcoming self-tolerance is a major hurdle, one such strategy is the use of Xenoantigens, that is the exact same antigen but from a different species that has considerable sequence homology, differing only by several amino acids which appear to the host as altered epitopes or as "altered self" and therefore tolerance can be broken causing a T-cell response against the endogenous self-antigen [210]. Veterinary xenogeneic vaccinations include a DNA plasmid vaccine encoding human Tyrosinase (TYR) [211] the only veterinary therapeutic tumour vaccine licensed by the United States department of Agriculture (USDA) for the use of oral and digital melanoma, now marketed as Oncept^{TM}.

Recent investigations reveal that the tumour microenvironment of metastatic DFT1 expressed B7-H1 and DFT1 cell lines could upregulate B7-H1[212]. Immune-suppressive tumour microenvironment created by tumour cells that escape 'immunoediting' allowing tumour growth and proliferation [213] where certain checkpoint pathways will be used advantageously by tumour cells to confer immune resistance [214]. Hence, checkpoint blockades (monoclonal antibodies) targeting Programmed Cell Death 1 (PD1 or PDCD1) and its ligand PD-L1 (B7-H1) and Cytotoxic T Lymphocyte Antigen 4 (CTLA-4) are now attractive therapeutical targets [215]. Recent views consider cancer immunotherapy invaluable although a single treatment mode may be suitable for some cases, more combinatorial approach will be needed for others [216, 217].

Our research has highlighted ERBB3 as a potential therapeutic target however treatment of Tasmanian devils with DFT1 with therapeutic regimes such as chemotherapy and radiotherapy are impractical. However, a combinatorial approach using therapeutic cancer vaccines including inactivated allogenic DFT1 cancer vaccine, ERBB3 monoclonal antibody, ERBB3 Peptide or xenogeneic vaccine in combination with anti-immune checkpoint blockade therapy would be easier to implement in the field as well as providing a sustained immunological response against DFT1.

Conclusion

ERBB3 had previously avoided scrutiny due to its kinase inactivity; however, ERBB3 has now been the subject of intense investigation over the past decade and is now recognised as a potent partner of the epidermal growth receptor family. ERBB3 upregulation during developmental, dedifferentiation and regenerative processes encapsulates the Schwann cell's inherent plasticity and imparts certain characteristics of malignant transformation advantageous to transmission of DFT1. Our pilot study has shown for the first time that ERBB3 is consistently expressed immunohistochemically and that ERBB3 is also elevated in the serum of Tasmanian devils with advanced DFT1 and cutaneous lymphoma. Therefore, our research indicates that serum ERBB3 has the potential to be employed as a biomarker of DFT1 or CL in Tasmanian devils to assist conservationists in the management and welfare of Tasmanian devils and species survival. The simplicity of the ELISA Serum ERBB3 methodology is easily incorporated into routine laboratory batch testing and equally applied to include rapid turnaround of results for urgent cases. Extension of this research is necessary to include greater numbers of healthy Tasmanian devils both with and without visible injuries, devils with large and small DFT1 lesions as well as pre-clinical DFT1. This will firmly establish the normal reference range for serum ERBB3 from which potential pre-clinical DFT1 may be identified. In addition, ERBB3 is now recognised as a therapeutic target and therefore the potential exists to consider modes of administration in addition to existing whole cell vaccination such as ERBB3 monoclonal antibody, peptide or xenogeneic vaccines including checkpoint inhibitors. A combinatorial immunotherapeutic approach will enhance cytotoxic destruction, provide long term immunity from DFT1 and therefore eradicate this transmissible tumour from the wild.

Supporting information

S1 Fig. ERBB3 Orthologue protein alignment.
(DOCX)

Acknowledgments

This research was funded by the Dr Eric Guiler Save the Tasmanian Devil Research Grant and we are extremely grateful to Save the Tasmanian Devil Program especially the program manager David Pemberton, University of Tasmania, Department of Primary Industries, Water and Environment and the University of Adelaide for their continued support. We are grateful to all STDP field staff including Colette Harmsen, DPIPWE staff including veterinary officer Sarah Peck and senior keeper David Schaap. Pathologists Jim Taylor, Graeme Knowles, Andrew Davis. Librarians Margaret Quill and Toni Venettacci. Molecular biologists Richard Morrison and Teresa Wilson. Histological Support from Alistair Townsend, Tony Van Galen and Dhirendra Prasad—Royal Hobart Hospital, Mike Burley—Hobart Pathology, Dr Terry Brain and Karen Wolfswinkel—Launceston General Hospital, Jann Brauer—Launceston Pathology and Catherine Marshall—Mt Pleasant laboratories.

Author Contributions

Conceptualization: DH ES.

Data curation: DH.

Formal analysis: DH DK RT.

Funding acquisition: DH SS ES.

Investigation: DH DK RT SS ES.

Methodology: DH DK RT SS ES.

Project administration: DH SS ES.

Resources: DH DK RT SS ES SP.

Supervision: SS ES SP.

Validation: DH DK RT SS ES SP.

Visualization: DH DK RT SS ES SP.

Writing – original draft: DH.

Writing – review & editing: DH DK RT SS ES SP.

References

1. Guiler ER. Tasmanian devils in agriculture. Tasmanian Journal of Agriculture. 1970; 41(2):134-&.
2. Munday BL. Marsupial disease. Proceedings No36 of Course for Veterinarians—Fauna. 1978:335–85.
3. Griner LA. Neoplasms in Tasmanian devils (Sarcophilus harrisii) J Natl Cancer Inst. 1979; 62(3):589–95. PMID: 283288
4. Canfield PJ, Hartley WJ, Reddacliff GL. Spontanious proliferations in Australian marsupials—A survey and review .2.Dasyurids and Bandicoots. J Comp Pathol. 1990; 103(2):147–58. PMID: 2246390
5. Canfield PJ, Cunningham AA. Disease and mortality in Australasian marsupials held at London zoo, 1872–1972 J Zoo Wildl Med. 1993; 24(2):158–67.
6. Ladds P. Pathology of Australian native wildlife. Ladds P, editor. Collingwood, Australia: CSIRO Publishing; 2009. 640 p.
7. Scheelings TF, Dobson EC, Hooper C. Cutaneous T-cell lymphoma in two captive Tasmanian devils (Sarcophilus harrisii) J Zoo Wildl Med. 2014; 45(2):367–71. https://doi.org/10.1638/2013-0217R.1 PMID: 25000700
8. Loh R, Bergfeld J, Hayes D, O'Hara A, Pyecroft S, Raidal S, et al. The pathology of devil facial tumor disease (DFTD) in Tasmanian devils (Sarcophilus harrisii). Vet Pathol. 2006; 43(6):890–5. https://doi.org/10.1354/vp.43-6-890 PMID: 17099145
9. Hawkins CE, Baars C, Hesterman H, Hocking GJ, Jones ME, Lazenby B, et al. Emerging disease and population decline of an island endemic, the Tasmanian devil Sarcophilus harrisii. Biol Conserv. 2006; 131(2):307–24.
10. Chadwick B. Outbreak of facial tumours in Tasmanian devils. Journal of Wildlife Diseases. 2003; 39 (4Supplement):7–8.
11. Pearse AM, Swift K. Transmission of devil facial-tumour disease—An uncanny similarity in the karyotype of these malignant tumours means that they could be infective. Nature. 2006; 439(7076):549-. https://doi.org/10.1038/439549a PMID: 16452970
12. McCallum H, Jones M, Hawkins C, Hamede R, Lachish S, Sinn DL, et al. Transmission dynamics of Tasmanian devil facial tumor disease may lead to disease-induced extinction. Ecology. 2009; 90 (12):3379–92. PMID: 20120807
13. Hamede RK, McCallum H, Jones M. Biting injuries and transmission of Tasmanian devil facial tumour disease. J Anim Ecol. 2013; 82(1):182–90. https://doi.org/10.1111/j.1365-2656.2012.02025.x PMID: 22943286
14. Pye R, Hamede R, Siddle HV, Caldwell A, Knowles GW, Swift K, et al. Demonstration of immune responses against devil facial tumour disease in wild Tasmanian devils. Biology Letters. 2016; 12(10).
15. Karu N, Wilson R, Hamede R, Jones M, Woods GM, Hilder EF, et al. Discovery of Biomarkers for Tasmanian Devil Cancer (DFTD) by Metabolic Profiling of Serum. J Proteome Res. 2016; 15(10):3827–40. https://doi.org/10.1021/acs.jproteome.6b00629 PMID: 27599268
16. Loh R, Hayes D, Mahjoor A, O'Hara A, Pyecroft S, Raidal S. The immunohistochemical characterization of devil facial tumor disease (DFTD) in the Tasmanian Devil (Sarcophilus harrisii). Vet Pathol. 2006; 43(6):896–903. https://doi.org/10.1354/vp.43-6-896 PMID: 17099146

17. Pyecroft SB, Pearse AM, Loh R, Swift K, Belov K, Fox N, et al. Towards a case definition for devil facial tumour disease: What is it? EcoHealth. 2007; 4(3):346–51.
18. Murchison EP, Tovar C, Hsu A, Bender HS, Kheradpour P, Rebbeck CA, et al. The Tasmanian Devil Transcriptome Reveals Schwann Cell Origins of a Clonally Transmissible Cancer. Science. 2010; 327 (5961):84–7. https://doi.org/10.1126/science.1180616 PMID: 20044575
19. Siddle HV, Kreiss A, Tovar C, Yuen CK, Cheng YY, Belov K, et al. Reversible epigenetic down-regulation of MHC molecules by devil facial tumour disease illustrates immune escape by a contagious cancer. Proc Natl Acad Sci U S A. 2013; 110(13):5103–8. https://doi.org/10.1073/pnas.1219920110 PMID: 23479617
20. Siddle HV, Kaufman J. Immunology of naturally transmissible tumours. Immunology. 2015; 144 (1):11–20. https://doi.org/10.1111/imm.12377 PMID: 25187312
21. Woods GM, Howson LJ, Brown GK, Tovar C, Kreiss A, Corcoran LM, et al. Immunology of a Transmissible Cancer Spreading among Tasmanian Devils. J Immunol. 2015; 195(1):23–9. https://doi.org/10.4049/jimmunol.1500131 PMID: 26092814
22. Pearse AM, Swift K, Hodson P, Hua B, McCallum H, Pyecroft S, et al. Evolution in a transmissible cancer: a study of the chromosomal changes in devil facial tumor (DFT) as it spreads through the wild Tasmanian devil population. Cancer Genet. 2012; 205(3):101–12. https://doi.org/10.1016/j.cancergen.2011.12.001 PMID: 22469509
23. Deakin JE, Bender HS, Pearse AM, Rens W, O'Brien PCM, Ferguson-Smith MA, et al. Genomic Restructuring in the Tasmanian Devil Facial Tumour: Chromosome Painting and Gene Mapping Provide Clues to Evolution of a Transmissible Tumour. PLoS genetics. 2012; 8(2).
24. Lachish S, Jones M, McCallum H. The impact of disease on the survival and population growth rate of the Tasmanian devil. J Anim Ecol. 2007; 76(5):926–36. https://doi.org/10.1111/j.1365-2656.2007.01272.x PMID: 17714271
25. McCallum H, Tompkins DM, Jones M, Lachish S, Marvanek S, Lazenby B, et al. Distribution and impacts of Tasmanian devil facial tumor disease. EcoHealth. 2007; 4(3):318–25.
26. Jones ME, Cockburn A, Hamede R, Hawkins C, Hesterman H, Lachish S, et al. Life-history change in disease-ravaged Tasmanian devil populations. Proc Natl Acad Sci U S A. 2008; 105(29):10023–7. https://doi.org/10.1073/pnas.0711236105 PMID: 18626026
27. Hogg CJ, Grueber CE, Pemberton D, Fox S, Lee AV, Ivy JA, et al. "Devil Tools & Tech": A Synergy of Conservation Research and Management Practice. Conserv Lett. 2017; 10(1):133–8.
28. Pye RJ, Pemberton D, Tovar C, Tubio JMC, Dun KA, Fox S, et al. A second transmissible cancer in Tasmanian devils. Proc Natl Acad Sci U S A. 2016; 113(2):374–9. https://doi.org/10.1073/pnas.1519691113 PMID: 26711993
29. Britsch S. The neuregulin-I/ErbB signaling system in development and disease. Advances in anatomy, embryology, and cell biology. 2007; 190:1–65.
30. Schlessinger J. Cell signaling by receptor tyrosine kinases. Cell. 2000; 103(2):211–25. PMID: 11057895
31. Blume-Jensen P, Hunter T. Oncogenic kinase signalling. Nature. 2001; 411(6835):355–65. https://doi.org/10.1038/35077225 PMID: 11357143
32. Lemmon MA, Schlessinger J. Cell Signaling by Receptor Tyrosine Kinases. Cell. 2010; 141(7):1117–34. https://doi.org/10.1016/j.cell.2010.06.011 PMID: 20602996
33. Sithanandam G, Anderson LM. The ERBB3 receptor in cancer and cancer gene therapy. Cancer Gene Ther. 2008; 15(7):413–48. https://doi.org/10.1038/cgt.2008.15 PMID: 18404164
34. Hsieh AC, Moasser MM. Targeting HER proteins in cancer therapy and the role of the non-target HER3. Br J Cancer. 2007; 97(4):453–7. https://doi.org/10.1038/sj.bjc.6603910 PMID: 17667926
35. Roskoski R. The ErbB/HER family of protein-tyrosine kinases and cancer. Pharmacol Res. 2014; 79:34–74. https://doi.org/10.1016/j.phrs.2013.11.002 PMID: 24269963
36. Wilson KJ, Gilmore JL, Foley J, Lemmon MA, Riese DJ. Functional selectivity of EGF family peptide growth factors: Implications for cancer. Pharmacol Ther. 2009; 122(1):1–8. https://doi.org/10.1016/j.pharmthera.2008.11.008 PMID: 19135477
37. Falls DL. Neuregulins: functions, forms, and signaling strategies. Exp Cell Res. 2003; 284(1):14–30. PMID: 12648463
38. Montero JC, Rodriguez-Barrueco R, Ocana A, Diaz-Rodriguez E, Esparis-Ogando A, Pandiella A. Neuregulins and cancer. Clin Cancer Res. 2008; 14(11):3237–41. https://doi.org/10.1158/1078-0432.CCR-07-5133 PMID: 18519747
39. Mei L, Nave KA. Neuregulin-ERBB Signaling in the Nervous System and Neuropsychiatric Diseases. Neuron. 2014; 83(1):27–49. https://doi.org/10.1016/j.neuron.2014.06.007 PMID: 24991953

40. Yarden Y, Sliwkowski MX. Untangling the ErbB signalling network. Nat Rev Mol Cell Biol. 2001; 2 (2):127–37. https://doi.org/10.1038/35052073 PMID: 11252954

41. Citri A, Yarden Y. EGF-ERBB signalling: towards the systems level. Nat Rev Mol Cell Biol. 2006; 7 (7):505–16. https://doi.org/10.1038/nrm1962 PMID: 16829981

42. Warren CM, Landgraf R. Signaling through ERBB receptors: Multiple layers of diversity and control. Cell Signal. 2006; 18(7):923–33. https://doi.org/10.1016/j.cellsig.2005.12.007 PMID: 16460914

43. Li YW, Tennekoon GI, Birnbaum M, Marchionni MA, Rutkowski JL. Neuregulin signaling through a PI3K/Akt/Bad pathway in Schwann cell survival. Mol Cell Neurosci. 2001; 17(4):761–7. https://doi.org/10.1006/mcne.2000.0967 PMID: 11312610

44. Olayioye MA, Neve RM, Lane HA, Hynes NE. The ErbB signaling network: receptor heterodimerization in development and cancer. Embo J. 2000; 19(13):3159–67. https://doi.org/10.1093/emboj/19.13.3159 PMID: 10880430

45. Guy PM, Platko JV, Cantley LC, Cerione RA, Carraway KL. Insect cell-expressed P180(ERBB3) possesses an impaired tyrosine kinase-activity Proc Natl Acad Sci U S A. 1994; 91(17):8132–6. PMID: 8058768

46. Klapper LN, Glathe S, Vaisman N, Hynes NE, Andrews GC, Sela M, et al. The ErbB-2/HER2 oncoprotein of human carcinomas may function solely as a shared coreceptor for multiple stroma-derived growth factors. Proc Natl Acad Sci U S A. 1999; 96(9):4995–5000. PMID: 10220407

47. Shi FM, Telesco SE, Liu YT, Radhakrishnan R, Lemmon MA. ErbB3/HER3 intracellular domain is competent to bind ATP and catalyze autophosphorylation. Proc Natl Acad Sci U S A. 2010; 107 (17):7692–7. https://doi.org/10.1073/pnas.1002753107 PMID: 20351256

48. Zhang XW, Gureasko J, Shen K, Cole PA, Kuriyan J. An allosteric mechanism for activation of the kinase domain of epidermal growth factor receptor. Cell. 2006; 125(6):1137–49. https://doi.org/10.1016/j.cell.2006.05.013 PMID: 16777603

49. Kraus MH, Issing W, Miki T, Popescu NC, Aaronson SA. Isolation and characterization of ERBB3, a 3rd member of the ERBB/epidemal growth factor receptor family: Evidence for overexpression in a subset of human mammary tumours. Proc Natl Acad Sci U S A. 1989; 86(23):9193–7. PMID: 2687875

50. Yarden Y, Peles E. Biochemical analysis of the ligand for the Neu oncogene receptor Biochemistry. 1991; 30(14):3543–50. PMID: 1672825

51. Lemoine NR, Barnes DM, Hollywood DP, Hughes CM, Smith P, Dublin E, et al. Expression of the ERBB3 gene product in breast cancer Br J Cancer. 1992; 66(6):1116–21. PMID: 1333787

52. Alimandi M, Romano A, Curia MC, Muraro R, Fedi P, Aaronson SA, et al. Cooperative signalling of ERBB3 and ERBB2 in neoplastic transformation and human mammary carcinomas Oncogene. 1995; 10(9):1813–21. PMID: 7538656

53. Siegel PM, Ryan ED, Cardiff RD, Muller WJ. Elevated expression of activated forms of Neu/ErbB-2 and ErbB-3 are involved in the induction of mammary tumors in transgenic mice: implications for human breast cancer. Embo J. 1999; 18(8):2149–64. https://doi.org/10.1093/emboj/18.8.2149 PMID: 10205169

54. Holbro T, Civenni G, Hynes NE. The ErbB receptors and their role in cancer progression. Exp Cell Res. 2003; 284(1):99–110. PMID: 12648469

55. Vaught DB, Stanford JC, Young C, Hicks DJ, Wheeler F, Rinehart C, et al. HER3 Is Required for HER2-Induced Preneoplastic Changes to the Breast Epithelium and Tumor Formation. Cancer Res. 2012; 72(10):2672–82. https://doi.org/10.1158/0008-5472.CAN-11-3594 PMID: 22461506

56. Rajkumar T, Gullick WJ. The type 1 growth factor receptors in human breast cancer Breast Cancer Res Treat. 1994; 29(1):3–9. PMID: 7912566

57. Reschke M, Mihic-Probst D, van der Horst EH, Knyazev P, Wild PJ, Hutterer M, et al. HER3 is a determinant for poor prognosis in melanoma. Clin Cancer Res. 2008; 14(16):5188–97. https://doi.org/10.1158/1078-0432.CCR-08-0186 PMID: 18698037

58. Jaiswal BS, Kljavin NM, Stawiski EW, Chan E, Parikh C, Durinck S, et al. Oncogenic ERBB3 Mutations in Human Cancers. Cancer Cell. 2013; 23(5):603–17. https://doi.org/10.1016/j.ccr.2013.04.012 PMID: 23680147

59. Gullick WJ. The c-erb/HER3 receptor in human cancer. Cancer Surv. 1996; 27:339–49. PMID: 8909809

60. Jiang N, Saba NF, Chen ZG. Advances in Targeting HER3 as an Anticancer Therapy. Chemotherapy research and practice. 2012; 2012:817304. https://doi.org/10.1155/2012/817304 PMID: 23198146

61. Kim JH, Im KS, Kim NH, Yhee JY, Nho WG, Sur JH. Expression of HER-2 and nuclear localization of HER-3 protein in canine mammary tumors: Histopathological and immunohistochemical study. Vet J. 2011; 189(3):318–22. https://doi.org/10.1016/j.tvjl.2010.08.012 PMID: 20947393

62. Doster AR, Yhee JY, Kim JH, Im KS, Sur JH. CDX-2 and HER-3 Expression in Canine Gastric and Colorectal Adenocarcinomas. J Comp Pathol. 2011; 145(1):12–9. https://doi.org/10.1016/j.jcpa.2010.11.007 PMID: 21238975

63. Matsuyama S, Nakamura M, Yonezawa K, Shimada T, Ohashi F, Takamori Y, et al. Expression patterns of the erbB subfamily mRNA in canine benign and malignant mammary tumors. J Vet Med Sci. 2001; 63(9):949–54. PMID: 11642281

64. Katoh M, Yazaki Y, Sugimura T, Terada M. c-erbb3 gene encodes secreted as well as transmembrane receptor tyrosine kinase Biochem Biophys Res Commun. 1993; 192(3):1189–97. https://doi.org/10.1006/bbrc.1993.1542 PMID: 7685162

65. Lee H, Maihle NJ. Isolation and characterization of four alternate c-erbB3 transcripts expressed in ovarian carcinoma-derived cell lines and normal human tissues. Oncogene. 1998; 16(25):3243–52. https://doi.org/10.1038/sj.onc.1201866 PMID: 9681822

66. Peck S, Corkrey R, Hamede R, Jones M, Canfield P. Hematologic and serum biochemical reference intervals for wild Tasmanian devils (Sarcophilus harrisii). Vet Clin Pathol. 2015; 44(4):519–29. https://doi.org/10.1111/vcp.12304 PMID: 26613213

67. Roepstorff K, Grovdal L, Grandal M, Lerdrup M, van Deurs B. Endocytic downregulation of ErbB receptors: mechanisms and relevance in cancer. Histochem Cell Biol. 2008; 129(5):563–78. https://doi.org/10.1007/s00418-008-0401-3 PMID: 18288481

68. Sorkin A, Goh LK. Endocytosis and intracellular trafficking of ErbBs. Exp Cell Res. 2009; 315(4):683–96. PMID: 19278030

69. Waterman H, Sabanai I, Geiger B, Yarden Y. Alternative intracellular routing of ErbB receptors may determine signaling potency. J Biol Chem. 1998; 273(22):13819–27. PMID: 9593726

70. Waterman H, Yarden Y. Molecular mechanisms underlying endocytosis and sorting of ErbB receptor tyrosine kinases. FEBS Lett. 2001; 490(3):142–52. PMID: 11223029

71. Baulida J, Kraus MH, Alimandi M, DiFiore PP, Carpenter G. All ErbB receptors other than the epidermal growth factor receptor are endocytosis impaired. J Biol Chem. 1996; 271(9):5251–7. PMID: 8617810

72. Mayor S, Pagano RE. Pathways of clathrin-independent endocytosis. Nat Rev Mol Cell Biol. 2007; 8(8):603–12. https://doi.org/10.1038/nrm2216 PMID: 17609668

73. Le Roy C, Wrana JL. Clathrin- and non-clathrin-mediated endocytic regulation of cell signalling. Nat Rev Mol Cell Biol. 2005; 6(2):112–26. https://doi.org/10.1038/nrm1571 PMID: 15687999

74. Sak MM, Breen K, Ronning SB, Pedersen NM, Bertelsen V, Stang E, et al. The oncoprotein ErbB3 is endocytosed in the absence of added ligand in a clathrin-dependent manner. Carcinogenesis. 2012; 33(5):1031–9. https://doi.org/10.1093/carcin/bgs128 PMID: 22436610

75. Qiu XB, Goldberg AL. Nrdp1/FLRF is a ubiquitin ligase promoting ubiquitination and degradation of the epidermal growth factor receptor family member, ErbB3. Proc Natl Acad Sci U S A. 2002; 99(23):14843–8. https://doi.org/10.1073/pnas.232580999 PMID: 12411582

76. Diamonti AJ, Guy PM, Ivanof C, Wong K, Sweeney C, Carraway KL. An RBCC protein implicated in maintenance of steady-state neuregulin receptor levels. Proc Natl Acad Sci U S A. 2002; 99(5):2866–71. https://doi.org/10.1073/pnas.052709799 PMID: 11867753

77. Bouyain S, Leahy DJ. Structure-based mutagenesis of the substrate-recognition domain of Nrdp1/FLRF identifies the binding site for the receptor tyrosine kinase ErbB3. Protein Sci. 2007; 16(4):654–61. https://doi.org/10.1110/ps.062700307 PMID: 17384230

78. Cao ZW, Wu XL, Yen L, Sweeney C, Carraway KL. Neuregulin-induced ErbB3 downregulation is mediated by a protein stability cascade involving the E3 ubiquitin ligase Nrdp1. Mol Cell Biol. 2007; 27(6):2180–8. https://doi.org/10.1128/MCB.01245-06 PMID: 17210635

79. Huang Z, Choi BK, Mujoo K, Fan X, Fa M, Mukherjee S, et al. The E3 ubiquitin ligase NEDD4 negatively regulates HER3/ErbB3 level and signaling. Oncogene. 2015; 34(9):1105–15. https://doi.org/10.1038/onc.2014.56 PMID: 24662824

80. Mosesson Y, Mills GB, Yarden Y. Derailed endocytosis: an emerging feature of cancer. Nat Rev Cancer. 2008; 8(11):835–50. https://doi.org/10.1038/nrc2521 PMID: 18948996

81. Maramotti S, Paci M, Manzotti G, Rapicetta C, Gugnoni M, Galeone C, et al. Soluble Epidermal Growth Factor Receptors (sEGFRs) in Cancer: Biological Aspects and Clinical Relevance. Int J Mol Sci. 2016; 17(4).

82. Baron AT, Cora EM, Lafky JM, Boardman CH, Buenafe MC, Rademaker A, et al. Soluble epidermal growth factor receptor (sEGFR/sErbB1) as a potential risk, screening, and diagnostic serum biomarker of epithelial ovarian cancer. Cancer Epidemiol Biomarkers Prev. 2003; 12(2):103–13. PMID: 12582019

83. Pitteri SJ, Amon LM, Buson TB, Zhang YZ, Johnson MM, Chin A, et al. Detection of Elevated Plasma Levels of Epidermal Growth Factor Receptor Before Breast Cancer Diagnosis among Hormone

Therapy Users. Cancer Res. 2010; 70(21):8598–606. https://doi.org/10.1158/0008-5472.CAN-10-1676 PMID: 20959476

84. Baron AT, Wilken JA, Haggstrom DE, Goodrich ST, Maihle NJ. Clinical implementation of soluble EGFR (sEGFR) as a theragnostic serum biomarker of breast, lung and ovarian cancer. IDrugs. 2009; 12(5):302–8. PMID: 19431095

85. Baric M, Kulic A, Sirotkovic-Skerlev M, Plavetic ND, Vidovic M, Horvatic-Herceg G, et al. Circulating Her-2/Neu Extracellular Domain in Breast Cancer Patients-Correlation with Prognosis and Clinico-pathological Parameters Including Steroid Receptor, Her-2/Neu Receptor Coexpression. Pathol Oncol Res. 2015; 21(3):589–95. https://doi.org/10.1007/s12253-014-9859-6 PMID: 25367073

86. Lam L, McAndrew N, Yee M, Fu T, Tchou JC, Zhang HT. Challenges in the clinical utility of the serum test for HER2 ECD. Biochim Biophys Acta-Rev Cancer. 2012; 1826(1):199–208.

87. Siampanopoulou M, Galaktidou G, Dimasis N, Gotzamani-Psarrakou A. Profiling serum HER-2/NEU in prostate cancer. Hippokratia. 2013; 17(2):108–12. PMID: 24376312

88. Carney WP. The emerging role of monitoring serum HER-2/neu oncoprotein levels in women with metastatic breast cancer. Lab Med. 2003; 34(1):58–64.

89. Rio C, Buxbaum JD, Peschon JJ, Corfas G. Tumor necrosis factor-alpha-converting enzyme is required for cleavage of erbB4/HER4. J Biol Chem. 2000; 275(14):10379–87. PMID: 10744726

90. Feng SM, Sartor CI, Hunter D, Zhou H, Yang XH, Caskey LS, et al. The HER4 cytoplasmic domain, but not its c terminus, inhibits mammary cell proliferation. Mol Endocrinol. 2007; 21(8):1861–76. https://doi.org/10.1210/me.2006-0101 PMID: 17505063

91. Feng SM, Muraoka-Cook RS, Hunter D, Sandahl MA, Caskey LS, Miyazawa K, et al. The E3 Ubiquitin Ligase WWP1 Selectively Targets HER4 and Its Proteolytically Derived Signaling Isoforms for Degradation. Mol Cell Biol. 2009; 29(3):892–906. https://doi.org/10.1128/MCB.00595-08 PMID: 19047365

92. Vakar-Lopez F, Cheng CJ, Kim J, Shi GG, Troncoso P, Tu SM, et al. Up-regulation of MDA-BF-1, a secreted isoform of ErbB3, in metastatic prostate cancer cells and activated osteoblasts in bone marrow. J Pathol. 2004; 203(2):688–95. https://doi.org/10.1002/path.1568 PMID: 15141384

93. Chen NY, Ye XC, Chu K, Navone NM, Sage EH, Yu-Lee LY, et al. A secreted isoform of ErbB3 promotes osteonectin expression in bone and enhances the invasiveness of prostate cancer cells. Cancer Res. 2007; 67(14):6544–8. https://doi.org/10.1158/0008-5472.CAN-07-1330 PMID: 17638862

94. Lin SH, Cheng CJ, Lee YC, Ye X, Tsai WW, Kim J, et al. A 45-kDa ErbB3 secreted by prostate cancer cells promotes bone formation. Oncogene. 2008; 27(39):5195–203. https://doi.org/10.1038/onc.2008.156 PMID: 18490922

95. Lin SH, Lee YC, Choueiri MB, Wen SJ, Mathew P, Ye XC, et al. Soluble ErbB3 levels in bone marrow and plasma of men with prostate cancer. Clin Cancer Res. 2008; 14(12):3729–36. https://doi.org/10.1158/1078-0432.CCR-08-0472 PMID: 18559590

96. Hsieh SY, He JR, Yu MC, Lee WC, Chen TC, Lo SJ, et al. Secreted ERBB3 Isoforms Are Serum Markers for Early Hepatoma in Patients with Chronic Hepatitis and Cirrhosis. J Proteome Res. 2011; 10(10):4715–24. https://doi.org/10.1021/pr200519q PMID: 21877752

97. Srinivasan R, Leverton KE, Sheldon H, Hurst HC, Sarraf C, Gullick WJ. Intracellular expression of the truncated extracellular domain of c-erbB-3/HER3. Cell Signal. 2001; 13(5):321–30. PMID: 11369513

98. Takahashi M, Hasegawa Y, Ikeda Y, Wada Y, Tajiri M, Ariki S, et al. Suppression of Heregulin beta Signaling by the Single N-Glycan Deletion Mutant of Soluble ErbB3 Protein. J Biol Chem. 2013; 288(46):32910–21. https://doi.org/10.1074/jbc.M113.491902 PMID: 24097984

99. Funayama T, Nakanishi T, Takahashi K, Taniguchi S, Takigawa M, Matsumura T. Overexpression of c-erbB-3 in various stages of human squamous cell carcinomas. Oncology. 1998; 55(2):161–7. PMID: 9499191

100. Raabe TD, Deadwyler G, Varga JW, Devries GH. Localization of neuregulin Isoforms and erbB receptors in myelinating glial cells. Glia. 2004; 45(2):197–207. https://doi.org/10.1002/glia.10311 PMID: 14730713

101. Adilakshmi T, Ness-Myers J, Madrid-Aliste C, Fiser A, Tapinos N. A Nuclear Variant of ErbB3 Receptor Tyrosine Kinase Regulates Ezrin Distribution and Schwann Cell Myelination. J Neurosci. 2011; 31(13):5106–19. https://doi.org/10.1523/JNEUROSCI.5635-10.2011 PMID: 21451047

102. Koumakpayi IH, Le Page C, Delvoye N, Saad F, Mes-Masson AM. Macropinocytosis Inhibitors and Arf6 Regulate ErbB3 Nuclear Localization in Prostate Cancer Cells. Mol Carcinog. 2011; 50(11):901–12. https://doi.org/10.1002/mc.20766 PMID: 21438025

103. Koumakpayi IH, Diallo JS, Le Page C, Lessard L, Gleave M, Begin LR, et al. Expression and nuclear localization of ErbB3 in prostate cancer. Clin Cancer Res. 2006; 12(9):2730–7. https://doi.org/10.1158/1078-0432.CCR-05-2242 PMID: 16675564

104. Cheng CJ, Ye XC, Vakar-Lopez F, Kim J, Tu SM, Chen DT, et al. Bone microenvironment and androgen status modulate subcellular localization of ErbB3 in prostate cancer cells. Mol Cancer Res. 2007; 5(7):675–84. https://doi.org/10.1158/1541-7786.MCR-06-0306 PMID: 17634423

105. Reif R, Adawy A, Vartak N, Schroder J, Gunther G, Ghallab A, et al. Activated ErbB3 Translocates to the Nucleus via Clathrin-independent Endocytosis, Which Is Associated with Proliferating Cells. J Biol Chem. 2016; 291(8):3837–47. https://doi.org/10.1074/jbc.M115.686782 PMID: 26719328

106. Offterdinger M, Schofer C, Weipoltshammer K, Grunt TW. c-erbB-3: a nuclear protein in mammary epithelial cells. J Cell Biol. 2002; 157(6):929–39. https://doi.org/10.1083/jcb.200109033 PMID: 12045181

107. Lee H, Akita RW, Sliwkowski MX, Maihle NJ. A naturally occurring secreted human ErbB3 receptor isoform inhibits heregulin-stimulated activation of ErbB2, ErbB3, and ErbB4. Cancer Res. 2001; 61 (11):4467–73. PMID: 11389077

108. Brand TM, Iida M, Luthar N, Wleklinski MJ, Starr MM, Wheeler DL. Mapping C-Terminal Transactivation Domains of the Nuclear HER Family Receptor Tyrosine Kinase HER3. PLoS One. 2013; 8(8).

109. Maihle NJ, Lee H. Soluble ErbB3 methods of detection and antibodies United States patent and Trade Mark Office. 2010;Patent number US 7,744,882(June 29, 2010):1–39 [cited 14th July 2016) available from: http://patft.uspto.gov/netacgi/nph-Parser?Sect1=PTO1&Sect2=HITOFF&d=PALL&p=1&u=%2Fnetahtml%2FPTO%2Fsrchnum.htm&r=1&f=G&l=50&s1=7,744,882.PN.&OS=PN/7,744,882&RS=PN/7,744,882.

110. Beeton N, McCallum H. Models predict that culling is not a feasible strategy to prevent extinction of Tasmanian devils from facial tumour disease. J Appl Ecol. 2011; 48(6):1315–23.

111. Mirsky R, Jessen KR. The neurobiology of Schwann cells. Brain Pathol. 1999; 9(2):293–311. PMID: 10219747

112. Fricker FR, Antunes-Martins A, Galino J, Paramsothy R, La Russa F, Perkins J, et al. Axonal neuregulin 1 is a rate limiting but not essential factor for nerve remyelination. Brain. 2013; 136:2279–97. https://doi.org/10.1093/brain/awt148 PMID: 23801741

113. Fricker FR, Lago N, Balarajah S, Tsantoulas C, Tanna S, Zhu N, et al. Axonally Derived Neuregulin-1 Is Required for Remyelination and Regeneration after Nerve Injury in Adulthood. J Neurosci. 2011; 31 (9):3225–33. https://doi.org/10.1523/JNEUROSCI.2568-10.2011 PMID: 21368034

114. Ronchi G, Haastert-Talini K, Fornasari BE, Perroteau I, Geuna S, Gambarotta G. The Neuregulin1/ErbB system is selectively regulated during peripheral nerve degeneration and regeneration. Eur J Neurosci. 2016; 43(3):351–64. https://doi.org/10.1111/ejn.12974 PMID: 26061116

115. Carroll SL. Molecular mechanisms promoting the pathogenesis of Schwann cell neoplasms. Acta Neuropathol. 2012; 123(3):321–48. https://doi.org/10.1007/s00401-011-0928-6 PMID: 22160322

116. Rodriguez FJ, Stratakis CA, Evans DG. Genetic predisposition to peripheral nerve neoplasia: diagnostic criteria and pathogenesis of neurofibromatoses, Carney complex, and related syndromes. Acta Neuropathol. 2012; 123(3):349–67. https://doi.org/10.1007/s00401-011-0935-7 PMID: 22210082

117. Rodriguez FJ, Folpe AL, Giannini C, Perry A. Pathology of peripheral nerve sheath tumors: diagnostic overview and update on selected diagnostic problems. Acta Neuropathol. 2012; 123(3):295–319. https://doi.org/10.1007/s00401-012-0954-z PMID: 22327363

118. Akahane K, Kato K, Ogiso S, Sakaguchi K, Hashimoto M, Ishikawa A, et al. Malignant granular cell tumor of the breast: case report and literature review. Beast Cancer. 2015; 22(3):317–23.

119. Bourdeaut F, Ribeiro A, Paris R, Pierron G, Couturier J, Peuchmaur M, et al. In neuroblastic tumours, Schwann cells do not harbour the genetic alterations of neuroblasts but may nevertheless share the same clonal origin. Oncogene. 2008; 27(21):3066–71. https://doi.org/10.1038/sj.onc.1210965 PMID: 18071318

120. Omi K, Kitano Y, Agawa H, Kadota K. An immunohistochemical study of peripheral neuroblastoma, ganglioneuroblastoma, anaplastic ganglioglioma, schwannoma and neurofibroma in cattle J Comp Pathol. 1994; 111(1):1–14. PMID: 7962722

121. Kagawa Y, Hirayama K, Tagami M, Tsunoda N, Yoshino T, Matsui T, et al. Immunohistochemical analysis of equine pulmonary granular cell tumours. J Comp Pathol. 2001; 124(2–3):122–7. https://doi.org/10.1053/jcpa.2000.0439 PMID: 11222008

122. Chijiwa K, Uchida K, Tateyama S. Immunohistochemical evaluation of canine peripheral nerve sheath tumors and other soft tissue sarcomas. Vet Pathol. 2004; 41(4):307–18. https://doi.org/10.1354/vp.41-4-307 PMID: 15232130

123. Schoniger S, Valentine BA, Fernandez CJ, Summers BA. Cutaneous Schwannomas in 22 Horses. Vet Pathol. 2011; 48(2):433–42. https://doi.org/10.1177/0300985810377072 PMID: 20716761

124. Duke FD, Teixeira LBC, Galle LE, Green N, Dubielzig RR. Malignant Uveal Schwannoma With Peripheral Nerve Extension in a 12-Week-Old Color-Dilute Labrador Retriever. Vet Pathol. 2015; 52(1):181–5. https://doi.org/10.1177/0300985814522811 PMID: 24513800

125. Stonecypher MS, Byer SJ, Grizzle WE, Carroll SL. Activation of the neuregulin-1/ErbB signaling pathway promotes the proliferation of neoplastic Schwann cells in human malignant peripheral nerve sheath tumors. Oncogene. 2005; 24(36):5589–605. https://doi.org/10.1038/sj.onc.1208730 PMID: 15897877

126. Izycka-Swieszewska E, Wozniak A, Drozynska E, Kot J, Grajkowska W, Klepacka T, et al. Expression and significance of HER family receptors in neuroblastic tumors. Clin Exp Metastasis. 2011; 28 (3):271–82. https://doi.org/10.1007/s10585-010-9369-1 PMID: 21203803

127. Wilzen A, Krona C, Sveinbjornsson B, Kristiansson E, Dalevi D, Ora I, et al. ERBB3 is a marker of a ganglioneuroblastoma/ganglioneuroma-like expression profile in neuroblastic tumours. Mol Cancer. 2013;12.

128. Lee PR, Cohen JE, Fields RD. Immune system evasion by peripheral nerve sheath tumor. Neurosci Lett. 2006; 397(1–2):126–9. https://doi.org/10.1016/j.neulet.2005.12.027 PMID: 16406348

129. Horste GMZ, Hu W, Hartung HP, Lehmann HC, Kieseier BC. The immunocompetence of Schwann cells. Muscle & Nerve. 2008; 37(1):3–13.

130. Tzekova N, Heinen A, Kury P. Molecules Involved in the Crosstalk Between Immune- and Peripheral Nerve Schwann Cells. J Clin Immunol. 2014; 34:S86–S104. https://doi.org/10.1007/s10875-014-0015-6 PMID: 24740512

131. Stern DF. ERBB3/HER3 and ERBB2/HER2 duet in mammary development and breast cancer. J Mammary Gland Biol Neoplasia. 2008; 13(2):215–23. https://doi.org/10.1007/s10911-008-9083-7 PMID: 18454306

132. Nahta R. Deciphering the role of insulin-like growth factor-I receptor in trastuzumab resistance. Chemotherapy research and practice. 2012; 2012:648965. https://doi.org/10.1155/2012/648965 PMID: 22830017

133. Huang XP, Gao LZ, Wang SL, McManaman JL, Thor AD, Yang XH, et al. Heterotrimerization of the Growth Factor Receptors erbB2, erbB3, and Insulin-like Growth Factor-I Receptor in Breast Cancer Cells Resistant to Herceptin. Cancer Res. 2010; 70(3):1204–14. https://doi.org/10.1158/0008-5472.CAN-09-3321 PMID: 20103628

134. Engelman JA, Zejnullahu K, Mitsudomi T, Song YC, Hyland C, Park JO, et al. MET amplification leads to gefitinib resistance in lung cancer by activating ERBB3 signaling. Science. 2007; 316(5827):1039–43. https://doi.org/10.1126/science.1141478 PMID: 17463250

135. Yun C, Gang L, Gu RM, Xu W, Ming XZ, Chen HQ. Essential role of Her3 in two signaling transduction patterns: Her2/Her3 and MET/Her3 in proliferation of human gastric cancer. Mol Carcinog. 2015; 54 (12):1700–9. https://doi.org/10.1002/mc.22241 PMID: 25400108

136. Wang XC, Batty KM, Crowe PJ, Goldstein D, Yang JL. The potential of panHER inhibition in cancer. Front Oncol. 2015; 5.

137. Dey N, Williams C, Leyland-Jones B, De P. A critical role for HER3 in HER2-amplified and non-amplified breast cancers: function of a kinase-dead RTK. Am J Transl Res. 2015; 7(4):733–50. PMID: 26064441

138. Sergina NV, Rausch M, Wang DH, Blair J, Hann B, Shokat KM, et al. Escape from HER-family tyrosine kinase inhibitor therapy by the kinase-inactive HER3. Nature. 2007; 445(7126):437–41. https://doi.org/10.1038/nature05474 PMID: 17206155

139. Liu BL, Ordonez-Ercan D, Fan ZY, Edgerton SM, Yang XH, Thor AD. Downregulation of erbB3 abrogates erbB2-mediated tamoxifen resistance in breast cancer cells. International Journal of Cancer. 2007; 120(9):1874–82. https://doi.org/10.1002/ijc.22423 PMID: 17266042

140. Sithanandam G, Fornwald LW, Fields J, Anderson LM. Inactivation of ErbB3 by siRNA promotes apoptosis and attenuates growth and invasiveness of human lung adenocarcinoma cell line A549. Oncogene. 2005; 24(11):1847–59. https://doi.org/10.1038/sj.onc.1208381 PMID: 15688028

141. Amin DN, Sergina N, Lim L, Goga A, Moasser MM. HER3 signalling is regulated through a multitude of redundant mechanisms in HER2-driven tumour cells. Biochem J. 2012; 447:417–25. https://doi.org/10.1042/BJ20120724 PMID: 22853430

142. Hamburger AW. The role of ErbB3 and its binding partners in breast cancer progression and resistance to hormone and tyrosine kinase directed therapies. J Mammary Gland Biol Neoplasia. 2008; 13 (2):225–33. https://doi.org/10.1007/s10911-008-9077-5 PMID: 18425425

143. Tinoco G, Warsch S, Gluck S, Avancha K, Montero AJ. Treating Breast Cancer in the 21st Century: Emerging Biological Therapies. J Cancer. 2013; 4(2):117–32. https://doi.org/10.7150/jca.4925 PMID: 23386910

144. Baselga J, Swain SM. Novel anticancer targets: revisiting ERBB2 and discovering ERBB3. Nat Rev Cancer. 2009; 9(7):463–75. https://doi.org/10.1038/nrc2656 PMID: 19536107

145. Kruser TJ, Wheeler DL. Mechanisms of resistance to HER family targeting antibodies. Exp Cell Res. 2010; 316(7):1083–100. https://doi.org/10.1016/j.yexcr.2010.01.009 PMID: 20064507

146. Aurisicchio L, Marra E, Roscilli G, Mancini R, Ciliberto G. The promise of anti-ErbB3 monoclonals as new cancer therapeutics. Oncotarget. 2012; 3(8):744–58. https://doi.org/10.18632/oncotarget.550 PMID: 22889873

147. Kol A, van Scheltinga A, Timmer-Bosscha H, Lamberts LE, Bensch F, de Vries EGE, et al. HER3, serious partner in crime Therapeutic approaches and potential biomarkers for effect of HER3-targeting. Pharmacol Ther. 2014; 143(1):1–11. https://doi.org/10.1016/j.pharmthera.2014.01.005 PMID: 24513440

148. Ma J, Lyu H, Huang JC, Liu BL. Targeting of erbB3 receptor to overcome resistance in cancer treatment. Mol Cancer. 2014; 13.

149. Lee Y, Ma J, Lyu H, Huang JC, Kim A, Liu BL. Role of erbB3 receptors in cancer therapeutic resistance. Acta Biochim Biophys Sin. 2014; 46(3):190–8. https://doi.org/10.1093/abbs/gmt150 PMID: 24449784

150. Zhang N, Chang Y, Rios A, An Z. HER3/ErbB3, an emerging cancer therapeutic target. Acta Biochim Biophys Sin. 2016; 48(1):39–48. https://doi.org/10.1093/abbs/gmv103 PMID: 26496898

151. van der Horst EH, Murgia M, Treder M, Ullrich A. Anti-HER-3 MAbs inhibit HER-3-mediated signaling in breast cancer cell lines resistant to anti-HER-2 antibodies. International Journal of Cancer. 2005; 115(4):519–27. https://doi.org/10.1002/ijc.20867 PMID: 15704104

152. Robinson MK, Hodge KM, Horak E, Sundberg AL, Russeva M, Shaller CC, et al. Targeting ErbB2 and ErbB3 with a bispecific single-chain Fv enhances targeting selectivity and induces a therapeutic effect in vitro. Br J Cancer. 2008; 99(9):1415–25. https://doi.org/10.1038/sj.bjc.6604700 PMID: 18841159

153. Treder M, Ogbagabriel S, Moor R, Schulze-Horsel U, Hettmann T, Rothe M, et al. Fully human anti-HER3 mAb U3-1287 (AMG 888) demonstrates unique in vitro and in vivo activities versus other HER family inhibitors in NSCLC models. EJC Suppl. 2008; 6(12):99-.

154. Schoeberl B, Pace EA, Fitzgerald JB, Harms BD, Xu LH, Nie L, et al. Therapeutically Targeting ErbB3: A Key Node in Ligand-Induced Activation of the ErbB Receptor-PI3K Axis. Sci Signal. 2009; 2(77).

155. Schoeberl B, Faber AC, Li DN, Liang MC, Crosby K, Onsum M, et al. An ErbB3 Antibody, MM-121, Is Active in Cancers with Ligand-Dependent Activation. Cancer Res. 2010; 70(6):2485–94. https://doi.org/10.1158/0008-5472.CAN-09-3145 PMID: 20215504

156. Huang JC, Wang SL, Lyu H, Cai B, Yang XH, Wang JX, et al. The anti-erbB3 antibody MM-121/SAR256212 in combination with trastuzumab exerts potent antitumor activity against trastuzumab-resistant breast cancer cells. Mol Cancer. 2013; 12.

157. Schaefer G, Haber L, Crocker LM, Shia S, Shao L, Dowbenko D, et al. A Two-in-One Antibody against HER3 and EGFR Has Superior Inhibitory Activity Compared with Monospecific Antibodies. Cancer Cell. 2011; 20(4):472–86. https://doi.org/10.1016/j.ccr.2011.09.003 PMID: 22014573

158. Huang S, Li CR, Armstrong EA, Peet CR, Saker J, Amler LC, et al. Dual Targeting of EGFR and HER3 with MEHD7945A Overcomes Acquired Resistance to EGFR Inhibitors and Radiation. Cancer Res. 2013; 73(2):824–33. https://doi.org/10.1158/0008-5472.CAN-12-1611 PMID: 23172311

159. Belleudi F, Marra E, Mazzetta F, Fattore L, Giovagnoli MR, Mancini R, et al. Monoclonal antibody-induced ErbB3 receptor internalization and degradation inhibits growth and migration of human melanoma cells. Cell Cycle. 2012; 11(7):1455–67. https://doi.org/10.4161/cc.19861 PMID: 22421160

160. McDonagh CF, Huhalov A, Harms BD, Adams S, Paragas V, Oyama S, et al. Antitumor Activity of a Novel Bispecific Antibody That Targets the ErbB2/ErbB3 Oncogenic Unit and Inhibits Heregulin-Induced Activation of ErbB3. Mol Cancer Ther. 2012; 11(3):582–93. https://doi.org/10.1158/1535-7163.MCT-11-0820 PMID: 22248472

161. Rajkumar T, Gullick WJ. A monoclonal antibody to the human c-erbb3 protein stimulates the anchorage independent growth of breast cancer cell lines Br J Cancer. 1994; 70(3):459–65. PMID: 8080731

162. Blackburn E, Zona S, Murphy ML, Brown IR, Chan SKW, Gullick WJ. A monoclonal antibody to the human HER3 receptor inhibits Neuregulin 1-beta binding and co-operates with Herceptin in inhibiting the growth of breast cancer derived cell lines. Breast Cancer Res Treat. 2012; 134(1):53–9. https://doi.org/10.1007/s10549-011-1908-1 PMID: 22169894

163. Lazrek Y, Dubreuil O, Garambois V, Gaborit N, Larbouret C, Le Clorennec C, et al. Anti-HER3 Domain 1 and 3 Antibodies Reduce Tumor Growth by Hindering HER2/HER3 Dimerization and AKT-Induced MDM2, XIAP, and Fox01 Phosphorylation. Neoplasia. 2013; 15(3):335-+. PMID: 23479511

164. Garner AP, Bialucha CU, Sprague ER, Garrett JT, Sheng Q, Li SR, et al. An Antibody That Locks HER3 in the Inactive Conformation Inhibits Tumor Growth Driven by HER2 or Neuregulin. Cancer Res. 2013; 73(19):6024–35. https://doi.org/10.1158/0008-5472.CAN-13-1198 PMID: 23928993

165. Garrett JT, Sutton CR, Kurupi R, Bialucha CU, Ettenberg SA, Collins SD, et al. Combination of Antibody That Inhibits Ligand-Independent HER3 Dimerization and a p110 alpha Inhibitor Potently Blocks PI3K Signaling and Growth of HER2+ Breast Cancers. Cancer Res. 2013; 73(19):6013–23. https://doi.org/10.1158/0008-5472.CAN-13-1191 PMID: 23918797

166. Sala G, Rapposelli IG, Ghasemi R, Piccolo E, Traini S, Capone E, et al. EV20, a Novel Anti-ErbB-3 Humanized Antibody, Promotes ErbB-3 Down-Regulation and Inhibits Tumor Growth In Vivo. Transl Oncol. 2013; 6(6):676–U293. PMID: 24466370

167. Mirschberger C, Schiller CB, Schraml M, Dimoudis N, Friess T, Gerdes CA, et al. RG7116, a Therapeutic Antibody That Binds the Inactive HER3 Receptor and Is Optimized for Immune Effector Activation. Cancer Res. 2013; 73(16):5183–94. https://doi.org/10.1158/0008-5472.CAN-13-0099 PMID: 23780344

168. Fitzgerald JB, Johnson BW, Baum J, Adams S, Iadevaia S, Tang J, et al. MM-141, an IGF-IR- and ErbB3-Directed Bispecific Antibody, Overcomes Network Adaptations That Limit Activity of IGF-IR Inhibitors. Mol Cancer Ther. 2014; 13(2):410–25. https://doi.org/10.1158/1535-7163.MCT-13-0255 PMID: 24282274

169. Francis D, Huang S, Werner L, Lantto J, Horak ID, Kragh M, et al. Sym013, novel pan-HER monoclonal antibody mixture, augments radiation response in human lung and head and neck tumors. Cancer Res. 2014; 74(19).

170. Zhang L, Castanaro C, Luan B, Yang K, Fan LF, Fairhurst JL, et al. ERBB3/HER2 Signaling Promotes Resistance to EGFR Blockade in Head and Neck and Colorectal Cancer Models. Mol Cancer Ther. 2014; 13(5):1345–55. https://doi.org/10.1158/1535-7163.MCT-13-1033 PMID: 24634416

171. Clarke N, Hopson C, Hahn A, Sully K, Germaschewski F, Yates J, et al. Preclinical pharmacologic characterization of GSK2849330, a monoclonal AccretaMab (R) antibody with optimized ADCC and CDC activity directed against HER3. Eur J Cancer. 2014; 50:98–9.

172. D'Souza JW, Reddy S, Goldsmith LE, Shchaveleva I, Marks JD, Litwin S, et al. Combining Anti-ERBB3 Antibodies Specific for Domain I and Domain III Enhances the Anti-Tumor Activity over the Individual Monoclonal Antibodies. PLoS One. 2014; 9(11).

173. Lee S, Greenlee EB, Amick JR, Ligon GF, Lillquist JS, Natoli EJ, et al. Inhibition of ErbB3 by a monoclonal antibody that locks the extracellular domain in an inactive configuration. Proc Natl Acad Sci U S A. 2015; 112(43):13225–30. https://doi.org/10.1073/pnas.1518361112 PMID: 26460020

174. Meetze K, Vincent S, Tyler S, Mazsa EK, Delpero AR, Bottega S, et al. Neuregulin 1 Expression Is a Predictive Biomarker for Response to AV-203, an ERBB3 Inhibitory Antibody, in Human Tumor Models. Clin Cancer Res. 2015; 21(5):1106–14. https://doi.org/10.1158/1078-0432.CCR-14-2407 PMID: 25542901

175. Gu JM, Yang JS, Chang Q, Liu ZH, Ghayur T, Gu JJ. Identification of Anti-EGFR and Anti-ErbB3 Dual Variable Domains Immunoglobulin (DVD-Ig) Proteins with Unique Activities. PLoS One. 2015; 10(5).

176. Gaborit N, Abdul-Hai A, Mancini M, Lindzen M, Lavi S, Leitner O, et al. Examination of HER3 targeting in cancer using monoclonal antibodies. Proc Natl Acad Sci U S A. 2015; 112(3):839–44. https://doi.org/10.1073/pnas.1423645112 PMID: 25564668

177. Huang XP, Gao LZ, Wang SL, Lee CK, Ordentlich P, Liu BL. HDAC Inhibitor SNDX-275 Induces Apoptosis in erbB2-Overexpressing Breast Cancer Cells via Down-regulation of erbB3 Expression. Cancer Res. 2009; 69(21):8403–11. https://doi.org/10.1158/0008-5472.CAN-09-2146 PMID: 19826038

178. Hickinson DM, Klinowska T, Speake G, Vincent J, Trigwell C, Anderton J, et al. AZD8931, an Equipotent, Reversible Inhibitor of Signaling by Epidermal Growth Factor Receptor, ERBB2 (HER2), and ERBB3: A Unique Agent for Simultaneous ERBB Receptor Blockade in Cancer. Clin Cancer Res. 2010; 16(4):1159–69. https://doi.org/10.1158/1078-0432.CCR-09-2353 PMID: 20145185

179. Foreman PK, Gore M, Kobel PA, Xu L, Yee H, Hannum C, et al. ErbB3 Inhibitory Surrobodies Inhibit Tumor Cell Proliferation In Vitro and In Vivo. Mol Cancer Ther. 2012; 11(7):1411–20. https://doi.org/10.1158/1535-7163.MCT-12-0068 PMID: 22553357

180. Wu YM, Zhang YX, Wang ML, Li Q, Qu ZX, Shi V, et al. Downregulation of HER3 by a Novel Antisense Oligonucleotide, EZN-3920, Improves the Antitumor Activity of EGFR and HER2 Tyrosine Kinase Inhibitors in Animal Models. Mol Cancer Ther. 2013; 12(4):427–37. https://doi.org/10.1158/1535-7163.MCT-12-0838 PMID: 23395887

181. Miller MJ, Foy KC, Overholser JP, Nahta R, Kaumaya PTP. HER-3 peptide vaccines/mimics: Combined therapy with IGF-1R, HER-2, and HER-1 peptides induces synergistic antitumor effects against breast and pancreatic cancer cells. OncoImmunology. 2014; 3(11).

182. Ren X-R, Wang J, Osada T, Mook RA Jr., Morse MA, Barak LSet al. Perhexiline promotes HER3 ablation through receptor internalization and inhibits tumor growth. Breast cancer research: BCR. 2015; 17 (1):528.

183. Ferreira RB, Law ME, Jahn SC, Davis BJ, Heldermon CD, Reinhard M, et al. Novel agents that down-regulate EGFR, HER2, and HER3 in parallel. Oncotarget. 2015; 6(12):10445–59. https://doi.org/10.18632/oncotarget.3398 PMID: 25865227

184. McCallum H. Models for managing wildlife disease. Parasitology. 2016; 143(7):805–20. https://doi.org/10.1017/S0031182015000980 PMID: 26283059

185. Lachish S, McCallum H, Mann D, Pukk CE, Jones ME. Evaluation of Selective Culling of Infected Individuals to Control Tasmanian Devil Facial Tumor Disease. Conserv Biol. 2010; 24(3):841–51. https://doi.org/10.1111/j.1523-1739.2009.01429.x PMID: 20088958

186. Aurisicchio L, Ciliberto G. Genetic cancer vaccines: current status and perspectives. Expert Opin Biol Ther. 2012; 12(8):1043–58. https://doi.org/10.1517/14712598.2012.689279 PMID: 22577875

187. Guo CQ, Manjili MH, Subjeck JR, Sarkar D, Fisher PB, Wang XY. Therapeutic Cancer Vaccines: Past, Present, and Future. In: Tew KD, Fisher PB, editors. Advances in Cancer Research, Vol 119. Advances in Cancer Research. 119. San Diego: Elsevier Academic Press Inc; 2013. p. 421–75.

188. Melero I, Gaudemack G, Gerritsen W, Huber C, Parmiani G, Scholl S, et al. Therapeutic vaccines for cancer: an overview of clinical trials. Nat Rev Clin Oncol. 2014; 11(9):509–24. https://doi.org/10.1038/nrclinonc.2014.111 PMID: 25001465

189. Melief CJM, van Hall T, Arens R, Ossendorp F, van der Burg SH. Therapeutic cancer vaccines. J Clin Invest. 2015; 125(9):3401–12. https://doi.org/10.1172/JCI80009 PMID: 26214521

190. Papaioannou NE, Beniata OV, Vitsos P, Tsitsilonis O, Samara P. Harnessing the immune system to improve cancer therapy. Ann Transl Med. 2016; 4(14).

191. Kazemi T, Younesi V, Jadidi-Niaragh F, Yousefi M. Immunotherapeutic approaches for cancer therapy: An updated review. Artif Cell Nanomed Biotechnol. 2016; 44(3):769–79.

192. Anderson K, Modiano J. Progress in Adaptive Immunotherapy for Cancer in Companion Animals: Success on the Path to a Cure. Veterinary Sciences. 2015; 2(4):363. https://doi.org/10.3390/vetsci2040363 PMID: 27066495

193. Bergman PJ. Immunotherapy in Veterinary Oncology. Vet Clin N Am-Small Anim Pract. 2014; 44 (5):925-+.

194. Regan D, Guth A, Coy J, Dow S. Cancer immunotherapy in veterinary medicine: Current options and new developments. Vet J. 2016; 207:20–8. https://doi.org/10.1016/j.tvjl.2015.10.008 PMID: 26545847

195. Fazekas J, Furdos I, Singer J, Jensen-Jarolim E. Why man's best friend, the dog, could also benefit from an anti-HER-2 vaccine. Oncol Lett. 2016; 12(4):2271–6. https://doi.org/10.3892/ol.2016.5001 PMID: 27698788

196. Singer J, Fazekas J, Wang W, Weichselbaumer M, Matz M, Mader A, et al. Generation of a Canine Anti-EGFR (ErbB-1) Antibody for Passive Immunotherapy in Dog Cancer Patients. Mol Cancer Ther. 2014; 13(7):1777–90. https://doi.org/10.1158/1535-7163.MCT-13-0288 PMID: 24755200

197. Ito D, Brewer S, Modiano JF, Beall MJ. Development of a novel anti-canine CD20 monoclonal antibody with diagnostic and therapeutic potential. Leuk Lymphoma. 2015; 56(1):219–25. https://doi.org/10.3109/10428194.2014.914193 PMID: 24724777

198. Brown GK, Kreiss A, Lyons AB, Woods GM. Natural Killer Cell Mediated Cytotoxic Responses in the Tasmanian Devil. PLoS One. 2011; 6(9).

199. Pinfold TL, Brown GK, Bettiol SS, Woods GM. Mouse Model of Devil Facial Tumour Disease Establishes That an Effective Immune Response Can be Generated Against the Cancer Cells. Frontiers in immunology. 2014; 5:251. https://doi.org/10.3389/fimmu.2014.00251 PMID: 24904594

200. Howson LJ, Morris KM, Kobayashi T, Tovar C, Kreiss A, Papenfuss AT, et al. Identification of Dendritic Cells, B Cell and T Cell Subsets in Tasmanian Devil Lymphoid Tissue; Evidence for Poor Immune Cell Infiltration into Devil Facial Tumors. Anat Rec. 2014; 297(5):925–38.

201. Kreiss A, Brown GK, Tovar C, Lyons AB, Woods GM. Evidence for induction of humoral and cytotoxic immune responses against devil facial tumor disease cells in Tasmanian devils (Sarcophilus harrisii) immunized with killed cell preparations. Vaccine. 2015; 33(26):3016–25. https://doi.org/10.1016/j.vaccine.2015.01.039 PMID: 25708088

202. Slingluff CL. The Present and Future of Peptide Vaccines for Cancer Single or Multiple, Long or Short, Alone or in Combination? Cancer J. 2011; 17(5):343–50. https://doi.org/10.1097/PPO.0b013e318233e5b2 PMID: 21952285

203. Foy KC, Wygle RM, Miller MJ, Overholser JP, Bekaii-Saab T, Kaumaya PTP. Peptide Vaccines and Peptidomimetics of EGFR (HER-1) Ligand Binding Domain Inhibit Cancer Cell Growth In Vitro and In Vivo. J Immunol. 2013; 191(1):217–27. https://doi.org/10.4049/jimmunol.1300231 PMID: 23698748

204. Overholser J, Ambegaokar KH, Eze SM, Sanabria-Figueroa E, Nahta R, Bekaii-Saab T, et al. Anti-Tumor Effects of Peptide Therapeutic and Peptide Vaccine Antibody Co-targeting HER-1 and HER-2

in Esophageal Cancer (EC) and HER-1 and IGF-1R in Triple-Negative Breast Cancer (TNBC). Vaccines. 2015; 3(3):519–43. https://doi.org/10.3390/vaccines3030519 PMID: 26350593

205. Allen SD, Garrett JT, Rawale SV, Jones AL, Phillips G, Forni G, et al. Peptide vaccines of the HER-2/neu dimerization loop are effective in inhibiting mammary tumor growth in vivo. J Immunol. 2007; 179 (1):472–82. PMID: 17579068

206. Gil EY, Jo UH, Lee HJ, Kang J, Seo JH, Lee ES, et al. Vaccination with ErbB-2 peptides prevents cancer stem cell expansion and suppresses the development of spontaneous tumors in MMTV-PyMT transgenic mice. Breast Cancer Res Treat. 2014; 147(1):69–80. https://doi.org/10.1007/s10549-014-3086-4 PMID: 25104444

207. Clifton GT, Peoples GE, Mittendorf EA. The development and use of the E75 (HER2 369–377) peptide vaccine. Future Oncol. 2016; 12(11):1321–9. https://doi.org/10.2217/fon-2015-0054 PMID: 27044454

208. Kaumaya PTP. A paradigm shift: Cancer therapy with peptide-based B-cell epitopes and peptide immunotherapeutics targeting multiple solid tumor types: Emerging concepts and validation of combination immunotherapy. Human Vaccines Immunother. 2015; 11(6):1368–86.

209. Ly LV, Sluijter M, van der Burg SH, Jager MJ, van Hall T. Effective Cooperation of Monoclonal Antibody and Peptide Vaccine for the Treatment of Mouse Melanoma. J Immunol. 2013; 190(1):489–96. https://doi.org/10.4049/jimmunol.1200135 PMID: 23203930

210. Cavallo F, Aurisicchio L, Mancini R, Ciliberto G. Xenogene vaccination in the therapy of cancer. Expert Opin Biol Ther. 2014; 14(10):1427–42. https://doi.org/10.1517/14712598.2014.927433 PMID: 25023219

211. Bergman PJ, Camps-Palau MA, McKnight JA, Leibman NF, Craft DM, Leung C, et al. Development of a xenogeneic DNA vaccine program for canine malignant melanoma at the Animal Medical Center. Vaccine. 2006; 24(21):4582–5. https://doi.org/10.1016/j.vaccine.2005.08.027 PMID: 16188351

212. Flies A, Woods G, Lyons AB, Hayball J. B7-H1 (PD-L1) is expressed in the Tasmanian devil facial tumor microenvironment and is strongly upregulated in response to IFN-gamma. Eur J Immunol. 2016; 46:1095-.

213. Muenst S, Laubli H, Soysal SD, Zippelius A, Tzankov A, Hoeller S. The immune system and cancer evasion strategies: therapeutic concepts. J Intern Med. 2016; 279(6):541–62. https://doi.org/10.1111/joim.12470 PMID: 26748421

214. Pardoll DM. The blockade of immune checkpoints in cancer immunotherapy. Nat Rev Cancer. 2012; 12(4):252–64. https://doi.org/10.1038/nrc3239 PMID: 22437870

215. Topalian SL, Drake CG, Pardoll DM. Immune Checkpoint Blockade: A Common Denominator Approach to Cancer Therapy. Cancer Cell. 2015; 27(4):450–61. https://doi.org/10.1016/j.ccell.2015.03.001 PMID: 25858804

216. Chen DS, Mellman I. Oncology Meets Immunology: The Cancer-Immunity Cycle. Immunity. 2013; 39 (1):1–10. https://doi.org/10.1016/j.immuni.2013.07.012 PMID: 23890059

217. van der Burg SH, Arens R, Ossendorp F, van Hall T, Melief AJM. Vaccines for established cancer: overcoming the challenges posed by immune evasion. Nat Rev Cancer. 2016; 16(4):219–33. https://doi.org/10.1038/nrc.2016.16 PMID: 26965076

Appendix 3 has been removed for copyright or proprietary reasons.

Pye, R. J., Pemberton, D., Tovar, C., Tubio, J. M. C., Dun, K. A., Fox, S. et al., 2016. A second transmissible cancer in Tasmanian devils. Proc Natl Acad Sci U S A., 113(2), 374-9. doi: 10.1073/pnas.1519691113 (includes supporting material)

Article

Cancer Cell

The Origins and Vulnerabilities of Two Transmissible Cancers in Tasmanian Devils

Graphical Abstract

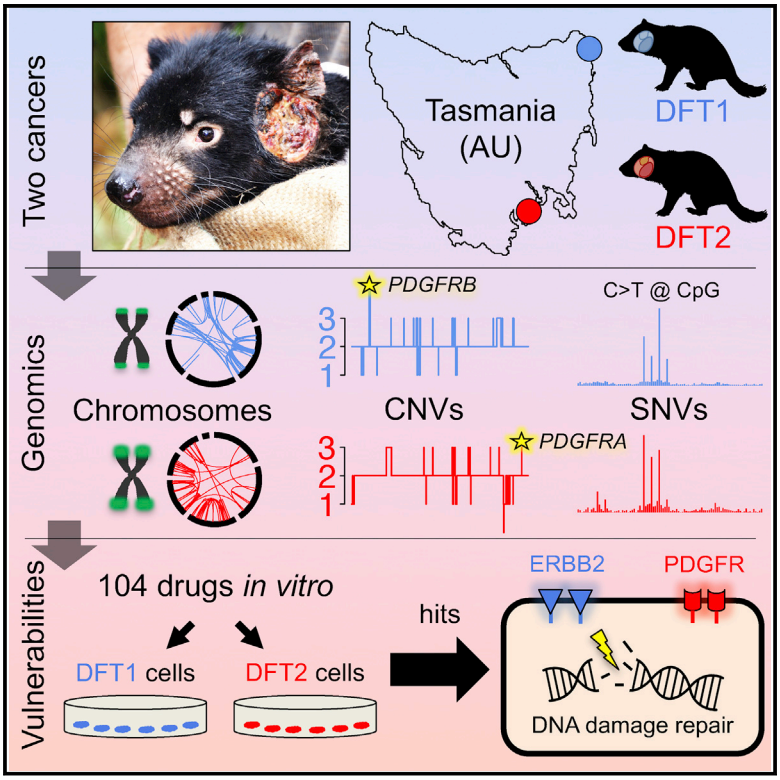

Highlights

- Tasmanian devil transmissible cancers arose from similar tissues in two individuals
- Similar mutation patterns and driver candidates imply common oncogenic processes
- Losses at *B2M* and Y chromosome loci suggest selection to escape immune detection
- Receptor tyrosine kinases and DNA repair factors implicated as therapeutic targets

Authors

Maximilian R. Stammnitz, Tim H.H. Coorens, Kevin C. Gori, ..., Mathew J. Garnett, Zemin Ning, Elizabeth P. Murchison

Correspondence

epm27@cam.ac.uk

In Brief

Stammnitz et al. show that the two transmissible cancer clones that affect Tasmanian devils are very similar in their tissues-of-origin, mutational patterns and driver gene candidates. Importantly, these cancers are both highly sensitive to inhibitors of some receptor tyrosine kinases as well as to inhibitors of DNA repair.

Stammnitz et al., 2018, Cancer Cell *33*, 607–619
April 9, 2018
https://doi.org/10.1016/j.ccell.2018.03.013

CellPress

Cancer Cell
Article

The Origins and Vulnerabilities of Two Transmissible Cancers in Tasmanian Devils

Maximilian R. Stammnitz,[1] Tim H.H. Coorens,[1,7] Kevin C. Gori,[1,7] Dane Hayes,[2,3] Beiyuan Fu,[4] Jinhong Wang,[1] Daniel E. Martin-Herranz,[1] Ludmil B. Alexandrov,[4,8] Adrian Baez-Ortega,[1] Syd Barthorpe,[4] Alexandra Beck,[4] Francesca Giordano,[4] Graeme W. Knowles,[2] Young Mi Kwon,[1] George Hall,[4] Stacey Price,[4] Ruth J. Pye,[5] Jose M.C. Tubio,[1] Hannah V.T. Siddle,[6] Sukhwinder Singh Sohal,[3] Gregory M. Woods,[5] Ultan McDermott,[4] Fengtang Yang,[4] Mathew J. Garnett,[4] Zemin Ning,[4] and Elizabeth P. Murchison[1,9,*]

[1]Transmissible Cancer Group, Department of Veterinary Medicine, University of Cambridge, Cambridge CB3 0ES, UK
[2]Mount Pleasant Laboratories, Tasmanian Department of Primary Industries, Parks, Water and the Environment, Prospect, TAS 7250, Australia
[3]School of Health Sciences, Faculty of Health, University of Tasmania, Launceston, TAS 7248, Australia
[4]Wellcome Trust Sanger Institute, Wellcome Genome Campus, Hinxton CB10 1SA, UK
[5]Menzies Institute for Medical Research, University of Tasmania, Hobart, TAS 7000, Australia
[6]Centre for Biological Sciences, University of Southampton, Southampton SO17 1BJ, UK
[7]These authors contributed equally
[8]Present address: Department of Cellular and Molecular Medicine, University of California, San Diego, La Jolla, CA 92093, USA
[9]Lead Contact
*Correspondence: epm27@cam.ac.uk
https://doi.org/10.1016/j.ccell.2018.03.013

SUMMARY

Transmissible cancers are clonal lineages that spread through populations via contagious cancer cells. Although rare in nature, two facial tumor clones affect Tasmanian devils. Here we perform comparative genetic and functional characterization of these lineages. The two cancers have similar patterns of mutation and show no evidence of exposure to exogenous mutagens or viruses. Genes encoding PDGF receptors have copy number gains and are present on extrachromosomal double minutes. Drug screening indicates causative roles for receptor tyrosine kinases and sensitivity to inhibitors of DNA repair. Y chromosome loss from a male clone infecting a female host suggests immunoediting. These results imply that Tasmanian devils may have inherent susceptibility to transmissible cancers and present a suite of therapeutic compounds for use in conservation.

INTRODUCTION

Tasmanian devils (*Sarcophilus harrisii*) are marsupial carnivores endemic to the Australian island of Tasmania. This species is considered endangered due to the emergence of a clonally transmissible cancer known as devil facial tumor 1 (DFT1) (Pearse and Swift, 2006). DFT1 presents as facial and oral tumors, and the disease is contagious between animals by the transfer of living cancer cells by biting (Hamede et al., 2013; Pearse and Swift, 2006). First observed in north-east Tasmania in 1996, DFT1 is a somatic clone that originally arose from the cells of an individual female devil (Deakin et al., 2012; Hawkins et al., 2006; Murchison et al., 2012). The lineage spawned by this animal has subsequently spread widely throughout Tasmania, causing significant declines in devil populations (Hawkins et al., 2006; Lazenby et al., 2018).

In 2014, routine diagnostic screening revealed a second transmissible cancer in Tasmanian devils (Pye et al., 2016b). This

Significance

Transmissible cancers are malignant clones that "metastasize" between individuals. The mechanisms whereby such cancers emerge, spread, and escape the allogeneic immune system are poorly understood. Remarkably, despite the rarity of known transmissible cancers in nature, Tasmanian devils harbor two distinct transmissible facial tumor clones. Here, we investigate the underlying mechanisms of devil transmissible cancers by performing comparative genetic and functional analyses of the two clones. The cancers show striking similarities in their tissues-of-origin, genome architectures, mutational patterns, driver gene candidates, and drug vulnerabilities, suggesting that they arose via similar processes. Both cancers carry deletions at loci relevant for immunogenicity. Importantly, common dependence on receptor tyrosine kinases and DNA repair pathways provides opportunities for targeted therapy and Tasmanian devil conservation.

cancer, DFT2, causes oral and facial tumors that are grossly indistinguishable from those caused by DFT1 (Pye et al., 2016b). However, DFT2 tumors are histologically, cytogenetically, and genetically distinct from DFT1. Indeed, karyotype evidence suggests that DFT2 arose from the somatic cells of a male animal, in contrast to the female origin of DFT1 (Pye et al., 2016b). To date, DFT2 has been confirmed in only 11 devils, all located on the Channel Peninsula in Tasmania's south-east (Kwon et al., 2018).

The discovery of a second transmissible cancer in Tasmanian devils was entirely unexpected and remains unexplained. Other than DFT1 and DFT2 in devils, only one other naturally occurring transmissible cancer is known in mammals, which is the 11,000-year-old canine transmissible venereal tumor in dogs (Murchison et al., 2014). Outside of mammals, only five transmissible cancers have been observed, all of which cause leukemia-like diseases in marine bivalves (Metzger et al., 2015, 2016). The scarcity of known transmissible cancers in nature suggests that such diseases emerge rarely. Furthermore, in Tasmanian devils, there were no reports of animals with facial tumors comparable with those caused by DFT1 and DFT2 prior to 1996 (Hawkins et al., 2006; Loh et al., 2006a). Thus, the recent identification of two transmissible cancers in Tasmanian devils, detected within an interval of 18 years, is very surprising, and suggests that exogenous or anthropogenic factors may contribute to risk of transmissible cancer development specifically in this species.

Despite an urgent need to further understand the molecular basis of transmissible cancers in Tasmanian devils, little is known of the underlying genetic changes that initially caused these cancers and that promote their colonization of allogeneic hosts. The genome of DFT1 indicates that this lineage has acquired several thousand mutations during its evolution (Murchison et al., 2012). Although some genes have been somatically altered (Miller et al., 2011; Murchison et al., 2012; Taylor et al., 2017), no "driver" mutations with a clear causative role in DFT1 emergence or evolution have been identified. Major histocompatibility complex (MHC) molecules are undetectable on the surface of most DFT1 cells, likely explaining the low immunogenicity of these cells in allogeneic hosts (Siddle et al., 2013). However, no mutations in genes involved in antigen presentation have been defined. DFT2 has not yet been characterized beyond a preliminary assessment of its histology, karyotype, and genetic profiles at microsatellite and MHC loci (Pye et al., 2016b).

Given the similar phenotypes of DFT1 and DFT2, the emergence of DFT2 provides an opportunity to understand the common factors that underlie transmissible cancers in Tasmanian devils. Here, we provide a comparative genetic and functional characterization of DFT1 and DFT2, analyzed alongside 46 normal devil genomes.

RESULTS

Tissues-of-Origin

DFT2 tumors are histologically distinct from those of DFT1 (Pye et al., 2016b). DFT2 is characterized by sheets of pleomorphic cells (amorphic to stellate and fusiform), whereas DFT1 is composed of pleomorphic round cells often arranged in bundles, cords, or packets (Loh et al., 2006a; Pye et al., 2016b). DFT1 expresses neuroectodermal markers, and is proposed to be of Schwann cell origin; indeed, a Schwann cell marker, PRX, is used to confirm DFT1 diagnosis (Loh et al., 2006b; Murchison et al., 2010; Tovar et al., 2011). DFT2 does not express PRX (Pye et al., 2016b) and its histogenesis remains unknown.

We used a panel of antibodies to broadly characterize the DFT2 tissue-of-origin by immunohistochemistry. Similar to DFT1, DFT2 is negative for cytokeratin and smooth muscle actin, and positive for vimentin, neural-specific enolase, and S100 (Figure S1). The similarity in tissue markers and gross phenotype between DFT1 and DFT2 suggests that these cancers arose from a similar cell type.

Germline Genotypes and Populations-of-Origin

To further understand the identities, locations and relationship between the DFT1 and DFT2 founder individuals, whose cells spawned the two lineages, we compared the germline alleles present in DFT1 and DFT2 with those in the devil population.

Tasmanian devil genetic analysis has revealed population substructure between eastern devil populations and those in the more isolated north-west (Brüniche-Olsen et al., 2014; Jones et al., 2004; Miller et al., 2011). Genotyping of DFT1 and DFT2 (Table S1) at 320 nuclear polymorphic loci, and comparison with 401 devils sampled from seven locations between 1999 and 2014 (Brüniche-Olsen et al., 2016), confirmed that both DFT1 and DFT2 arose from individuals with "eastern" genotypes (Figure 1). Further analysis indicated that DFT1 clustered most strongly with individuals sampled in north-east Tasmania (Mount William) in 2004, whereas DFT2 bore closest identity with individuals collected in 2014 from the Channel Peninsula (Figure 1). Overall, these findings are consistent with the notion that DFT1 and DFT2 arose within the areas in which they were first observed (Figure 1B), implying that both lineages may have been discovered relatively soon after their emergence.

The independent emergence of transmissible cancers from two Tasmanian devils both belonging to the eastern subpopulation suggests the possibility of inherited germline predisposition alleles that increase risk of transmissible cancer development. We investigated this hypothesis by sequencing the genomes of DFT1 and DFT2 (Table S1) and identifying and annotating their founder individuals' inherited germline single-nucleotide variant (SNV) and small insertion and deletion (indel) alleles (variants were considered likely to be germline if they were shared with $\geq$1 normal devil or if they were found in both DFT1 and DFT2, see the STAR Methods). Although a subset of these caused putative non-synonymous gene alterations in 908 genes (Table S1), none bore homology to known inherited cancer risk loci in humans (Forbes et al., 2015). Overall, although this approach revealed a number of candidate loci, we cannot confirm their involvement in DFT risk.

Virus Screen

We next investigated the possibility that exposure to exogenous pathogens, such as viruses, may increase the risk of DFT diseases developing in Tasmanian devils. We produced *de novo* assemblies of two DFT1 and two DFT2 genomes, and used whole genome and short read alignments to identify contigs that were exclusive to tumors and absent from four normal devils (see STAR Methods). This approach did not provide evidence for exogenous viral DNA in DFT1 or DFT2 (Table S1), consistent

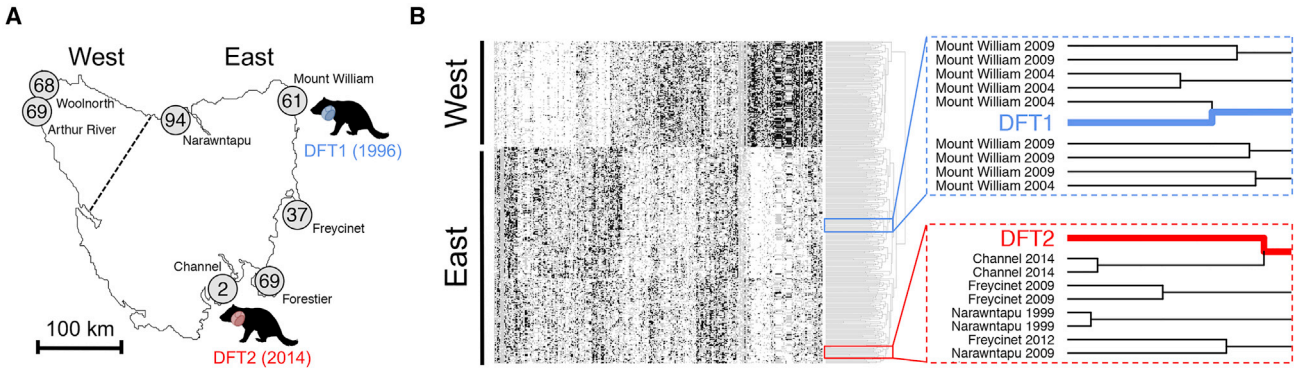

Figure 1. Origins of DFT1 and DFT2

(A) Map of Tasmania illustrating sampling locations of 400 devil individuals represented in (B). Number of individuals sampled from each location is labeled (Brüniche-Olsen et al., 2016). "East" and "West" denote the populations that cluster separately in (B), separated by dotted line. One individual was sampled from a captive population and is not shown on map. Devil silhouettes depict locations and year of first observations of DFT1 and DFT2.

(B) Hierarchical clustering of 320 SNP genotypes across a panel of 401 devils, DFT1 (blue) and DFT2 (red); individuals are represented as rows and loci as columns. Genotypes are coded as white (homozygous 1/1), black (homozygous 2/2), and gray (heterozygous 1/2). East and West populations, as defined in (A), are labeled. Right, detail of Euclidian distance dendrogram with sampling years and locations of devils neighboring DFT1 and DFT2 genotypes.

See also Table S1 and Figure S1.

with the results of previous screens for viruses in DFT1 using sequence alignments and transmission electron microscopy (Murchison et al., 2012; Pyecroft et al., 2007). However, we cannot exclude the potential involvement of DNA viruses that have not been maintained, small circular unintegrated DNA viruses not captured by our DNA extraction method, RNA viruses, or other pathogens in triggering DFT emergence.

Mutational Signatures

Further evidence for the involvement of exogenous agents in DFT1 and DFT2 pathogenesis might be gained from examination of mutational signatures (Alexandrov et al., 2013, 2015a; Baez-Ortega and Gori, 2017). The similarity in mutational spectra, a representation of the six SNV mutation types together with their immediate 5′ and 3′ contexts found in DFT1 and DFT2 tumors, suggests that similar mutational processes have operated in these two cancers (Figure 2A). We applied Markov Chain Monte Carlo sampling with a Bayesian statistical model to refit the 30 mutational signatures cataloged in human cancers (COSMIC, 2017) to pools of mutations in DFT1 and DFT2. This analysis revealed that refitting with human mutational signatures 1 and 5, both of which are "clock-like" age-associated signatures, which are almost universally active in human cancer and normal cells and are not indicative of exogenous mutational exposures (Alexandrov et al., 2013, 2015a; Blokzijl et al., 2016; Ju et al., 2017; Rahbari et al., 2016), adequately reconstructed the mutational spectra observed in both DFT1 and DFT2 (cosine similarity 0.93 and 0.95, respectively) (Figure 2B; Table S2).

Interestingly, neither DFT1 nor DFT2 genomes analyzed here bear imprints of exposure to UV light, a mutagen that leaves a readily recognizable mutational signature (Table S2). This contrasts with the transmissible venereal tumor in dogs, in which ~40% of mutations have been caused by UV (Murchison et al., 2014). Given that both DFT1 and DFT2 tumors are frequently located on external regions of the face, this observation suggests that either the nocturnal Tasmanian devil is rarely exposed to UV or, alternatively, that the cells that propagate DFT1 and DFT2 are not those on the surface of cutaneous tumors, but rather derive from non-exposed regions, such as the oral cavity or deep within the tumor mass.

Early Somatic Mutations

Our analysis has not provided evidence that exogenous exposures or germline risk contributed to DFT emergence. Next, we further characterized the functional consequences of putative somatic mutations in the two cancers. We identified 2,884 SNVs and 410 indels (DFT1), and 3,591 SNVs and 572 indels (DFT2), which were present in the genomes of two sequenced DFT1 tumors (86T and 88T, collected from Central Tasmania in 2005 and Eastern Tasmania in 2007, respectively) or two sequenced DFT2 tumors (202T2 and 203T3, both collected from the Channel Peninsula in 2014), but were not detected in the genomes of 46 normal devils (Figure 2C; Table S2). As we do not have germline DNA from the DFT1 or DFT2 founder devils, we cannot ascertain the provenance of these variants; however, a subset will be early somatic variants that occurred after emergence of each lineage and prior to divergence of the tumor isolates analyzed here (Figure 2C). Only 18 (18 SNVs, 0 indels) of these variants in DFT1 and 19 (16 SNVs, 3 indels) in DFT2 were predicted to be non-synonymous, with no intersection between the genes harboring non-synonymous variants in DFT1 and DFT2 (Figure 2C; Table S2). None of these putative early somatic non-synonymous SNV or indel mutations occurred in a set of genes with confirmed causative involvement in human cancer (http://cancer.sanger.ac.uk/cosmic/census/) (Tables S2 and S3). The majority of these mutations were predicted to be heterozygous (Table S2). However, we observed that DFT1 harbored a hemizygous nonsense mutation in *WWC3* (R945* in exon 21/24), and DFT2 carried a hemizygous truncating indel in *MPDZ* (S496X in exon 9/47); in both cases, the second copy was deleted, likely leading to complete loss-of-function (Tables S2 and S4). We genotyped these variants across eight additional geographically dispersed DFT1 tumors (*WWC3*) and two additional DFT2 tumors (*MPDZ*) (Table S2); in both cases, the relevant variant

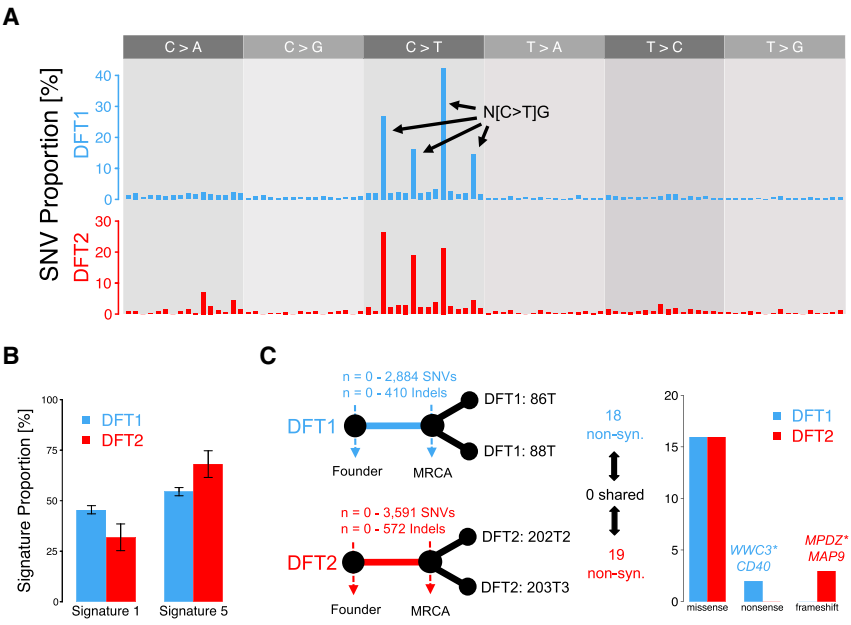

Figure 2. Single-Nucleotide Variants and Indels in DFT1 and DFT2

(A) Mutational spectra of single-nucleotide variants (SNVs). Only SNVs that are unique to one tumor within a lineage, and therefore likely to be somatic, are displayed (n = 6,812 [DFT1], n = 626 [DFT2]). Each bar represents a mutation category defined by the mutation type shown in upper gray panel, and its immediate 5′ and 3′ base context; mutation classes are presented in the order shown in (COSMIC, 2017), and prominent mutation types are labeled (N, any base). Mutation counts are normalized to corresponding nucleotide triplet frequencies in the devil genome.

(B) Best fit of two mutational signatures. Signatures 1 and 5, extracted from human cancers (Alexandrov et al., 2013), were fitted to SNVs derived from DFT1 and DFT2. DFT1 and DFT2 SNVs were represented by a pool of those that are unique to one tumor within each lineage. Error bars display 95% Bayesian credible intervals of the posterior probability after 10^5 Markov Chain Monte Carlo samples.

(C) Analysis of early somatic variants. Left, simplified phylogenetic trees represent origins of DFT1 and DFT2 from their respective founder devils, and their respective divergence after the most recent common ancestor (MRCA) of the tumor isolates analyzed here (86T and 88T, DFT1) and (202T2 and 203T3, DFT2). Plausible range of somatic SNV and indel counts within the trunk of each tree is indicated, with the upper bound defined by those variants shared between both tumor isolates in each lineage but not detected in 46 normal devil genomes. The upper bounds of early somatic non-synonymous mutations in each lineage is shown and, right, annotation of these variants is represented. * indicates the truncating mutations in *WWC3* and *MPDZ* are hemizygous as in both cases the second allele has been deleted.

See also Tables S2, S3, and S4.

was present in all tumors analyzed, suggesting that these variants may be somatic mutations acquired early, prior to clonal diversification. Interestingly, both *WWC3* and *MPDZ* are proposed to encode negative regulators of YAP1 and WWTR1/TAZ, core effectors of the Hippo signaling pathway, which has conserved roles in development, regeneration, and cancer (Han et al., 2017; Juan and Hong, 2016; Moroishi et al., 2015; Varelas et al., 2010; Zanconato et al., 2016). YAP1 and WWTR1/TAZ are transcriptional co-activators that shuttle between cytoplasm and nucleus; in both DFT1 and DFT2 cells, YAP1 and WWTR1/TAZ are expressed and show nuclear localization, indicating activity (Figure S1). The Hippo pathway has been implicated in several human cancer histotypes, and is of particular importance in Schwann cell cancers (Wu et al., 2018; Zanconato et al., 2016).

Cytogenetics and Structural Variants

Structural variants (SVs) are another source of somatic variation that may have contributed to DFT oncogenesis. Chromosome painting revealed that the DFT2 karyotype (Pye et al., 2016b) appears to have arisen via insertion of chromosome 6 into the pericentric region of chromosome 2, forming a large derived chromosome (Figure 3A). We used discordantly mapped paired-end sequence reads and PCR screens to identify putative somatic SVs in DFT1 and DFT2. The pattern of SVs in DFT1 revealed a cluster of rearrangements on chromosome 2 that was acquired prior to divergence of the tumors sequenced in this study (Figure 3B; Table S5). We also identified a focus of SVs on chromosome 1 in one DFT1 tumor, which marks the region from which the extrachromosomal double minutes (DMs) in this tumor derive (Taylor et al., 2017) (Figures 3A and 3B; Table S5). We identified 64 and 23 rearrangements involving genes in one or both DFT1 genomes or in one or both DFT2 genomes analyzed here, respectively, but not in 34 normal devil genomes (Table S5). These predicted three DFT1-specific in-frame fusion genes, *PDZD11-RFX2*, *CAMK2A-NEURL1B*, and *EZH2-ETNK2;* the latter two potential fusion genes were found in only one of two analyzed DFT1 tumors, and are thus unlikely to have arisen early in DFT1 tumor evolution (Tables S3 and S5). Genotyping of *PDZD11-RFX2*, however, confirmed its presence in eight additional geographically dispersed DFT1 tumors (Table S2), suggesting that it may be a somatic rearrangement that occurred early in the DFT1 lineage. *EZH2*, encoding a histone methyltransferase, is dysregulated in many cancers (Kim and Roberts, 2016), but it is unclear if the disruption of this gene in a subset of DFT1s has provided a selective advantage to this lineage (Table S3). Overall, the DFT2 genomes analyzed here have simpler structures and fewer rearrangements than those of the DFT1 genomes analyzed here. However, similar microhomology-mediated repair processes operated during clonal evolution of both DFT1 and DFT2 (Figure 3B; Table S5).

Telomeres

Rearrangements in cancer are frequently triggered by telomere crisis (Maciejowski and de Lange, 2017). Tasmanian devils have unusual telomeres characterized by extreme length dimorphism between homologs (Bender et al., 2012). This feature has been lost in DFT1, which carries uniformly short telomeres (Bender et al., 2012). We used fluorescence *in situ* hybridization (FISH) to examine telomere length in DFT2. Our analysis revealed that cells derived from DFT2 exhibited telomere length dimorphism between homologs similar to normal cells (Figure 3C), and indicated

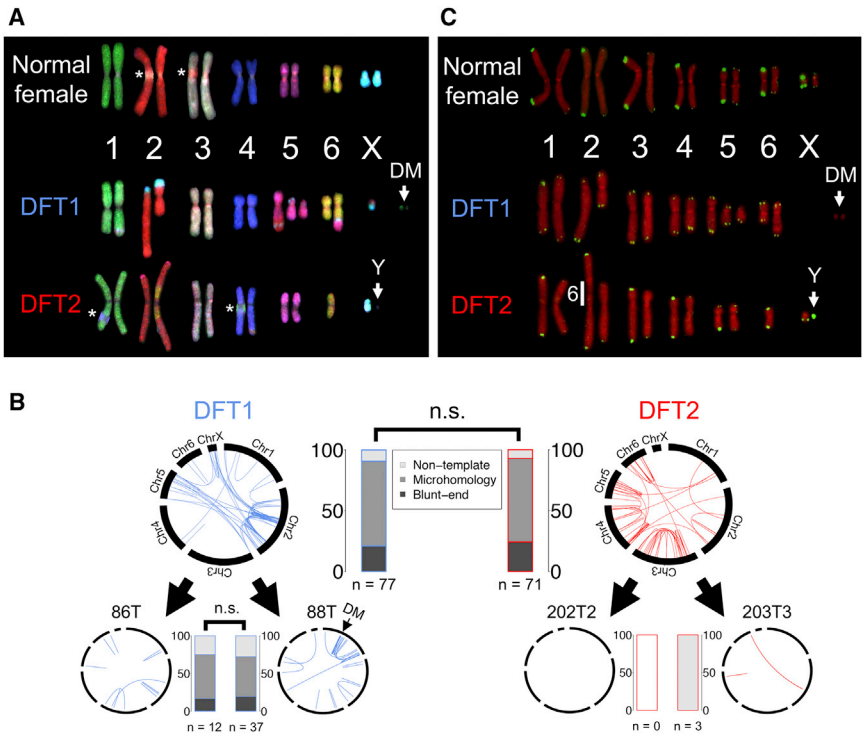

Figure 3. Structural Variation and Telomeres in DFT1 and DFT2

(A) Chromosome painting. Normal devil female, DFT1 (tumor 88T) and DFT2 (tumor 203T3) metaphases hybridized with devil chromosome-specific fluorescent probes. DM, double minutes; the Y chromosome lacks a specific probe and is indicated with "Y"; * indicates locations of overlap between chromosome arms that were present in images used to generate karyotypes.

(B) Structural variant (SV) mutations. Larger upper circos plots represent likely somatic SVs shared between 86T and 88T (DFT1) or 202T2 and 203T3 (DFT2), respectively, but that are not found in 34 normal devils. Lower circos plots represent SVs that are uniquely found in one of the sequenced tumors of the two lineages. DM, SVs involved in double minutes. Blue or red lines connect chromosomal coordinates involved in SV. Stacked bar plots indicate percentage of breakpoints displaying short regions of microhomology, non-templated sequence insertions or blunt ends. n.s., Pearson's chi square test, $p > 0.05$.

(C) Telomeres. Normal devil female, DFT1 (tumor 88T) and DFT2 (tumor 202T2) metaphases hybridized with telomere-specific fluorescent probes (green). Chromosomes are labeled red. DMs and Y chromosome are indicated, as well as site of integration of chromosome 6 into the derivative chromosome 2 in DFT2.

See also Tables S3 and S5.

that it was the chromosome 6 homolog with short telomeres that was incorporated into chromosome 2 to generate the large derivative chromosome in DFT2 (Figure 3C). Thus, although loss of telomere length dimorphism is not essential for the emergence of transmissible cancers in Tasmanian devils, this species' unusual telomere organization may contribute to risk of chromosomal rearrangement, which may predispose to DFT cancer.

Copy Number Variants

We next characterized copy number variants (CNVs) in the two cancers. A comparison of CNVs in DFT1 and DFT2 confirmed that all of the tumor isolates analyzed here are largely diploid (Figure 4A; Table S4). Most CNVs in DFT1 and DFT2 involved different genomic regions; however, an ~18.4 megabase hemizygous deletion on chromosome 3 was found in both lineages (Figure 4A; Table S4). This CNV, which was not detected in 46 normal devil genomes suggesting that it is possibly somatic (Figure S2), reduces dosage of 74 genes in both DFT1 and DFT2 (Figure 4B and Table S4). One gene in DFT1 (*MAST3*) (Murchison et al., 2012) and four genes in DFT2, including *HGF* and *TP73*, have undergone homozygous deletion (Figure 4B; Table S4); the other two homozygously deleted genes in DFT2, *CACNA2D1* and *ENSSHAG0000005243*, are linked to *HGF* and *TP73*, respectively. Interestingly, *TP73* acts downstream of Hippo pathway effectors to activate apoptosis (Moroishi et al., 2015).

Copy number gains have increased the dosage of 1,129 genes in DFT1 and 501 genes in DFT2. Strikingly, we observed that genes encoding the two platelet-derived growth factor receptors (PDGFRs), *PDGFRA* and *PDGFRB*, were respectively gained in copy number in DFT2 (copy number 4, focal amplification) and some DFT1s (as part of extrachromosomal DMs) (Figure 4C; Tables S3 and S4). This correlated with strong expression of both PDGFRs in DFT1 and DFT2 (Figure 4C). Interestingly, both *PDGFA* and *PDGFB*, encoding ligands for PDGFRs, have undergone copy number gains in DFT1 (and *PDGFA* is additionally involved in a SV in DFT1 [Murchison et al., 2012; Tables S4 and S5]). Furthermore, *ERBB3* showed copy number gains in DFT1 and is expressed in DFT1 (Hayes et al., 2017; Taylor et al., 2017), and a subset of DFT1s carried gains of *NRG2*, encoding an ERBB ligand (Figure 4B; Tables S3 and S4).

Immune Genes and Loss of Y Chromosome

DFT clones must escape the host immune system despite their status as allogeneic grafts. Interestingly, *B2M*, encoding a component of MHC class I, has undergone hemizygous deletion in DFT1 (Figure 4D). This copy number loss may have contributed to the downregulation of MHC observed in DFT1, resulting in this lineage's low immunogenicity (Siddle et al., 2013). We also observed that DFT1 carried a heterozygous truncating mutation in *CD40*, encoding an immune co-stimulatory molecule that may be expressed together with MHC class II by Schwann cells (Figures 2C and 4B) (Duan et al., 2007; Meyer zu Hörste et al., 2010).

DFT2 faces a further potential immunological challenge due to its possession of the Y chromosome. This lineage arose in a male devil and has, to date, usually been observed in males (of the 11 reported cases of DFT2, 9 involve a male host [Kwon et al., 2018]). This apparent bias toward male hosts raises the possibility that females may be less susceptible to DFT2 due to immunogenicity of antigens derived from the Y chromosome. We investigated the stability of the Y chromosome in DFT2 by PCR amplifying the Y-linked *SRY* locus in a panel of DFT tumors and their male and female hosts (Figure 4E; Table S6). As

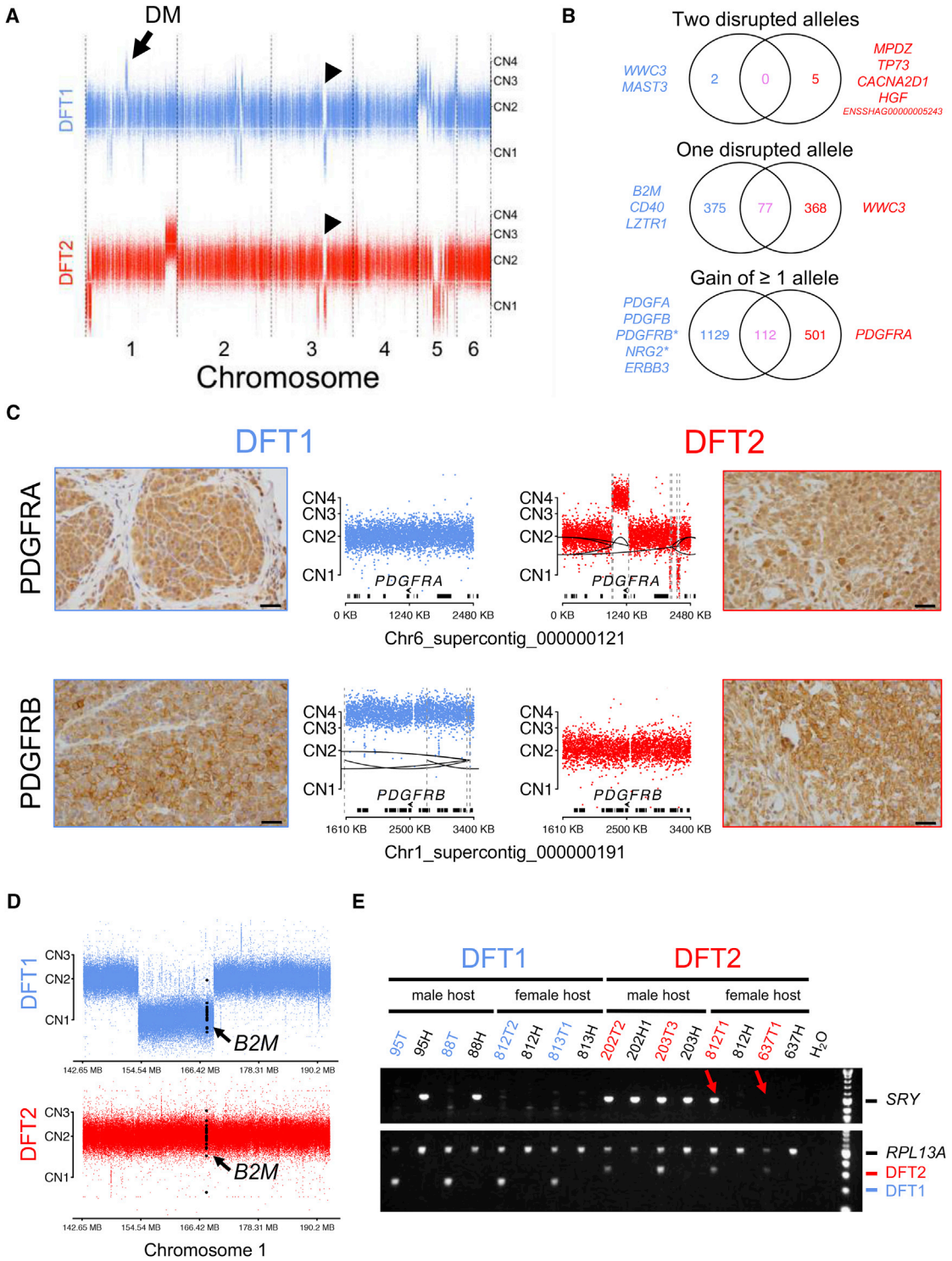

Figure 4. Copy Number Variation and Functional Annotation in DFT1 and DFT2

(A) DFT1 (tumor 88T) and DFT2 (tumor 202T2) autosomal copy number generated using read counts at 735,281 SNP loci. Each dot represents $\log_2$R, where R = (read depth in tumor)/(read depth in 203H), at a single SNP. CN, copy number. Arrow, chromosomal origin of DMs; arrowheads, hemizygous deletion identified in both DFT1 and DFT2.

(B) Illustration of gene alterations. In each Venn diagram, number of genes altered in ≥1 DFT1 tumors are shown in blue on the left, and number of genes altered in ≥1 DFT2 tumors are shown in red on the right; numbers of genes that are similarly altered in ≥1 DFT1 and ≥1 DFT2 tumor are shown in pink in the center of each diagram. Only autosomal genes are considered and 'disrupted' alleles include only predicted loss-of-function alterations. Genes-of-interest are written in text beside diagrams. * indicates these genes are amplified on extrachromosomal DMs.

(legend continued on next page)

expected, Y chromosome DNA was not detected in DFT1, which is derived from a female founder devil, regardless of the gender of the host (Figure 4E). In DFT2, Y chromosome DNA was present in DFT2 tumors in male hosts, as well as in one DFT2 tumor in a female host, Devil 812 (Devil 812 also carried two DFT1 tumors [Kwon et al., 2018]). However, the Y chromosome locus could not be detected in the DFT2 tumor derived from the second female host, Devil 637 (Figure 4E).

DFT1 and DFT2 Drug Screen

To gain further insight into the signaling pathways which promote DFT1 and DFT2 growth and survival, and to uncover potential therapeutic vulnerabilities, we performed a high-throughput *in vitro* drug sensitivity screen. Four DFT1 cell lines and two DFT2 cell lines (Table S7) were treated with a 7-point titration (1,000-fold concentration range) of 104 pre-clinical and clinical compounds with activity against a wide range of molecular targets (Figure 5A; Table S7) prior to cell viability quantification. Hierarchical clustering based on half maximal inhibitory concentration (IC_{50}) values indicated that DFT1 and DFT2 are distinguishable from each other based on their drug sensitivity (Figure 5B); however, the two cancers share a striking overall similarity in drug response profile compared with several hundred human cancer cell lines (Figures 5C–5F; Table S7 [Yang et al., 2013]).

Both DFT1 and DFT2 are sensitive to a suite of inhibitors of receptor tyrosine kinases (RTKs) (Figure 5C). In particular, DFT1 cell lines are remarkably responsive to Afatinib, an inhibitor of ERBB2 and EGFR (DFT1 cell lines top 0.4%–1.1% most sensitive of 959 cell lines, geometric mean DFT1 IC_{50}: 9.8 nM) (Figure 5C). This sensitivity is likely mediated by ERBB2 inhibition, as DFT1 is resistant to Gefitinib and Erlotinib, agents that specifically target EGFR (Table S7). Remarkably, DFT1 cell lines show significantly greater sensitivity to Afatinib than a panel of *ERBB2*-amplified human breast cancer cell lines (Figure 5E; geometric mean DFT1 IC_{50}: 9.8 nM, geometric mean $ERBB2^{+}$ Breast cancer cell lines IC_{50}: 314.9 nM; $p = 0.000516$, Wilcoxon rank-sum test). DFT2, on the other hand, is highly sensitive to Axitinib, a compound with activity against PDGFR, KIT, and vascular endothelial growth factor receptor (VEGFR) (DFT2 cell lines top 0.2%–0.4% most sensitive of 854 cell lines, geometric mean DFT2 IC_{50}: 5.0 nM) (Figure 5C). In addition, both DFT1 and DFT2 show sensitivity to Dasatinib, a tyrosine kinase inhibitor whose targets include PDGFR, ABL, SRC, ephrins, and KIT (geometric mean DFT1 IC_{50}: 7.5 nM; geometric mean DFT2 IC_{50}: 6.4 nM) (Figure 5C). Both DFT1 and DFT2 are markedly sensitive to CHEK1/CHEK2 inhibitor AZD7762, and poly-ADP ribose polymerase (PARP) inhibitors Talazoparib and Olaparib, suggesting that DFT cancers are intolerant of DNA damage (Figure 5D; Table S7), perhaps explaining the remarkable genomic stability observed in DFT1 (Deakin et al., 2012; Murchison et al., 2012). The response of DFT cell lines to Talazoparib was particularly notable and is comparable with that of highly sensitive human Ewing's sarcoma cell lines (geometric mean DFT1 IC_{50}: 33.1 nM, top 0.2%–2.0% of 922 cell lines, geometric mean DFT2 IC_{50}: 74.2 nM, top 0.7%–5.2% of 922 cell lines, geometric mean Ewing's IC_{50}: 330.2 nM, top 0.3%–72.1% of 922 cell lines) (Brenner et al., 2012; Garnett et al., 2012) (Figure 5F). This sensitivity likely does not reflect defects in homologous recombination, as we do not detect evidence for COSMIC mutational signature 3 (Figure 2A; Table S2) (Alexandrov et al., 2015b; Alexandrov et al., 2013; COSMIC, 2017; Nik-Zainal et al., 2012; Nik-Zainal et al., 2016). Altogether, this screen highlights key vulnerabilities inherent to DFT cells and strongly implicates RTK signaling in driving oncogenesis of both DFT1 and DFT2.

DISCUSSION

DFT2 has changed our perception of the nature of transmissible cancers. Previously, transmissible cancers were believed to arise very rarely in nature, with the existing examples representing exceptional cases that had overcome strong natural barriers. Indeed, the observation that all sampled transmissible venereal tumors in dogs belong to a single clone which originated several thousand years ago (Murgia et al., 2006; Rebbeck et al., 2009; Strakova et al., 2016) suggests that such canine cancers appear and disperse infrequently. However, the emergence of DFT2, together with the discovery of several transmissible cancers in marine bivalves (Metzger et al., 2015, 2016), suggests that some species may have a particular vulnerability for the development of this type of disease and that, at least in these species, transmissible cancers may be spawned relatively frequently.

The reason for Tasmanian devils' apparent susceptibility to transmissible cancers is not clear. The striking similarities in tissues-of-origin, genome architectures, mutational processes, driver gene candidates, and drug vulnerabilities, strongly suggest that DFT1 and DFT2 belong to the same cancer type and arose via similar oncogenic mechanisms. DFTs are likely of neuroectodermal origin, and may show differentiation toward the neural crest-derived Schwann cell lineage (Murchison et al., 2010). The closest human cancer histotype to DFT is not clear (Loh et al., 2006b), and comparative studies with human and veterinary cancers are further hampered by lack of knowledge of the body site from which DFT cancers first arise. It is notable that, although Tasmanian devils are reported to have high frequencies of host-derived neoplasia (Griner, 1979), no lesions have been described that are consistent with pre-transmissible DFT; given that hundreds of wild and captive devils are routinely monitored

(C) Copy number and immunohistochemistry for *PDGFRA* and *PDGFRB*. Reads mapping within 500 base pair genomic bins were counted and normalized using cn.MOPS (Klambauer et al., 2012); each dot represents $\log_2$R for a single bin, where R = (read count tumor)/(read count 203H). CN, copy number. Structural variants are represented by dashed gray lines connected by black lines. Genes are represented as black bars, and locations and orientations of *PDGFRA* and *PDGFRB* are shown. Brown stain reports expression, counterstained with blue hematoxylin. Scale bar, 30 μm.

(D) Copy number at *B2M* locus. Copy number was determined and displayed as in (C). Bins within *B2M* are colored in black. CN, copy number.

(E) PCR amplification of the Y chromosome-linked *SRY* locus. DFT1 tumors (95T, 88T, 812T2, and 813T1) and DFT2 tumors (202T2, 203T3, 812T1, and 637T1) are labeled in blue and red, respectively, and DFT1 hosts (95H, 88H, 812H, and 813H) and DFT2 hosts (202H1, 203H, 812H, and 637H) are displayed in black. The upper panel shows *SRY* product and the lower panel shows positive control (*RPL13A*) and diagnostic amplification product for confirmation of DFT1 or DFT2 (Kwon et al., 2018). Red arrows highlight presence (812T1) or absence (637T1) of an *SRY* band in DFT2 tumors infecting female Tasmanian devils.

See also Tables S3, S4, S5, S6, and Figure S2.

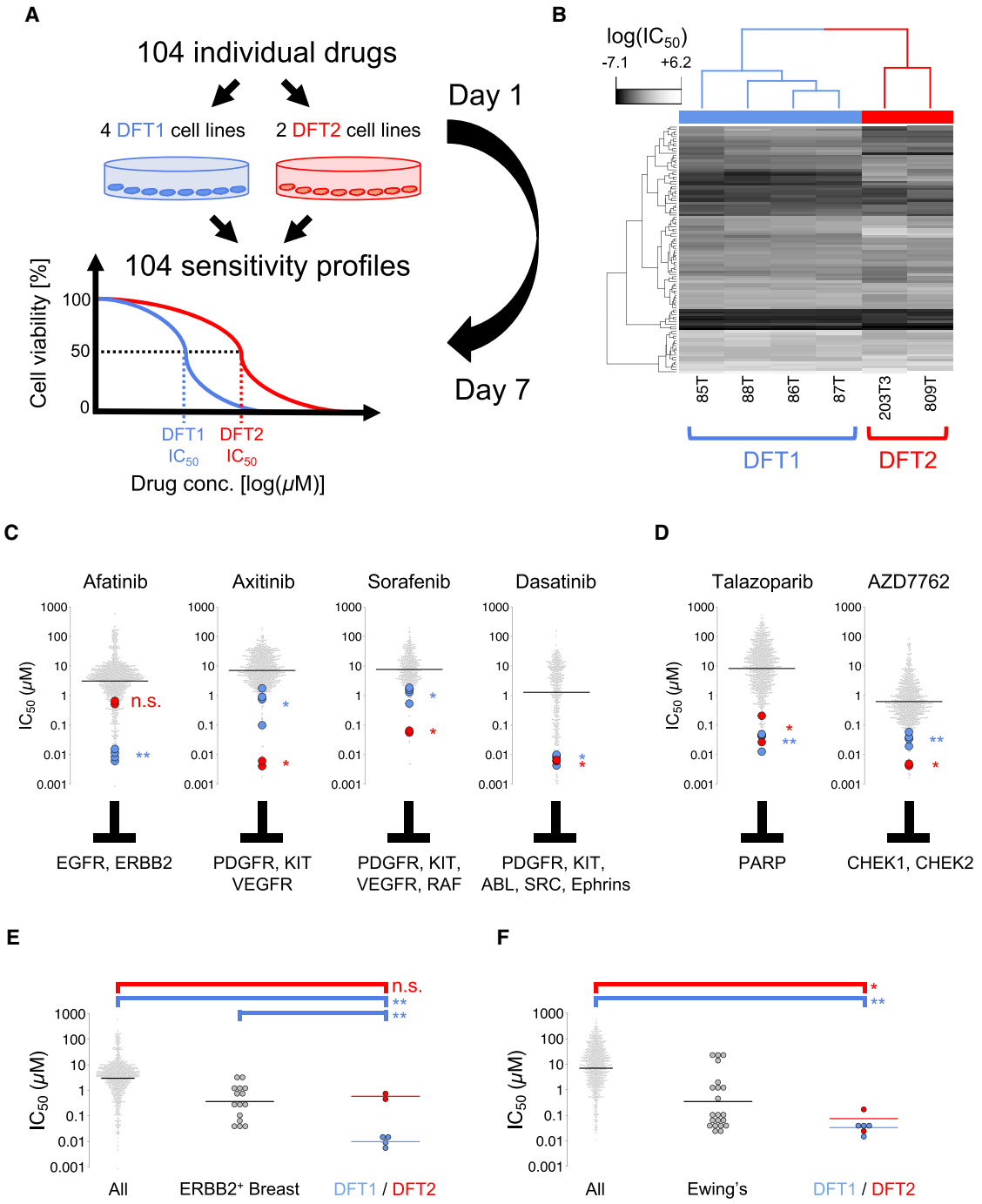

Figure 5. DFT1 and DFT2 Drug Screen

(A) Four DFT1 (85T, 86T, 87T, and 88T) and two DFT2 (203T3 and 809T) cell lines were screened against a panel of 104 drugs under clinical and pre-clinical investigation in human oncology. Cell viability was measured after 144 hr.

(B) Hierarchical clustering of $\log_e$ (IC_{50}) values for 6 DFT cell lines (columns) screened with 104 compounds (rows).

(C and D) IC_{50} for DFT1 (blue) and DFT2 (red) cell lines for four receptor tyrosine kinase (RTK) inhibitors (C) or two DNA repair inhibitors (D). Gray dots represent human cancer cell lines (GDSC set). Drug molecular targets are indicated. Horizontal bars represent geometric mean IC_{50}. *$p < 0.05$, **$p < 0.001$; n.s., not significant, Wilcoxon rank-sum test for DFT1 and DFT2 compared with human cell lines.

(E) Afatinib IC_{50} for 953 human cancer cell lines (All), 15 *ERBB2*-amplified human breast cancer cell lines (ERBB2$^+$ breast), and DFT1 and DFT2 cell lines. Horizontal bars represent geometric mean IC_{50}. **$p < 0.001$; n.s., not significant, Wilcoxon rank-sum test.

(F) Talazoparib IC_{50} for 922 human cancer cell lines (All), 21 Ewing's sarcoma cell lines (Ewing's), and DFT1 and DFT2 cell lines. Horizontal bars represent geometric mean IC_{50}. *$p < 0.05$, **$p < 0.001$; Wilcoxon rank-sum test.

See also Table S7.

each year, this suggests that either such lesions are difficult to detect or recognize or that DFT cancers arise rarely but carry a high risk of becoming transmissible. Importantly, we cannot completely negate the possibility that DFT1 and/or DFT2 arose via a horizontal DNA transfer event involving an ancestral DFT cell and a normal cell (Pye et al., 2016b); however, the lack of germline and somatic genetic similarity between DFT1 and DFT2 suggests that this scenario is unlikely.

We investigated genetic and phenotypic features of DFT1 and DFT2, and compared the two lineages with each other and with catalogs of known human cancer genes and drug sensitivity profiles. These data suggest an important role for RTK signaling, most likely involving ERBB2 (DFT1 only) and PDGFRs (DFT1 and DFT2), in sustaining growth and survival of DFT cancers. In this context, it is likely that copy number gains involving PDGFR genes may have provided selective advantage in these cancers. Furthermore, we noted that *PDGFRB* has been amplified on DMs in some DFT1s, and may be the positively selected driver required to maintain this extrachromosomal DNA. We did not identify any mutations in *ERBB2* in DFT1. However, we observed copy number gains involving *ERBB3*, encoding an ERBB2 heterodimerization partner, and *NRG2,* encoding an ERBB3 ligand (Hynes and Lane, 2005; Taylor et al., 2017), suggesting a possible mechanism for ERBB2 activation. Both DFTs show remarkably few perturbations in known cancer genes, and only two genes in DFT1 and five genes in DFT2 are predicted to have undergone biallelic loss-of-function. Thus, the observation that DFT1 and DFT2 both harbor predicted two-hit loss-of-function mutations in genes encoding proposed regulators and effectors of Hippo signaling (*WWC3, MPDZ, TP73*), together with evidence for activity of Hippo effectors YAP1 and WWTR1/TAZ in DFT1 and DFT2 cells, raises the possibility that this pathway is involved in DFT cancers in Tasmanian devils. The Hippo pathway plays conserved roles in differentiation, proliferation, and regeneration in several tissues (Moroishi et al., 2015; Yu et al., 2015; Zanconato et al., 2016), and in the Schwann cell context drives transcriptional upregulation of PDGF and ERBB signaling components (Deng et al., 2017; Wu et al., 2018).

DFT clones must escape the host immune system despite their status as allogeneic grafts. Although low Tasmanian devil population genetic diversity may reduce capacity for foreign tissue detection (Miller et al., 2011; Siddle et al., 2007), this species' rejection of skin allografts (Kreiss et al., 2011) suggests that DFT1 and DFT2 clones have specific adaptations favoring immune escape. Our analysis did not identify any genomic aberrations common to both cancers that might underlie such adaptations, raising the possibilities that they may be epigenetically controlled (Siddle et al., 2013), or that DFT cancers arise from cell types that already harbor low immunogenicity. Nevertheless, it is possible that hemizygous deletion of *B2M* may have contributed to downregulation of MHC class I in DFT1, although the remaining intact copy can be robustly expressed in response to the inflammatory cytokine, interferon gamma (Siddle et al., 2013). In DFT2, both copies of *B2M* remain intact, and *B2M* expression has been detected in at least a subset of tumor cells (H. Siddle, unpublished data). This suggests that DFT1 and DFT2 may have adopted different strategies for immune evasion, although the significance of these findings is not yet confirmed. Loss of Y chromosome DNA in DFT2 may have rendered this cancer less immunogenic in female hosts, although we cannot exclude the possibility that this loss is selectively neutral. If Y chromosome loss is indeed a selective advantage to the lineage, we may expect in future to observe Y-null DFT2 strains, perhaps derived from several independent Y chromosome loss events, becoming dominant in the population. Despite limited understanding of the mechanisms of DFT immune evasion, recent observations of natural immune responses against DFT1 (Pye et al., 2016a), as well as allele frequency shifts indicative of selection in DFT1-affected populations (Epstein et al., 2016), suggest that some devils may be capable of mounting immune responses against DFT cancers.

Altogether, our findings present the possibility that transmissible cancers may be a part of Tasmanian devils' natural ecology. Indeed, we did not find evidence for the involvement of exogenous exposures or pathogens in DFT carcinogenesis, nor did we identify any known cancer predisposition alleles in the inherited genomes of the DFT1 or DFT2 founder devils. Thus, it seems plausible that additional DFTs occurred in the past but escaped detection, perhaps because they remained in localized populations or because they existed prior to the nineteenth-century arrival of European documenters.

It is worth speculating about biological features specific to devils that may spur DFT cancer development. Devils bite each other frequently around the facial area, often causing significant tissue injury (Hamede et al., 2013). Given the important roles for Hippo and RTK signaling in wound-healing responses (Zanconato et al., 2016), particularly in Schwann cells (Mindos et al., 2017; Fex Svennigsen and Dahlin, 2013), it is tempting to speculate that DFT cancers may arise from aberrant maintenance of proliferative cells involved in tissue repair after injury. Under this model, the facial biting behavior of Tasmanian devils may predispose these animals to emergence of cancers via tissue injury, simultaneously providing a route of cell transmission. Furthermore, it is possible that anthropogenic factors may have indirectly increased the risk of DFT emergence or spread in recent years. For instance, it is possible that some modern land use practices, such as pastoralism, may have provided favorable conditions for devils, leading to elevations in local devil densities (Guiler, 1970, 1982; Jones et al., 2004); this might have led to increased intra-specific competition, perhaps increasing interactions and fights, which may in turn have raised probabilities of DFTs arising or spreading. Road construction may have caused increased connectivity between devil populations, providing more opportunities for DFTs to spread. Finally, persecution of devils by European colonists (Hawkins et al., 2006) may have contributed to this species' low genetic diversity (Jones et al., 2004), a possible risk factor for DFT immune escape and disease spread (Siddle et al., 2007). In future, it will be important to continue to monitor Tasmanian devils for evidence of additional DFT clones and to track the evolution and spread of DFT1 and DFT2.

At present, there are few options for DFT treatment, and most animals succumb to disease. Given the failure of conventional chemotherapy agents against DFT1 (Phalen et al., 2013), the potential for orally delivered, targeted therapies offer considerable promise. We have shown that DFT1 and DFT2 are exquisitely sensitive to a suite of RTK inhibitors, including those targeting PDGFRs (DFT1 and DFT2) and ERBB2 (DFT1 only), as well as

to inhibitors of DNA repair. The recent success of experimental immunotherapy regimens against DFT1 (Tovar et al., 2017) opens the possibility that therapies which combine RTK or PARP inhibition with immune activation may present new opportunities for combatting DFT clones and saving the Tasmanian devil.

DFT1 and DFT2 arose from two unremarkable individuals, which gave rise to cancers with strikingly similar, but subtly different, histologic, genomic, and drug sensitivity phenotypes. We have shown that, at least in Tasmanian devils, relatively simple genomic changes coupled with incessant growth factor signaling spur the transition from somatic cell to parasitic clonal lineage. Transmissible cancers in Tasmanian devils exploit a perverse niche created by their host species and illustrate one context in which runaway selfish evolution can thrive.

STAR★METHODS

Detailed methods are provided in the online version of this paper and include the following:

- KEY RESOURCES TABLE
- CONTACT FOR REAGENT AND RESOURCE SHARING
- EXPERIMENTAL MODEL AND SUBJECT DETAILS
  - Tissue Sampling and Ethics
  - Cell Lines and Cell Culture
- METHOD DETAILS
  - Cytogenetics
  - Histology
  - Immunohistochemistry
  - Sample Processing and Sequencing
  - Published Normal Devil Genomes
  - Whole Genome Amplification
  - SNV Validation
  - SNV Genotyping across Normal Panel
  - SNV Genotyping of *WWC3* and *MPDZ* Mutations
  - SV Validation
  - SV Genotyping across Normal Panel
  - SV Genotyping of *PDZD11-RFX2*
  - DFT Diagnostic PCRs
  - Y Chromosome PCRs
  - Drug Screen
- QUANTIFICATION AND STATISTICAL ANALYSES
  - Devil Population Analysis
  - SNV and Indel Analysis
  - Copy Number Analysis
  - Structural Variant Analysis
  - Mutational Signature Analysis
  - Virus Screen and PAV Analysis
  - Drug Screen IC_{50} Analysis
- DATA AND SOFTWARE AVAILABILITY

SUPPLEMENTAL INFORMATION

Supplemental Information includes two figures and seven tables and can be found with this article online at https://doi.org/10.1016/j.ccell.2018.03.013.

ACKNOWLEDGMENTS

We give particular thanks to Mike Stratton, and to members of the Wellcome Trust Sanger Institute Sample Management, Core IT, and Cancer Genome Project IT Departments for their support. We are grateful to Anna Brüniche-Olsen, Alison Caldwell, Tasha Czarny, Samantha Fox, Rodrigo Hamede, Paul Kitts, Alexandre Kreiss, Billie Lazenby, Nick Mooney, Máire Ní Leathlobhair, David Pemberton, Aylwyn Scally and Andrea Strakova for logistical and technical assistance and for helpful discussions. This work was supported by grants from Wellcome (102942/Z/13/A and WT098051). Support was also provided by the National Science Foundation (DEB-1316549), Eric Guiler Tasmanian Devil Research Grants, and a Philip Leverhulme Prize awarded by the Leverhulme Trust. M.R.S. is supported by a scholarship from the Gates Cambridge Trust. Work in the M.J.G. lab is supported by funding from CRUK (C44943/A22536), SU2C (SU2C-AACR-DT1213) and Wellcome (102696). Devil silhouette image credits to Bob Comix: http://bit.ly/2hFQPaC, licensed under a Creative Commons Attribution-Share Alike 4.0 License.

AUTHOR CONTRIBUTIONS

E.P.M. conceived, designed, and supervised the study. M.R.S., T.H.H.C., K.C.G., D.E.M.-H., A.B.-O., and Y.M.K. carried out computational analyses. D.H., G.W.K., and S.S.S. generated IHC images and analyzed histology. M.R.S. and E.P.M. analyzed ancestral Tasmanian devil data. F.G., G.H., and Z.N. provided genome assemblies and performed a subtractive screen. M.R.S. and T.H.H.C. investigated viral and Y chromosome scaffolds. B.F. and F.Y. performed chromosome and telomere FISH experiments. M.R.S., T.H.H.C., K.C.G., D.E.M.-H., J.M.C.T., and E.P.M. analyzed SNV, indel, CNV, and SV mutations from sequencing data. J.W. and M.R.S. performed validation PCRs. L.B.A., S.B., A.B., S.P., U.McD., and M.J.G. conducted drug screen experiments. M.R.S., E.P.M., and M.J.G. analyzed drug screen data. Y.M.K. extracted DNA from tissue biopsies and cell lines. H.V.T.S., R.J.P., and G.M.W. provided cell lines and experimental suggestions. E.P.M. and M.R.S. wrote the paper. All authors read and approved the manuscript.

DECLARATION OF INTERESTS

The authors declare no competing financial interests.

Received: November 14, 2017
Revised: January 23, 2018
Accepted: March 11, 2018
Published: April 9, 2018

REFERENCES

Alexandrov, L.B., Nik-Zainal, S., Wedge, D.C., Aparicio, S.A., Behjati, S., Biankin, A.V., Bignell, G.R., Bolli, N., Borg, A., Borresen-Dale, A.L., et al. (2013). Signatures of mutational processes in human cancer. Nature *500*, 415–421.

Alexandrov, L.B., Jones, P.H., Wedge, D.C., Sale, J.E., Campbell, P.J., Nik-Zainal, S., and Stratton, M.R. (2015a). Clock-like mutational processes in human somatic cells. Nat. Genet. *47*, 1402–1407.

Alexandrov, L.B., Nik-Zainal, S., Siu, H.C., Leung, S.Y., and Stratton, M.R. (2015b). A mutational signature in gastric cancer suggests therapeutic strategies. Nat. Commun. *6*, 8683.

Baez-Ortega, A., and Gori, K. (2017). Computational approaches for discovery of mutational signatures in cancer. Brief. Bioinform. https://doi.org/10.1093/bib/bbx082.

Bean, J., Brennan, C., Shih, J.Y., Riely, G., Viale, A., Wang, L., Chitale, D., Motoi, N., Szoke, J., Broderick, S., et al. (2007). MET amplification occurs with or without T790M mutations in EGFR mutant lung tumors with acquired resistance to gefitinib or erlotinib. Proc. Natl. Acad. Sci. USA *104*, 20932–20937.

Bender, H.S., Murchison, E.P., Pickett, H.A., Deakin, J.E., Strong, M.A., Conlan, C., McMillan, D.A., Neumann, A.A., Greider, C.W., Hannon, G.J., et al. (2012). Extreme telomere length dimorphism in the Tasmanian devil and related marsupials suggests parental control of telomere length. PLoS One *7*, e46195.

Benson, G. (1999). Tandem repeats finder: a program to analyze DNA sequences. Nucleic Acids Res. *27*, 573–580.

Blokzijl, F., de Ligt, J., Jager, M., Sasselli, V., Roerink, S., Sasaki, N., Huch, M., Boymans, S., Kuijk, E., Prins, P., et al. (2016). Tissue-specific mutation accumulation in human adult stem cells during life. Nature *538*, 260–264.

Boetzer, M., Henkel, C.V., Jansen, H.J., Butler, D., and Pirovano, W. (2011). Scaffolding pre-assembled contigs using SSPACE. Bioinformatics *27*, 578–579.

Brenner, J.C., Feng, F.Y., Han, S., Patel, S., Goyal, S.V., Bou-Maroun, L.M., Liu, M., Lonigro, R., Prensner, J.R., Tomlins, S.A., et al. (2012). PARP-1 inhibition as a targeted strategy to treat Ewing's sarcoma. Cancer Res. *72*, 1608–1613.

Brüniche-Olsen, A., Jones, M.E., Austin, J.J., Burridge, C.P., and Holland, B.R. (2014). Extensive population decline in the Tasmanian devil predates European settlement and devil facial tumour disease. Biol. Lett. *10*, 20140619.

Brüniche-Olsen, A., Austin, J.J., Jones, M.E., Holland, B.R., and Burridge, C.P. (2016). Detecting selection on temporal and spatial scales: a genomic time-series assessment of selective responses to devil facial tumor disease. PLoS One *11*, e0147875.

Camacho, C., Coulouris, G., Avagyan, V., Ma, N., Papadopoulos, J., Bealer, K., and Madden, T.L. (2009). BLAST+: architecture and applications. BMC Bioinformatics *10*, 421.

Carpenter, B., Gelman, A., Hoffman, M.D., Lee, D., Goodrich, B., Betancourt, M., Brubaker, M., Guo, J., Li, P., and Riddell, A. (2017). Stan: a probabilistic programming language. J. Stat. Softw. *76*, 1–32.

Chen, K., Chen, L., Fan, X., Wallis, J., Ding, L., and Weinstock, G. (2014). TIGRA: a targeted iterative graph routing assembler for breakpoint assembly. Genome Res. *24*, 310–317.

COSMIC. (2017). COSMIC signatures of mutational processes in human cancer. http://cancer.sanger.ac.uk/cosmic/signatures.

Deakin, J.E., Bender, H.S., Pearse, A.M., Rens, W., O'Brien, P.C., Ferguson-Smith, M.A., Cheng, Y., Morris, K., Taylor, R., Stuart, A., et al. (2012). Genomic restructuring in the Tasmanian devil facial tumour: chromosome painting and gene mapping provide clues to evolution of a transmissible tumour. PLoS Genet. *8*, e1002483.

Deng, Y., Wu, L.M.N., Bai, S., Zhao, C., Wang, H., Wang, J., Xu, L., Sakabe, M., Zhou, W., Xin, M., et al. (2017). A reciprocal regulatory loop between TAZ/YAP and G-protein Galphas regulates Schwann cell proliferation and myelination. Nat. Commun. *8*, 15161.

DePristo, M.A., Banks, E., Poplin, R., Garimella, K.V., Maguire, J.R., Hartl, C., Philippakis, A.A., del Angel, G., Rivas, M.A., Hanna, M., et al. (2011). A framework for variation discovery and genotyping using next-generation DNA sequencing data. Nat. Genet. *43*, 491–498.

Duan, R.S., Jin, T., Yang, X., Mix, E., Adem, A., and Zhu, J. (2007). Apolipoprotein E deficiency enhances the antigen-presenting capacity of Schwann cells. Glia *55*, 772–776.

Epstein, B., Jones, M., Hamede, R., Hendricks, S., McCallum, H., Murchison, E.P., Schonfeld, B., Wiench, C., Hohenlohe, P., and Storfer, A. (2016). Rapid evolutionary response to a transmissible cancer in Tasmanian devils. Nat. Commun. *7*, 12684.

Fex Svennigsen, A., and Dahlin, L.B. (2013). Repair of the peripheral nerve-remyelination that works. Brain Sci. *3*, 1182–1197.

Forbes, S.A., Beare, D., Gunasekaran, P., Leung, K., Bindal, N., Boutselakis, H., Ding, M., Bamford, S., Cole, C., Ward, S., et al. (2015). COSMIC: exploring the world's knowledge of somatic mutations in human cancer. Nucleic Acids Res. *43*, D805–D811.

Garnett, M.J., Edelman, E.J., Heidorn, S.J., Greenman, C.D., Dastur, A., Lau, K.W., Greninger, P., Thompson, I.R., Luo, X., Soares, J., et al. (2012). Systematic identification of genomic markers of drug sensitivity in cancer cells. Nature *483*, 570–575.

Giordano, F., Stammnitz, M.R., Murchison, E.P., and Ning, Z. (2018). scanPAV: a pipeline for extracting presence-absence variations in genome pairs. Bioinformatics. https://doi.org/10.1093/bioinformatics/bty189.

Griner, L.A. (1979). Neoplasms in Tasmanian devils (*Sarcophilus harrisii*). J. Natl. Cancer Inst. *62*, 589–595.

Gu, Z., Gu, L., Eils, R., Schlesner, M., and Brors, B. (2014). circlize Implements and enhances circular visualization in R. Bioinformatics *30*, 2811–2812.

Guiler, E.R. (1970). Observations on the Tasmanian devil, *Sarcophilus harrisii* (marsupialia: dasyuridae). Aust. J. Zool. *18*, 49–62.

Guiler, E.R. (1982). Temporal and spatial distribution of the Tasmanian devil, *Sarcophilus harrisii* (dasyuridae: marsupialia). Papers and Proceedings of the Royal Society of Tasmania *116*, 153–163.

Hamede, R.K., McCallum, H., and Jones, M. (2013). Biting injuries and transmission of Tasmanian devil facial tumour disease. J. Anim. Ecol. *82*, 182–190.

Han, Q., Lin, X., Zhang, X., Jiang, G., Zhang, Y., Miao, Y., Rong, X., Zheng, X., Han, Y., Han, X., et al. (2017). WWC3 regulates the Wnt and Hippo pathways via Dishevelled proteins and large tumour suppressor 1, to suppress lung cancer invasion and metastasis. J. Pathol. *242*, 435–447.

Hawkins, C.E., Baars, C., Hesterman, H., Hocking, G.J., Jones, M.E., Lazenby, B., Mann, D., Mooney, N., Pemberton, D., Pyecroft, S., et al. (2006). Emerging disease and population decline of an island endemic, the Tasmanian devil *Sarcophilus harrisii*. Biol. Conservat. *131*, 307–324.

Hayes, D.A., Kunde, D.A., Taylor, R.L., Pyecroft, S.B., Sohal, S.S., and Snow, E.T. (2017). ERBB3: a potential serum biomarker for early detection and therapeutic target for devil facial tumour 1 (DFT1). PLoS One *12*, e0177919.

Huber, W., Carey, V.J., Gentleman, R., Anders, S., Carlson, M., Carvalho, B.S., Bravo, H.C., Davis, S., Gatto, L., Girke, T., et al. (2015). Orchestrating high-throughput genomic analysis with Bioconductor. Nat. Methods *12*, 115–121.

Hynes, N.E., and Lane, H.A. (2005). ERBB receptors and cancer: the complexity of targeted inhibitors. Nat. Rev. Cancer *5*, 341–354.

Jones, M.E., Paetkau, D., Geffen, E., and Moritz, C. (2004). Genetic diversity and population structure of Tasmanian devils, the largest marsupial carnivore. Mol. Ecol. *13*, 2197–2209.

Ju, Y.S., Martincorena, I., Gerstung, M., Petljak, M., Alexandrov, L.B., Rahbari, R., Wedge, D.C., Davies, H.R., Ramakrishna, M., Fullam, A., et al. (2017). Somatic mutations reveal asymmetric cellular dynamics in the early human embryo. Nature *543*, 714–718.

Juan, W.C., and Hong, W. (2016). Targeting the hippo signaling pathway for tissue regeneration and cancer therapy. Genes (Basel) *7*, https://doi.org/10.3390/genes7090055.

Kent, W.J. (2002). BLAT—the BLAST-like alignment tool. Genome Res. *12*, 656–664.

Kim, K.H., and Roberts, C.W. (2016). Targeting EZH2 in cancer. Nat. Med. *22*, 128–134.

Klambauer, G., Schwarzbauer, K., Mayr, A., Clevert, D.A., Mitterecker, A., Bodenhofer, U., and Hochreiter, S. (2012). cn.MOPS: mixture of Poissons for discovering copy number variations in next-generation sequencing data with a low false discovery rate. Nucleic Acids Res. *40*, e69.

Kreiss, A., Cheng, Y., Kimble, F., Wells, B., Donovan, S., Belov, K., and Woods, G.M. (2011). Allorecognition in the Tasmanian devil (*Sarcophilus harrisii*), an endangered marsupial species with limited genetic diversity. PLoS One *6*, e22402.

Kwon, Y.M., Stammnitz, M.R., Wang, J., Knowles, G.W., Pye, R.J., Hamede, R.K., and Murchison, E.P. (2018). Tasman-PCR: A genetic diagnostic assay for Tasmanian devil facial tumour diseases. bioRxiv. https://doi.org/10.1101/287847.

Lazenby, B.T., Tobler, M.W., Brown, W.E., Hawkins, C.E., Hocking, G.J., Hume, F., Huxtable, S., Iles, P., Jones, M.E., Lawrence, C., et al. (2018). Density trends and demographic signals uncover the long-term impact of transmissible cancer in Tasmanian devils. J. Appl. Ecol. https://doi.org/10.1111/1365-2664.13088.

Li, H. (2012). Exploring single-sample SNP and INDEL calling with whole-genome de novo assembly. Bioinformatics *28*, 1838–1844.

Li, H. (2013). Aligning sequence reads, clone sequences and assembly contigs with BWA-MEM. arXiv, 1303.3997.

Li, H., and Durbin, R. (2009). Fast and accurate short read alignment with Burrows-Wheeler transform. Bioinformatics *25*, 1754–1760.

Li, D., Ambrogio, L., Shimamura, T., Kubo, S., Takahashi, M., Chirieac, L.R., Padera, R.F., Shapiro, G.I., Baum, A., Himmelsbach, F., et al. (2008). BIBW2992, an irreversible EGFR/HER2 inhibitor highly effective in preclinical lung cancer models. Oncogene *27*, 4702–4711.

Li, H., Handsaker, B., Wysoker, A., Fennell, T., Ruan, J., Homer, N., Marth, G., Abecasis, G., and Durbin, R.; 1000 Genome Project Data Processing, Subgroup (2009). The sequence alignment/map format and SAMtools. Bioinformatics *25*, 2078–2079.

Li, R., Zhu, H., Ruan, J., Qian, W., Fang, X., Shi, Z., Li, Y., Li, S., Shan, G., Kristiansen, K., et al. (2010). De novo assembly of human genomes with massively parallel short read sequencing. Genome Res. *20*, 265–272.

Loh, R., Bergfeld, J., Hayes, D., O'Hara, A., Pyecroft, S., Raidal, S., and Sharpe, R. (2006a). The pathology of devil facial tumor disease (DFTD) in Tasmanian devils (*Sarcophilus harrisii*). Vet. Pathol. *43*, 890–895.

Loh, R., Hayes, D., Mahjoor, A., O'Hara, A., Pyecroft, S., and Raidal, S. (2006b). The immunohistochemical characterization of devil facial tumor disease (DFTD) in the Tasmanian devil (*Sarcophilus harrisii*). Vet. Pathol. *43*, 896–903.

Maciejowski, J., and de Lange, T. (2017). Telomeres in cancer: tumour suppression and genome instability. Nat. Rev. Mol. Cell Biol. *18*, 175–186.

McLaren, W., Pritchard, B., Rios, D., Chen, Y., Flicek, P., and Cunningham, F. (2010). Deriving the consequences of genomic variants with the ensembl API and SNP effect predictor. Bioinformatics *26*, 2069–2070.

Metzger, M.J., Reinisch, C., Sherry, J., and Goff, S.P. (2015). Horizontal transmission of clonal cancer cells causes leukemia in soft-shell clams. Cell *161*, 255–263.

Metzger, M.J., Villalba, A., Carballal, M.J., Iglesias, D., Sherry, J., Reinisch, C., Muttray, A.F., Baldwin, S.A., and Goff, S.P. (2016). Widespread transmission of independent cancer lineages within multiple bivalve species. Nature *534*, 705–709.

Meyer zu Hörste, G., Heidenreich, H., Mausberg, A.K., Lehmann, H.C., ten Asbroek, A.L., Saavedra, J.T., Baas, F., Hartung, H.P., Wiendl, H., and Kieseier, B.C. (2010). Mouse Schwann cells activate MHC class I and II restricted T-cell responses, but require external peptide processing for MHC class II presentation. Neurobiol. Dis. *37*, 483–490.

Mikkelsen, T.S., Wakefield, M.J., Aken, B., Amemiya, C.T., Chang, J.L., Duke, S., Garber, M., Gentles, A.J., Goodstadt, L., Heger, A., et al. (2007). Genome of the marsupial *Monodelphis domestica* reveals innovation in non-coding sequences. Nature *447*, 167–177.

Miller, W., Hayes, V.M., Ratan, A., Petersen, D.C., Wittekindt, N.E., Miller, J., Walenz, B., Knight, J., Qi, J., Zhao, F., et al. (2011). Genetic diversity and population structure of the endangered marsupial *Sarcophilus harrisii* (Tasmanian devil). Proc. Natl. Acad. Sci. USA *108*, 12348–12353.

Mindos, T., Dun, X.P., North, K., Doddrell, R.D., Schulz, A., Edwards, P., Russell, J., Gray, B., Roberts, S.L., Shivane, A., et al. (2017). Merlin controls the repair capacity of Schwann cells after injury by regulating Hippo/YAP activity. J. Cell Biol. *216*, 495–510.

Moroishi, T., Hansen, C.G., and Guan, K.L. (2015). The emerging roles of YAP and TAZ in cancer. Nat. Rev. Cancer *15*, 73–79.

Mullikin, J.C., and Ning, Z. (2003). The phusion assembler. Genome Res. *13*, 81–90.

Murchison, E.P., Tovar, C., Hsu, A., Bender, H.S., Kheradpour, P., Rebbeck, C.A., Obendorf, D., Conlan, C., Bahlo, M., Blizzard, C.A., et al. (2010). The Tasmanian devil transcriptome reveals Schwann cell origins of a clonally transmissible cancer. Science *327*, 84–87.

Murchison, E.P., Schulz-Trieglaff, O.B., Ning, Z., Alexandrov, L.B., Bauer, M.J., Fu, B., Hims, M., Ding, Z., Ivakhno, S., Stewart, C., et al. (2012). Genome sequencing and analysis of the Tasmanian devil and its transmissible cancer. Cell *148*, 780–791.

Murchison, E.P., Wedge, D.C., Alexandrov, L.B., Fu, B., Martincorena, I., Ning, Z., Tubio, J.M.C., Werner, E.I., Allen, J., De Nardi, A.B., et al. (2014). Transmissible [corrected] dog cancer genome reveals the origin and history of an ancient cell lineage. Science *343*, 437–440.

Murgia, C., Pritchard, J.K., Kim, S.Y., Fassati, A., and Weiss, R.A. (2006). Clonal origin and evolution of a transmissible cancer. Cell *126*, 477–487.

Nik-Zainal, S., Alexandrov, L.B., Wedge, D.C., Van Loo, P., Greenman, C.D., Raine, K., Jones, D., Hinton, J., Marshall, J., Stebbings, L.A., et al. (2012). Mutational processes molding the genomes of 21 breast cancers. Cell *149*, 979–993.

Nik-Zainal, S., Davies, H., Staaf, J., Ramakrishna, M., Glodzik, D., Zou, X., Martincorena, I., Alexandrov, L.B., Martin, S., Wedge, D.C., et al. (2016). Landscape of somatic mutations in 560 breast cancer whole-genome sequences. Nature *534*, 47–54.

O'Neill, R.J., Eldridge, M.D., Crozier, R.H., and Graves, J.A. (1997). Low levels of sequence divergence in rock wallabies (Petrogale) suggest a lack of positive directional selection in SRY. Mol. Biol. Evol. *14*, 350–353.

O'Neill, R.J.W., Brennan, F.E., Delbridge, M.L., Crozier, R.H., and Graves, J.A.M. (1998). De novo insertion of an intron into the mammalian sex determining gene, SRY. Proc. Natl. Acad. Sci. USA *95*, 1653–1657.

Pearse, A.M., and Swift, K. (2006). Allograft theory: transmission of devil facial-tumour disease. Nature *439*, 549.

Phalen, D.N., Frimberger, A., Pyecroft, S., Peck, S., Harmsen, C., Lola, S., de Mello Mattos, B., Li, K.M., McLachlan, A.J., and Moore, A. (2013). Vincristine chemotherapy trials and pharmacokinetics in tasmanian devils with Tasmanian devil facial tumor disease. PLoS One *8*, e65133.

Pye, R.J., Hamede, R., Siddle, H.V., Caldwell, A., Knowles, G.W., Swift, K., Kreiss, A., Jones, M.E., Lyons, A.B., and Woods, G.M. (2016a). Demonstration of immune responses against devil facial tumour disease in wild Tasmanian devils. Biol. Lett. *12*, 20160553.

Pye, R.J., Pemberton, D., Tovar, C., Tubio, J.M., Dun, K.A., Fox, S., Darby, J., Hayes, D., Knowles, G.W., Kreiss, A., et al. (2016b). A second transmissible cancer in Tasmanian devils. Proc. Natl. Acad. Sci. USA *113*, 374–379.

Pyecroft, S.B., Pearse, A.M., Loh, R., Swift, K., Belov, K., Fox, N., Noonan, E., Hayes, D., Hyatt, A., Wang, L., et al. (2007). Towards a case definition for devil facial tumour disease: what is it? EcoHealth *4*, 346–351.

R Core Team (2015). R: A Language and Environment for Statistical Computing (R Foundation for Statistical Computing).

Rahbari, R., Wuster, A., Lindsay, S.J., Hardwick, R.J., Alexandrov, L.B., Turki, S.A., Dominiczak, A., Morris, A., Porteous, D., Smith, B., et al. (2016). Timing, rates and spectra of human germline mutation. Nat. Genet. *48*, 126–133.

Rebbeck, C.A., Thomas, R., Breen, M., Leroi, A.M., and Burt, A. (2009). Origins and evolution of a transmissible cancer. Evolution *63*, 2340–2349.

Rimmer, A., Phan, H., Mathieson, I., Iqbal, Z., Twigg, S.R.F., WGS500 Consortium, Wilkie, A.O.M., McVean, G., and Lunter, G. (2014). Integrating mapping-, assembly- and haplotype-based approaches for calling variants in clinical sequencing applications. Nat. Genet. *46*, 912–918.

Schulze, K., Imbeaud, S., Letouzé, E., Alexandrov, L.B., Calderaro, J., Rebouissou, S., Couchy, G., Meiller, C., Shinde, J., Soysouvanh, F., et al. (2015). Exome sequencing of hepatocellular carcinomas identifies new mutational signatures and potential therapeutic targets. Nat. Genet. *47*, 505–511.

Siddle, H.V., Kreiss, A., Eldridge, M.D.B., Noonan, E., Clarke, C.J., Pyecroft, S., Woods, G.M., and Belov, K. (2007). Transmission of a fatal clonal tumor by biting occurs due to depleted MHC diversity in a threatened carnivorous marsupial. Proc. Natl. Acad. Sci. USA *104*, 16221–16226.

Siddle, H.V., Kreiss, A., Tovar, C., Yuen, C.K., Cheng, Y., Belov, K., Swift, K., Pearse, A.M., Hamede, R., Jones, M.E., et al. (2013). Reversible epigenetic down-regulation of MHC molecules by devil facial tumour disease illustrates immune escape by a contagious cancer. Proc. Natl. Acad. Sci. USA *110*, 5103–5108.

Strakova, A., Ni Leathlobhair, M., Wang, G.D., Yin, T.T., Airikkala-Otter, I., Allen, J.L., Allum, K.M., Bansse-Issa, L., Bisson, J.L., Castillo Domracheva, A., et al. (2016). Mitochondrial genetic diversity, selection and recombination in a canine transmissible cancer. Elife *5*, https://doi.org/10.7554/eLife.14552.

Taylor, R.L., Zhang, Y., Schoning, J.P., and Deakin, J.E. (2017). Identification of candidate genes for devil facial tumour disease tumourigenesis. Sci. Rep. *7*, 8761.

Thorvaldsdóttir, H., Robinson, J.T., and Mesirov, J.P. (2013). Integrative Genomics Viewer (IGV): high-performance genomics data visualization and exploration. Brief. Bioinform. *14*, 178–192.

Tovar, C., Obendorf, D., Murchison, E.P., Papenfuss, A.T., Kreiss, A., and Woods, G.M. (2011). Tumor-specific diagnostic marker for transmissible facial tumors of Tasmanian devils: immunohistochemistry studies. Vet. Pathol. *48*, 1195–1203.

Tovar, C., Pye, R.J., Kreiss, A., Cheng, Y., Brown, G.K., Darby, J., Malley, R.C., Siddle, H.V., Skjodt, K., Kaufman, J., et al. (2017). Regression of devil facial tumour disease following immunotherapy in immunised Tasmanian devils. Sci. Rep. *7*, 43827.

Varelas, X., Samavarchi-Tehrani, P., Narimatsu, M., Weiss, A., Cockburn, K., Larsen, B.G., Rossant, J., and Wrana, J.L. (2010). The Crumbs complex couples cell density sensing to Hippo-dependent control of the TGF-beta-SMAD pathway. Dev. Cell *19*, 831–844.

Vis, D.J., Bombardelli, L., Lightfoot, H., Iorio, F., Garnett, M.J., and Wessels, L.F. (2016). Multilevel models improve precision and speed of IC50 estimates. Pharmacogenomics *17*, 691–700.

Wala, J.A., Bandopadhayay, P., Greenwald, N., O'Rourke, R., Sharpe, T., Stewart, C., Schumacher, S., Li, Y., Weischenfeldt, J., Yao, X., et al. (2018). SvABA: genome-widedetection of structural variants and indels by local assembly. GenomeRes. https://doi.org/10.1101/gr.221028.117.

Wright, B., Willet, C.E., Hamede, R., Jones, M., Belov, K., and Wade, C.M. (2017). Variants in the host genome may inhibit tumour growth in devil facial tumours: evidence from genome-wide association. Sci. Rep. *7*, 423.

Wu, L.M.N., Deng, Y., Wang, J., Zhao, C., Wang, J., Rao, R., Xu, L., Zhou, W., Choi, K., Rizvi, T.A., et al. (2018). Programming of Schwann cells by Lats1/2-TAZ/YAP signaling drives malignant peripheral nerve sheath tumorigenesis. Cancer Cell *33*, 292–308.

Yang, W., Soares, J., Greninger, P., Edelman, E.J., Lightfoot, H., Forbes, S., Bindal, N., Beare, D., Smith, J.A., Thompson, I.R., et al. (2013). Genomics of Drug Sensitivity in Cancer (GDSC): a resource for therapeutic biomarker discovery in cancer cells. Nucleic Acids Res. *41*, D955–D961.

Yu, F.X., Zhao, B., and Guan, K.L. (2015). Hippo pathway in organ size control, tissue homeostasis, and cancer. Cell *163*, 811–828.

Zanconato, F., Cordenonsi, M., and Piccolo, S. (2016). YAP/TAZ at the roots of cancer. Cancer Cell *29*, 783–803.

STAR★METHODS

KEY RESOURCES TABLE

REAGENT or RESOURCE	SOURCE	IDENTIFIER
Antibodies		
Monoclonal mouse anti-human Cytokeratin	Dako	Cat# M3515; RRID: AB_2132885
Monoclonal mouse anti-human Muscle Specific Actin	Leica Microsystems	Cat# NCL-MSA; RRID: AB_563409
Monoclonal mouse anti-human Neuron Specific Enolase	Dako	Cat# M0873; RRID: AB_2099322
Monoclonal mouse anti-human Smooth Muscle Antigen	Dako	Cat# M0851; RRID: AB_2223500
Monoclonal mouse anti-human Vimentin	Dako	Cat# M0725; RRID: AB_10013485
Monoclonal mouse anti-human YAP1	Sigma-Aldrich	Cat# WH0010413M1; RRID: AB_1844253
Monoclonal rabbit anti-human PDGFRB	Abcam	Cat# ab32570; RRID: AB_777165
Polyclonal rabbit anti-human PDGFRA	Abcam	Cat# ab124392; RRID: AB_10978090
Polyclonal rabbit anti-human Periaxin	Sigma-Aldrich	Cat# HPA001868; RRID: AB_2172440
Polyclonal rabbit anti-human S100	Dako	Cat# Z0311; RRID: AB_10013383
Polyclonal rabbit anti-human WWTR1/TAZ	Sigma-Aldrich	Cat# T4077; RRID: AB_1841213
Biological Samples		
Devil facial tumor disease 1 (DFT1) biopsy: 36T2	This paper	Table S2
Devil facial tumor disease 1 (DFT1) biopsy: 96T	This paper	Table S2
Devil facial tumor disease 1 (DFT1) biopsy: 221T	This paper	Table S2
Devil facial tumor disease 1 (DFT1) biopsy: 331T	This paper	Table S2
Devil facial tumor disease 1 (DFT1) biopsy: 333Ta	This paper	Table S2
Devil facial tumor disease 1 (DFT1) biopsy: 812T2	This paper	Table S6
Devil facial tumor disease 1 (DFT1) biopsy: 813T1	This paper	Table S6
Devil facial tumor disease 2 (DFT2) biopsy: 637T1	This paper	Table S6
Tasmanian devil buffy coat: 95H	This paper	Table S6
Tasmanian devil buffy coat: 124H	This paper	Table S2
Tasmanian devil ear biopsy: 122H1	This paper	Table S2
Tasmanian devil ear biopsy: 133H	This paper	Table S2
Tasmanian devil ear biopsy: 238H	This paper	Table S2
Tasmanian devil ear biopsy: 244H	This paper	Table S2
Tasmanian devil ear biopsy: 264H	This paper	Table S2
Tasmanian devil ear biopsy: 265H	This paper	Table S2
Tasmanian devil ear biopsy: 266H	This paper	Table S2
Tasmanian devil ear biopsy: 267H	This paper	Table S2
Tasmanian devil ear biopsy: 268H	This paper	Table S2
Tasmanian devil ear biopsy: 269H	This paper	Table S2
Tasmanian devil ear biopsy: 270H	This paper	Table S2
Tasmanian devil ear biopsy: 270H	This paper	Table S2
Tasmanian devil ear biopsy: 317H	This paper	Table S2
Tasmanian devil ear biopsy: 637H	This paper	Table S6
Tasmanian devil ear biopsy: 811H	This paper	Table S2
Tasmanian devil ear biopsy: 812H	This paper	Table S6
Tasmanian devil ear biopsy: 813H	This paper	Table S6
Tasmanian devil kidney biopsy: 203H	Pye et al., 2016b	SN-H; Tables S1 and S2
Tasmanian devil liver biopsy: 31H	Murchison et al., 2012	Male normal devil; Table S2
Tasmanian devil liver biopsy: 63H1	This paper	Table S2
Tasmanian devil liver biopsy: 110H	This paper	Table S2
Tasmanian devil liver biopsy: 112H	This paper	Table S2

(*Continued on next page*)

Continued

REAGENT or RESOURCE	SOURCE	IDENTIFIER
Tasmanian devil liver biopsy: 115H1	This paper	Table S2
Tasmanian devil liver biopsy: 117H	This paper	Table S2
Tasmanian devil liver biopsy: 119H	This paper	Table S2
Tasmanian devil liver biopsy: 134H1	This paper	Table S2
Tasmanian devil liver biopsy: 347H	This paper	Table S2
Tasmanian devil liver biopsy: 379H	This paper	Table S2
Tasmanian devil liver biopsy: 420H	This paper	Table S2
Tasmanian devil liver biopsy: 442H	This paper	Table S2
Tasmanian devil liver biopsy: 443H	This paper	Table S2
Tasmanian devil liver biopsy: 444H	This paper	Table S2
Tasmanian devil spleen biopsy: 11H1	This paper	Table S2
Tasmanian devil spleen biopsy: 202H1	Pye et al., 2016b	RV-H; Tables S1 and S2
Tasmanian devil spleen biopsy: 398H	This paper	Table S2
Chemicals, Peptides, and Recombinant Proteins		
Chemotherapeutic Compounds List	This paper	Table S7
Syto60	Thermo Fisher Scientific	Cat# S11342
Critical Commercial Assays		
Agilent SureSelect XT, HSQ	Agilent Technologies	Cat# G9611A
DNeasy Blood and Tissue kit	Qiagen	Cat# 69504
EZ-PCR Mycoplasma Test	Biological Industries	Cat# 20-700-20
Fluorescence-based live-cell assay	Thermo Fisher Scientific	Cat# L324
Genomic-Tip kit	Qiagen	Cat# 10223
illustra GenomiPhi V2 DNA Amplification kit	GE Healthcare	Cat# 25660030
MycoAlert Mycoplastma Detection kit	Lonza	Cat# LT07-118
NEBNext Sanger Sequencing Kit for MiSeq libraries	NEB	Cat# E7645S
QIAquick PCR Purification kit	Qiagen	Cat# 28106
Telomere PNA kit	Dako	Cat# K5327
Deposited Data		
Aligned sequencing reads of tumors and normals	This paper	ENA: PRJEB21902
Aligned sequencing reads of 12 normals from West Pencil Pine	Wright et al., 2017	ENA: PRJEB8782
COSMIC Cancer Gene Census	Forbes et al., 2015	http://cancer.sanger.ac.uk/census/
COSMIC consensus mutational signatures	Alexandrov et al., 2013	http://cancer.sanger.ac.uk/cosmic/signatures
Drug Sensitivity in Cancer (GDSC) IC50 data	Yang et al., 2013	http://www.cancerrxgene.org/downloads
RAD Sequencing data of 527 Tasmanian devils	Brüniche-Olsen et al., 2016	http://datadryad.org/resource/doi:10.5061/dryad.86bq5
Raw data	This paper	https://doi.org/10.17632/znfphvhmbv.1
Tasmanian devil reference genome 7.0	Murchison et al., 2012	https://www.ensembl.org/Sarcophilus_harrisii/
Tasmanian devil tumor and host contigs from de novo assemblies	This paper	ENA: PRJEB21902, https://doi.org/10.17632/znfphvhmbv.1
Experimental Models: Cell Lines		
Devil facial tumor disease 1 (DFT1): 85T	This paper	Tables S2 and S7
Devil facial tumor disease 1 (DFT1): 86T	Siddle et al., 2013	DFTD 1426; Tables S1, S2, S6, and S7
Devil facial tumor disease 1 (DFT1): 87T	Siddle et al., 2013	DFTD C5065; Tables S2 and S7
Devil facial tumor disease 1 (DFT1): 88T	Siddle et al., 2013	DFTD 4906; Tables S1, S2, S6, and S7
Devil facial tumor disease 1 (DFT1): 95T	This paper	Tables S2 and S6
Devil facial tumor disease 2 (DFT2): 202T2	Pye et al., 2016b	RV-T; Tables S1, S2, and S6
Devil facial tumor disease 2 (DFT2): 203T3	Pye et al., 2016b	SN-T; Tables S1, S2, S6, and S7

(*Continued on next page*)

Continued

REAGENT or RESOURCE	SOURCE	IDENTIFIER
Devil facial tumor disease 2 (DFT2): 338T	Pye et al., 2016b	JV-T; Table S2
Devil facial tumor disease 2 (DFT2): 339T	Pye et al., 2016b	NR-T; Table S2
Devil facial tumor disease 2 (DFT2): 809T1	This paper	Table S7
Tasmanian devil fibroblasts: 91H	Murchison et al., 2012	Female normal devil, reference animal; Table S2
Oligonucleotides		
DFT diagnostic oligos	Kwon et al., 2018	N/A
MPDZ forward: 5'-GGT CTT GGA TGA ACA AAA GAA GA-3'	This paper	N/A
MPDZ reverse: 5'-ACT GTA CGG CTG GCA CTG AT-3'	This paper	N/A
PDZD11-RFX2 forward: 5'- ACC GCC AAG TTT CAA ATC AG-3'	This paper	N/A
PDZD11-RFX2 reverse: 5'- TCC TCC AGG ATA CCT CTC CA-3'	This paper	N/A
Single Nucleotide Variant (SNV) Validation oligos	This paper	Table S2
SRY forward: 5'-GCG ACC GTT CAT TGA CGA AG-3'	This paper	N/A
SRY reverse: 5'-ACA GAT TTG GGG ACA CGA GG-3'	This paper	N/A
Structural Variant (SV) Validation oligos	This paper	Table S5
Tasmanian devil chromosome-specific FISH probes	Murchison et al., 2012	N/A
WWC3 forward: 5'-CAA AAA CTA AAG CAA AAA CCA AGA-3'	This paper	N/A
WWC3 reverse: 5'-CCA GAA GGC CTA TTG AAT TCC T-3'	This paper	N/A
Software and Algorithms		
alleleCount	Cancer Genome Project, Wellcome Trust Sanger Institute	https://github.com/cancerit/alleleCount
Breakpoints via Assembly (BRASS)	Cancer Genome Project, Wellcome Trust Sanger Institute	https://github.com/cancerit/BRASS
BWA-backtrack	Li and Durbin, 2009	http://bio-bwa.sourceforge.net/
BWA-MEM	Li, 2013	http://bio-bwa.sourceforge.net/
Fermi	Li, 2012	https://github.com/lh3/fermi
Integrative Genomics Viewer (IGV)	Thorvaldsdóttir et al., 2011	http://software.broadinstitute.org/software/igv/
Phusion2	Mullikin and Ning, 2003	http://www.sanger.ac.uk/science/tools/phusion2
PICARD	DePristo et al., 2011	http://broadinstitute.github.io/picard/
Platypus	Rimmer et al., 2014	http://www.well.ox.ac.uk/platypus
R Language and Environment for Statistical Computing	R Core Team, 2015	https://www.R-project.org/
R Bioconductor Suite	Huber et al., 2015	https://www.bioconductor.org/
R circlize package	Gu et al., 2014	https://github.com/jokergoo/circlize
R cn.MOPS package	Klambauer et al., 2012	http://www.bioinf.jku.at/software/cnmops/
R Stan interface	Carpenter et al., 2017	http://mc-stan.org/users/interfaces/rstan
Samtools	Li et al., 2009	http://samtools.sourceforge.net/
scanPAV	Giordano et al., 2018	https://github.com/wtsi-hpag/scanPAV
SOAPdenovo	Li et al., 2010	http://soap.genomics.org.cn/soapdenovo.html
Somatypus (cancer data adaptation of Platypus)	This paper	https://github.com/baezortega/somatypus
SSPACE	Boetzer et al., 2011	https://www.baseclear.com/genomics/bioinformatics/basetools/SSPACE
SvABA	Wala et al., 2017	https://github.com/walaj/svaba

(*Continued on next page*)

Continued

REAGENT or RESOURCE	SOURCE	IDENTIFIER
TIGRA Assembler	Chen et al., 2014	http://bioinformatics.mdanderson.org/main/TIGRA
Variant Effect Predictor (VEP)	McLaren et al., 2010	https://www.ensembl.org/info/docs/tools/vep/index.html
Other		
Custom R scripts for data analysis and reproduction	This paper	https://github.com/MaximilianStammnitz

CONTACT FOR REAGENT AND RESOURCE SHARING

Further information and requests for resources and reagents should be directed to and will be fulfilled by the lead contact, Elizabeth Murchison (epm27@cam.ac.uk). Tasmanian devil material can only be shared with the permission of the Tasmanian Government.

EXPERIMENTAL MODEL AND SUBJECT DETAILS

Tissue Sampling and Ethics

Tissues were sampled from wild Tasmanian devils that were subsequently released, or from animals euthanized for welfare reasons. All animal procedures were performed under a Standard Operating Procedure approved by the General Manager, Natural and Cultural Heritage Division, Tasmanian Government Department of Primary Industries, Parks, Water and the Environment (DPIPWE), in agreement with the DPIPWE Animal Ethics Committee, or under University of Tasmania Animal Ethics Committee Permit A0014976. The project was approved by the University of Cambridge Department of Veterinary Medicine Ethics and Welfare Committee, reference CR191.

Cell Lines and Cell Culture

DFT1 cell lines 86T and 88T have been previously described with the names 1426 and 4906 respectively (Siddle et al., 2013). DFT2 cell lines 202T2 and 203T3 cell lines were established as follows. Micro-biopsies of approximately 2 mm in diameter were collected into RPMI 1640 (Thermo Fisher Scientific, Waltham, MA, USA) with 2% vol./vol. antibiotic-antimycotic (Thermo Fisher Scientific). Biopsies were flushed through a tea-strainer sized metal mesh with amniomax (Thermo Fisher Scientific). Subsequently, cells were plated in 6 well flat-bottomed plates (Corning Inc., Corning, NY, USA) with 3 ml amniomax and 2% vol./vol. antibiotic-antimycotic, and placed at 35°C with 5% atm. CO_2. After 24 hr, medium was replaced and plates were incubated with the same conditions for an additional 48 hr. Cells were then transferred into T25 flasks with the same medium, and after reaching confluence approximately 48 hr later, flasks were split and media changed to RPMI 1640; 1% vol./vol. GlutaMAX (Thermo Fisher Scientific); 10% vol./vol. FCS (Bovogen Biologicals, Melbourne, VIC, Australia), 20% vol./vol. amniomax and 1% vol./vol. antibiotic-antimycotic. We used MycoAlert (Lonza, Basel, Switzerland) and EZ-Mycoplasma Test (Biological Industries, Kibbutz Beit-Haemek, Israel) kits to screen cell lines for Mycoplasma according to manufacturers' instructions. Details about dates of sampling and Mycoplasma status for cell lines sequenced in this study are indicated below.

Name	Year of Establishment	Year of DNA Extraction	Estimated Tumor Purity*	Mycoplasma
86T	2005	2009	100%	negative
88T	2007	2009	100%	negative
202T2	2014	2015	100%	positive
203T3	2014	2015	90-95%	negative

*See *SNV-based Tumor Purity Estimation* for methods.

Tables S1, S2, S6, and S7 and the Key Resources Table list information on all Tasmanian devil and DFT cell lines, as well as other samples used in this study.

METHOD DETAILS

Cytogenetics

Chromosome-specific probes were derived from flow sorted chromosomes and hybridized with metaphases as described (Murchison et al., 2012). For fluorescence *in situ* hybridization with telomeric probes, we used the Telomere PNA (Peptide Nucleic Acids)/Cy3

kit (Dako, Glostrup, Denmark). There are two nomenclature systems in use for Tasmanian devil chromosomes (Deakin et al., 2012; Pearse and Swift, 2006). These two systems differ in their designations of the two largest devil chromosomes, chromosomes 1 and 2. The chromosome named chromosome 1 in the first system is named chromosome 2 in the second system, and vice versa. In this study, we used the nomenclature adopted by Pearse and Swift (Pearse and Swift, 2006); this system is also used in the Tasmanian devil reference genome (Murchison et al., 2012).

Histology

Tasmanian devil tissues were fixed in 10% Neutral Buffered Formaldehyde (Australian Biostain, Traralgon, VIC, Australia) for 24 hr and selected tissues were cassetted (Techno Plas, St. Marys, SA, Australia) and processed overnight using a standard 15-hr overnight procedure in the TP 1050 tissue processor (Leica Microsystems, Wetzlar, Germany). Tissues were orientated on the EG1160 (Leica Microsystems), embedded in paraffin wax (Leica Microsystems) and sectioned at 3 microns using a Leica RM2245 microtome and adhered to microscope slides (Menzel Gläser, Thermo Fisher Scientific) for 20 min at 60°C. Sections were deparaffinized, rehydrated and stained using Jung autostainer XL (Leica Microsystems) for Hematoxylin (Australian Biostain) and Eosin, dehydrated, cleared, cover slipped (Leica Microsystems) and mounted in CV Mount (Leica Microsystems) (Hayes et al., 2017).

Immunohistochemistry

Tasmanian devil tissues and tumors were sectioned at 3 microns, floated onto Superfrost plus slides (Menzel Gläser) and subjected to standard deparaffinization and rehydration techniques using an automated stainer (Leica Microsystems). Antigen retrieval in tissue sections was conducted in citrate buffer at pH 6.0 (Reveal Decloaker, Biocare Medical, Pacheco, CA, USA) at 120°C for 8 min using a Pascal pressure chamber (Dako) then cooled to 20°C. Endogenous peroxidase activity was quenched using 3% hydrogen peroxide (Ajax Finechem, Thermo Fisher Scientific) in methanol (Ajax Finechem) for 30 min. Detection of primary antibodies was achieved using Mach1 Universal HRP-Polymer detection kit (Biocare Medical). Protein block (Background Sniper, Biocare Medical) was applied for 20 min prior to application of primary antibodies. Polyclonal rabbit anti-human PDGFRA 1:800 (Cat#ab124392, Abcam, Cambridge, UK), Monoclonal rabbit anti-human PDGFRB 1:50 (Cat#ab32570, Abcam), Polyclonal Rabbit anti-human S100 1:1500 (Cat#Z0311, Dako), Monoclonal Mouse anti-human Neuron Specific Enolase 1:200 (Cat#M0873, Dako), Monoclonal Mouse anti-human Cytokeratin 1:100 (Cat#M3515, Dako), Monoclonal Mouse anti-human Vimentin 1:800 (Cat#M0725, Dako), Monoclonal Mouse anti-human Smooth Muscle Antigen 1:200 (Cat#M0851, Dako), Monoclonal Mouse anti-human Muscle Specific Actin 1:50 (Cat#NCL-MSA, Leica Microsystems), Polyclonal Rabbit anti-human Periaxin 1:400 (Cat#HPA001868, Sigma-Aldrich, St. Louis, MO, USA), Monoclonal mouse anti-human YAP1 1:100 (Cat#WH0010413M1, Sigma-Aldrich) and Polyclonal rabbit anti-human WWTR1/TAZ 1:100 (Cat#T4077, Sigma-Aldrich) were diluted as indicated with antibody diluent (Dako) and applied to both devil tumor and normal devil control tissues at room temperature for 30 min. Negative control was omission of primary antibody with buffer substitution. Universal HRP-polymer was applied for 30 min (MRH538L10, Biocare Medical) followed by 1 drop of Betazoid DAB Chromogen 3,3 Diaminobenzidine (BDB900G, Biocare Medical) in 1 ml of substrate buffer (DB900, Biocare Medical) applied for 4 min. Tris-buffered saline (Biocare Medical) was used to rinse between all steps. Slides were rinsed, stained with Carazzi's Hematoxylin for 5 min, washed for 3 min in tap water, dehydrated, cleared, cover slipped (CV5030, Leica Microsystems) and mounted in CV mount (Leica Microsystems) (Hayes et al., 2017). Sections were viewed under light microscopy using Olympus BX41 (Olympus Corporation, Shinjuko, Tokyo, Japan) and selected areas were photographed using a digital camera (DP20, Olympus Corporation).

Sample Processing and Sequencing

DNA Extraction

DNA from all samples except for 86T and 88T was extracted using the DNeasy Blood and Tissue extraction kit (Qiagen, Hilden, Germany). DNA from 86T and 88T was extracted using the Genomic-Tip kit (Qiagen).

Library Preparation

500 ng of genomic DNA was fragmented (average size distribution 425 base pair (BP), LE220, Covaris, Woburn, MA, USA), purified, libraries prepared (Agilent SureSelect XT, HSQ, Agilent Technologies, Santa Clara, CA, USA), and index tags applied (Sanger 168 tag set). Index tagged samples were amplified (6 cycles of PCR, KAPA HiFi kit, KAPA Biosystems, Wilmington, MA, USA), quantified (1k assay, LabChip GX, PerkinElmer, Waltham, MA, USA), then pooled together in an equimolar fashion.

High-Coverage DNA Sequencing

Pooled samples were quantified (1K assay, Bioanalyzer, Agilent Technologies), normalized (~6 nM), and submitted to cluster formation for HiSeq V4 sequencing (125 BP paired-end (PE) reads, Illumina, San Diego, CA, USA). We sequenced the equivalent of two lanes per tumor, and one lane per host; however, sequencing was multiplexed across several lanes. The table below indicates average insert size, read length and average read depth for samples sequenced at high coverage in this study (see also Table S1).

ID	Average Sequencing Depth	Average Insert Size	Read Length
202H1	49 X	417 BP	125 PE
202T2	67 X	418 BP	125 PE
203H	45 X	428 BP	125 PE
203T3	70 X	429 BP	125 PE
86T	86 X	430 BP	125 PE
88T	67 X	428 BP	125 PE

Sequence reads were aligned to the Tasmanian devil reference genome Devil7.1, an in-house assembly which is identical to the publicly available Devil7.0 (http://www.ensembl.org/Sarcophilus_harrisii/Info/Index), except Devil7.1 excludes the mitochondrial contig. Throughout the study, we used custom scaffold identifiers. Correspondence between our scaffold identifiers and those used in Devil7.0 can be found at Mendeley Data (https://doi.org/10.17632/znfphvhmbv.1). Alignment was performed using BWA-backtrack (Li and Durbin, 2009) and duplicate flagging and removal was conducted using PICARD (DePristo et al., 2011).

Low-Coverage DNA Sequencing

Thirty normal genomes were additionally sequenced at low coverage (~1 X) (Table S2). Library preparation and sequencing were performed as described for high-coverage genomes. Reads were aligned to Devil7.1+MT with BWA-MEM.

Published Normal Devil Genomes

We included data from two previously sequenced normal Tasmanian devil genomes, 31H and 91H, in this study ((Murchison et al., 2012); 31H and 91H are the "male" and "female" normal genomes respectively). However, only a subset of 31H data (lanes 999#1, 999#2, 999#3, 999#4, 999#6, 1000#1, 1000#2, 1000#4, 1000#6, 1000#7, 1000#8, 1002#1, 1002#7, 1003#1, 1003#2, 1003#3, 1003#7) were included, as some lanes fell below sequencing quality thresholds (average sequencing coverage for this sample was ~17 X). Two previously sequenced DFT1 tumors from this study, 53T and 87T (Murchison et al., 2012), were not included in the current study, as they fell below sequencing quality thresholds. Twelve previously sequenced devil normal genomes were also used in this study (Wright et al., 2017) (Table S2). These were aligned to Devil7.1+MT with BWA-MEM.

Whole Genome Amplification

Whole genome amplification was performed to create DNA stocks for PCR screening. Depending on the concentration, 1-2 μl of DNA (concentration range ~20 to ~50 ng/μl) from each sample was used as input for whole genome amplification using the illustra GenomiPhi V2 DNA Amplification kit (GE Healthcare, Chicago, IL, USA).

SNV Validation

We performed experimental validation on a set of 96 single-nucleotide variants (SNVs) obtained through our computational filtering pipelines. The SNVs selected for validation were derived from computation sets found in both DFT1s (86T and 88T), both DFT2s (202T2 and 203T3) or in all four tumors (86T, 88T, 202T2, 203T3). Primers were designed around each SNV (Table S2) and used to amplify a ~500 BP region around the SNV site with conditions as follows. Template DNA was an equal volume pool of whole genome amplified DNA from 86T, 88T, 202T2 and 203T3.

Ingredient	Company	Volume (μl)
Water	-	6.2
Phusion HF buffer (5x)	Thermo Fisher Scientific	4.0
dNTP-mix (10 μM each)	Thermo Fisher Scientific	1.6
Primer forward (10 μM)	Sigma-Aldrich	3.0
Primer reverse (10 μM)	Sigma-Aldrich	3.0
Template DNA	-	2.0
Phusion HF Polymerase	Thermo Fisher Scientific	0.2
Total	-	20.0

Step	Duration (s)	Cycles
Initial melting (98°C)	300	1
Melting (98°C)	30	
Annealing (60°C)	30	35
Elongation (72°C)	45	
Final elongation (72°C)	300	1
Final cooling (4°C)	-	1

Amplification products were purified with the QIAquick PCR purification kit (Qiagen), and pooled in roughly equimolar quantities. Pooled amplicon DNA was quantified (dsDNA BR assay, Thermo Fisher Scientific), purified, libraries prepared (NEBNext Sanger Sequencing Kit, New England Biolabs, Ipswich, MA, USA), and index tags applied (Sanger 168 tag set). Index tagged samples were amplified (8 cycles of PCR, KAPA HiFi kit, KAPA Biosystems), quantified by qPCR (KAPA Library Quant Kit, KAPA Biosystems) and submitted to cluster formation for MiSeq sequencing (300 BP PE read length, Illumina).

12,831,254 sequence reads were obtained and aligned to 2000 BP windows around each of the 96 SNV loci in the Devil7.1 reference using BWA-MEM (Li, 2013); the 95 loci (one PCR failed) had a median read coverage of 70,941 X (range 1,730 X to 481,111 X). We manually inspected each of the 95 loci using the Integrative Genomics Viewer (IGV) (Thorvaldsdóttir et al., 2013) to ensure alignment accuracy. As the template DNA used in this experiment was a pool of DNA from four tumors, and each SNV was predicted to be present, at least in the heterozygous state, in at least two of the four tumors, the minimum variant allele fraction (VAF), for the predicted alternative allele was expected to be 0.25. In order to distinguish true alleles from background sequencing errors, we first used alleleCount (https://github.com/cancerit/alleleCount) to calculate VAF for the two nucleotide bases that were neither the reference allele nor predicted alternative allele. We fitted a gamma distribution to these "background VAFs" and used this distribution to test if our predicted alternative allele VAF was significantly different to background. Predicted alternative alleles with VAF values that fell above 95% of the cumulative probability under the gamma curve were defined as validated SNVs. Overall, 93/95 SNVs were validated, detailed in Table S2.

SNV Genotyping across Normal Panel

We PCR screened each of the 93 validated SNVs across a panel of 30 normal devils to confirm genotyping accuracy. Whole genome amplified DNA from 30 devils was distributed with equal volume into three pools of 10 devils (Table S2). PCRs were performed, amplicons were pooled, libraries prepared and MiSeq sequencing performed (see section SNV Validation) with 300 BP PE reads. 12,116,462 sequence reads were generated, and mapped to 2000 BP windows around each of the 95 SNV loci in Devil7.1 using BWA-MEM (Li, 2013) with a median read depth of 80,778 X (range 1,594 X to 328,569 X). Using the same approach outlined above (see section SNV Validation), we obtained the classification results summarized in Table S2.

SNV Genotyping of *WWC3* and *MPDZ* Mutations

To assess the somatic pervasiveness of hemizygous *WWC3* SNV (DFT1) and *MPDZ* indel (DFT2) predicted loss-of-function mutations, we used the following sequencing approach. We PCR amplified (primers *WWC3* forward and *WWC3* reverse, see Key Resources Table) a 200 BP region around the affected *WWC3* locus on exon 21 in ten tumors 36T2, 85T, 86T, 87T, 88T, 95T, 96T, 221T, 331T and 333Ta which cover a wide spatiotemporal range (Table S2). Similarly, a region around the frameshift *MPDZ* indel on exon 9 was amplified (primers *MPDZ* forward and *MPDZ* reverse, see Key Resources Table) in the four DFT2 tumors 202T2, 203T3, 338T and 339T (Table S2). PCR products were cleaned up with the QIAquick PCR Purification kit (Qiagen). Products were then capillary sequenced with the corresponding PCR primers *WWC3* forward and *MPDZ* forward (Key Resources Table).

Ingredient	Company	Volume (μl)
Water	-	5.5
PCR buffer (10x)	Qiagen	5.0
dNTP-mix (2.5 μM each)	Qiagen	4.0
Primer forward (10 μM)	Sigma-Aldrich	7.5
Primer reverse (10 μM)	Sigma-Aldrich	7.5
Template DNA	-	20.0
Taq Polymerase	Qiagen	0.5
Total	-	50.0

Step	Duration (s)	Cycles
Initial melting (94°C)	300	1
Melting (94°C)	30	35
Annealing (58°C)	30	
Elongation (72°C)	15	
Final elongation (72°C)	300	1
Final cooling (4°C)	-	1

SV Validation

Candidate Structural Variants (SVs) were validated with PCRs spanning breakpoints. PCR primers are listed in Table S5, and PCR conditions are listed below. Of the 345 candidate SVs, 345 (100%) were validated (Table S5). Candidate somatic SV amplicons were sequenced on the Illumina MiSeq platform. Amplicons were purified and libraries generated as described above in SNV Validation and were sequenced with 300 BP PE reads.

Ingredient	Company	Volume (μl)
Water	-	8.3
CoralLoad buffer (10x)	Qiagen	2.0
dNTP-mix (10 μM each)	Thermo Fisher Scientific	1.6
Primer forward (10 μM)	Sigma-Aldrich	3.0
Primer reverse (10 μM)	Sigma-Aldrich	3.0
Template DNA	-	2.0
Taq Polymerase	Qiagen	0.1
Total	-	20.0

Step	Duration (s)	Cycles
Initial melting (94°C)	300	1
Melting (94°C)	30	
Annealing (60°C)	30	35
Elongation (72°C)	90	
Final elongation (72°C)	300	1
Final cooling (4°C)	-	1

SV Genotyping across Normal Panel

We screened all PCR validated SVs across a panel of 34 normal devil genomes. Briefly, whole genome amplified DNA from 34 devils was pooled in equal volume into four pools (3 pools of 10 devils, and 1 pool of 4 devils that comprised DNA from 202H1, 203H, 31H and 91H; Table S2) and PCRs were conducted with the reagents and conditions as described above (see section SV Validation). SVs that amplified in any one of the normal pools were classed as germline, and those which were not amplified in any of the normal pools were retained as candidate somatic. The SVs predicted to be unique to a single tumor were validated by confirming their absence by PCR in other tumors (Table S5).

SV Genotyping of *PDZD11-RFX2*

In order to establish the somatic pervasiveness of a detected intron-to-intron structural variant interlinking genes *PDZD11* and *RFX2* across the DFT1 tumor phylogeny, we used a similar PCR strategy as described above for the *WWC3* and *MPDZ* mutation screening. Briefly, a 231 BP amplicon involving breakpoints on chromosomes 2 and X, was obtained in eight additional DFT1 tumors 36T2, 85T, 87T, 95T, 96T, 221T, 331T and 333Ta (Table S2). Primers used were *PDZD11-RFX2* forward and *PDZD11-RFX2* reverse (Key Resources Table), and PCR conditions are listed below.

Ingredient	Company	Volume (μl)
Water	-	5.3
CoralLoad buffer (10x)	Qiagen	2.0
dNTP-mix (10 μM each)	Thermo Fisher Scientific	1.6
Primer forward (10 μM)	Sigma-Aldrich	3.0
Primer reverse (10 μM)	Sigma-Aldrich	3.0
Template DNA	-	5.0
Taq Polymerase	Qiagen	0.1
Total	-	20.0

Step	Duration (s)	Cycles
Initial melting (94°C)	300	1
Melting (94°C)	30	
Annealing (60°C)	30	35
Elongation (72°C)	30	
Final elongation (72°C)	300	1
Final cooling (4°C)	-	1

DFT Diagnostic PCRs

A multiplex DFT diagnostic PCR has been developed to confirm DFT1 or DFT2 diagnosis (Kwon et al., 2018). Briefly, the PCR incorporates three primer sets, respectively targeting a DFT1-specific structural variant, a DFT2-specific structural variant, and the *RPL13A* locus, which acts as an internal positive control. The PCR was performed as described (Kwon et al., 2018).

Y Chromosome PCRs

Samples included in this analysis are listed in Table S6. Whole genome amplified DNA was used as a template for amplification of *SRY* or a set of DFT1/DFT2 diagnostic markers as follows with primers *SRY* forward and *SRY* reverse (Key Resource Table).

Ingredient	Company	Volume (μl)
Water	-	11.3
PCR buffer (10x)	Qiagen	2.0
dNTP-mix (10 μM each)	Thermo Fisher Scientific	1.6
Primer forward (10 μM)	Sigma-Aldrich	1.5
Primer reverse (10 μM)	Sigma-Aldrich	1.5
Template DNA	-	2.0
Taq Polymerase	Qiagen	0.1
Total	-	20.0

Step	Duration (s)	Cycles
Initial melting (94°C)	300	1
Melting (94°C)	30	38
Annealing (64°C)	30	
Elongation (72°C)	90	
Final elongation (72°C)	300	1
Final cooling (4°C)	-	1

Drug Screen

Automated High-throughput Screen

Details of cell lines used in drug screen are presented in Table S7. Cells were seeded into 384-well plates using a XRD-384 (FluidX, Brooks Automation, Chelmsford, MA, USA) reagent dispenser. The number of cells seeded was individually optimized for each cell line to maximize the dynamic range of the assay: 85T = 600, 86T = 1200, 87T = 2000, 88T = 1600, 203T3 = 3200, 809T = 1600. Compounds were stored in Storage Pods (Roylan Developments, Fetcham, UK) providing a moisture-free, low oxygen environment, and protection from UV damage. Compounds were screened using a 7-point dose response curve and a linear half-log dilution series covering a 1000-fold concentration range. The dosing of the compounds was carried out using an Echo 555 (Labcyte, San Jose, CA, USA) acoustic dispenser and the duration of drug treatment was 144 hr (6 days). Cell number at the end of 6 days was measured using CellTitre-Glo 2.0 (Promega, Madison, WI, USA) reagent. 85T, 86T, 87T and 88T cell lines were screened as a single technical replicate in each of two separate screening runs. 203T3 cell line was screened in duplicate in each of two separate screening runs. 809T was screened in duplicate in each of two separate screening runs for a proportion of compounds, and was screened as a single replicate on the remaining proportion of compounds. Fluorescence intensity data from screening plates for each dose response curve was fitted using a multi-level fixed effect model (Vis et al., 2016).

Manual Follow-up Screen

We performed a follow-up drug screen to further elucidate the drug sensitivity of DFT1 cell lines to dual EGFR and ERBB2 inhibitors. Specifically, DFT1 showed particular sensitivity to Afatinib, an inhibitor of both ERBB2 and EGFR (Table S7). The observation that DFT1 cell lines were resistant to Gefitinib, an inhibitor of EGFR, suggests that the sensitivity to Afatinib is mediated by ERBB2. We further tested this hypothesis by manually screening DFT1 cell lines (85T, 86T, 87T, 88T) and three human cancer cell line controls (A549, AU565 and PC-9) with Erlotinib and Gefitinib (EGFR inhibitors), and Lapatinib and Afatinib (EGFR and ERBB2 inhibitors), as displayed in Table S7.

The control human cancer cell lines have the following known sensitivities. PC-9 has a drug sensitive deletion in EGFR (E746-A750 in exon 19) and is thus susceptible to EGFR inhibitors (Bean et al., 2007; Li et al., 2008). PC-9 cells are known to be highly sensitive to Gefitinib, Afatinib, and Erlotinib while exhibiting only a very modest sensitivity to Lapatinib (Bean et al., 2007). AU565 is an ERBB2-dependent breast cancer cell line and as such is sensitive to the ERBB2 inhibitors Afatinib and Lapatinib, but is insensitive to drugs targeting only EGFR. A549 is a human lung adenocarcinoma cell line with an oncogenic KRAS G12S point mutation, displaying resistance to both EGFR and ERBB2 inhibitors (Li et al., 2008). DFT1 cell lines and A549 were grown in DMEM/F-12 media, AU565 and PC-9 were grown in RPMI-1640 media. All cells were maintained at 37°C and 5% CO_2.

Dose-response curves were obtained by setting up 96-well cell culture plates for each drug. DFT1 cells in each well were dosed with drugs at exponentially decreasing concentration. The maximum drug concentration was 1 μM. The cells were cultured in the presence of drugs for 48 hr. A fluorescence-based live-cell assay (Thermo Fisher Scientific) was used to detect cell viability. After live-cell detection, the cells were fixed overnight. On the next day, the cells were prepared for fixed cell detection. Cells were washed two times with 200 μl/well of water and stained with Syto60 1:5000 (Thermo Fisher Scientific). After 1 hr of incubation at room temperature, plates were washed two times with 200 μl/well of water. Lastly, 100 μl of water was added to each well and the plate was detected. The experiment was repeated in triplicates for each cell line and drug. IC_{50} values from this experiment are shown below as $\log_e(\mu M)$ concentrations, indicate that DFT1 is resistant to Erlotinib, and that 3 of 4 DFT1 cell lines here tested show sensitivity to Lapatinib under these conditions (Table S7).

QUANTIFICATION AND STATISTICAL ANALYSES

Bioinformatics downstream analyses of ancestral data, mutational calls and drug screen results were performed in the R language for statistical computing (R Core Team, 2015), using existing Bioconductor libraries (Huber et al., 2015) and customized scripts.

Devil Population Analysis

We genotyped tumors 86T and 88T (DFT1), tumors 202T2 and 203T3 (DFT2), and normal devils 202H1, 203H and 91H against a panel of previously ascertained variants (Brüniche-Olsen et al., 2016). Of the 2,281 variants described by Brüniche-Olsen et al., we excluded (i) indels, (ii) single nucleotide polymorphisms (SNPs) falling into RADseq-fragments ambiguously mapping to the reference genome (i.e. >2 mismatching bases or one or more alignment gaps of total length >2 BP), (iii) SNPs mapping in windows of 5 BP around simple repeats, 500 BP around contig ends or 1,000 BP around scaffold ends, (iv) SNPs mapping to the X chromosome and (v) SNPs falling into regions which are non-diploid in any of the tumor samples (Table S4). In addition, using the genotypes provided by Brüniche-Olsen et al., we excluded those SNPs which showed limited variation across the population. Specifically, for each SNP we computed the proportion of individuals that shared identical genotypes. SNPs were ranked by the proportion of individuals sharing identical genotypes, and those SNPs which were within the group of 60% least varying across the population were excluded. Finally, if >1 SNP mapped to the same RADseq fragment, only the SNP mapping closest to the 5' end of the fragment (with respect to the reference) was selected for further analysis. These steps provided a final set of 320 SNPs.

Of the 527 individuals genotyped in (Brüniche-Olsen et al., 2016), we excluded any individual with missing genotype data at more than 20% of loci. For the remaining 398 individuals, we extracted the genotypes assigned in (Brüniche-Olsen et al., 2016). Genotypes across DFT1 tumors 86T and 88T, DFT2 tumors 202T2 and 203T3, as well as normal devils 91H, 202H1 and 203H were genotyped at the 320 SNP loci using alleleCount (https://github.com/cancerit/alleleCount). Sites with <7 read coverage were marked as missing data, and remaining sites were coded as follows:

(i) homozygous 1/1: >70% reads support allele 1
(ii) heterozygous 1/2: >30% and <70% reads support alleles 1 and 2
(iii) homozygous 2/2: >70% reads support allele 2

Our 1 and 2 allele definitions were used as per Brüniche-Olsen et al. (2016). Missing genotypes across all 405 individuals were imputed by adopting the genotypes of the closest related SNP, as measured by Euclidian distance across the sample set.

Hierarchical clustering was then performed by applying the default R hclust() function (method: 'complete'), defining each genotype value as follows:

(i) homozygous 1/1: 0
(ii) heterozygous 1/2: 0.5
(iii) homozygous 2/2: 1

SNV and Indel Analysis

SNV and Indel Calling

We used Platypus version 0.8.1 for detecting and genotyping single nucleotide variants (SNVs) and small insertions and deletions (indels) (Rimmer et al., 2014). Variants were ascertained from the high-coverage genomes sequenced in this study (86T, 88T, 202T2, 203T3, 202H1, 203H) as well as from two previously sequenced devil genomes (31H, 91H) (Tables S1 and S2). Platypus was run twice on each BAM file with two different settings: (i) default mode with additional flags –minReads=3 and –minPosterior=0, (ii) default mode with –minReads=3, –minPosterior=0, –minFlank=0 and –trimReadFlank=10. Variants flagged with badReads, MQ, strandBias, SC and QD were removed, and remaining variants were merged into a single file and genotyped across each sample. Genotyped variants flagged with badReads, MQ, strandBias, SC and QD were removed for both SNVs and indels. The final variant list contained 1,882,666 SNVs and 356,570 indels genotyped across the set of tumors (86T, 88T, 202T2, 203T3) and hosts (202H1, 203H, 91H, 31H). The following post-processing steps were applied to our set of genotyped SNVs and indels.

(i) Homozygous-variant-in-reference filter. Sample 91H was used to assemble the Tasmanian devil reference genome (Murchison et al., 2012). This implies that variants called with a high variant allele fraction (VAF, proportion of reads at a base position supporting the variant allele) in this sample are likely to represent reference assembly errors. Thus, SNVs and indels called with VAF >0.9 in sample 91H were discarded from our variant list.
(ii) Strand bias filter. In regions with total coverage ≥11 across all eight samples, we rejected variant calls with less than 20% support on either forward or reverse sequencing strands. In regions with total coverage <11 reads across all samples, we removed variants that had less than two supporting reads in either forward or reverse direction.
(iii) Sequencing noise filter. Low-VAF SNVs and indels were found across all samples, including hosts, and therefore likely reflect consistent sequencing noise or alignment artefacts in these positions. A variant with VAF <0.2 in all samples with ≥1 supporting reads was discarded if at least one of the host samples had ≥1 supporting reads.
(iv) Simple repeats regions filter. SNVs and indels lying within a 5 BP window around simple repeat regions, as annotated by Tandem Repeat Finder (Benson, 1999), were discarded.
(v) Regions filter. The Tasmanian devil reference genome (Devil7.1) is a scaffold-level assembly, consisting of 237,291 contigs assembled into 35,974 scaffolds. We rejected any variant mapping within 500 BP from the start or end of a contig, or within 1000 BP from the start of end of a scaffold. In addition, variant calls mapping to scaffolds not assigned to a chromosome were discarded.

Combined, these filtering steps left 988,972 SNVs and 194,250 indels. We further genotyped these across our panel of 30 low-coverage normal devil genomes and 12 previously published normal devil genomes (Wright et al., 2017) using Platypus with settings –minPosterior=0 and –minReads=0.

SNV and Indel Subsetting

We classified our variants into different categories, outlined below. Number of variants in each set is indicated in table below.

(i) Germline variants, which are present in the Tasmanian devil population, were defined as variants which had ≥5 supporting sequence reads in high-coverage normal genomes 91H, 202H1 or 203H, or ≥1 supporting sequence read in genome 31H and 42 low-coverage normal genomes (samples listed in Table S2).
(ii) Potentially somatic variants are shared between both tumors of the same lineage, or all four tumors, with ≥5 reads in each tumor, but have <5 reads in each of the three high-coverage normal devil genomes 91H, 202H1 and 203H, and 0 reads in genome 31H and 42 low-coverage normal devil genomes (Table S2). This set includes the following three subsets:

DFT1 Potentially Somatic Variants. Present with ≥5 reads in 86T and 88T, but ≤5 reads in DFT2 tumors and 202H1, 203H and 91H normal devil genomes, and 0 reads in genome 31H and 42 low-coverage normal devil genomes (Table S2). These represent both germline variation that was inherited by the DFT1 founder devil, but that is not captured in the DFT2 founder devil, nor in the normal genomes examined here; and somatic variants that were acquired before divergence of 86T and 88T.
DFT2 Potentially Somatic Variants. Present with ≥5 reads in 202T2 and 203T3, but ≤5 reads in DFT1 tumors and normal devil genomes 202H1, 203H and 91H, and 0 reads in genome 31H and 42 low-coverage normal devil genomes (Table S2). These represent both germline variation that was inherited by the DFT2 founder devil, but that is not captured in the DFT1 founder devil, nor the normal genomes examined here; and somatic variants that were acquired before divergence of 202T2 and 203T3.
DFT1 and DFT2 Potentially Somatic Variants. Present with ≥5 reads in 86T, 88T, 202T2 and 203T3, but ≤5 reads in normal devil genomes 202H1, 203H and 91H, and 0 reads in genome 31H and 42 low-coverage normal devil genomes (Table S2). These potentially represent both germline variation that was inherited by both the DFT1 and DFT2 founder devil, but that is not captured in the normal genomes examined here; and somatic variants that were acquired by DFT1 before the divergence of 86T and 88T, and were also independently acquired by DFT2 before the divergence of 202T2 and 203T3.

(iii) Tumor-unique variants are those variants that are present with ≥5 reads in only one tumor, and are supported by <5 reads in every other tumor and normal genomes 91H, 202H1 and 203H, as well as 0 reads in genome 31H and 42 additional normal genomes (Table S2). These variants could be newly arising somatic mutations that occurred after divergence of 86T-88T or 202T2-203T3 from their most recent common ancestor (MRCA) tumors; or germline variants inherited by the DFT1 or DFT2 founder devils but not shared with the normal panel, or somatic mutations that arose before the MRCA of 86T-88T or 202T2-203T3, that were subsequently lost in one tumor due to back mutation or copy number loss.
(iv) Remainder variants comprise SNVs or indels which are either (i) represented by support from ≥5 reads in at least one DFT1 and one DFT2 tumor, but not found with ≥5 reads in all four tumors, not found with ≥5 reads in any high-coverage normal genomes (202H1, 203H, 91H) or with >0 reads in 31H and 42 low-coverage hosts (Table S2); or (ii) supported by <5 reads in ascertainment panel samples (86T, 88T, 202T2, 203T3, 202H1, 203H, 91H).

The table below indicates number of variants belonging to each category outlined above. Panels on right indicate with "x" the presence and "-" the absence of variants belonging to each category within each sample.

Set	SNVs	Indels	86T	88T	202T2	203T3	Normal Devils
Total	988,972	194,250					
Germline	974,040	191,001	x	x	x	x	x
DFT1 potentially somatic	2,796	387	x	x	-	-	-
DFT2 potentially somatic	3,503	549	-	-	x	x	-
DFT1/DFT2 potentially somatic	88	23	x	x	x	x	-
86T tumor-unique	3229	477	x	-	-	-	-
88T tumor-unique	3583	566	-	x	-	-	-
202T2 tumor-unique	231	19	-	-	x	-	-
203T3 tumor-unique	398	66	-	-	-	x	-
Remainder	1,104	1,162	x	x	x	x	x

Genome browser visual assessments of 75 individual variant calls yielded false positive call rates of <5% for SNVs (2/75) and <15% for indels (9/75).

SNV and Indel Annotation

Of the 602 genes in the COSMIC Cancer Gene Census (http://cancer.sanger.ac.uk/census/; downloaded on 17/05/2016), 490 were annotated in the Ensembl Devil7.0 genebuild (http://www.ensembl.org/Sarcophilus_harrisii/Info/Index). An additional 69 genes were annotated only in the NCBI 101 annotation gene set (https://www.ncbi.nlm.nih.gov/genome/annotation_euk/Sarcophilus_harrisii/101/; downloaded on 17/05/2016), but were not in the Ensembl gene set; thus, 43 cancer genes were not detectable in the Tasmanian devil reference genome (Table S3). SNV and indel subsets were annotated with the Ensembl variant effect predictor (VEP) using default settings (McLaren et al., 2010) (Tables S2, S3, and S4). We also ran an alternative variant caller, SAMtools mpileup, specifically on the COSMIC Cancer Gene Census gene set (Table S3) and searched manually for additional protein-altering variants, however, this did not detect additional variants.

SNV-Based Tumor Purity Estimation

Tumor DNA sequenced in this study was derived from cell lines, and thus is likely to be relatively pure. However, it is possible, particularly for early passage cell lines, that host cells remain in culture. We assessed the purity of 86T, 88T, 202T2 and 203T3 by examining VAF of germline SNVs. This analysis revealed that 86T, 88T and 202T2 contain only tumor DNA, whereas 203T3 had approximately 5-10% host DNA at the time when DNA was collected for sequencing.

Copy Number Analysis

Scaffold Exclusion

The Tasmanian devil genome Devil7.1 has 35,974 scaffolds, most of which are assigned to chromosomes (Murchison et al., 2012), with scaffolds ordered along chromosomes using synteny with the opossum genome (Mikkelsen et al., 2007; Murchison et al., 2012). Short scaffolds, for which synteny with the opossum genome could not be determined, are placed at the end of each chromosome. We excluded these latter scaffolds from copy number analysis, together with the entire X chromosome. Coordinates of excluded scaffolds are listed below.

Chromosome	Excluded Scaffolds
1	Chr1_supercontig_000000399 to Chr1_supercontig_000006728
2	Chr2_supercontig_000000501 to Chr2_supercontig_000008380
3	Chr3_supercontig_000000417 to Chr3_supercontig_000007196
4	Chr4_supercontig_000000317 to Chr4_supercontig_000006728
5	Chr5_supercontig_000000218 to Chr5_supercontig_000003187
6	Chr6_supercontig_000000194 to Chr6_supercontig_000002843
X	Chrx_supercontig_000000000 to Chrx_supercontig_000002377
Un	ChrU_supercontig_000000000 to ChrU_supercontig_000000439

Copy Number Calling

We used the read-depth based algorithm cn.MOPS to assign copy numbers to genomic segments of our four high-coverage tumor genomes (Klambauer et al., 2012). Samples 91H, 202H1 and 203H served as normal controls. Briefly, read-depths were counted in 500 BP bins across selected scaffolds using cn.MOPS getReadCountsFromBAM(), and coverage was normalized to the mode. After modelling copy number posterior likelihoods between copy number (CN) 0 and CN6 for each 500 BP bin in each sample, the cn.MOPS circular binary segmentation algorithm was invoked with a 3 x 500 BP minimum length parameter for non-CN2 segments.

Copy Number Filtering

Each candidate copy number variant (CNV) (defined as a segment with CN≠2) was filtered through a number of steps. First, the minimum size of copy number changes specific to a unique tumor within either the DFT1 or DFT2 lineage (tumor-unique CNVs) was set to 5000 BP, i.e. at least 10 neighboring bins of 500 BP. To further validate tumor-unique CNV segments, we conducted quantitative, lineage-specific sequence read count comparisons. CNVs were only retained when their dispersions significantly differed ($p<0.01$) between 86T-88T or 202T2-203T3, as measured by a paired two-sided Student's t-test. For segments with insignificantly differing read count distributions, copy number posterior likelihoods from cn.MOPS were pooled between both tumors. The highest scoring median value was then chosen for assigning the same segmental copy number to both 86T and 88T or 202T2 and 203T3. Table S4 lists copy number segments and assignments.

Copy Number Annotation

Non-diploid copy number segments were intersected with the set of Ensembl genes (Devil7.0) (Tables S3 and S4). Genes that were completely or partially represented on non-diploid segments, such that loss of one copy or gain of one or more copies was predicted, were considered to be involved in a CNV (Figure 4A, Tables S3 and S4).

To validate gene copy number annotations in COSMIC Cancer Gene Census genes (http://cancer.sanger.ac.uk/census/; downloaded on 17/05/2016), and to obtain calls of those COSMIC genes falling into previously excluded scaffolds (see *Scaffold Exclusion*), and which are not annotated by Ensembl, we conducted an independent, parallel copy number assessment (Table S3). 559/602 COSMIC Cancer Gene Census genes are annotated in the devil reference genome in the Ensembl and/or NCBI gene sets (see SNV and Indel Annotation). To search for the remaining 43 genes, which were annotated neither by Ensembl nor NCBI, we obtained transcript sequences for each gene's opossum – or if this was not available – human orthologue. We used BLAT (Kent, 2002) to align the gene transcript to the devil genome; this approach allowed us to preliminary annotate an additional 4 genes. Next, each gene's footprint was defined as the genomic interval between the start of the first exon and the end of the last exon of each gene. Gene footprints were divided into bins of 500 BP, or – in the case when the gene region would be partitioned into fewer than 10 bins – into bins of 50 BP. For each bin in each sample, the average coverage was collected from the aligned reads using the SAMtools bedcov function (Li et al., 2009). Samples were divided into the following groups: DFT1 (86T, 88T), DFT2 (202T2, 203T3) and host (31H, 91H, 202H1, 203H). An ANOVA test was used to identify gene loci with a heterogeneous distribution of coverage, where the mean of one group differed significantly from the other two with a confidence level of 0.0001. Tukey's range test was then performed to establish which samples had a different mean. A threshold difference of 0.25 was used in order to call a copy number gain or loss after a significant difference was determined. This threshold was also used to assign individual copy number variants to specific samples.

CNV Genotyping across Normal Panel

We analyzed copy number changes on chromosome 3 in our panel of 46 normal devil genomes as follows. Sequencing reads falling into 10,000 BP windows tiled along the chromosome were counted by cn.MOPS getReadCountsFromBAM() (Klambauer et al., 2012). Bin counts were normalized by the average sequencing depth across the whole respective sample, as listed in Table S2.

Structural Variant Analysis

Structural Variant Calling

We used Breakpoints via Assembly (BRASS), a tool that uses discordantly mapped read pairs, for detecting structural variants (SVs). A minimum of two discordant reads detecting a breakpoint in any one sample was required to make a call. SVs were ascertained from tumors 86T, 88T, 202T2 and 203T3, and normal genomes 91H, 31H, 202H1 and 203H.

Structural Variant Filtering

We rejected SV calls for which at least one end fell within a scaffold not assigned to a chromosome. Only calls with a total of >10 supporting reads across all eight samples (86T, 88T, 202T2, 203T3, 31H, 91H, 202H1, 203H) were retained. Moreover, any SV prediction with >2 combined supporting reads across any of the four normals 31H, 91H, 202H1, and 203H was discarded as a likely germline polymorphism. Somatic and potentially somatic SVs were defined as having >10 supporting reads in individual tumors or both tumors of a lineage respectively, together with <3 supporting reads in all other samples combined.

Structural Variant Display

Circos plots of the set of SVs that were not detected in the normal panel are displayed in Figure 3B using the R circlize package (Gu et al., 2014).

Structural Variant Breakpoint Assembly

Exact breakpoint types and corresponding single-base resolution were reconstructed through an in-house analysis pipeline centered around the TIGRA assembler (Chen et al., 2014). Briefly, the structural variant breakpoint predictions identified by BRASS were given as input to TIGRA. TIGRA was used to select structural variant-supporting reads from tumors (86T, 88T, 202T2 and 203T3), and from them assemble contigs spanning the structural variant breakpoints. These contigs were realigned to the devil reference sequence using BWA-MEM (Li, 2013). We selected those contigs that mapped to both scaffold locations predicted by BRASS. We analyzed these alignments to determine the precise location of the breakpoint, to base pair resolution, and to categorize each as either non-templated sequence insertions, microhomologies, or blunt-end breakpoints (Table S5). Of these selected contigs, those with the highest scoring alignments were aligned against the MiSeq amplicon reads. The resulting contig-amplicon read alignments

were manually inspected using IGV to further validate the breakpoint junction sequences (Thorvaldsdóttir et al., 2013). As an additional check, the results obtained through our TIGRA pipeline were also reproduced using the assembly based structural variant caller SvABA (Wala et al., 2018).

Structural Variant Annotation

SV breakpoints were intersected with Ensembl gene predictions. SVs that were predicted within a gene footprint are annotated in Table S5. Strand and frame information was used to predict the potential for SVs to create in-frame fusion genes (Tables S3 and S5).

Mutational Signature Analysis

SNV Spectra for Somatic Mutational Signatures

The set of tumor-unique SNVs for each tumor (see SNV and Indel Subsetting) were extracted, together with their immediate 5' and 3' contexts (96 mutation types). 86T and 88T tumor-unique variants were pooled, and 202T2 and 203T3 tumor-unique variants were pooled, generating DFT1 and DFT2 somatic mutation sets, respectively. Triplet frequency normalization was done as follows. We counted frequencies of the 32 pyrimidine-context nucleotide triplet combinations in the variant-calling accessible (see SNV and Indel Calling) Devil7.1 reference. Each of the 96 observed mutation counts were then divided by its corresponding triplet frequency, prior to rescaling the sum of mutational proportions to 100%.

Normalization of COSMIC Mutational Signatures

The thirty consensus mutational signatures derived from human cancers which are available in the COSMIC database (http://cancer.sanger.ac.uk/cosmic/signatures; downloaded on 01/06/2017) and are relative to the human genome were normalized as follows: we counted frequencies of the 32 pyrimidine-context nucleotide triplet combinations in the human reference genome GRCh37 (hg19). Each of the 96 mutation proportions of each COSMIC signature were then divided by its corresponding triplet frequency, yielding a species-agnostic mutational signature, prior to rescaling the sum of mutational proportions to 100%.

Fitting COSMIC Mutational Signatures DFT1 and DFT2 Spectra

We developed a Bayesian multinomial mixture model to refit known COSMIC mutational signatures to devil DFT1 and DFT2 somatic spectra. The fitting is done using Markov Chain Monte Carlo sampling (MCMC), using the No-U-Turn sampler implemented in the Stan programming language (Carpenter et al., 2017). In the model, the mutational signatures are interpreted as the probability parameters of independent multinomial distributions, and the observed mutation counts in the 96 mutational categories are treated as draws from a mixture of these multinomials. The MCMC process samples mixture weights that specify the degree to which each signature contributes to the observed mutations. We use a symmetrical, uniform Dirichlet distribution as our prior on the mixture weights.

Model specification:

$W \sim \text{Dirichlet}(1)$	Prior on mixture weights
$\theta = WS$	Multinomial mixture probabilities
$M \sim \text{Multinomial}(\theta)$	Likelihood

M: 1×96 vector of mutation counts by category;
1: 1×K vector, each entry is 1;
W: 1×K vector of mixture weights;
S: K×96 matrix of mutational signatures;
K: number of mutational signatures;
θ: 1×96 vector of multinomial probabilities resulting from the mixture of mutational signatures, S, according to weights, W.

Given that human signatures 1 and 5 are almost universal in human cancer and normal tissues (Alexandrov et al., 2013, 2015a; Blokzijl et al., 2016; Ju et al., 2017; Rahbari et al., 2016), we first fitted human signatures 1 and 5 to pooled DFT1 (6,812 variants) and DFT2 (629 variants) variants.

Next, we assessed the improvement of fit when introducing the remaining 28 known human signatures. We assessed cosine similarities between the DFT-unique spectra and double-fits of signatures 1, 5, as well as of any triple-fits of signatures 1, 5, N $\in$ [2-4,6-30] (Table S2). In order to avoid overfitting, we set a minimum threshold of 0.02 cosine similarity increase between 1, 5 and any 1, 5, N signature combinations for significance, as previously described (Schulze et al., 2015). However, only signature combinations 1, 5, 6 and 1, 5, 14 and 1, 5, 15 withstood this criterion in case of the fitting to the DFT1-unique spectrum (Δ0.0479 for signature combination 1, 5, 6; Δ0.0492 for signature combination 1, 5, 14; Δ0.0669 for signature combination 1, 5, 15), whereas no combinations surpassed Δ0.02 in the case of DFT2-unique variants (Table S2). As we did not detect the additional hallmarks of signature 6 and 15 (large numbers of small (<3 BP) indels at mono/polynucleotide repeats) or signature 14 (high numbers of somatic mutations (>200 per megabase), see http://cancer.sanger.ac.uk/cosmic/signatures; last access on 05/10/2017), we believe that it is unlikely that these signatures are present.

Virus Screen and PAV Analysis

De Novo Genome Assembly

De novo assemblies were produced from four tumor genomes (86T and 88T (DFT1) and 202T2 and 203T3 (DFT2)) and two host genomes (202H1 and 203H). We used Fermi (Li, 2012) to perform base error corrections for raw reads, to remove erroneous sequencing data and to generate a contig-wise assembly. We also ran Phusion2 (Mullikin and Ning, 2003) to obtain a second assembly with the base error corrected short reads. SOAPdenovo (Li et al., 2010) was used to process the cleaned reads in a third assembly run, which was improved using SSPACE (Boetzer et al., 2011). Next, Fermi/Phusion2 contigs were aligned to the SOAP scaffolds and assembly gaps closed when a piece of Fermi/Phusion2 sequence bridged two neighboring SOAP scaffolds.

Presence/Absence Variation (PAV) Analysis

Presence/absence variations (PAVs) are the sequences that are present in one genome assembly, but which are undetectable in another. We focused on identifying PAV contigs that were present one or more of the four tumor *de novo* assemblies, but which were absent from the reference genome. We first built an alignment index for absence in the reference assembly Devil7.1 using SMALT (https://sourceforge.net/projects/smalt/). In order to reduce CPU time, we shredded each tumor assembly into 1 kilobase fragments while removing 'N' bases, prior to alignment against the indexed absence (Devil7.1) assembly. Last, we filtered out small repetitive elements placed at ambiguous locations. We have integrated this software into a pipeline, scanPAV, which can be downloaded from https://github.com/wtsi-hpag/scanPAV/ (Giordano et al., 2018). This method produced a set of PAV candidate contigs which had evidence for presence in one or more tumor genome assembly, but which appeared to be absent from the devil reference genome. We further filtered these candidate tumor-specific PAV contigs by aligning sequence reads derived from the reference genome (91H) to them. Contigs with 91H sequence coverage >10 X were removed.

To further filter candidate PAV contigs for absence across a panel of normal devil genomes, the set of candidate tumor-unique PAV contigs were concatenated with Devil7.1 to create four Devil7.1+PAV assemblies, with each assembly carrying the set of PAVs unique to one of the four tumors. Next, we extracted the set of sequence reads from tumors 86T, 88T, 202T2 and 203T3 and normal devils 31H, 91H, 202H1 and 203H which previously did not map to Devil7.1, and aligned these to Devil7.1+PAV using BWA-MEM (Li, 2013). We measured the read depth of each candidate PAV contig in each sample, and retained those contigs that had read depth of at least 40% mean whole genome read depth in at least one tumor (thresholds were as follows, 86T – 34.4 X, 88T – 26.8 X, 202T2 – 26.8 X, 203T3 – 28.0 X), but that did not reach 20% whole genome read depth in any host (thus plausibly representing a single copy integration event in tumors but not in normal genomes); the thresholds for hosts were as follows: 31H – 3.4 X, 91H – 13.0 X, 202H1 – 9.8 X, 203H – 9.0 X. After this filtering, a total of 139 candidate tumor-specific PAV contigs remained (Table S1). The tumor-specificity of these contigs was assessed by aligning reads from the other three tumors to each individual tumor's set of candidate PAVs. The contigs were further evaluated by comparing against the NCBI 'nt' sequence database with the default 'dc-megablast' option in BLAST+ 2.6.0 (Camacho et al., 2009). The top hit was annotated, including target species name, ID, BLAST identity, hit length, E-value and bitscore (Table S1).

Y Chromosome Contig Identification

We used genome assemblies of a male host, 202H1, as well as DFT2 tumors 202T2 and 203T3 to identify Y chromosome contigs that were present in these assemblies but which were absent in the female Tasmanian devil reference genome Devil7.1. Contigs identified in 202H1, 202T2 and 203T3 which were absent in the reference genome were screened using BLAT (Kent, 2002) for the presence of a $\sim$ 825 BP dasyurid-specific intron located within the *SRY* gene (O'Neill et al., 1998). As an input query, we used the intronic *SRY* sequence of the stripe-faced dunnart (*Sminthopsis macroura*). Identified sequences were used as seeds for alignments of the neighboring exons with *SRY* cDNA sequences identified in rock wallabies (O'Neill et al., 1997).

Contigs devil-202H_4481 (202H1, length: 84,660 BP), devil-202T_3709 (202T2, length: 84,684 BP) and devil-203T_28242 (203T3, length: 70,068 BP) were identified as Y chromosomal sequences harboring *SRY*.

Drug Screen IC_{50} Analysis

IC_{50} drug sensitivity values for different cell lines, as derived from our high-throughput screen, were used as an input for $\log_e(IC_{50})$ hierarchical clustering. This was performed by applying the default R hclust() function (method: 'complete') on the Euclidian distance matrix derived from each pairwise drug and cell line combination. Figure 5B shows data for 6 DFT cell lines clustered with 104 compounds. IC_{50} data from human cell lines was obtained from the Genomics of Drug Sensitivity in Cancer (GDSC) database (http://www.cancerrxgene.org/, downloaded on 07/05/2017, Yang et al. (2013)).

DATA AND SOFTWARE AVAILABILITY

The accession number for genomic data reported in this paper is ENA: PRJEB21902. Additional materials such as IHC and FISH images, mutational calls, Devil7.0 to Devil7.1 translations, genome assembly contigs and PAVs can be found on Mendeley Data (https://doi.org/10.17632/znfphvhmbv.1). Code used in this study is made available on Github (https://github.com/MaximilianStammnitz).

Cancer Cell, Volume *33*

Supplemental Information

The Origins and Vulnerabilities of Two Transmissible Cancers in Tasmanian Devils

Maximilian R. Stammnitz, Tim H.H. Coorens, Kevin C. Gori, Dane Hayes, Beiyuan Fu, Jinhong Wang, Daniel E. Martin-Herranz, Ludmil B. Alexandrov, Adrian Baez-Ortega, Syd Barthorpe, Alexandra Beck, Francesca Giordano, Graeme W. Knowles, Young Mi Kwon, George Hall, Stacey Price, Ruth J. Pye, Jose M.C. Tubio, Hannah V.T. Siddle, Sukhwinder Singh Sohal, Gregory M. Woods, Ultan McDermott, Fengtang Yang, Mathew J. Garnett, Zemin Ning, and Elizabeth P. Murchison

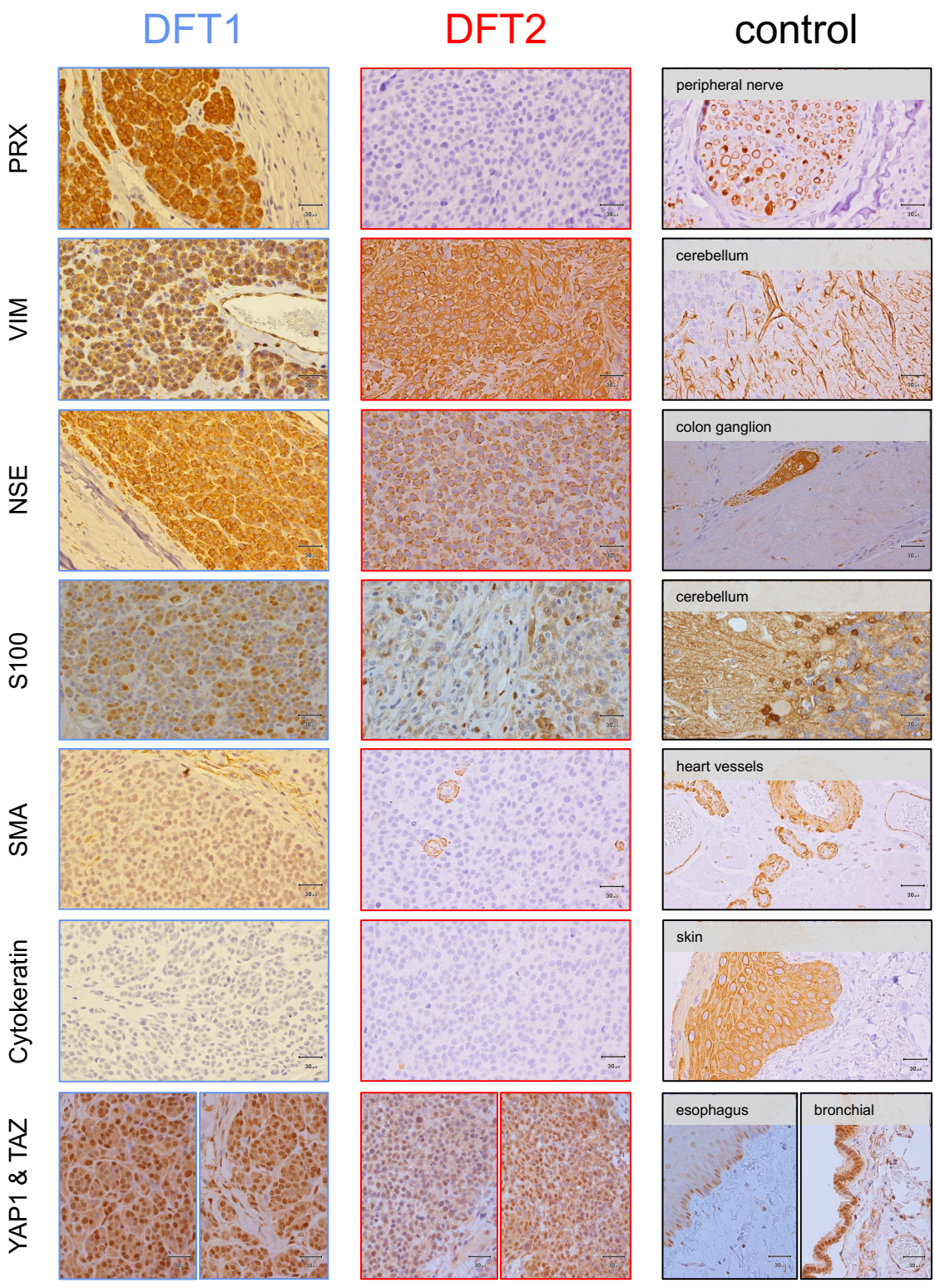

Figure S1, related to Figure 1: Immunohistochemistry.
DFT1 (left), DFT2 (center) and control (right) tissues stained with tissue lineage markers (Loh et al., 2006). PRX is included as a control (Pye et al., 2016b). Scale bar, 30 μm. PRX, periaxin; VIM, vimentin; NSE, neural specific enolase; SMA, smooth muscle actin; YAP1 (bottom left panels), yes-associated protein 1; TAZ/WWTR1 (bottom right panels), transcriptional coactivator with PDZ-binding motif/WW domain-containing transcription regulator 1. Nuclear localization of YAP1 and TAZ/WWTR1 indicates dephosphorylated, active states of the proteins (Moroishi et al., 2015; Wu et al., 2018).

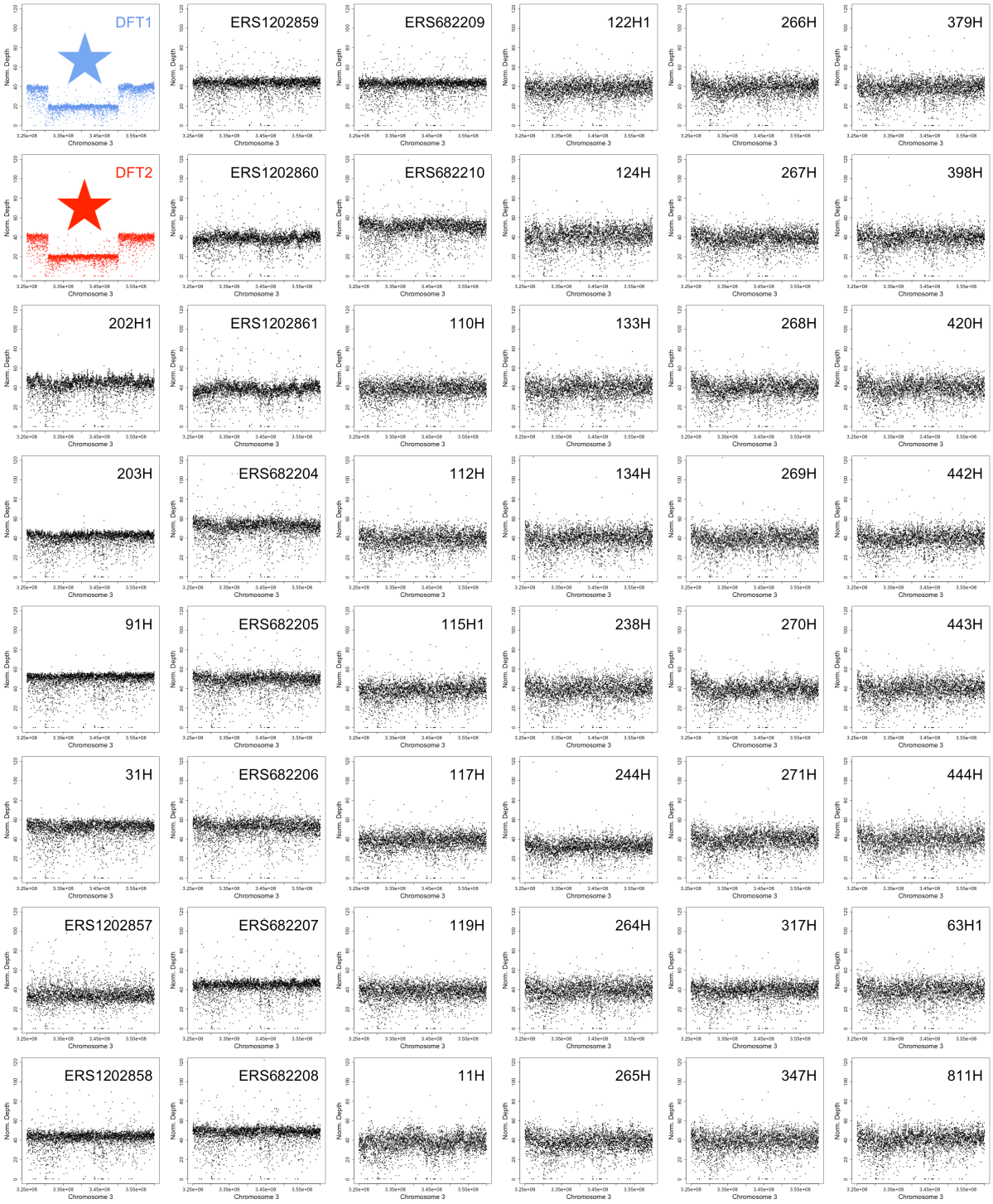

Figure S2, related to Figure 4: Genomic copy number at chromosome 3 locus in DFT1, DFT2 and 46 normal Tasmanian devil genomes.

Copy numbers of DFT1, DFT2 and 46 normal Tasmanian devil genomes at the chromosome 3 locus that has undergone hemizygous deletion in both DFT1 and DFT2 (Chr3_SC_000000273 position 360,001 to Chr3_SC_000000312 position 30,000). Dots represent number of sequence reads mapping in 10,000 base pair non-overlapping bins normalized to average sequencing depth. The region that has undergone hemizygous deletion in DFT1 and DFT2 is marked with a blue and red star, respectively.

Appendix - 7A

ERBB3: A potential target for both early detection and treatment of Devil Facial Tumour 1 (DFT1)

Dane A. Hayes [1, 2, 3], Dale A. Kunde [3], Robyn L. Taylor [2, 4], Stephen B. Pyecroft [5], Sukhwinder Singh Sohal[3], Elizabeth T. Snow [3].

[1]Department of Primary Industries, Parks Water and Environment, Animal Health Laboratory, Launceston, Tasmania, Australia. [2]Save the Tasmanian Devil Program, University of Tasmania, Hobart, Tasmania, Australia. [3]School of Health Sciences, Faculty of Health, University of Tasmania, Launceston, Tasmania, Australia. [4]Department of Primary Industries, Parks Water and Environment, Resource Management and Conservation, Hobart, Tasmania, Australia. [5]School of Animal & Veterinary Sciences, Faculty of Science, University of Adelaide, Roseworthy Campus, Roseworthy, South Australia.

Abstract

Devil Facial Tumour 1 (DFT1) is one of two transmissible neoplasms of Tasmanian devils (*Sarcophilus harrisii*) predominantly affecting their facial regions. DFT1's cellular origin is that of Schwann cell lineage where lesions are evident macroscopically late in the disease. Conversely, the pre-clinical timeframe from cellular transmission to appearance of DFT1 remains uncertain demonstrating the importance of an effective pre-clinical biomarker. We show that ERBB3, a marker expressed normally by the developing neural crest and Schwann cells, is immunohistohemically expressed by DFT1, therefore the potential of ERBB3 as a biomarker was explored. Under the hypothesis that serum ERBB3 levels may increase as DFT1 invades local and distant tissues our pilot study determined serum ERBB3 levels in normal Tasmanian devils and Tasmanian devils with DFT1. Compared to the baseline serum ERBB3 levels in unaffected Tasmanian devils, Tasmanian devils with DFT1 showed significant elevation of serum ERBB3 levels. Interestingly Tasmanian devils with cutaneous lymphoma (CL) also showed elevation of serum ERBB3 levels when compared to the baseline serum levels of Tasmanian devils without DFT1. Thus, elevated serum ERBB3 levels in otherwise healthy looking devils could predict possible DFT1 or CL in captive or wild devil populations and would have implications on the management, welfare and survival of Tasmanian devils. ERBB3 is also a therapeutic target and therefore the potential exists to consider modes of administration that may eradicate DFT1 from the wild.

Introduction

Devil Facial Tumour 1 (DFT1) is one of two transmissible neoplasms of Tasmanian devils (*Sarcophilus harrisii*) predominantly affecting their facial regions. DFT1's cellular origin is that of Schwann cell lineage where lesions are evident macroscopically late in the disease. Conversely, the pre-clinical timeframe from cellular transmission to appearance of DFT1 remains uncertain demonstrating the importance of an effective pre-clinical biomarker.

ERBB3 is expressed in early embryonal development and plays an integral role in the development of the neural crest and Schwann cells. ERBB3 is one of four members of the Epidermal Growth Factor (EGF) family representing a complex group of type 1 transmembrane receptor tyrosine kinase (RTK) designated *EGFR/ERBB1/HER1, ERBB2/HER2, ERBB3/HER3* and *ERBB4/HER4*. ERBB3 is upregulated in a number of human cancers such as breast, colon, gastric, ovarian and prostate but seldom reported in animal cancers.

DFT1's expression of ERBB3 immunohistochemically expression led us to postulate that excess extracellular domain (ECD) may circulate in the host's plasma and present itself as a possible candidate biomarker for DFT1.

Methods

A pilot study of thirty-five Tasmanian devils including clinically healthy Tasmanian devils (CHD, n=15), clinically healthy devils with dermatopathy (CHDD, n=4), Tasmanian devils with clinical DFT1 (DFT1, n=8) and Tasmanian devils with cutaneous lymphoma (CL, n=12)

Briefly, paraffin embedded tissues were processed using standard Histological and Immunohistochemical methods using citrate buffer antigen retrieval, Biocare Medical universal HRP detection kit and monoclonal rabbit anti-human ERBB3 (Abcam, clone SP71, ab93739, 1:50). Serum ERBB3 levels were measured using the RayBio anti-human ERBB3 ELISA Kit according to the manufacturer's instructions. The ELISA standard curve was plotted using Prism v5 and results for each serum interpolated and corrected for dilution. The significance of differences in serum ERBB3 between groups was determined using a Kruskal-Wallis test with Dunn's Multiple Comparison utilizing Prism v5.

Results

DFT1 histology (Fig 1A) Haematoxylin and Eosin. ERBB3 IHC revealed moderate to strong expression in 75% of cells in all strains of DFT1 (Fig 1B). Higher magnification (Fig 1C). Devil skin and subcutis (Fig 1E), peripheral nerve was seldom positive for ERBB3 (red arrow) in keeping with downregulation of ERBB3 in the adult in contrast to DFT1 ERBB3 expression (black arrow). ERBB3 in Tasmanian devil lymphoid follicle (Fig 1F). Trigeminal nerve section (Fig 1I) showed ERBB3 expression in nerve bodies (black arrow) and occasional ERBB3 expression in the adaxonal area (red arrows). Positive control devil bowel (Fig 1G) and negative controls DFT1 (Fig 1D), bowel (Fig 1H) and Trigeminal nerve (Fig 1J).

Serum ERBB3 levels are shown in figure 2. Serum ERBB3 in the Fifteen Tasmanian devils without neoplasia ranged from <30-663 pg/ml with a median of 32 pg/mL (30 – 220; interquartile range). Serum ERBB3 levels in the eight Tasmanian devils (devils 16-23) with clinical DFT1 ranged from 766-18,254 pg/ml with median of 3051 pg/mL (1060 – 10879; interquartile range. In the twelve Tasmanian devils with cutaneous lymphoma (devils 24-35) serum ERBB3 levels ranged from <30-20,021 pg/ml with a median of 1485 pg/mL (289 – 7901; interquartile range). In summary, serum ERBB3 levels are elevated in devils with DFT1 and CL when compared to clinically healthy devils.

Discussion

ERBB3 had previously avoided scrutiny due to its kinase inactivity; however, ERBB3 has now been the subject of intense investigation over the past decade and recognised now as a potent partner of the epidermal growth receptor family. ERBB3 upregulation during developmental, dedifferentiation and regenerative processes encapsulates the Schwann cell's inherent plasticity and imparts certain characteristics of malignant transformation advantageous to transmission of DFT1. Our pilot study has shown for the first time that ERBB3 is consistently expressed immunohistochemically and that ERBB3 is also elevated in the serum of Tasmanian devils with advanced DFT1 and cutaneous lymphoma. Therefore, our research indicates that serum ERBB3 has the potential to be utilised as a biomarker of DFT1 or CL in Tasmanian devils to assist conservationists in the management and welfare of Tasmanian devils and species survival. The simplicity of the ELISA Serum ERBB3 methodology is easily incorporated into routine laboratory batch testing, equally it can be applied to include rapid turnaround of results for urgent cases. Extension of this research is necessary to include greater numbers of healthy Tasmanian devils both with and without visible injuries, devils with large and small DFT1 lesions as well as pre-clinical DFT1. This will firmly establish the normal reference range for serum ERBB3 from which potential pre-clinical DFT1 devils may be identified. In addition, because ERBB3 is now recognised as a therapeutic target, potential exists to consider modes of administration in addition to existing whole cell vaccination such as ERBB3 monoclonal antibody, peptide or xenogeneic vaccines including checkpoint inhibitors. A combinatorial immunotherapeutic approach will enhance cytotoxic destruction, provide long-term immunity from DFT1 and therefore eradicate this transmissible tumour from the wild

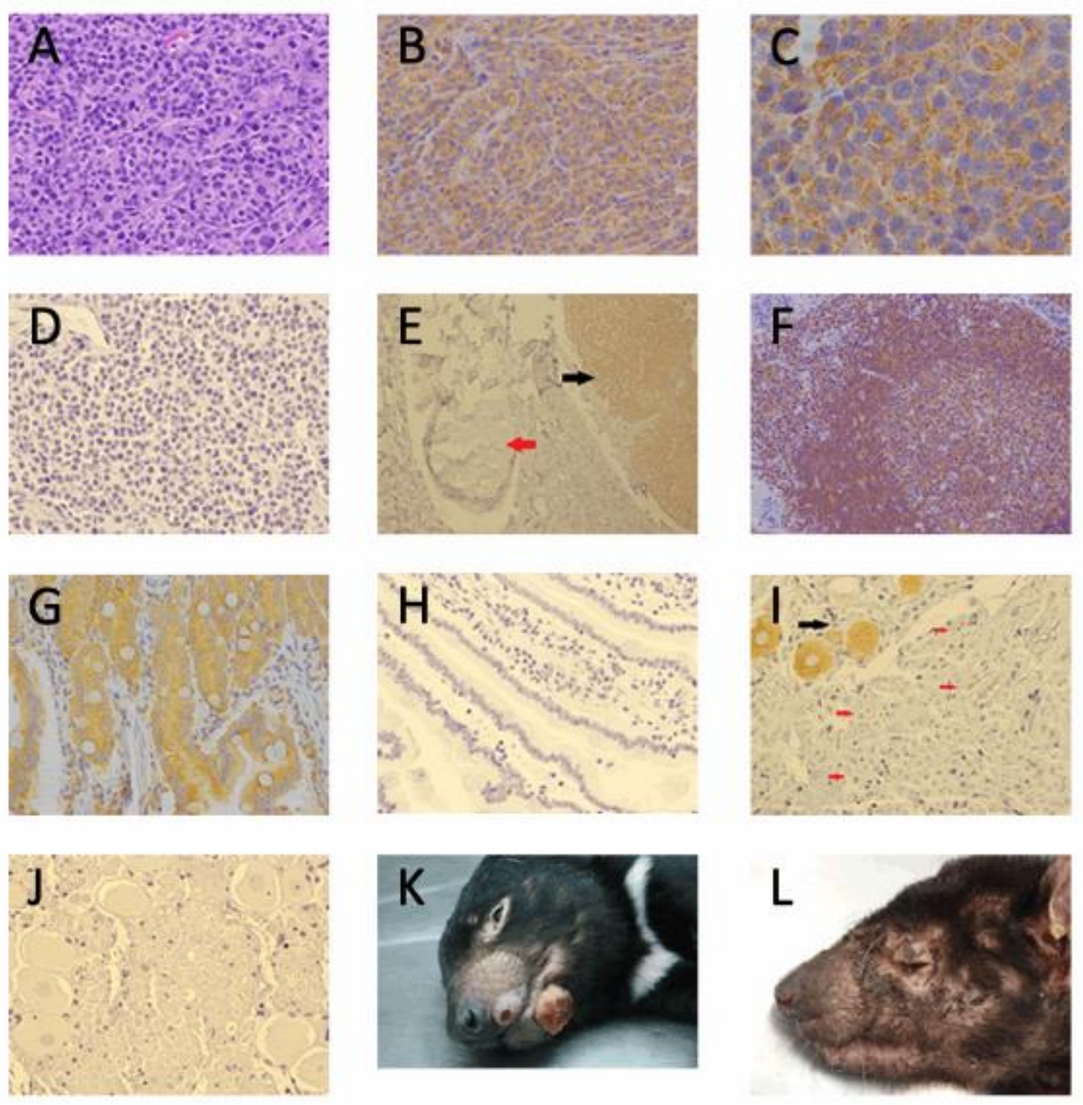

Figure 1. DFT1 staining and skin manifestation.
(A) Haematoxylin and Eosin stained DFT1 x40, (**B)** ERBB3 Immunohistochemical expression in DFT1 strain 3 x40, (**C)** ERBB3 immunohistochemical expression in DFT1 strain 3 x100, (**D)** DFT1 negative control, (**E)** Tasmanian devil skin and subcutis section with peripheral nerve (red arrow) and DFT1 (black arrow) x10, **(F)** Tasmanian devil lymph node ERBB3 expression lymphoid follicle x20, (**G)** Tasmanian devil bowel ERBB3 positive control x40, (**H)** ERBB3 IHC negative control bowel, (**I)** trigeminal nerve shows ERBB3 positive nerve body (black arrow) and occasional adaxonal ERBB3 positivity (red arrows) x40, (**J)** ERBB3 IHC negative control trigeminal nerve, (**K)** Tasmanian Devil gross appearance of DFT1. Photo credit: DPIPWE archive, (**L)** Tasmanian devil gross appearance cutaneous lymphoma. Photo credit DPIPWE archive.

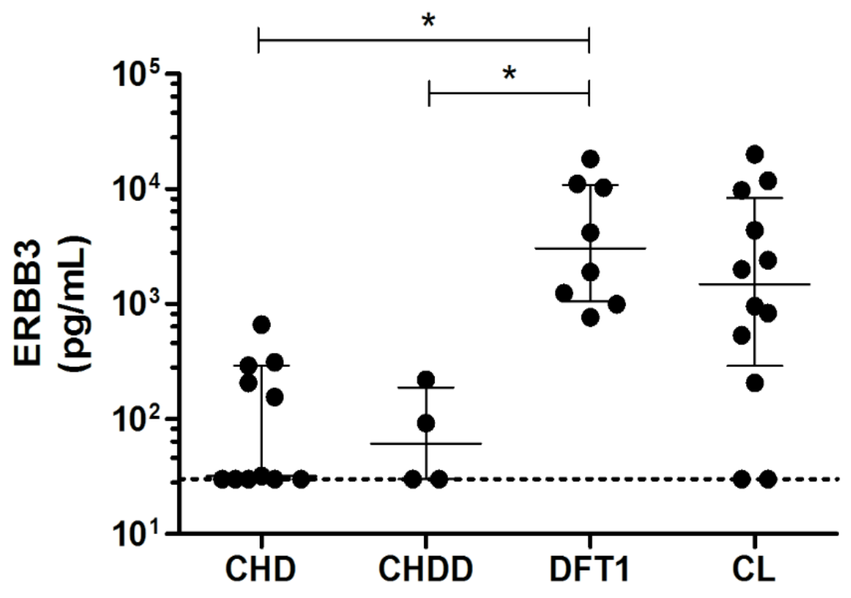

Figure 2. Serum ERBB3 levels in Tasmanian devils.
Serum ERBB3 levels were measured by ELISA in clinically healthy Tasmanian devils CHD (n=11), clinically healthy Tasmanian devils with dermatopathy CHDD (n=4), clinically diagnosed DFT1 (n=8) and those with cutaneous lymphoma CL (n=12). Horizontal dashed line indicates the limit of detection of the ELISA assay at 30 pg/mL. Results of individual devils are shown with the median and interquartile range identified by the whiskers. Significance testing using a Kruskal-Wallis test with Dunn's Multiple Comparison Testing shown with * representing $p < 0.05$.

Acknowledgements and References

This research was funded by the Dr Eric Guiler Save the Tasmanian Devil Research Grant and we are extremely grateful to Save the Tasmanian Devil Program. Full article and references can be found at PLOSONE https://doi.org/10.1371/journal.pone.0177919

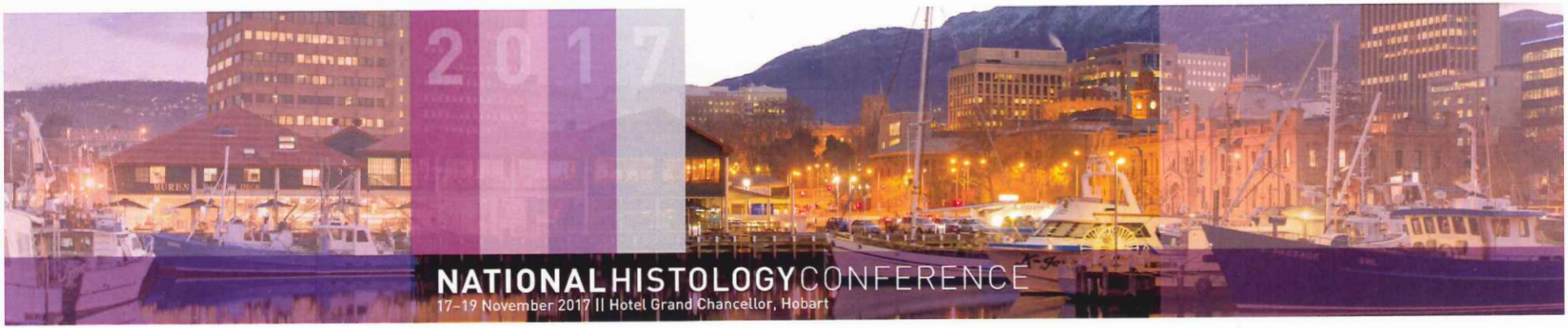

Appendix - 7B

First Poster Prize

presented to

DANE HAYES

for

ERBB3: A potential serum biomarker for early detection and therapeutic target for Devil Facial Tumour 1 (DFT1)

HGSA
HISTOLOGY GROUP OF SOUTH AUSTRALIA

HISTOTECHNOLOGY
SOCIETY OF NSW

HGV

HQ